Lectures on Radiation Dosimetry Physics:

A Deeper Look into the Foundations of Clinical Protocols

by Michael W. Kissick and Sharareh Fakhraei

Lectures on Radiation Dosimetry Physics:

A Deeper Look into the
Foundations of Clinical Protocols

Lectures on Radiation Dosimetry Physics:

A Deeper Look into the
Foundations of Clinical Protocols

Michael W. Kissick
and Sharareh Fakhraei

Information in this book is provided for instructional use only. The authors have taken care that the information and recommendations contained herein are accurate and compatible with the standards generally accepted at the time of publication. Nevertheless, it is difficult to ensure that all the information given is entirely accurate for all circumstances. The authors and publisher cannot assume responsibility for the validity of all materials or for any damage or harm incurred as a result of the use of this information.

Printed in the United States of America

Contents

Preface

This book covers essential physics concepts for understanding and calculating problems in the physical energy deposited in matter from ionizing radiation. The focus of application is on medical uses, both imaging and radiation therapy. There is more weight on radiation therapy throughout the book because of the much greater need for accuracy and precision in that field.

Modern protocols can guide a person toward uncertainties of only 0.5% in the energy deposited per unit mass, the dose. In order to achieve this remarkably low level of uncertainty, one must fully understand all of the subtleties along the way. That is the purpose of this book.

This book starts with the basic science of ionizing radiation and culminates with the modern calibration protocol used in all U.S. radiotherapy clinics today—the American Association of Physicists in Medicine Task Group Report Number 51 (TG-51) and its predecessor, TG-21. The important equations of TG-21 are derived and then connected to TG-51. Since TG-21 is based on cavity theory more explicitly, this approach is something like teaching one how to drive a car with a manual transmission before teaching the much easier automatic transmission.

The aim of this work is to provide a deep understanding of all the pieces that underlie these practical protocols. The aim of this book is not to teach one how to use these protocols. It should be of interest to those who already have a basic education in this field, but who wish to expand and deepen their knowledge without all of the overhead of a large textbook. The information contained herein provides a more intuitive grasp of the physics concepts used in radiation dosimetry in medial applications, especially, but not limited to, radiation therapy physics.

Our use of figures here is conceptual only, and the reader should not read precise values from any figure herein.

This book is based on course notes from Medical Physics 501, a quite famous course in the Medical Physics Department of the University of Wisconsin–Madison. All of this material derives very heavily from Frank "Herb" Attix, the course's original instructor. It also benefited from Thomas Rockwell Mackie, the course's second instructor, who innovated by more properly organizing the material. It is imperative that gratitude also be extended to the many students of this course over the years who have offered input and suggestions along the way, especially students during the years 2010 to 2013 when D. Dunkerly, Q. Guererro, and N. Weiss were especially helpful to us in optimizing these class notes.

This work also draws upon many others, including Paul DeLuca and others in the University of Wisconsin–Madison medical physics and human oncology departments. Also helpful were many of the faculty of the nuclear engineering departments of both Pennsylvania State University and the University of Wisconsin–Madison.

Michael W. Kissick and
Sharareh Fakhraei

Dedication

We dedicate this book to professor Thomas "Rock" Mackie, the previous Medical Physics 501 instructor, upon whose notes this book is founded.

Michael Kissick and
Sharareh Fakhraei

1

Ionizing Radiation and What It Does in the Body

Among the very first applications of ionizing radiation were medical applications. The whole story starts when Wilhelm Roentgen discovered the x-ray in the 1890s. He was experimenting with Crookes tubes (early gaseous electronics, Figure 1.1), which accelerated electrons from a simple cathode to a simple anode. A mysterious, penetrating "ray" was observed to expose film that was out of sight in a desk drawer. The discovery of the x-ray was followed by the discovery of radiation by Henri Becquerel. Shortly after that, Marie Curie was the first to actually use radioactivity for cancer treatments with radium. She was also the first to measure the stopping power of charged particles.

Ionizing radiation has enough energy to remove electrons and leave atoms ionized. Since electrons are liberated with 4–25 eV of energy, ionizing radiation is defined to have at least this energy. Photons are considered to be ionizing with this minimum energy. A photon's energy, E_{photon}, is conveniently calculated as follows:

$$E_{photon} = h\nu = \frac{hc}{\lambda} = \frac{(4.136 \times 10^{-18})(2.998 \times 10^{17})}{\lambda} \ (keV \cdot s)(nm/s) = \frac{1.24 \ keV \cdot nm}{\lambda}. \tag{1.1}$$

Here, h is the Planck constant, c is the speed of light in vacuum, and λ is the photon's wavelength. With the help of Equation (1.1), it is clear that ionizing photons should have wavelengths up to about 310 nm as follows:

$$E_{photon} = 4\,eV \Rightarrow 4 \times 10^{-3}\,keV = \frac{1.24 \ keV \cdot nm}{\lambda} \Rightarrow \lambda = 310\,nm. \tag{1.2}$$

Ultraviolet (UV) photons with wavelengths from 10 nm to 400 nm satisfy this condition. However, since UV photons hardly penetrate tissues, they will not be considered "ionizing" for medical purposes.

The two types of ionizing photons are as follows, but note that they are not distinguished by energy:

- "γ-rays" come from nuclear processes, such as nuclear shell transitions or anti-matter annihilation events.
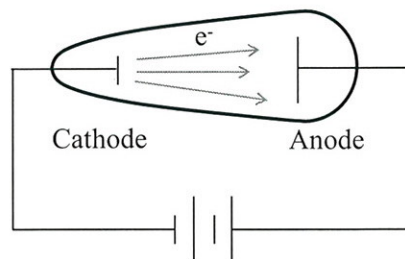
Figure 1.1. The geometry of early gaseous electronics.

1

Table 1.1: Specifying Different Types of X-ray Photons by Their Accelerating Voltage

Photon's Energy Range	X-ray Type
0.1–20 kV	Low-energy or "soft rays" or "Grentz rays" (mostly absorbed in skin)
20–120 kV	Diagnostic range
120–300 kV	Orthovoltage
300 kV–1 MV	Intermediate-energy rays or supervoltage (heroic efforts)
Above 1 MV	Megavoltage (needs microwave technology)

- "x-rays" are caused by electronic processes (i.e., bremsstrahlung or continuous x-rays from Crookes tubes) or atomic processes such as electron shell transitions (i.e., characteristic or fluorescence x-rays).

Further, x-ray photons in the medical field have energies specified by their accelerating voltage. Table 1.1 demonstrates classification of x-ray types based on their energy range.

For comparison, some examples of typical energies and wavelengths are as follows:

- Thermal kinetic energy (K.E.): $\sim (2/3)kT = (2/3)(1.38 \times 10^{-23} J/K)(295K) = 17 \times 10^{-3} eV$

- Radar–super high frequency (SHF): $\lambda \sim 10cm,\ \nu = 3.0 GHz,\ h\nu = 12.4 \times 10^{-3} eV$

- Radio–900 kHz: $\lambda \sim 333m,\ h\nu = (6.63 \times 10^{-34} J \cdot s)(900 \times 10^{3} s^{-1}) = 3.7 \times 10^{-9} eV$

- 35 MV linac photon: $\lambda \sim 35.0 \times 10^{-5} nm\ \ll$ atomic size

There are two types of particles to consider in ionizing radiation. First, uncharged particles, such as photons and neutrons, have random discrete interactions with other particles, but other than these stochastic interactions, they do not interact with matter. Second, as charged particles slow down continuously, they lose energy in a predictable way aside from lateral scatter and range straggling. These charged particles transfer the particle's energy to matter from the many overlapping electromagnetic interactions. The charged particles, therefore, cause the dose, the energy deposited per mass. They are considered "directly ionizing." This is in contrast to the uncharged particles, which are said to not have a range, but instead are attenuated exponentially. The uncharged particles can penetrate a significant distance. The uncharged particles cause dose by first transferring some or all of their energy to the charged particles. In this way, uncharged particles are said to be "indirectly ionizing."

The SI unit of dose is the gray (Gy), and the historical unit is the rad. Grays and rads are related to each other and defined as follows:

$$100 \text{ rad} = 1 \text{ Gy} = 1 \text{ J/kg}. \tag{1.3}$$

In the subject of "health physics," often the uncharged particles—the photons and neutrons—are the main focus because of their larger range for shielding concerns. The subject of this book is "radiation dosimetry." The focus here is the transfer of energy first from uncharged to charged particles (step 1), and then from the charged particles to matter (step 2). This two-step process is illustrated in Figure 1.2.

Note also in Figure 1.2 that there are two common uncharged particles to consider: photons and neutrons. Both can be thought of as carriers of energy with discrete interactions that transfer energy. Neutrons differ in that they are much more likely to induce nuclear reactions. In a water-rich environment like the human body, proton recoil events are the main way that energetic charged particles are generated by neutrons. However, many of these recoil protons will create energetic electrons as well. Neutrons are more complicated and much less common in medical applications at this time. This book concentrates on photons. Photons are, by far, the uncharged particle that most medical applications use.
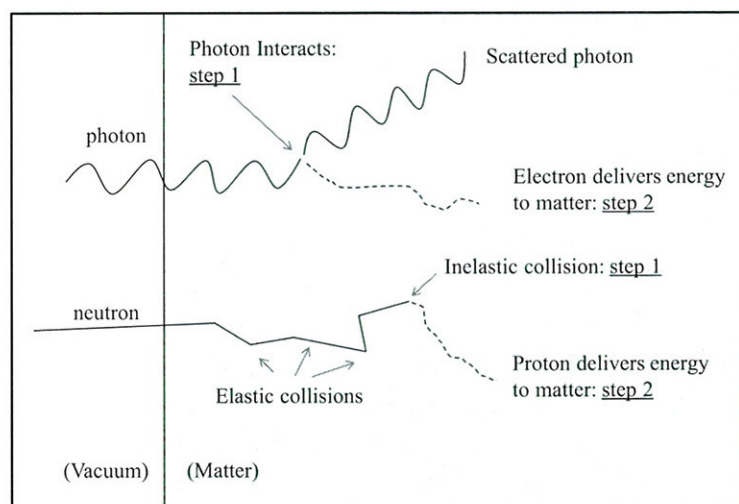
Figure 1.2. Energy transfer to the matter by indirectly ionizing radiation. Note that the dotted lines are where dose gets deposited.

The energy deposited causes both ionizations and excitations, and one difficulty we have is that dosimeters tend to be sensitive to either one or the other. This is one reason we need to calibrate dosimeters. Biological damage will come from both types of radiation.

As a thought experiment, imagine many close, discrete interactions for a charged particle that has a typical stopping power of about 2 MeV/cm (for a kinetic energy of a few MeV for an electron say, and stopping power will be further defined in later chapters). Now consider a 1 g/cm³ material and assume 20 eV/event. Then the number of events per cm is something like the following:

$$\left.\frac{\text{events}}{\text{cm}}\right|_{\text{charge}} = \frac{2 \times 10^6 \text{ eV/cm}}{20 \text{ eV / event}} \approx 10^5 \text{ events / cm.} \tag{1.4}$$

The charged particles we will mostly be interested in here are electrons, but Table 1.2 lists other charged particles that have been used or considered in medicine.

Electrons can be accelerated by many means such as Van de Graff generators, linear accelerators, betatrons, microtrons, and cathode ray tubes (and Crookes tubes). Note how very much lighter these particles are relative to other particles in Table 1.2. Negatrons are electrons, and positrons are anti-electrons. Beta particles are electrons emitted from the nucleus. Knock-on electrons, or delta rays, are electrons emitted from atoms by another charged particle. An Auger electron is an electron emitted by the atom as a whole in an electronic transition.

Muons are heavy electrons, and are leptons that have spin 1/2 and follow Fermi statistics.

Table 1.2: Charged Particles That Have Been Used for Radiotherapy
(Note that if the atomic number of an ion, $Z>1$, it may not be completely ionized.)

Particle	Electron/ Positron	Muon	Pion not 0	Proton ^{1}H	Deuteron ^{2}H	Triton ^{3}H	Alpha ^{4}He	"Heavy" Ions
Charge	±1	±1	±1	+1	+1	+1	+2	+Z
Rest mass (MeV)	0.511	105.7	139.6	938.3	1875.6	2809	3727	Nuclear Mass

Charged pions are produced by charged particle collisions with a nucleus. They have some use in experimental radiotherapy. They have two quarks: $u\bar{d}$. Note:

$$\pi^{+/-} \rightarrow \mu^{+/-} + v'^{-}_{\mu}, \tag{1.5}$$

$$\pi^{+/-} \rightarrow e^{+/-} + v'^{-}_{e}. \tag{1.6}$$

Protons are used clinically in radiotherapy. Neutrons will release protons from collisions. Protons are usually produced in synchrotrons and various types of cyclotrons.

Alpha particles are helium nuclei emitted as alpha decay from unstable nuclei. They are often spallation products, for example from carbon, which can be thought of as three alphas stuck together.

The heaviest nuclei typically conceived of for radiotherapy is carbon, often not completely ionized.

Biology is not a focus of this book. Physical dose is the focus. Very briefly, though, biological effects are caused by chemical effects that are originally caused by physical effects from the charged particle's deposition of energy. To get an idea of magnitude in radiation therapy, a typical dose that kills a tumor is about 60 Gy = 60 J/ kg. Note that 4.18 J = 1 calorie. Assuming a tumor is mostly water with 1 g/cc, and say it has a volume of 30 cc, it requires 1 calorie to raise 1 g of water 1 degree Celsius.

$$\left(60 \text{ J/kg}\right)\left(30 \text{ cc}\right)\left(\frac{0.001 \text{ kg}}{\text{cc}}\right)\left(\frac{1 \text{ calorie}}{4 \text{ J}}\right) = 0.5 \text{ calorie}. \tag{1.7}$$

Therefore, radiation therapy is not killing tumors by injecting high amounts of energy. In fact, one could argue that it kills by injecting very low-entropy energy. The high-energy photons create a lot of free radicals that can damage DNA. For the most part, a tumor cell is killed by trying to reproduce itself with badly damaged DNA. The amount of energy from a lethal therapy photon beam is extremely small. The energy density of a therapy radiation field on our body is about 10^{-3} calories/g, but by contrast, the energy density from food as our body processes it is around 10^3 calories/g. An example would be sugar metabolism:

$$(20 \text{ MJ/kg})\left(\frac{1 \text{ kg}}{10^3 \text{ g}}\right)\left(\frac{10^6 \text{ J}}{1 \text{ MJ}}\right)\left(\frac{1 \text{ cal}}{4.18 \text{J}}\right) = 4.8 \text{ kcal/g}. \tag{1.8}$$

Note that we are only about 5% to 10% efficient in getting food energy: i.e., celery has negative net calories. Most of the biological effects are mediated by the process of radiolysis of water, and the simplest possible view of water radiolysis is the following[†]:

$$e^{-}_{fast} \rightarrow H_2O \rightarrow H_2O^* \rightarrow \dot{H} + \dot{O}H, \tag{1.9}$$

which leads to free radicals[‡]:

$$e^{-}_{fast} \rightarrow H_2O \rightarrow H_2O^+ + e^{-}, \tag{1.10}$$

which leads to ion radicals. Whether ionizations or excitations dominate, the damage will depend on time scales. Both ion radicals and free radicals, as well as the original fast-charged particle, can cause DNA damage, but free radicals last the longest (see Table 1.3), and they diffuse and bind to the DNA backbone (ribose, a sugar). If the bond breaks one strand of the DNA, it can more easily be repaired over a few hours. Hence, dose rate is important to consider (but never is handled well for health physics considerations, which is very unfortunate).

[†] * = excitation
[‡] + = ionization
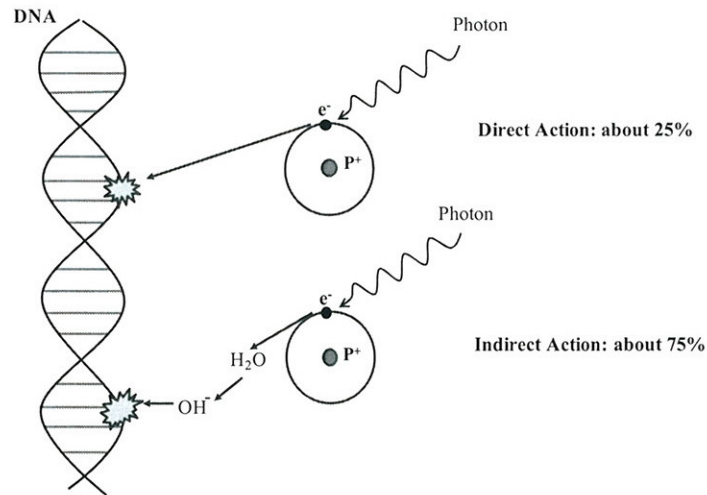
Figure 1.3. Direct and indirect action.

We learned above that uncharged particles are indirectly ionizing, and charged particles are directly ionizing. These terms need to be strictly distinguished from "direct action" and "indirect action." Indirect action refers to DNA damage from radicals and other byproducts of ionizations and excitations. Contrast this with direct action, in which the charged particle damages the DNA directly (Figure 1.3). Free radicals, part of indirect action, cause about 70% to 75% of DNA damage in radiotherapy. The time scales of various processes in radiation therapy are listed in Table 1.3: note the time scale span of almost 30 orders of magnitude.

The chemistry and biology quickly gets very complicated from here.

There is a related quantity to dose called **dose equivalent**, H. The dose equivalent is used to estimate risk for health physics applications from longer-term exposures; it is not meant to calculate damage or risk in specific cases.

$$H = DQN. \tag{1.11}$$

Table 1.3: The Biological Process from First Principles Would Require Decades of Orders of Magnitude in Characteristic Time Scales

Process	Time Scale
Photon interaction	10^{-20}–10^{-18} s photon travel, atom
Fast electron	10^{-16}–10^{-14} s electron travel, cell
Ion radical	10^{-10}–10^{-9} s ion radical lifetime
Free radical	10^{-6}–10^{-5} s free radical lifetime
Chemical changes, breaking bonds	10^{-4}–10^{-2} s reaction rate dependent
Human DNA repair*	10^{3}–10^{4} s based on clinical data
Biological effects	10^{4}–10^{9} s depends on effect

*See Bentzen 1999; *in vivo* repair is longer than in *in vitro* studies.
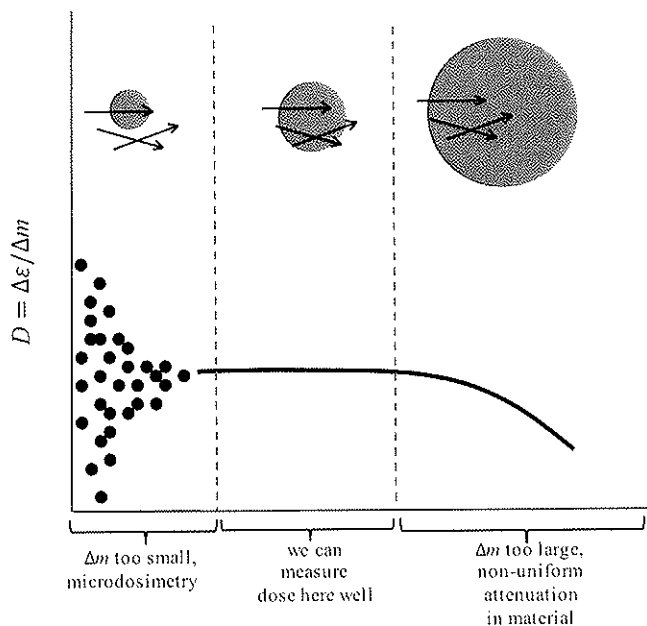
Figure 1.4. There is an optimal sensitive volume in which to measure dose.

Here, H is dose equivalent, and N is the product of all other factors, including demographic factors like age, health, etc. We will always assume N is unity here. The quantity Q is quality factor, a weighting for the *type* (includes energy) of radiation, and D is physical dose.

The SI unit for dose equivalent is the sievert, or Sv. The historical unit is the rem[*], where 100 rem $=1$ Sv $=1$ J/kg. We will not use H in this book, but it is good to understand it. The International Commission on Radiological Protection (ICRP) values for quality factor are listed in Table 1.4.

An essential point to be made is that finding the absorbed physical dose is harder than you might think (see Figure 1.4). The quantity "dose" is defined as the energy absorbed, $\Delta\varepsilon$, per unit mass that absorbed this energy, Δm. We will see that our dosimeters only directly measure part of the energy (except for a good calorimeter, which actually measures the total energy that eventually ends up as heat). As we have already seen, that thermal

Table 1.4: The ICRP Values for Quality Factor

Q	Particle	Particle Energy
1	Photons, Electrons, Muons	All
5	Neutrons	E < 10 keV
10	Neutrons	10 keV < E < 100 keV
20	Neutrons	100 keV < E < 2 MeV
10	Neutrons	2 MeV < E < 20 MeV
5	Neutrons	20 MeV < E
5	Protons	E < 2 MeV
20	Alphas, other...	All

[*]The term rem stands for roentgen equivalent in man.

energy produced is extremely small. The other issue is that the size of Δm can affect the limit away from a few random events toward many events—recall the central limit theorem.

We will want to move in a limit from the stochastic nature of radiation toward a continuous field approach to radiation in order to determine dose analytically, the expectation value of the energy deposited per mass. We will formally define dose again later.

We will see as this book progresses that the big issues for dosimetry are the following:

1. conversion to energetic charged particles,
2. ionization versus excitation,
3. deposition of only a small amount of energy, and
4. the incorrect cancellation of fluence effects due to spatial equilibrium concerns, especially at material interfaces.

References

AAPM. (1983). Radiotherapy Task Group 21. "A protocol for the determination of absorbed dose from high-energy photon and electron beams." *Med. Phys.* 10:741–71.

Attix, F.H. *Introduction to Radiological Physics and Radiation Dosimetry.* Weinheim, Germany: WILEY-VCH Verlag GmbH & Co. KGaA, 2004.

Almond, P.R., P.J. Biggs, B.M. Coursey, W.F. Hanson, M.S. Huq, R. Nath, and D.W.O. Rogers. (1999). Radiotherapy Task Group 51. "AAPM's TG-51 protocol for clinical reference dosimetry of high-energy photon and electron beams." *Med. Phys.* 26:1847–70.

Bentzen, S.M., M.I. Saunders, and S. Dische. (1999). "Repair halftimes estimated from observations of treatment-related morbidity after CHART or conventional radiotherapy in head and neck cancer." *Radiother Oncol.* 53:219–26.

2

Radiation Fields
and Their Statistics

Ionizing radiation is stochastic (random) and quantized by its basic nature. Randomness comes from at least three sources: (1) more than two-body collisions are indeterminate, (2) photon and neutron interactions are *spatially* random, and (3) radioactive decay is *temporally* random. The latter two sources are luckily well characterized by Poisson statistics. However, we want to approximate ionizing radiation with a continuous field description, a non-quantized description that has values at every point. Consider that a stochastic quantity, N_i, comes from the ith measurement of n measurements. The mean value and the standard deviation of all n measurements are defined respectively as follows:

$$\bar{N} = \frac{\sum_{i=1}^{n} N_i}{n},$$ (2.1)

and

$$\sigma = \sqrt{\frac{\sum_{i=1}^{n} (N_i - \bar{N})^2}{n-1}}.$$ (2.2)

With enough particles (interactions/decays/etc.), the Poisson distribution for each particle interaction becomes a Gaussian, with its mean getting closer to the expectation value.

$$N_e = \lim_{n \to \infty} \bar{N} = \lim_{n \to \infty} \frac{\sum_{i=1}^{n} N_i}{n}.$$ (2.3)

The larger the number of measurements n becomes, the smaller the potential deviation from N_e would be. For a single random set of measurements, the standard deviation is as follows:

$$\sigma = \sqrt{N_e} \cong \sqrt{\bar{N}}.$$ (2.4)

Accuracy refers to systematic type errors in N_e. Precision refers to estimates of proximity to N_e. The variance of the mean of these n values will be given by:

$$\sigma_{\bar{N}} = \sigma / \sqrt{n}.$$ (2.5)

Example Problem: To survey background radiation over a certain open field, one would measure the number of counts detected at a few locations. At each location, there is a choice to keep retaking and keep averaging the data to increase precision for that location's reading. By what factor does the precision improve when five readings are averaged at each location instead of just taking one reading?

Solution: At each location, there is a reading based on n instances averaged together. Here we compare $n=5$ to $n=1$. The average counts per reading at each location is $\bar{N}$. The uncertainty will be estimated from the standard deviation for Poisson statistics; radioactive decay detection often follows Poisson statistics. Therefore, the Poisson uncertainty for each reading instance is $\sigma = \sqrt{\bar{N}}$. If one averages $n=5$ readings, then the variation of the average will be $\sigma_{\bar{N}} = \sigma / \sqrt{n}$. The overall counts will be reported for each location as $\bar{N} \pm \sigma_{\bar{N}}$. Even if N remains the same between $n=1$ and $n=5$, such that the "accuracy" is the same, the "precision" will improve by a factor $\sqrt{5} = 2.24$. If one were to have worked in count rate, the answer remains the same. The time window, Δt, is just divided through all steps to make the stated count rate result as $\dot{\bar{N}} \pm \sigma_{\bar{N}} = \frac{1}{\Delta t}(\bar{N} \pm \sigma_{\bar{N}})$.

Fluence and Fluence Rate

The first non-stochastic field quantity we define is **fluence**, Φ. Fluence is a scalar quantity for a vector field of particles. The most straightforward definition of fluence uses the concept of a differential volume, dv, about a point, P. Consider **every** bisecting circle area, da, and count the *expectation number of particles* that cross it, N_e (Figure 2.1). Thus the fluence is defined as the following:

$$\Phi = \frac{dN_e}{da},$$ (2.6)

and has units of fluence in cm^{-2} or particles per area.

There is another fluence definition referred as **Chilton's fluence**. In this alternative, the volume, V, is used instead of the subtle area above. This definition uses the sum of all i^{th} particle's path lengths, l_i, that are considered to be straight through V. That is:

$$\Phi = \lim_{\substack{N \to \infty \\ V \to 0}} \left(\frac{1}{V} \sum_{i=1}^{N} l_i \right).$$ (2.7)
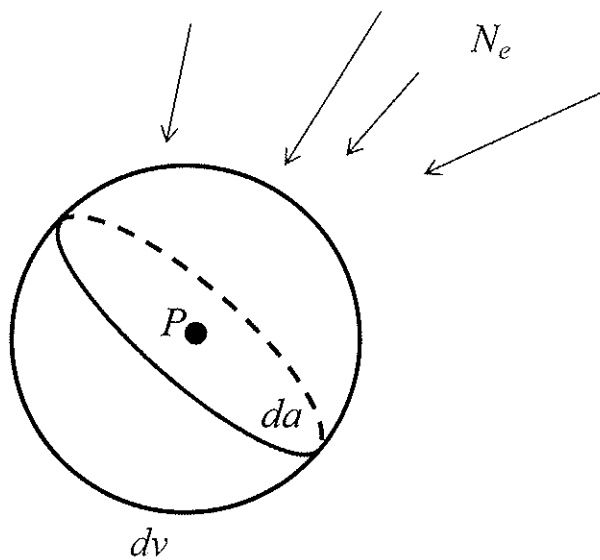
Figure 2.1. Geometry of imaginary volume dv around point P.
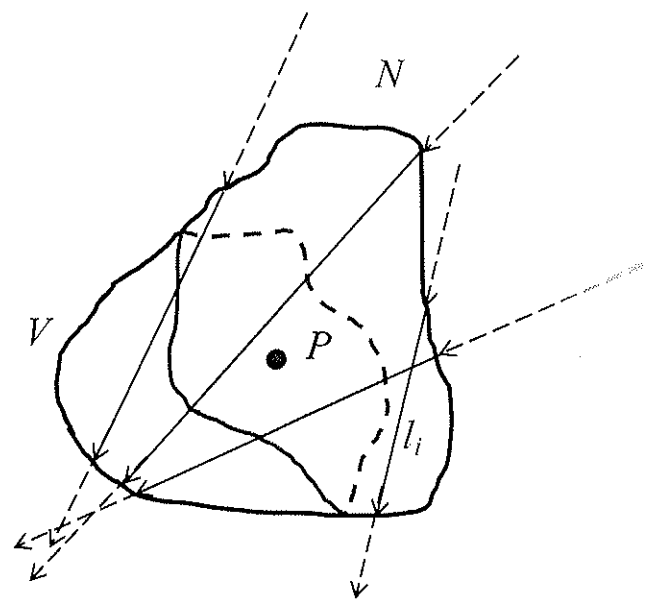
Figure 2.2. Geometry of Chilton's fluence.

If $l = l_i\big|_{\text{any } i}$, then the Chilton's fluence is defined as Equation (2.8):

$$\Phi = \frac{Nl}{V}.$$

(2.8)

The units of Chilton's fluence (Figure 2.2) will remain the same as the previous fluence. The **fluence rate** is simply defined:

$$\dot{\Phi} = \frac{d\Phi}{dt}.$$

(2.9)

The units of fluence rate is $cm^{-2} \cdot s^{-1}$ or the rate of particles per area.

Energy Fluence and Energy Fluence Rate

Refer back to Figure 2.1. Energy is imparted from every direction. **Radiant energy**, R, is the expectation value of the (kinetic) energy carried by N_e particles, which strike the differential volume, dv. For particles with mass, like protons or electrons, radiant energy is given by the following:

$$R = T \cdot N_e,$$

(2.10)

where T is the kinetic energy of the particles (assuming they are monoenergetic). For massless particles, such as photons, with frequency v, however, T is replaced by the photon's energy, hv, as follows:

$$R = hv \cdot N_e.$$

(2.11)

Now, we can define the next non-stochastic quantity, **energy fluence**, Ψ, as follows:

$$\Psi = \frac{dR}{da}.$$

(2.12)

Energy fluence has the units of $J \cdot cm^{-2}$ or energy per area. It is also appropriate to express the energy fluence in units of $eV \cdot cm^{-2}$. Recall that "eV" is the energy of singly charged particles accelerated in 1 volt. Energy fluence of monoenergetic particles with mass is given by the following:

$$\Psi = T \cdot \Phi$$

(2.13)

and for massless monoenergetic particles:

$$\Psi = hv \cdot \Phi.$$

(2.14)

As above, the **energy fluence rate** is defined by the following:

$$\dot{\Psi} = \frac{d\Psi}{dt},$$

(2.15)

and has the units of $eV \cdot cm^{-2} s^{-1}$ or the rate of energy per area. If there is an energy spectrum of particles, then one can consider these relations as valid for each energy bin, and one can then integrate over all the energy bins. Since energy is the end goal for dosimetry, and since the energy spectrum is often fundamental and needs to be considered, the energy fluence is more often useful, and the energy can cancel to make integrals easier: see the example at the end of this chapter.

Angular Distributions

We can calculate differential distributions if the above fluence variables are continuous, and this is a prime advantage for a field description. The limits in the definitions provide us with a particle *field* description. Each particle has a position, direction, energy, and time, and these are all independent, continuous quantities that comprise a multi-dimensional phase space. Therefore, consider that there are at least eight parameters that describe a particle: type (species, charge, mass, spin, etc.); current position (x_0, y_0, z_0); direction to the next position (polar angles: θ, β); energy (kinetic, T or hv); and time. For a field of particles of the same type, there is a seven-dimensional (phase) space that allows for a seven-dimensional characterization of the radiation field, spectrum, or distribution of all these quantities:

$$\Phi'(x, y, z, \theta, \beta, T, t) = \frac{d^7\Phi}{dxdydzd\theta d\beta dTdt}. \tag{2.16}$$

The field is completely specified at point P at location coordinates (x, y, z). The **differential fluence rate** is defined by the following:

$$\Phi'(\dots, t) = \dot{\Phi}'(\dots) = \frac{d^{\#}\dot{\Phi}}{d(\text{variables})}. \tag{2.17}$$

In fact, many analytical treatments result in a differential cross section, fundamentally. It is important to understand some key aspects of the analytical geometry associated with this math. In Figure 2.3, the quantity $d\Omega$ is a differential solid angle. The units of $d\Omega$ is *steradians* (sr). The following differential solid angle is more easily understood by referring to Figure 2.3:

$$d\Omega = \frac{r^2 \sin\theta d\theta d\beta}{r^2} = \sin\theta d\theta d\beta. \tag{2.18}$$
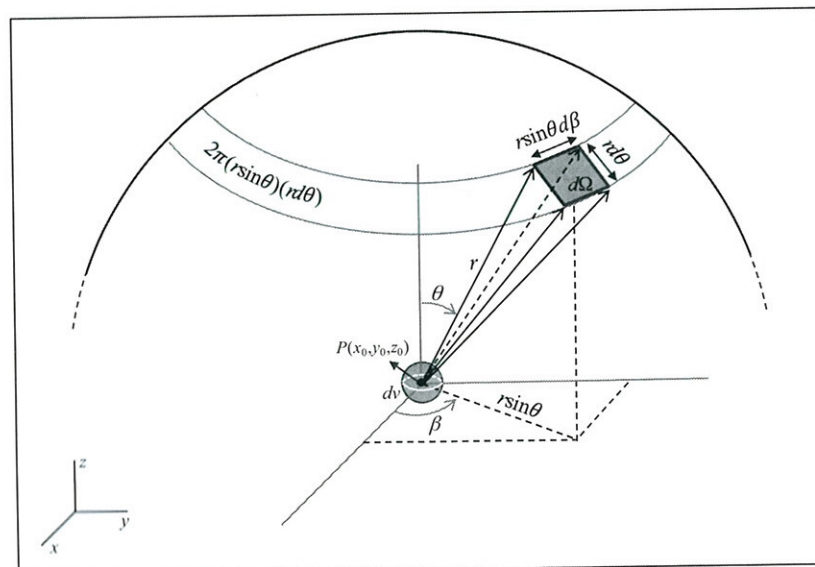
Figure 2.3. The geometry of angular distributions and solid angle where P is located at position (x_0, y_0, z_0).
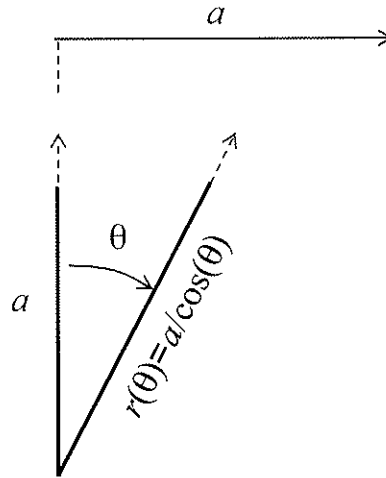
Figure 2.4. Average radius of a disk using angular distributions.

Often the interaction is azimuthally symmetric, and the following notion is used for a differential solid angle that has integrated over the azimuthal angle, β, as follows:

$$d\Omega_\theta = \frac{2\pi r^2 \sin\theta d\theta}{r^2} = 2\pi \sin\theta d\theta. \tag{2.19}$$

It is important to note that often both versions of the differential solid angle are used, and sometimes in the same treatment. With integration over the polar angles, one obtains the following:

$$\int_{\Omega=0}^{4\pi} \dot\Phi'(\Omega)d\Omega \Rightarrow \int_{\theta=0}^{\pi}\int_{\beta=0}^{2\pi} \dot\Phi'(\Omega)\sin\theta d\theta d\beta. \tag{2.20}$$

Note that the integrand, the $\sin(\theta)$ is a Jacobian. It is a conversion essentially between polar and spherical coordinate aspects of the integrand. This is an important factor. Here is an example of how to use the $\sin(\theta)$ factor:
Example Problem: Refer to Figure 2.4 above. Find the average radius of a disk at a distance away from the center that equals the radius of the disk.
Solution: In order to find the average of a given quantity, y, one generally performs the following integral:

$$\bar{y} = \frac{\int_{E=0}^{\infty} yN(E)dE}{\int_{E=0}^{\infty} N(E)dE}, \tag{2.21}$$

In the above equation, the variable E in the distribution $N(E)$ could be the particle energy, for example. Therefore, using the general concept in Equation (2.21), the average radius is calculated as follows:

$$\bar{r} = \int\limits_{\theta=0}^{\pi/4}\int\limits_{\beta=0}^{2\pi} r(\theta,\beta)\sin(\theta)d\theta d\beta \bigg/ \int\limits_{\theta=0}^{\pi/4}\int\limits_{\beta=0}^{2\pi}\sin(\theta)d\theta d\beta$$

$$= \frac{1}{2\pi(2-\sqrt{2})/2}\int\limits_{\theta=0}^{\pi/4}\int\limits_{\beta=0}^{2\pi} r(\theta,\beta)\sin(\theta)d\theta d\beta$$

$$= \frac{1}{2\pi(2-\sqrt{2})/2}\int\limits_{\beta=0}^{2\pi} d\beta \int\limits_{\theta=0}^{\pi/4}\frac{a\cdot\sin(\theta)}{\cos(\theta)}d\theta$$

$$= a\cdot\frac{2\pi}{2\pi(2-\sqrt{2})/2}\cdot\left[-\ln(\cos(\theta))\right]_0^{\pi/4} = 2a\cdot(0.3466)/(2-\sqrt{2}) = (1.18)a$$

Often, the problem is independent of the azimuthal angle, β, so $\dot{\Phi}'(\theta) = 2\pi\sin\theta\,\dot{\Phi}'(\Omega)$. It is also common to see a mixture of θ and Ω.

Energy Distributions

The energy spectrum of the fluence rate is the following:

$$\dot{\Phi}'(T) = \frac{d\dot{\Phi}}{dT} = \int\limits_{\theta=0}^{\pi}\int\limits_{\beta=0}^{2\pi}\dot{\Phi}'(\Omega,T)\sin\theta d\theta d\beta, \tag{2.22}$$

therefore,

$$\dot{\Phi} = \int\limits_{T=0}^{T_{max}}\dot{\Phi}'(T)dT. \tag{2.23}$$

Note that T here is the particle energy. Since the fluence rate is related to the energy fluence rate by the following:

$$\dot{\Psi}'(T) = T\dot{\Phi}'(T), \tag{2.24}$$

thus,

$$\dot{\Psi} = \int\limits_{T=0}^{T_{max}}\dot{\Psi}'(T)dT = \int\limits_{T=0}^{T_{max}}T\dot{\Phi}'(T)dT. \tag{2.25}$$

Of course, for photons, T will be replaced with $h\nu$.

Because one is often concerned with the energy distribution, it is often more convenient to work with energy fluence. Here is a simple example of how using the energy fluence can be helpful. The following piecewise function describes the spectrum of fluence rate in Figure 2.5.

$$\dot{\Phi}'(T) = \frac{a}{T} \quad \text{for} \quad 0 < T < T',$$

$$\dot{\Phi}'(T) = b \quad \text{for} \quad T' < T < T_{max}.$$

By integrating over energy we can get the fluence rate as the following:

$$\dot{\Phi} = \int\limits_0^{T'}\frac{a}{T}dT + \int\limits_{T'}^{T_{max}}bdT = a\ln(T'/0) + b(T_{max}-T').$$
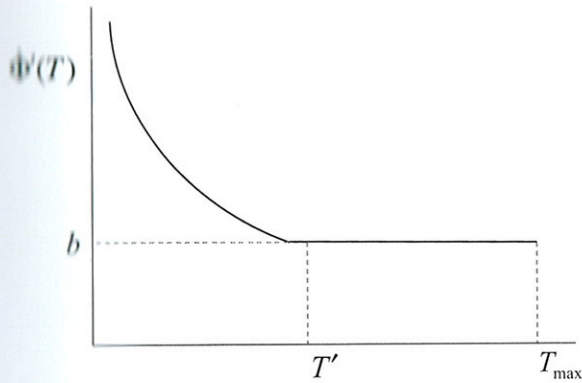
Figure 2.5. Fluence rate spectrum for the example.
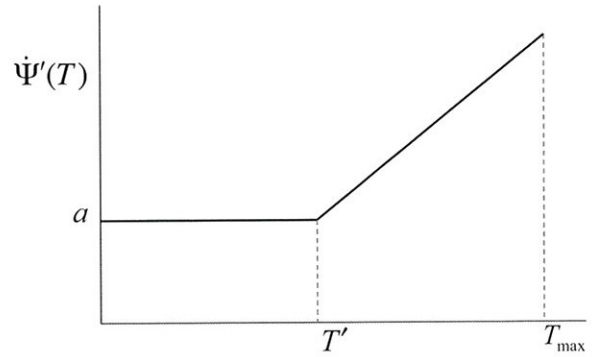
Figure 2.6. Energy fluence rate spectrum for the example.

By applying Equation (2.24), the spectrum of energy fluence rate is given by the following (see Figure 2.6):

$$\dot{\Psi}'(T) = a \quad \text{for} \quad 0 < T < T',$$

$$\dot{\Psi}'(T) = bT \quad \text{for} \quad T' < T < T_{max}.$$

Sometimes we want to work with energy fluence instead of fluence by integrating over energy the energy fluence, like the following:

$$\Psi = \int_0^{T'} a \, dT + \int_{T'}^{T_{max}} bT \, dT = aT' + b(T_{max}^2 - T'^2)/2.$$

Further, one can use the condition at the discontinuity that $a = bT'$. Note that the units of a, a distribution value, would be $\dfrac{keV}{cm^2 \cdot s \cdot keV}$ or energy rate per area per energy bin.

References

Attix, F.H. *Introduction to Radiological Physics and Radiation Dosimetry*. Weinheim, Germany: WILEY-VCH Verlag GmbH & Co. KGaA, 2004.

3

Photon Interactions

Ionizing photons are primarily known by two names: x-rays and (gamma) γ-rays. They are electromagnetic, indirectly ionizing particles with energies ranging from hundreds of eVs to tens of MeVs or greater.

X-rays are electromagnetic radiation caused by electronic processes. Photons emitted by electrons when transiting from higher to lower atomic energy levels are called characteristic or fluorescent x-rays. Photons emitted when charged particles interact with a strong electrostatic field are called bremsstrahlung or continuous x-rays. However, γ-rays are electromagnetic radiation caused by processes other than from electromagnetic force. This type of radiation is emitted from either the nuclear decays or from the annihilation of matter and antimatter. Note that there is no distinction between x-rays and γ-rays based on energy, hv.

Photon interactions with matter generally result in charged particles being liberated, thereby transferring energy to matter from the charged particles. In general, six interactions will be considered in radiological physics: photoelectric effect, Compton effect, pair production, triplet production, Rayleigh scattering, and photonuclear interactions. Among these interactions, photoelectric effect, Compton effect, and pair/triplet production are important interactions for medical dosimetry. The main variables or dependencies of these interactions are atomic number, z, and energy of the incoming photon, hv.

Table 3.1 summarizes the emission properties of six interactions. In the photoelectric effect, the Compton effect, and triplet production, fluorescent photons are not always emitted. In pair and triplet production, annihilation photons are emitted when a positron annihilates with an electron, generally away from the site of the photon interaction. Also, fluorescent x-rays can be emitted from triplet production. Rayleigh scattering, which happens when scattering body size is much smaller than the photon wavelength, is only a redirection of photons, and the reason why the sky is blue. Rayleigh scattering is important in radiological physics only for scattering out of nar-

Table 3.1: Principal Photon Interactions and Their Products
(Note that many more photonuclear interactions are possible, but most with very small cross sections.)

Interaction		Scattered Photons	Uncharged Particle Emitted	Charged Particle Emitted	Charged Particle Created
Photoelectric Effect			yes	yes	
Compton Effect		yes	yes	yes	
Pair Production			yes		yes
Triplet Production			yes	yes	yes
Rayleigh Scatter		yes			
Photonuclear Interactions	(γ,n)		yes		
	(γ,p)		yes	yes	

row beams, and it is purely elastic. Photonuclear interactions—such as (γ,α) and $(\gamma,2\alpha)$, for example—are also possible, and so forth.

Cross Sections and the Attenuation Coefficient

The key concept to describe interactions of particles in matter is the cross section. Consider n photons in a radiation field of area a hitting a thin slab of thickness dl of matter (Figure 3.1).

The differential probability of a certain interaction occurring between a photon and an atom[†] of the matter in the slab, dP, is proportional to the thickness of the slab, dl, the number of targets per unit volume in the matter, and also the type of the interaction. The number of targets per unit volume is $N_A\rho/A$, where N_A is Avogadro's number ($N_A = 6.022 \times 10^{23}$ mole^{-1}), A is molecular weight (with units of g/mole), and the quantity ρ is gravimetric density (with units of g/cm^3). It is important to note that $N_A\rho/A$ has the units of $\dfrac{(\text{mole}^{-1})(\text{g/cm}^3)}{\text{g}\cdot\text{mole}^{-1}} = \text{cm}^{-3}$

The cross section, σ, is then defined as follows:

$$dP = dl(N_A\rho/A)\sigma. \tag{3.1}$$

A common unit for the cross section is the *barn* (1 *barn* $= 10^{-24}$ cm^2). It represents the probability of something hitting a target such as an atom or a nucleus. Someone once said *"big as a barn!"*.

The number of interactions, like thinking in probabilities, is obtained by a product of the field density or the fluence, $\Phi(\equiv n/a)$, and the area of each target[‡], $_a\sigma$ (the atomic cross section, as indicated by the preceding subscript "a"). Therefore, the number of interactions per target is $_a\sigma\cdot\Phi$.

The number of interactions per unit volume is then $[_a\sigma(N_A\rho/A)]\cdot(n/a)$ with the units of $\dfrac{\text{cm}^2}{\text{cm}^2}\dfrac{\text{cm}^{-3}}{} = \text{cm}^{-3}$.

$(N_A\rho/A)$: Targets per unit volume

Photons trajectory

$_a\sigma$

dl
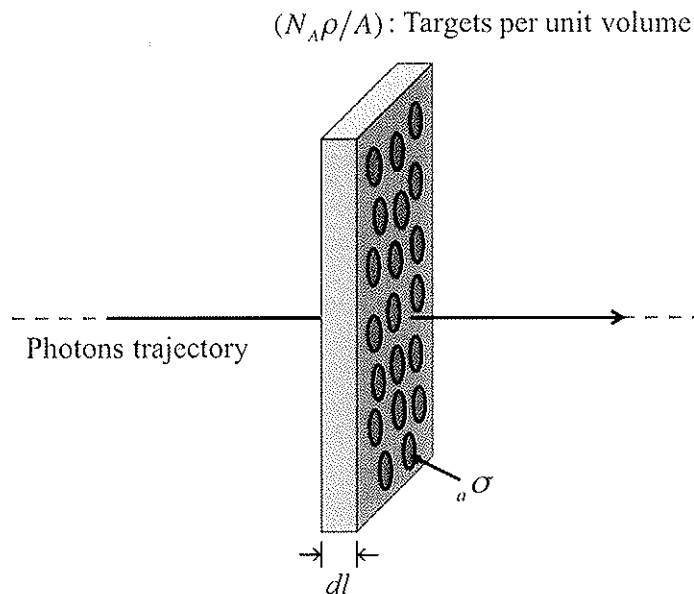
Figure: 3.1. General geometry for the derivation of the attenuation coefficient.

[†]The photoelectric effect treats electrons not as individuals, but as a group. Other interactions treat them individually.
[‡]Here each target is an atom, but a cross section is a general term that can apply to larger or smaller units of matter.

Consider that the number of interactions is equal to the loss of fluence from the photon field, such that a positive interaction means a loss (−) of a photon (fluence). Therefore, we have the following:

$$\left[{}_a\sigma(N_A\rho / A) \right] \cdot (n/a) = {}_a\sigma(N_A\rho / A)\Phi = -\frac{d\Phi}{dl}. \tag{3.2}$$

According to Equation (3.2), the rate of fluence loss is proportional to the fluence itself. Therefore, an exponential loss results:

$$\frac{d\Phi}{dl} = -({}_a\sigma N_A\rho / A)\Phi. \tag{3.3}$$

The **attenuation coefficient** is defined as the following:

$$\mu = {}_a\sigma N_A\rho / A. \tag{3.4}$$

The units of the attenuation coefficient is cm^{-1}. Therefore, Equation (3.3) will turn into the following:

$$\frac{d\Phi}{dl} = -\mu\Phi. \tag{3.5}$$

The solution of this differential equation is the uncollided fluence at a distance l as follows:

$$\Phi(l) = \Phi_0 e^{-\mu \cdot l}. \tag{3.6}$$

Here, Φ_0 is the fluence at the surface of the material. The first listings of μ/ρ started with Barkla and Sadler (1907), then upgraded by Allen (1935), Victoreen (1949), McMaster (1969), and Johns and Cunningham (1983).

The **mean free path** is the average distance traveled by the photon. The probability that the photon survives to l without a collision is then $e^{-\mu \cdot l}$. The probability that a photon survives to l and then in dl at l it has a collision is then $e^{-\mu \cdot l} \cdot \mu dl$. The mean free path, λ, is then found by the following average:

$$\lambda = \int_0^\infty l(e^{-\mu \cdot l} \cdot \mu dl) = \mu\int_0^\infty l e^{-\mu \cdot l} dl = 1/\mu. \tag{3.7}$$

If $\mu l \ll 1$, a Taylor series expansion, keeping only the linear term, gives the following:

$$\Phi(l) = \Phi_0 e^{-\mu \cdot l} \approx \Phi_0(1 - \mu l). \tag{3.8}$$

Example Problem: Consider two photon attenuation processes, each with their own attenuation coefficients: $\mu_1 + \mu_2 = \mu$. There are two questions:

A) What is the total number of interactions by process 1?

B) If the target is thin, how can the expression be simplified?

Solution: First note that the total number of interactions of both types will affect the available (uninteracted) fluence at a given point, l. So, the total number of interactions of both types is just (original fluence) − (uninteracted fluence):

$$\Phi_0 - \Phi(l) = \Phi_0(1 - e^{-\mu \cdot l}).$$

Next note that the relative probability of interacting by process 1 at any point is just $\dfrac{\mu_1}{\mu_1 + \mu_2}$. Finally, the number of interactions by process 1 is the *relative* probability of interacting by process 1 times the total number of interactions, and this is the answer to question A:

$$\left(\frac{\mu_1}{\mu_1 + \mu_2}\right) \cdot (1 - e^{-\mu \cdot l}).$$

Now for the next part. Note that if the target is thin, we can Taylor series expand and drop higher-order terms to get the following:

$$\Phi_0 - \Phi(l) \approx \Phi_0 \{1 - [1 - (\mu_1 + \mu_2) \cdot l]\}.$$

Therefore:

$$\left(\frac{\mu_1}{\mu_1 + \mu_2}\right) \cdot (1 - e^{-\mu \cdot l}) \approx \left(\frac{\mu_1}{\mu_1 + \mu_2}\right) \cdot \{1 - [1 - (\mu_1 + \mu_2) \cdot l]\} = \mu_1 \cdot l,$$

and

$$\mu_1 \cdot l \approx 1 - e^{-\mu_1 \cdot l}.$$

This is the answer to the question B, but a common mistake is that many people make this the answer for A.

In Compton interactions, the target is each electron instead of each atom. In cases like this, we need to replace the atomic cross section with the cross section of each electron, for z electrons per atom, $_e\sigma$ as follows[†]:

$$_a\sigma = z \cdot {_e\sigma}. \tag{3.9}$$

This leads us to the following:

$$\mu = {_e\sigma} N_A \rho z / A. \tag{3.10}$$

There are further groupings of these quantities. The density is often divided out as follows[‡]:

$$\frac{\mu}{\rho} = (_e\sigma)\left(\frac{z}{A/N_A}\right). \tag{3.11}$$

This is the **mass attenuation coefficient**. Notice that the quantity $N_A z/A$ is (atoms/mole) × (electrons/atom) / (grams/mole). Except for hydrogen, if monoisotopic, when converted to atomic mass units, u, this ratio is mostly constant near 0.5 and drops to about 0.4 at very high atomic numbers. It is basically the "*proton*" to "*neutron + proton*" ratio. In this sense, the cross section for the electron here is just a probability of an interaction as the following:

$$_e\sigma \propto \frac{\mu}{\rho}. \tag{3.12}$$

Because the density is divided out in the mass attenuation coefficient, this coefficient is independent of the material *phase*. i.e., water and ice have the same mass attenuation coefficient. Table 3.2 illustrates atomic number to

---

[†]Note how this just counts electrons and ignores its bound state. It is very much a probability argument.
[‡]Note that most sources would have used a capital "Z" instead of the lower-case z we use here.

Table 3.2: Atomic Number to Mass Number Ratio

Material	z/A
Hydrogen -1	1.00
Tritium (Hydrogen -3)	0.33
Helium	0.50
Carbon	0.50
Water	0.55
Muscle	0.56
Lithium Fluoride	0.46
Air	0.50

mass number ratio (z/A) for various materials. Note that the number of protons and the atomic mass tend to be proportional if there are enough particles. Hydrogen is a special case, therefore.

Terma, Kerma, and Collision Kerma

As we said in the first chapter, the main focus of this book is calculating physical dose. However, in order to get closer to calculate dose, we need to first define some non-stochastic quantities that come from a field description of the radiation field.

The first non-stochastic quantity is **terma.** For photons, terma is defined as the total energy released per unit mass. Terma is expressed by the following:

$$T = \frac{\mu}{\rho} \Psi.$$

(3.13)

Note that the focus with this quantity is on the primary radiation beam or field's energy and attenuation. No mention at all is made of what *happens* with this beam energy that is released. Terma has the units of $\frac{J}{kg}$. It has the same units as dose, but is quite far from dose. Yet, it is the first step in that direction.

Kerma is the second non-stochastic quantity that gets us closer to the calculation of dose. It is defined as the kinetic energy released per unit mass. In fact, kerma indicates how much of the released energy gets to charged particles. These charged particles may subsequently radiate photons again, but that is not yet considered. Kerma is expressed as the following:

$$K = \frac{\mu_{tr}}{\rho} \Psi.$$

(3.14)

Kerma has the units of $\frac{J}{kg}$. Again, the same units as dose, but is still not dose. Yet, it is the next step in that direction. In this part, we need to define mass energy transfer coefficient, $\frac{\mu_{tr}}{\rho}$. It is defined via the average energy transferred to charged particles per interaction, $\overline{T}$, by the following:

$$\frac{\mu_{tr}}{\rho} = \frac{\overline{T}}{h\nu} \cdot \frac{\mu}{\rho}.$$

(3.15)

Notice that $\dfrac{\mu_{tr}}{\rho} < \dfrac{\mu}{\rho}$, since $\dfrac{\overline{T}}{h\nu} < 1$. By means of Equation (3.15), the average fraction of energy transferred to charged particles per interaction is determined as follows:

$$\frac{\overline{T}}{h\nu} = \frac{\mu_{tr}}{\mu}. \qquad (3.16)$$

Critical to this definition is an understanding of $\overline{T}$. Assume that for each i of n photon interactions there is an amount of energy given to charged particles, $(\varepsilon_{tr})_i$. Then,

$$\overline{T} = (1/n)\sum_{i=1}^{n}(\varepsilon_{tr})_i. \qquad (3.17)$$

For a photon with energy $h\nu$ interacting at a point, the energy transferred to charged particles, $(\varepsilon_{tr})_i$, will depend on the *type* of the interaction. Figure 3.2 represents some examples of how energy transferred, ε_{tr}, depends on the type of interaction.

All one cares about here is the transfer at a point to charges, but subsequent or other photons that carry some energy elsewhere are not considered here. Eventually, what we really want is energy absorbed "locally." Central to the issue of what we consider "local" is the definition of dose in a subtle way.

The third quantity to define as we approach the concept of dose is **collision kerma**, which can be equal to dose in some situations. It considers charged particles subsequently radiating photons again. A most critical shift in focus now happens to how the *kinetic* energy gets deposited, but not yet dose due to geometry concerns of the

Photoelectric effect $\varepsilon_{tr} = T_{e^-} + T_{Auger}$

Compton effect $\varepsilon_{tr} = T_{e^-}$

Pair Production $\varepsilon_{tr} = T_{e^-} + T_{e^+}$
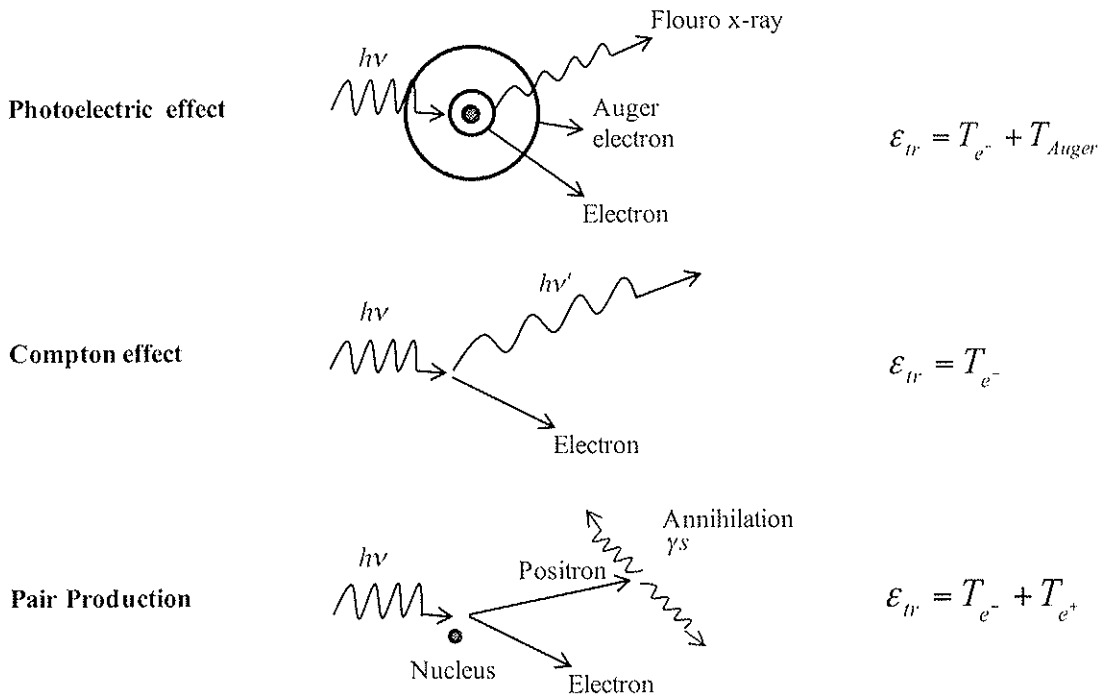
Figure 3.2. Examples of ε_{tr} depend on the type of interaction. Note that in the photoelectric effect, Auger electrons are not necessarily produced. Also, for pair production (if no annihilation-in-flight): $\varepsilon_{tr} = h\nu - 1.022$ MeV + (1.022 MeV − 1.022 MeV). In other words, annihilation takes the rest mass and leaves with it right away, depositing nothing locally. This is discussed further in later chapters.

radiation transport. The issue remaining, as we get close to dose, is locality: does what comes into a point equal what leaves (handled more later). Collision kerma is defined as follows:

$$K_c = \frac{\mu_{en}}{\rho} \Psi.$$

(3.18)

Collision kerma has the same units as dose, and it is close to dose. In order to define the mass energy absorption coefficient, $\frac{\mu_{en}}{\rho}$, we need to first introduce two new quantities. The first quantity is net energy transferred to charged particles, ε_{tr}^{net}. Specifically, this quantity relates to energy deposited within the *ranges* of the charged particles: the photons from radiative losses mostly deposit energy outside of these ranges. We want to stay local here, close to a "point." However, we know that photons carry energy around, and those photons are not to be included here. The second quantity to introduce is the average fraction of incident kinetic energy transferred by photon radiation, g. It is expressed as the following:

$$g = \frac{\text{average subsequent photon radiation energy}}{\overline{T}}.$$

(3.19)

Notice that for low-energy photons and low-z materials, $g \sim 0$. The fraction of energy *not* radiatively transferred, and can thus be deposited locally, is $(1-g)$. The local issue gets difficult at high energy because the charged particle range is close to the photon mean free path. A measure of the amount of energy that stays local is the following:

$$(1-g) = \frac{(1/n)\sum_{i=1}^{n}(\varepsilon_{tr}^{net})_i}{(1/n)\sum_{i=1}^{n}(\varepsilon_{tr})_i}.$$

(3.20)

Therefore, the mass energy absorption coefficient is defined as follows:

$$\frac{\mu_{en}}{\rho} = (1-g)\frac{\mu_{tr}}{\rho}.$$

(3.21)

Compton effect

$$\varepsilon_{tr}^{net} = T_{e^-}^{initial} - T_{e^-}^{final}$$

$T_{e^-}^{initial}$

hv

hv'

hv''

$T_{e^-}^{final} = 0$

Pair Production

hv

Nucleus ● $T_{e^+}^{initial}$

$T_{e^+}^{initial}$

$T_{e^+}^{final} \neq 0$

γs

$$\varepsilon_{tr}^{net} = \left[T_{e^-}^{initial} - T_{e^-}^{final} \right] + \left[T_{e^+}^{initial} - T_{e^+}^{final} \right] - hv''$$

$T_{.}^{final} = 0$

hv''
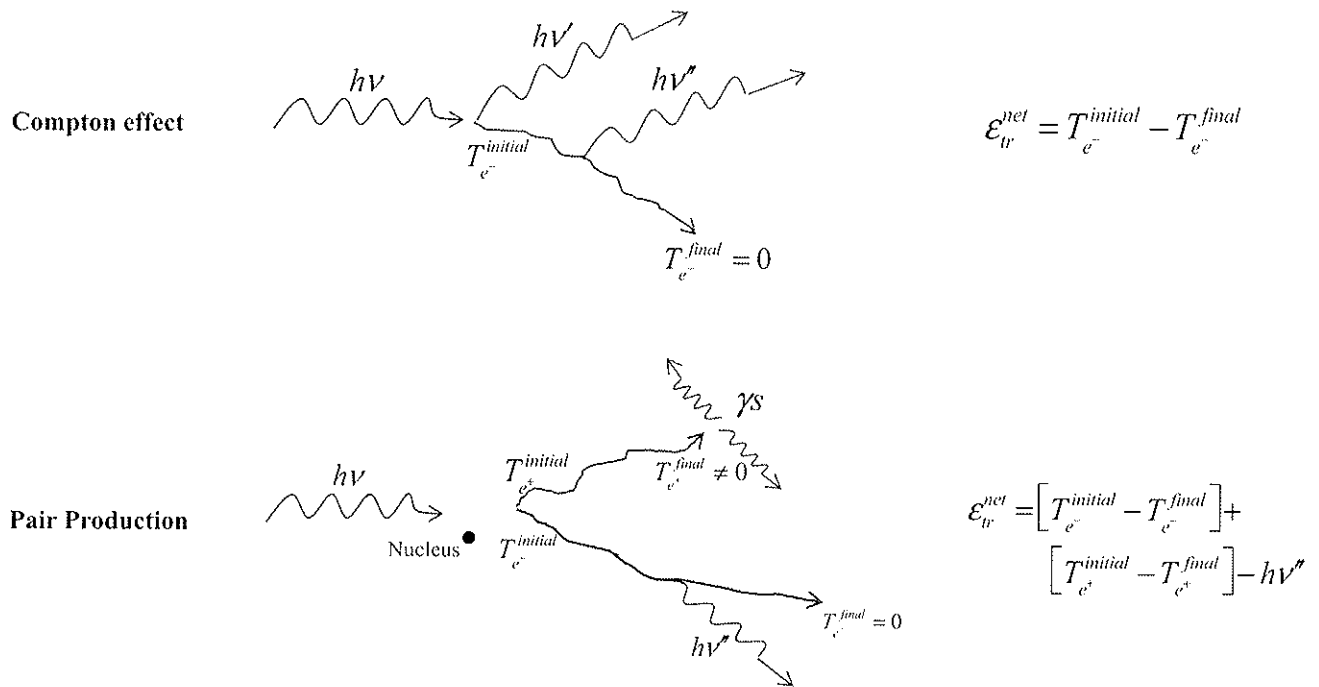
Figure 3.3. Calculating ε_{tr}^{net} for Compton effect and pair production. hv'' represents bremsstrahlung photons. Note that for pair production, if no annihilation-in-flight: $\varepsilon_{tr} = \varepsilon_{tr}^{net} - hv - 1.022$ MeV $+ (1.022$ MeV $- 1.022$ MeV). In the figure, annihilation-in-flight is implied, and the annihilation photons will carry the remaining kinetic energy of the positron, $T_{e^+}^{final}$, as well as their rest mass.

Figure 3.3 shows examples of calculation of ε_{tr}^{net} for Compton effect and pair production. Note that bremsstrahlung photons (hv'') and the annihilation photons are generally "far" from the point of interaction, yet are still included in this quantity. These are non-stochastic field quantities that map all subsequent energy transfers back to the original point of interaction. That is why they are approximations of dose.

Figure 3.4 also demonstrates calculating ε_{tr}^{net} for the photoelectric effect. It is important to mention that the photoelectric effect dominates at low energy where the subsequent bremsstrahlung is negligible for the photoelectron and, certainly, the Auger electrons. Therefore, $hv'' \sim 0$, and $\varepsilon_{tr}^{net} = \varepsilon_{tr}$ for this interaction.

The central issue here is to connect measured (dose) and calculated (collision kerma) quantities. The quantities terma, kerma, and collision kerma are so-called "point-quantities," meaning that they are ideally continuous,

Photoelectric effect

$hv \ll MeV$

Flouro x-ray, hv'

M
L
K

Auger electron, T_{Auger}

Photoelectron, T_{e^-}

$$\varepsilon_{tr}^{net} = T_{e^-} + T_{Auger}$$
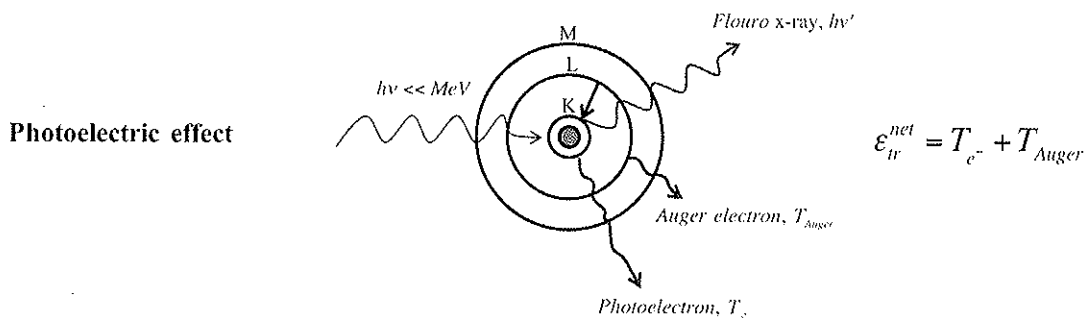
Figure 3.4. Calculating ε_{tr}^{net} for photoelectric effect.

such that mathematical operations like derivatives can be obtained. They are all proportional to energy fluence. Dose, however, is a *measured* quantity (fundamentally), and can be related to the above in some circumstances. The main focus of this book will examine how to connect dose to collision kerma.

Dose Definition

The calculated dose is an expectation value of energy imparted to matter per unit mass at a point. Dose is measured in a volume, so it is not a point quantity technically. There is a concept called "equilibrium" that allows for all points inside that volume to be the same in the relevant ways, but that will come later. Consider just the *energy imparted*, ε, the energy deposited in a specified volume, v. Figure 3.5 shows examples of calculated energy imparted for photoelectric effect, Compton effect, and pair production.

Photoelectric effect
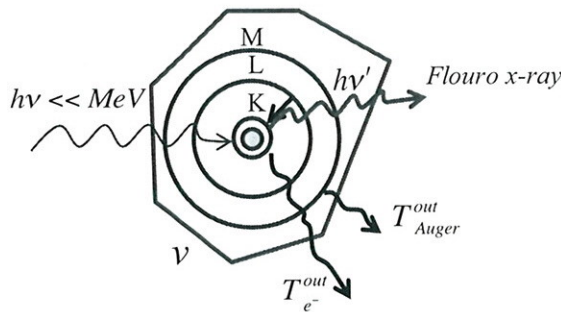
$$\varepsilon = h\nu - h\nu' - (T_{e^-}^{out} + T_{Auger}^{out})$$

Compton effect
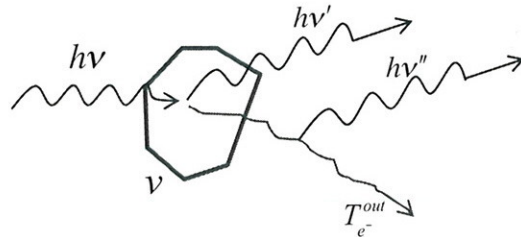
$$\varepsilon = h\nu - h\nu' - T_{e^-}^{out}$$

Pair Production
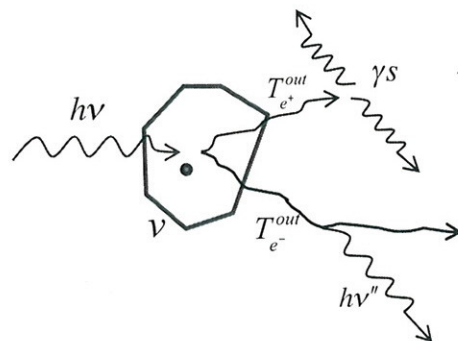
$$\varepsilon = h\nu - \left[T_{e^-}^{out} + T_{e^+}^{out} \right] - 1.022\,\text{MeV}$$

Figure 3.5. Calculating energy imparted, ε, for photoelectric effect, Compton effect, and pair production. Notice that the photoelectric effect dominates at low energy, and here, too, it leads to a simplification that is usually true for low energies: that is $T_{e^-}^{out} \sim 0$ and $T_{Auger}^{out} \sim 0$. The terms with "out" superscripts are the energies with which these particles leave the volume, v.

The dose is now just the expectation value of the energy imparted divided by the mass of the *small[†]* volume. It is expressed as the following:

$$Dose \equiv \frac{\Delta \bar{\varepsilon}}{(\Delta m = \rho \Delta V)}.$$

(3.22)

Note that *it is not possible to write an equation relating the absorbed dose directly to the fluence or energy fluence*. Therefore, the volume size of *v* is ideally *dv*, but it is never that in practice. See Attix (2004) pages 26 and 27.

Narrow and Broad Beam Geometry of Photons

Any reasonable dose measurement needs to consider the effects of scatter and geometry. The volume *v* above necessitates the move away from a pure point quantity. It also brings to mind the issue of the finiteness of geometry. Therefore, we discuss two important kinds of geometry: narrow beam geometry and broad beam geometry.

A convenient stochastic quantity to define here is **radiant energy**. Radiant energy, *R*, is the energy contained in the radiation, charged and uncharged. Consider the geometry of Figure 3.6. Here, only a narrow beam gets through. The rest is scattered away or absorbed. Therefore, in this geometry, ideally only lateral out-scattering or no scattering exists. In this case, the attenuator, which also scatters, has a straightforward result: ideally, any interaction at all will eliminate a photon from being detected. Therefore, the radiant energy detected, R_{det}, will be as follows with the total attenuation coefficient:

$$R_{det}(l) = R_{0det}e^{-\mu \cdot l}.$$

(3.23)

Now consider the geometry of Figure 3.7 with a loss of collimation. Ideally here, lateral in-scattering equals lateral out-scattering. Thus, the radiant energy detected, R_{det}, will be as follows, approximated with the energy absorption coefficient:

$$R_{det}(l) = R_{0det}e^{-\mu_{en} \cdot l}.$$

(3.24)

However, we are not ever in the ideal situation, and the relationship between in-scattering (scattering into the beam, laterally) and out-scattering (scattering out of the beam, laterally) can be complex. *Mostly*, though, out-
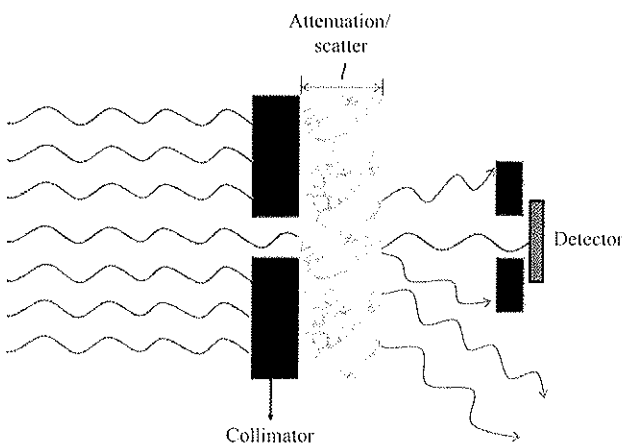
Figure 3.6. Narrow beam geometry.
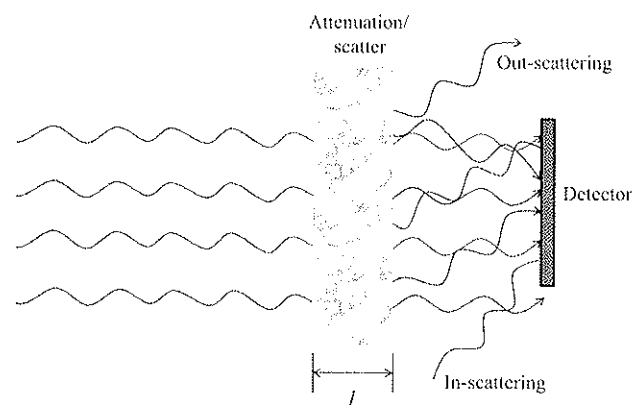
Figure 3.7. Broad beam geometry

[†]Ideally, the region *v* or *dv* here should be small enough so that all photons escape.

Attenuation/scatter (sphere)

Detector

Point source
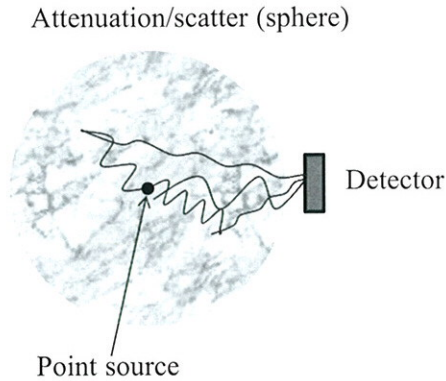
Figure 3.8. Example geometry showing in-scattering larger than out-scattering.

scattering is greater than in-scattering. In that case, the relation between **effective attenuation coefficient**, μ', energy absorption coefficient, and attenuation coefficient is as follows:

$$\mu_{en} < \mu' < \mu. \qquad \text{(out-scattering>in-scattering)} \tag{3.25}$$

If out-scattering is less than in-scattering (Figure 3.8), the effective attenuation coefficient is negative. This situation tends to happen at shallow depths. Also see Attix (2004) Figure 3.4, page 49.

This all leads to the concept of the **buildup factor**, B. buildup factor is a measure of the beam intensity to the primary (i.e., photons that have not yet interacted) beam component intensity:

$$B = \frac{\text{intensity of primary} + \text{secondary radiation}}{\text{intensity of primary radiation only}}. \tag{3.26}$$

IF there is no inverse-square law (not point source, parallel beam instead), then

$$R(l) = R_0 B(l) e^{-\mu l} = R_0 e^{-\mu'(l)l}. \tag{3.27}$$

For more discussions about radiant energy and how it connects to the energy imparted, please see Attix (2004) chapters 2 and 3. The effective attenuation coefficient is defined as the following:

$$\mu'(l) = \mu - \frac{\ln B(l)}{l}. \tag{3.28}$$

Notice that in a narrow beam geometry, $B=1$, but in general, $B>1$. Also note that the effective attenuation coefficient is a function of distance or depth, l. A cautionary final note is in order here. It was pointed out to us in Attix (2004) Chapter 3, that a mean effective attenuation coefficient is not well-defined there, but it is an average with respect to distance and not energy, as one might think at first. As a result, it was pointed out to us that the relationships between the backscatter factor, the mean attenuation coefficient, and a few figures and equations could have been tighter in Attix (2004) Chapter 3.

References

Allen, S.J.M. *X-Rays in Theory and Experiment.* A.H. Compton and S.K. Allison, Eds. New York: Van Nostrand, 1935.

Attix, F.H. *Introduction to Radiological Physics and Radiation Dosimetry.* Weinheim, Germany: WILEY-VCH Verlag GmbH & Co. KGaA, 2004.

Barkla, C.G. and C.A. Sadler. (1907). "Secondary x-rays and the atomic weight of nickel." *Phil. Mag.* 14:408–22.

Hubbell, J.H., W.H. McMaster, N.K. Del Grande, and J.H. Mallett. "X-Ray Cross Sections and Attenuation Coefficients." In *International Tables for X-Ray Crystallography,* Vol. 4, J.A. Ibers and W.C. Hamilton, Eds. Birmingham: Kynoch Press, 1974.

Johns, H.E. and J.R. Cunningham. *The Physics of Radiology,* 4th Ed. Springfield, IL: Thomas, 1983.

McMaster W.H., N.K. Del Grande, J.H. Mallet, and J.H. Hubbell. (1969, 1970). Compilation of x-ray cross sections. *Lawrence Livermore National Laboratory Report* UCRL-50174 (section I 1970, section II 1969, section III).

Victoreen, J.A. (1949). "The calculation of x-ray mass absorption coefficient." *J. Appl. Phys.* 20:1141–7.

4

Photoelectric Effect

In 1905, Albert Einstein won the Nobel Prize for explaining the photoelectric effect with quanta of energy. It was an initial demonstration of quantum mechanics. Since the photoelectric effect dominates at low energies ($h\nu << m_0 c^2$), it is a major contributor to imaging physics, especially in mammography, where this effect is completely dominant.

The photoelectric effect is a "coherent interaction" (an interaction with the entire atom) that results in the photon being absorbed and its energy transferred to the kinetic energy of an orbital electron, T_{e^-}, once the binding energy, E_b, price has been paid. Subsequent relaxation often occurs[†]. Figure 4.1 shows the geometry of this effect. The photon is an electromagnetic, transverse wave. Therefore, the push is mostly in the electric field direction, and the photoelectron tends to come off perpendicular to the direction of the incident photon. The angle of the photoelectron relative to the incident photon is θ_{e^-}. At low energies, it is near 90 degrees, but as the energy increases, it becomes more forwardly directed from relativistic effects.

Based on conservation of energy, we can have the following expression:

$$T_{e^-} = h\nu - E_b - T_A \cong h\nu - E_b. \tag{4.1}$$

The atom recoil energy, T_A, is typically neglected since the nucleus is usually so much heavier that it is approximately stationary. Note that the binding energy is only large enough for our interests for K and L transitions typically, and mostly just K for therapy and most imaging issues. It is also worth mentioning that the binding energy represents an energy well. It is actually negative in that sense, but here we just assume it is the magnitude (positive here).
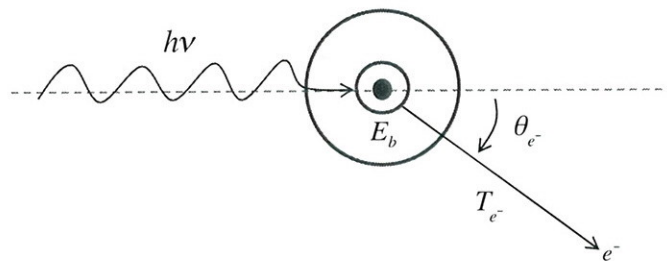
Figure 4.1. Photoelectric effect geometry. Concentric circles emphasize its coherent nature.

[†] There is a subsequent relaxation by either fluorescent photons or Auger electrons or both, and there is ambiguity as to whether these relaxations are considered part of the "interaction" per se.

The photoelectric effect cannot remove an electron from a given shell, n, if it does not have at least the binding energy for that shell, $(E_b)_n$. The threshold for photoelectric effect is the following:

$$(h\nu)_{min} = (E_b)_n \cdot \left(1 + \frac{(E_b)_n}{2M_a c^2}\right). \tag{4.2}$$

Of course, $(E_b)_n \ll M_a c^2$, and note that $(E_b)_n > 0$ here. Therefore, $(h\nu)_{min} \sim (E_b)_n$. Participation of this particular electron is most probable at photon energy just above $(E_b)_n$. This leads to a property that materials tend to be transparent to their own characteristic radiation, i.e., tungsten filter of a tungsten target to get tungsten characteristic radiation separate from many bremsstrahlung photons. In other words, most often the photoelectric effect will occur with an orbital shell that has a binding energy closer to, but lower than, the incident photon energy. For example, gold K-shell electrons are bound with $(E_b)_{K,gold} = 80.7$ keV. A photon with 80.6 keV could not liberate the gold K-shell electrons. The next highest energy is the L_1 shell at 14.4 keV.

There are sharp discontinuities of the probability of the photoelectric effect occurring at the binding energies. These discontinuities are called "edges" (see Figure 4.2). The **participation fraction**, P_n, is the fraction of photoelectric events attributed to shell n. It is calculated by finding the relative reduction in the cross section at the shell "edge" discontinuity as the following:

$$P_K = \frac{\tau_{above\,K} - \tau_{below\,K}}{\tau_{above\,K}}, \tag{4.3}$$

where $\tau_{above\,K}$ and $\tau_{below\,K}$ are the **photoelectric attenuation coefficients** just above and below the K-edge in Figure 4.2. The least rigorous aspect of the participation fraction is that it is assumed to be independent of energy above the shell edge: consider the extension of the line from just below the K-edge.

The L-shell participation fraction, P_L, is the fraction of the events that an L-shell participates in energies below the K-edge. The fraction of events from the L-shell, with an energy *above* the K-edge, is given by $(1-P_K)P_L$. It is the probability of not having a K-shell event times the probability of having an L-shell event.
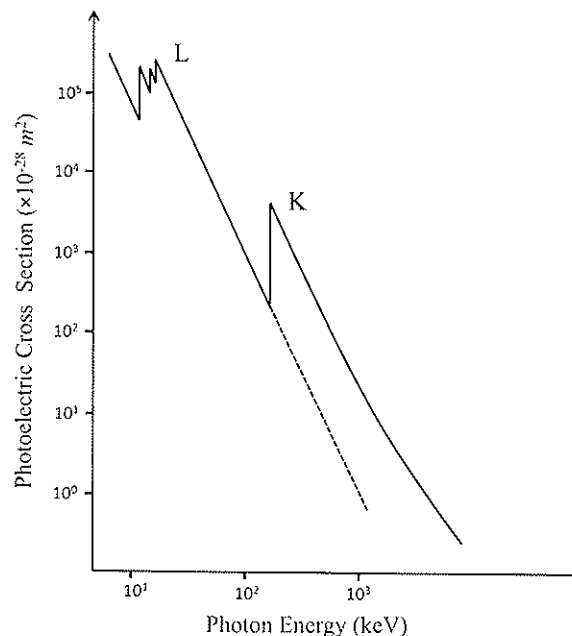
Figure 4.2. Photoelectric cross section for atomic number near 82. The dotted partial extension of L-shell shows that the enhancement of the K-shell can be approximated as a constant factor, especially near the edge.

Differential Cross Section for Photoelectric Effect (K-shell)

Before the Heitler theory described below, there was only the Compton scattering Klein–Nishina theory in 1929, which is discussed more in the next chapter. The cross section for photoelectric absorption had to be found by subtracting the Compton scatter from the total observed cross section. Note that at low energy, it is just these two interactions:

$$(\mu / \rho) - (\sigma_c / \rho) = (\sigma_{pe} / \rho). \tag{4.4}$$

Then in 1954, Heitler approximated just the K-shell contribution to the photoelectric differential cross section. For an unpolarized beam, the photoelectric differential cross section is given by the following:

$$\frac{d_a\tau_K}{d\Omega_0} \cong \left(\frac{z}{137}\right)^5 r_0^2 \left(\frac{m_0c^2}{hv}\right)^{7/2} 4\pi\sqrt{2} \left(\frac{\sin^2\theta_e}{\left(1 - \frac{pc}{m_0c^2}\cos\theta_e\right)^4}\right). \tag{4.5}$$

Here $m_0 = 9.10938215 \times 10^{-31}$ kg is the electron mass, r_0 is the classical electron radius[†], P is the photoelectron momentum, and $r_0^2 = 7.94 \times 10^{-26}$ cm^2. The number $1/137$ is the fine-structure constant, which is usually denoted as α.

$$\alpha = \frac{2\pi e^2}{hc} = \frac{e^2}{\hbar c} = \frac{1}{137}. \tag{4.6}$$

Note that $\left(\frac{1}{137}\right)^2 \frac{m_0c^2}{2} = 13.6$ eV is the binding energy for the hydrogen atom.

It is very common to see differential cross sections and related quantities plotted and described versus angle as equally as versus solid angle, and even for an equation to mix the two. This is confusing, but quite common.

Therefore, the K-shell contribution to the integrated cross section per atom, $_a\tau_K$, is as the following (note that it must be per atom and not per electron since this reaction involves the whole atom):

$$_a\tau_K = 2\pi \int_{\theta_e=0}^{\pi} \left(d_a\tau_K / d\Omega_0\right)\sin\theta_e \, d\theta_e = 4\sqrt{2}\left(\frac{z}{137}\right)^5 r_0^2 \left(\frac{m_0c^2}{hv}\right)^{7/2}. \tag{4.7}$$

Notice that for K-shell, $_a\tau_K \sim \dfrac{z^5}{(hv)^{3.5}}$. However, since $A \sim Z$ for atomic numbers greater than 1 tend to have Z/A constant at about 0.5 (see Chapter 3, Table 3.2). For all shells, the integrated cross section follows by[‡] the following:

$$_a\tau \sim \frac{N_A}{A} \cdot \frac{z^{4\to5}}{(hv)^{2\to3}} \sim \frac{z^{3\to4}}{(hv)^{2\to3}}. \tag{4.8}$$

The photoelectric effect exhibits a rapid decrease with energy, and is dominant only at low energies. Also, the photoelectric effect exhibits a strong dependence on atomic number, z. Applications of this attenuation behavior

---

[†] This comes from the days when they tried to find radiation resistance for electrons. r_0 is related to the width of spectral lines of freely radiating atoms: $\Delta\lambda = (4\pi/3)r_0 = 1.18 \times 10^{-14}$ m. See Feynman (1963) lectures I-32-1.
[‡] In Attix page 140, Eq. 7.30, the upper end of the exponent range is chosen. Many textbooks neglect to tell that there is a range.

include lead shielding, which is very effective at diagnostic energies (<100 keV) and bone, which is much more visible on diagnostic radiographic x-ray film because of its high calcium content (Z_{Ca} = 22 is a relatively high-z material compared to water). Note that for a mixture or compounds, one can define an **effective atomic number**, z_{eff}. The effective z is determined by elemental composition and energy. If Z_i is the atomic number of the ith element, then ε_i is defined as the following:

$$\varepsilon_i \equiv \frac{\text{Number of electrons in element } i}{\text{Total number of electrons}}, \tag{4.9}$$

then the approximation for z_{eff} for $m \geq 1$ would calculate as the following:

$$z_{eff} = \left(\sum_i \varepsilon_i Z_i^{m-1} \right)^{1/m-1}, \tag{4.10}$$

where, for photoelectric effect, $4 < m < 5$, for Compton effect, $m = 1$ and for pair production, $m = 2$. It is important to notice which process dominates at a given energy, because the exponent represents the dependencies for each interaction. The z_{eff} depends on energy mainly because it depends on which photon process dominates. The issue of effective atomic number deserves more discussion. For more description of effective atomic number, such as the $m = 1$ case, see Murty (1965) and Shivaramu (1999, 2000, 2001).

Fluorescent Photons and Auger Electrons

One method of de-excitation from the shell vacancy caused by the photoelectric effect is to release a fluorescent x-ray (Figure 4.3) when an outer shell electron leaves an outer shell for the vacancy in the (more negative energy) inner shell (recall that we are considering shell binding energies to be positive for now).

The energy of the fluorescent x-ray is determined by the following:

$$h\nu_{fluoro} = (E_b)_{inner} - (E_b)_{outer}. \tag{4.11}$$

The **fluorescence yield**, Y_n, is the probability of a transition to shell n, resulting in a fluorescent photon. Fluorescence is more likely for high atomic number materials. For transition to K-shell the z-dependence in fluorescence yield is $Y_K \sim z^{4 \to 5}$. Recall that the photoelectric effect atomic cross section is $_a\tau \sim z^{4 \to 5}$. We should expect that the fluorescence probability will have the same dependence, since it's like the reverse process. That is, except that it happens between two bound states.

Figure 4.3. Fluorescent photon and auger electron for a relaxation of K-shell.

Auger electron emission competes with fluorescence. It is the emission of an electron from an outer shell to carry excitation energy away that resulted from the photoelectric effect shell disturbance. Assume for now that *the probability of Auger emission ~z,* Then, heuristically,

$$\frac{(\text{probability/atom})_{fluor}}{(\text{probability/atom})_{Auger}} = \frac{Y_K}{1-Y_K} \approx \frac{az^{4\rightarrow5}}{z} \propto az^{3\rightarrow4}, \tag{4.12}$$

which leads to the following:

$$Y_K \approx \frac{az^{3\rightarrow4}}{1+az^{3\rightarrow4}} \approx \frac{z^{3\rightarrow4}}{1/a+z^{3\rightarrow4}}. \tag{4.13}$$

This is not bad since empirically we find the following[†]:

$$Y_K = \frac{(0.957)z^4}{(9.84\times10^5)+z^4}. \tag{4.14}$$

For low-z materials, we find that $Y_K \approx 0$, and for high-z materials, it is $Y_K \approx 0.957$, so the assumption about Auger production being proportional to z seems reasonable. For more discussion on this topic, see Attix (2004) pages 142–3.

There is ambiguity as to whether subsequent relaxations are considered part of the energy and net-energy transfer for a single photon interaction energy transfer calculation.

Example Problems: Consider three cases related to Figure 4.4 and calculate energy transfer and net energy transfer for each case.

Case 1: If *no relaxations* considered, or if all relaxations by *fluorescence.*

Case 2: If all relaxations are from *Auger,* and there is *no fluorescence.*

Case 3: If just the pictured single fluorescence photon is considered.

Solutions:

Case 1: If *no relaxations* considered, or if all relaxations by *fluorescence,* then:

$$\varepsilon_{tr} = \varepsilon_{tr}^{net} = T_{e^-} = h\nu - (E_B)_K = 100\,\text{keV} - 88\,\text{keV} = 12\,\text{keV}.$$

Case 2: If all relaxations are from *Auger,* and there is *no fluorescence:*

$$\varepsilon_{tr} = \varepsilon_{tr}^{net} = T_{e^-} + T_{Auger} = h\nu = 100\,\text{keV}.$$
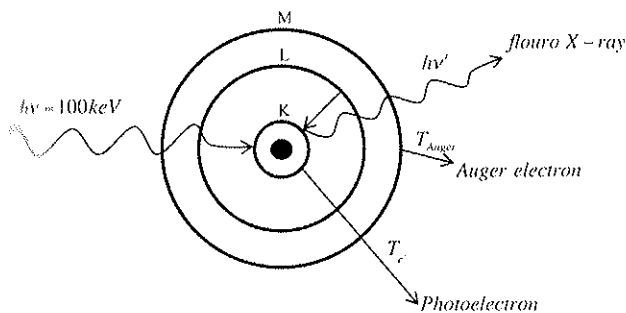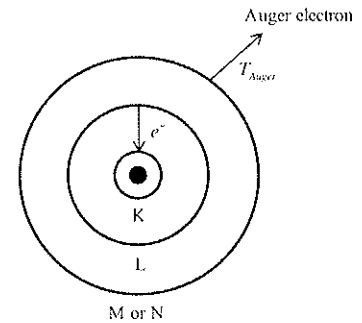
Figure 4.4. Energy transfer for photoelectric effect. Let's assume in this example it is Pb: $(E_B)_K = 88$ keV, and $(E_B)_L = 16$ keV.

$$\varepsilon_{tr} = T_{e^-} + T_{Auger}$$

Figure 4.5. Auger emission.

[†] See Hubble (1994).

Case 3: If just the pictured single fluorescence photon is considered:

$$\varepsilon_{tr} = \varepsilon_{tr}^{net} = h\nu - h\nu' = 100 \text{ keV} - (88 \text{ keV} - 16 \text{ keV}) = 28 \text{ keV}.$$

It is very common for a test problem to omit this subtlety. In situations where the atom cannot or is less likely to emit a fluorescent photon, then Auger emission can release energy. For example, an M-shell releases energy via Auger after a transition from L to K shells—presumably the K-shell vacancy was caused by a photoelectric interaction (Figure 4.5).

The energy of the Auger electron is found by getting energy from electrons moving into K, and paying for leaving L and then paying again for leaving M:

$$(T_{Auger})_M = (E_b)_K - (E_b)_L - (E_b)_M. \tag{4.15}$$

In general, the energy of Auger electrons are calculated as follows:

$$T_{Auger} = (E_b)_{vacancy} - (E_b)_{fill} - (E_b)_{Auger}. \tag{4.16}$$

The Auger electron can come from any shell, even the same as the filling shell. Then it is called a **Coster–Kronig** electron. Of course, there needs to be the condition met that $[(E_b)_{vacancy} - (E_b)_{fill}] > (E_b)_{Auger}$. Notice how we are quickly led to a possible chain of vacancies and a potentially high charge until all the vacancy shell binding energy is released and eventually conduction band electrons fill the vacancies. *It can be complex.*

Both fluorescent x-rays and Auger electrons are emitted isotropically as one might expect from a coherent, whole-atom process like each of these.

Mass Energy Transfer Coefficient for the Photoelectric Effect

The final result of this chapter is what gets transferred to charged particles. Both the photoelectron with $h\nu - E_b$ of kinetic energy, and the Auger electrons, which also release a fraction of the E_b, will contribute to the transfer of energy to charged particle kinetic energy. If the atom de-excites with only Auger electrons, then *all* of the original $h\nu$ will go to charged particles. i.e., the entire photoelectron binding energy is eventually all recovered. It can be ambiguous as to whether relaxations are part of the photoelectric "interaction."

Any fluorescent photons will decrease the energy transfer to charged particles. Above the K-edge, the mass energy transfer coefficient for photoelectric effect is approximately as follows:

$$\frac{\tau_{tr}}{\rho} = \frac{\tau}{\rho}\left(\frac{h\nu - P_K \cdot Y_K \cdot (h\overline{\nu})_K - (1 - P_K) \cdot P_L \cdot Y_L \cdot (h\overline{\nu})_L}{h\nu}\right). \tag{4.17}$$

The term $(1 - P_K)P_L Y_L (h\overline{\nu})_L$ approximates the contribution of energy from fluorescent photons from vacancies from the L-shell for incident photon energy above the K-edge and implicitly assumes that P_L is independent of the average photon energy, $h\overline{\nu}$. The quantities $(h\overline{\nu})_K$ and $(h\overline{\nu})_L$ are the fluorescence x-ray average energy for transitions into these shells from all other shells as weighted by the probability of each transition. They may be approximated by their respective binding energies, (E_b), like in biological tissues: low enough z, and high enough $h\nu$.

Below the K-edge, the mass energy transfer coefficient is approximately as the following:

$$\frac{\tau_{tr}}{\rho} = \frac{\tau}{\rho}\left(\frac{h\nu - P_L \cdot Y_L \cdot (h\overline{\nu})_L}{h\nu}\right). \tag{4.18}$$

We are ignoring contributions from shells *beyond L* because they are small. What matters for the energy transfer coefficients and for dosimetry is *average* energy transferred to charged particles from a large number of interactions.

References

Attix, F.H. *Introduction to Radiological Physics and Radiation Dosimetry*. Weinheim, Germany: WILEY-VCH Verlag GmbH & Co. KGaA, 2004.

Feynman, R.P., R.B. Leighton, and M. Sands. *The Feynman Lectures on Physics*, vol 1. Redwood City, CA: Addison-Wesley, 1963.

Heitler, W. *The Quantum Theory of Radiation*, 3rd ed. Oxford: Clarendon, 1954.

Hubbell, J.H., P.N. Trehan, N. Singh, B. Chand, D. Mehta, and M.L. Garg. (1994). "A Review, Bibliography, and Tabulation of K, L, and Higher atomic shell x-ray Fluorescence Yields. *J. Phys. Chem. Ref. Data* 23:339–64.

Klein, O. and T. Nishina. (1929). "Über die Streuung von Strahlung durch freie Elektronen nach der neuen relativistischen Quantendynamik von Dirac." *Zeitschrift für Physik*, 52:853–68.

Mayneord, R.C. (1965). "Effective Atomic Numbers of Heterogeneous Materials." *Nature* 207:398–99.

Shivaramu and V. Ramprasath. (2000). "Effective atomic numbers for photon energy absorption and energy dependence of some thermoluminescent dosimetric compounds." *Nucl. Instrum. Methods Phys. Res. B.* 168:294–304.

Shivaramu, R. Amutha, and V. Ramprasath. (1999). "Effective Atomic Numbers and Mass Attenuation Coefficients of Some Thermoluminescen Dosimetric Compounds for Total Photon Interaction." *Nucl. Sci. Eng.* 132:148–53.

Shivaramu, R. Vijayakumar, L. Rajasekaran, and N. Ramamurthy. (2001). "Effective atomic numbers for photon energy absorption of some low-Z substances of dosimetric interest." *Radiat. Phys. Chem.* 62:371–77.

5

Compton Scattering Effect

Arthur Holly Compton at Washington University in St. Louis discovered the Compton effect in 1923 and got the Nobel Prize in 1927. The geometry of the Compton effect and respective energies and momentums of incident and scattered photons and the electron are described visually in Figure 5.1.

The Compton effect dominates at intermediate incident photon energies, near the electron rest mass: $h\nu \sim m_0c^2$. At these energies—which are much bigger than shell-binding energies—the scattering becomes inelastic with energy given to an electron that is ejected from the atom. However, the dominant physics is a simple two-body collision that treats the electron as unbound to first order.

Straightforward kinematics provides a complete solution as follows:

$$hv' = \frac{hv}{1 + \alpha_0(1 - \cos\phi)}, \tag{5.1}$$

$$T_{e} = hv - hv' = \frac{hv \cdot \alpha_0(1 - \cos\phi)}{1 + \alpha_0(1 - \cos\phi)}, \tag{5.2}$$

$$\tan\theta = \frac{1}{(1 + \alpha_0)\tan(\phi/2)}. \tag{5.3}$$

Here $\alpha_0 \equiv \dfrac{hv}{m_0c^2}$. Note that here are three equations and four unknowns, $(hv', T_{e}, \phi, \theta)$, so given any of these unknowns in addition to hv, then all quantities are determined.

For the low-energy limit ($hv \ll m_0c^2$), energy of the scattered photon would be almost the same as incident photon ($hv' \cong hv$) and independent of scattering angle. This is the completely elastic limit of **Thomson scatter-**
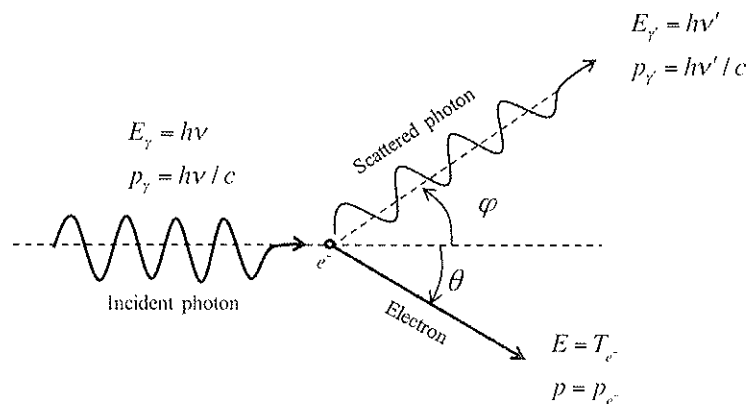

Figure 5.1. Geometry of the Compton effect, a simple two-body collision.

ing. Also, $hv' = hv$ is the result of $\phi = 0$, and there is effectively *no event*. From Equations (5.1) and (5.2), it is clear that for $\phi = 0$, the energy of the electron would be zero, $(T_{e^-} = 0)$ and then θ_{max} would occur as the following:

$$\theta \Rightarrow \theta_{max} = \arctan\left(\frac{1}{(1+\alpha_0)\tan(0)}\right) \Rightarrow 90°. \tag{5.4}$$

In contrast, when the scattered photon has a minimum amount of energy, then it corresponds to the case where $\phi \Rightarrow \phi_{max} = 180°$ and thus the scattered electron has the maximum energy as the following:

$$T_{e^-} \Rightarrow (T_{e^-})_{max} = hv\frac{2\alpha_0}{1+2\alpha_0}. \tag{5.5}$$

There are also two other cases that are important for shielding, because scattered photon angles greater than 90° relative to a normally incident beam will backscatter out of the surface:

$$\lim_{hv \to \infty}\left(hv'\big|_{\phi=90°}\right) = m_0c^2, \tag{5.6}$$

$$\lim_{hv \to \infty}\left(hv'\big|_{\phi=180°}\right) = m_0c^2/2. \tag{5.7}$$

Differential Cross Section for Compton Effect

The differential cross section for Compton effect per electron was derived by **Klein and Nishina** (1929), assuming unpolarized photons and unbound electrons with azimuthal symmetry as in the following:

$$\frac{d_e\sigma}{d\Omega_\phi} = \frac{r_0^2}{2}\left(\frac{hv'}{hv}\right)^2\left(\frac{hv}{hv'}+\frac{hv'}{hv}-\sin^2\phi\right). \tag{5.8}$$

Here, $r_0 = 2.818 \times 10^{-13}$ cm is the classical electron radius. The quantity Ω_ϕ can be understood in Figure 5.2. Note that the differential cross section is *per electron* and independent of z.
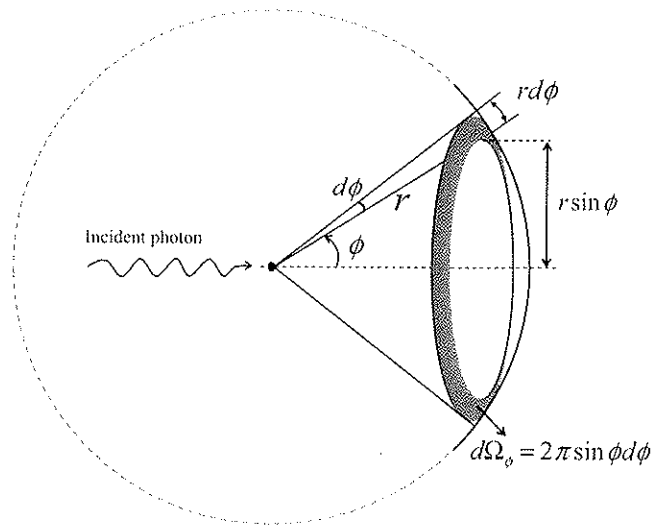
Figure 5.2. Differential annulus for azimuthally symmetric interactions with a Jacobian $\sin\phi$.

The number of scattered photons per unit azimuthal solid angle is illustrated in Figure 5.3. The peanut-shaped plot in Figure 5.3 does change with polarization effects included[*]. Figure 5.4 demonstrates differential
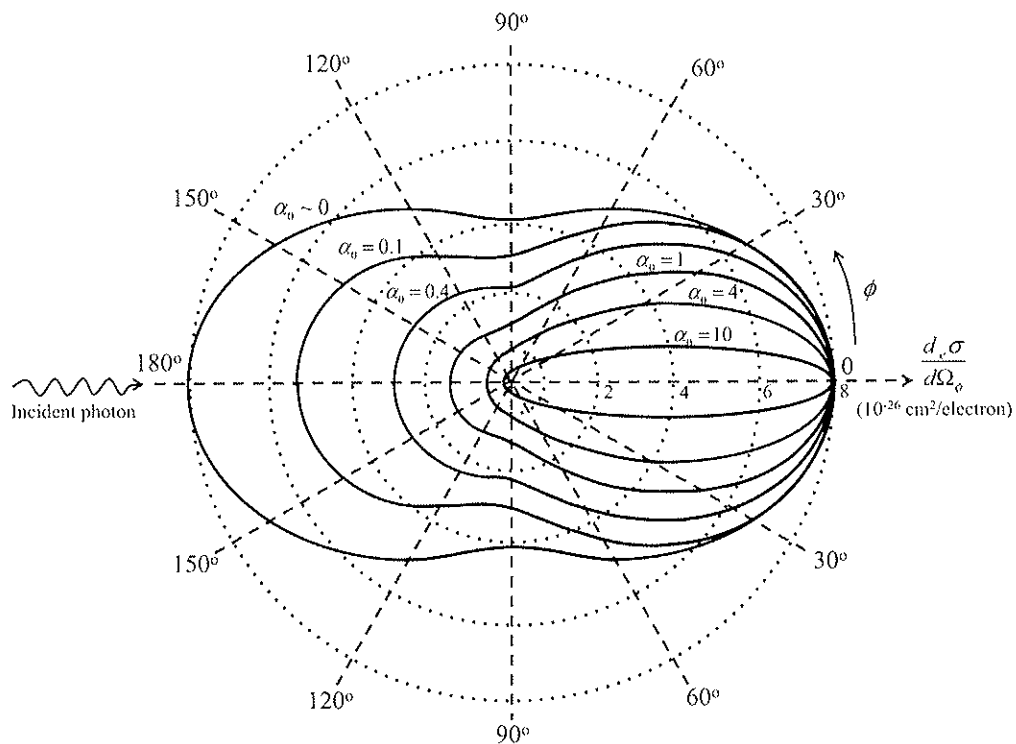
Figure 5.3. The number of scattered photons per unit azimuthal solid angle. Note that higher energies are forward directed. This figure was calculated with Equation (5.8).
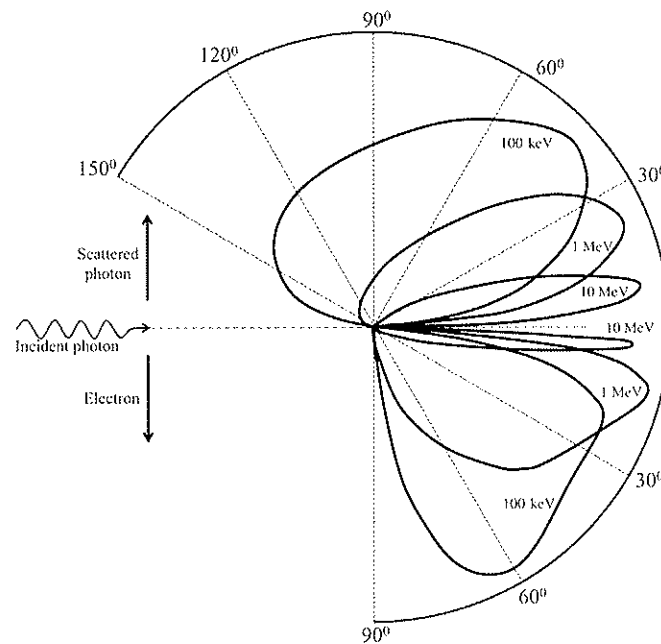
Figure 5.4. Differential cross sections per unit angle for Klein–Nishina scattering of photons for Compton electrons and scattered photons. Adapted from Hendee with permission.

cross sections per unit *angle* (not a solid angle as above). A plot of this differential cross section per angle would have the lines pushed to the origin at $\phi = 0$ and $\phi = 180$ because of the $\sin\phi$.

By integration over angles, the Klein–Nishina cross section per electron is the following:

$$_e\sigma = \int_0^\pi \frac{d_e\sigma}{d\Omega_\phi} \cdot \frac{d\Omega_\phi}{d\phi} d\phi = \int_0^\pi \frac{d_e\sigma}{d\Omega_\phi} \cdot 2\pi \sin\phi d\phi. \tag{5.9}$$

This gives us the cross section as follows:

$$_e\sigma = 2\pi r_0^2 \left\{ \left(\frac{1+\alpha_0}{\alpha_0^2} \right) \cdot \left(\frac{2(1+\alpha_0)}{1+2\alpha_0} - \frac{\ln(1+2\alpha_0)}{\alpha_0} \right) + \frac{\ln(1+2\alpha_0)}{2\alpha_0} - \frac{1+3\alpha_0}{(1+2\alpha_0)^2} \right\}. \tag{5.10}$$

Pay attention that for *low* incident photon energy limit, $_e\sigma$ is expanded in powers of relative energy:

$$_e\sigma = \frac{8\pi}{3} r_0^2 \left\{ 1 - 2\alpha_0 + 5.2\alpha_0^2 - 13.3\alpha_0^3 + ... \right\}. \tag{5.11}$$

Notice how this approaches the Thomson limit as $\alpha_0 \to 0$. The low-energy Thomson scattering limit is then the following:

$$\frac{d_e\sigma}{d\Omega_\phi} = \frac{r_0^2}{2} \left(1 + \cos^2\phi \right). \tag{5.12}$$

If one integrates this differential cross section, the answer would be as follows:

$$_e\sigma = \int_0^\pi \frac{d_e\sigma}{d\Omega_\phi} \cdot \frac{d\Omega_\phi}{d\phi} d\phi,$$

$$= \int_0^\pi \frac{d_e\sigma}{d\Omega_\phi} \cdot 2\pi \sin\phi d\phi, \tag{5.13}$$

$$= \frac{8\pi}{3} r_0^2 = 6.65 \times 10^{-25} (\text{cm}^2 / \text{electron}).$$

For *large* incident photon energy limit, $(\alpha_0 \gg 1)$, however, the cross section per electron is as follows:

$$_e\sigma \approx \frac{\pi}{2\alpha_0} r_0^2 \left[1 + 2 \cdot \ln(2\alpha_0) \right]. \tag{5.14}$$

It decreases with energy at high energies.

The mass attenuation coefficient for the Compton effect is $\frac{\sigma}{\rho} = {}_e\sigma \frac{N_A z}{A}$, and its units are cm^2/g.

Remember that the cross section per atom is related to the cross section per electron as $_a\sigma = {}_e\sigma \cdot z$.

Differential Cross Section Relative to Recoil Electron Energy

One can obtain the differential cross section relative to recoil electron energy by performing the chain rule as follows:

[See Jackson (1999) pages 694–7.

$$\frac{d_e\sigma}{dT_e} = \frac{d_e\sigma}{d\Omega_\phi} \cdot \frac{d\Omega_\phi}{d\phi} \cdot \frac{d\phi}{dT_e}.$$

(5.15)

Differentiating Equation (5.2) leads us to $\dfrac{d\phi}{dT_e}$ as the following:

$$\frac{d\phi}{dT_e} = \left\{ \frac{h\nu\alpha_0 \sin\phi}{[1 + \alpha_0(1 - \cos\phi)]^2} \right\}^{-1}.$$

(5.16)

Here, with $\dfrac{d\Omega_\phi}{d\phi} = 2\pi\sin\phi$ and the help of Equations (5.8) and (5.15), the differential cross section relative to recoil electron energy would be the following:

$$\frac{d_e\sigma}{dT_e} = \frac{\pi r_0^2}{\alpha_0 h\nu} \left(2 - \frac{2T_e}{\alpha_0(h\nu - T_e)} + \frac{T_e^2}{\alpha_0^2(h\nu - T_e)^2} + \frac{T_e^2}{h\nu(h\nu - T_e)} \right).$$

(5.17)

In pulse height spectra from NaI detectors, one often sees the **Compton edge**. It is caused by the $(h\nu - T_e)$ term. At low photon energies, $\dfrac{d_e\sigma}{dT_e}$ is proportional to $(h\nu)^{-2}$. Other than this, it is almost independent of T_e. The backscatter edge happens at the low end. It is often seen from backscatter out of shielding material stacked next to the detector. Figures 6.6 and 6.7 from Anderson (1984) show the Compton edge and the backscatter edge, respectively. Note that the Compton electron and its scattered photon must add to the original energy entering the interaction. Therefore, the Compton edge plus the backscatter peak equal the full energy peak in a detector spectrum.

Mass Energy Transfer Coefficient for the Compton Effect

Only the recoil electron kinetic energy will contribute significantly to the energy transfer. There will be some de-excitation with fluorescent x-rays and Auger electrons, but they contribute a relatively very small amount compared to the scattered photon and the recoil electron. The energy transfer cross section can be obtained from a differential distribution as follows:

$$_e\sigma_{tr} = \int_{T_e=0}^{T_{max}} \frac{d_e\sigma}{dT_e} \frac{T_e}{h\nu} dT_e.$$

(5.18)

So the mass energy transfer coefficient is related to the cross section as follows:

$$\frac{\sigma_{tr}}{\rho} = \frac{\bar{T}_e}{h\nu} \frac{\sigma}{\rho} = {}_e\sigma_{tr} \frac{N_A Z}{A}.$$

(5.19)

See Attix (2004) Appendix D.1 for $_e\sigma$ components. Figure 7.7 of Attix (2004), illustrates $\dfrac{\bar{T}_e}{h\nu}$ and $\dfrac{h\nu'}{h\nu}$ ratios. At low incident energies, (<1.0 MeV), most of the energy is given to the scattered photon, but at high energies, the recoil electron receives more kinetic energy. But note that this electron cannot ever receive all of it.

Therefore, the mass energy transfer coefficient is small at low energies. That is, $\frac{\sigma_{tr}}{\rho} < \frac{\sigma}{\rho}$. However, at high energies, the mass energy transfer coefficient is almost equal to mass attenuation coefficient ($\frac{\sigma_{tr}}{\rho} \cong \frac{\sigma}{\rho}$), but it can never be equal.

There is also a **mass scattering coefficient** with an analogous definition, but using the scattered photon energy as follows:

$$\frac{\sigma_s}{\rho} = \frac{hv'}{hv} \cdot \frac{\sigma}{\rho}. \tag{5.20}$$

So, we can have the following expression:

$$\frac{\sigma}{\rho} = \frac{\sigma_{tr}}{\rho} + \frac{\sigma_s}{\rho}. \tag{5.21}$$

Note that we have excluded the binding energy for this interaction and assumed that the electron was free. In reality, there is a small correction that you should be aware of.

Binding Energy Correction for the Klein–Nishina Cross Section

At low incident photon energies and in high-z materials, one should correct for the fact that electrons are bound. The correction is mostly not very significant since these regimes are where the photoelectric effect dominates.

We need to multiply the Klein–Nishina differential cross sections by the **form factor function**. It is a function of atomic number and energy:

$$\frac{d_a\sigma}{d\Omega_\phi} = F(T_e, z)\frac{d_a\sigma_{K-N}}{d\Omega_\phi}, \tag{5.22}$$

where,

$$\frac{d_a\sigma_{K-N}}{d\Omega_\phi} = z \cdot \frac{d_e\sigma_{K-N}}{d\Omega_\phi}. \tag{5.23}$$

The scattering coefficient for carbon at 10 keV is plotted in Johns and Cunningham (1983) page 183, Figure 6.6.

The Compton effect has clinical relevance. The scattered photon is the main health physics (shielding) concern. At intermediate energies, it is independent of z. Therefore, the contrast for imaging can be bad, but the tomotherapy machine uses megavoltage computed tomography (MVCT) to avoid metal artifacts. Also, scattered photons degrade images for nuclear medicine imaging.

References

Anderson, D.W. *Absorption of Ionizing Radiation*. Baltimore: University Park Press, 1984.
Attix, F.H. *Introduction to Radiological Physics and Radiation Dosimetry*. Weinheim, Germany: WILEY-VCH Verlag GmbH & Co. KGaA, 2004.
Evans, R.D. *The Atomic Nucleus*. Malabar, Florida: Krieger Publishing Co., 1955.
Hendee, W.R. *Medical Radiation Physics*. Chicago: Year Book Medical Publishers, Inc., 1970.
Jackson, J.D. *Classical Electrodynamics*, 3rd Ed. New York: Wiley, 1999.
Johns, H.E. and J.R. Cunningham. *The Physics of Radiology*, 4th Ed. Springfield, IL: Thomas, 1983.
Klein, O. and T. Nishina. (1929). "Über die Streuung von Strahlung durch freie Elektronen nach der neuen relativistischen Quantendynamik von Dirac." *Zeitschrift für Physik* 52:853–68.

6

Pair (and Triplet) Production Effect

In both pair and triplet production, an electron (or "negatron") and a positron (anti-electron) are produced spontaneously as a photon interacts with a strong electric field from either a nucleus (pair production) or an electron (triplet production). These interactions are dominant at high incident photon energy ($hv \gg m_0 c^2$). The geometry of pair production and triplet production are illustrated respectively in Figures 6.1 and 6.4.

After some math, the threshold energy for these effects to take place is the following:

$$(hv)_{min} = 2m_0 c^2 \left(1 + \frac{2m_0 c^2}{2Mc^2} \right), \tag{6.1}$$

where, m_0 is the rest mass of an electron. For pair production, $M = M_{nucleus} \gg m_0$, and for triplet production, $M = m_0$.

Assuming that the recoil of the nucleus is small, the available kinetic energy for both pair and triplet production is simply as follows:

$$T_{avail} = hv - (hv)_{min}^{pair} = hv - 2m_0 c^2. \tag{6.2}$$

Notice that for both pair and triplet production, the available kinetic energy is the same, even though the threshold differs. For pair production, the threshold energy is $2m_0 c^2 = 1.022$ MeV, and this is used for both pair and triplet available kinetic energy in Equation (6.2).
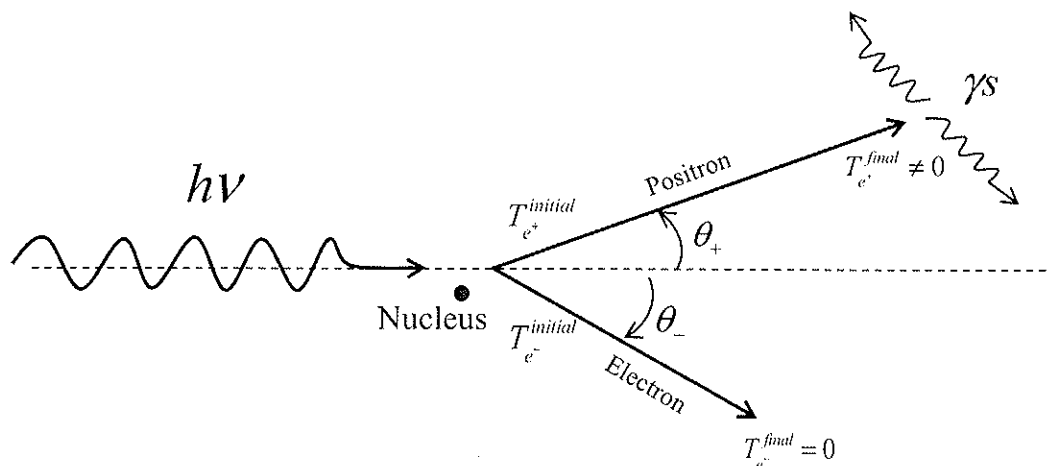

Figure 6.1. The geometry of pair production with annihilation in flight indicated.

Pair Production

In pair production effect (Figure 6.1), the mean kinetic energy given to each of the two particles is half of the available kinetic energy[*].

$$\overline{T}_{e^{\pm}} = \frac{T_{avail}}{2}.$$

(6.3)

The mean angle given to each of the two particles with respect to the incident photon direction is as follows:

$$\overline{\theta}_{\pm} = \frac{m_0 c^2}{\overline{T}_{e^{\pm}}}.$$

(6.4)

The unit of the $\overline{\theta}_{\pm}$ is radians. Note that $1/T$ dependence is similar to bremsstrahlung (and that's not all, as we will see). Higher-energy particles get more forward-directed.

Cross Section for Pair Production

Bethe and Heitler (1934) derived the atomic differential cross section for pair production as follows:

$$\frac{d_a \kappa_{pair}}{d\overline{T}_{e^{\pm}}} = \sigma_0 \frac{z^2}{T_{avail}} P.$$

(6.5)

where, the quantity σ_0 is defined as follows:

$$\sigma_0 = \frac{r_0^2}{137} = 4.80 \times 10^{-28} \ (\text{cm}^2 / \text{atom}).$$

(6.6)

Remember that $\left(\frac{1}{137}\right) = \alpha$ is the fine structure constant. The quantity r_0 is the classical electron radius, and it also represents the range of the strong nuclear force.

$$r_0 = \frac{e^2}{m_0 c^2} = 2.8179 \times 10^{-15} \, \text{m}.$$

(6.7)

Notice that in Equation (6.5) all of the complications are in P. It is a function of photon energy and almost independent of atomic number, z (see Figure 7.18 of Attix).

The cross section is then obtained by integrating the differential cross section as follows:

$$_a \kappa_{pair} = \sigma_0 z^2 \int_{T_{e^{\pm}}=0}^{T_{avail}} \frac{P}{T_{avail}} d(T_{e^{\pm}}) = \sigma_0 z^2 \int_0^1 P d(T_{e^{\pm}} / T_{avail}),$$

(6.8)

Here, $\int_0^1 d(T_{e^{\pm}} / T_{avail}) = 1$, and using Equation (6.9) to define an average P, ($\overline{P}$):

$$\overline{P} = \int_0^1 P d(T_{e^{\pm}} / T_{avail}) \bigg/ \int_0^1 d(T_{e^{\pm}} / T_{avail}),$$

(6.9)

---

[*]Actually, the positron gets a bit more energy because of the push from the positively charged nucleus.

the cross section for pair production is given by the following:

$$_a\kappa_{pair} = \sigma_0 z^2 \overline{P}.$$ (6.10)

This $\overline{P}$ also has little z dependence.

If the interaction is too far from the nucleus, then many orbital electrons will screen the nuclear electric field. When screening can be neglected, $(2m_0c^2 << h\nu << 137m_0c^2z^{-1/3})$, there is no z dependence and just a weak logarithmic dependence on energy:

$$\overline{P} \approx \frac{28}{9} \ln \frac{2h\nu}{m_0c^2} - \frac{218}{27}.$$ (6.11)

When screening is maximized at high energy, $(h\nu >> 137m_0c^2z^{-1/3})$, there is a weak logarithmic z dependence and basically no energy dependence:

$$\overline{P} \approx \frac{28}{9} \ln(183z^{-1/3}) - \frac{2}{27}.$$ (6.12)

At energies around m_0c^2, no analytical form is possible. We can use the approximation that $_a\kappa_{pair}$ is proportional to z^2 for all photon energies.

The pair production mass attenuation coefficient is related to the cross section as follows:

$$\frac{\kappa}{\rho} = {}_a\kappa \frac{N_A}{A},$$ (6.13)

and its units are cm²/g.

The Similarity between Pair Production and Bremsstrahlung

There is a concept about anti-particles proposed by Paul Dirac in 1930 that says the negative energy root from $E^2 = (pc)^2 + (m_0c^2)^2$ is an anti-particle. This came out of the Schrödinger equation with some relativity.

A photon with enough energy, and an electric field to exchange momentum with, can liberate something out of the infinite sea of negative energy (the "Dirac sea," completely filled and occupied states = vacuum), and the hole left behind is the anti-matter (Figure 6.2).
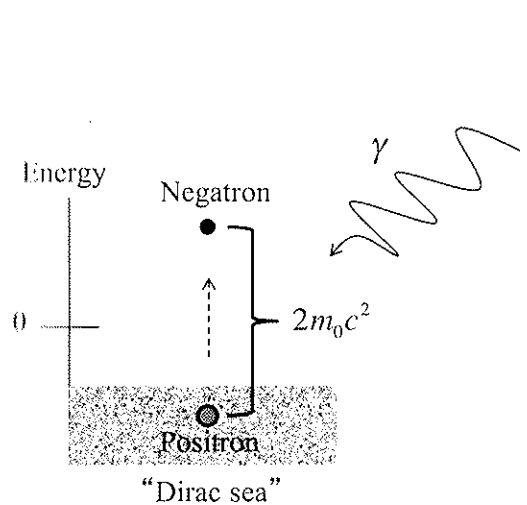
Figure 6.2. The Dirac conception of pair production.
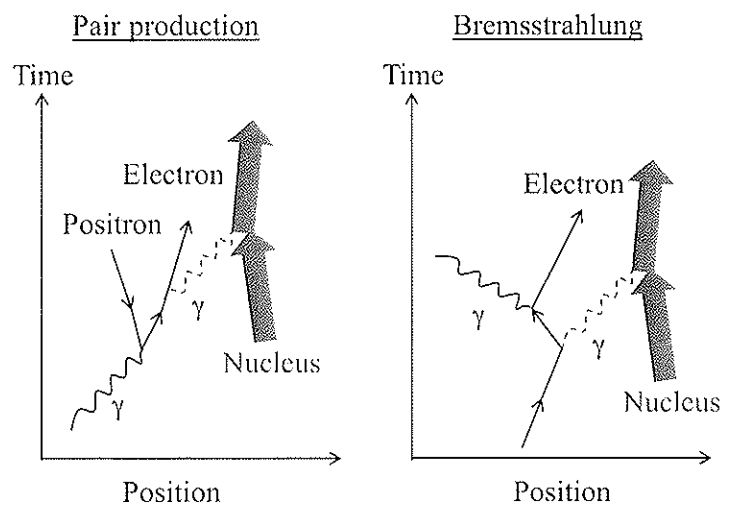
Figure 6.3. Feynman diagram similarities between bremsstrahlung and pair production.

Another mathematical oddity is that one can perhaps view the positron as moving backwards in time. This is used in Feynman diagrams, where the similarity between bremsstrahlung and pair production is profoundly obvious (see Figure 6.3).

The cross sections (cm²/atom) of pair production and bremsstrahlung are *very* similar. For pair production at very high energies and bremsstrahlung (radiative losses), the cross sections are respectively as the following:

$$_a\kappa_{pair} = \frac{r_0^2}{137}z^2\left(\frac{28}{9}\ln(183z^{-1/3}) - \frac{2}{27}\right).$$

(6.14)

$$\sigma_\gamma = \frac{r_0^2}{137}z^2\left(\frac{36}{9}\ln(183z^{-1/3}) - \frac{4}{18}\right).$$

(6.15)

Therefore,

$$_a\kappa_{pair} \approx \frac{7}{9}\sigma_\gamma.$$

(6.16)

Triplet Production

The electric field is now from an electron, a very light particle that becomes indistinguishable from the created particle. Therefore, triplet production (Figure 6.4) happens instead of pair production.

The mean kinetic energy given to each of the three particles is a third of the available kinetic energy[†]:

$$\bar{T}_{e^-} = \frac{T_{avail}}{3}.$$

(6.17)

Of course, since $M = m_0$ in Equation (6.1), the threshold is now $4m_0c^2$. It is all due to momentum conservation.
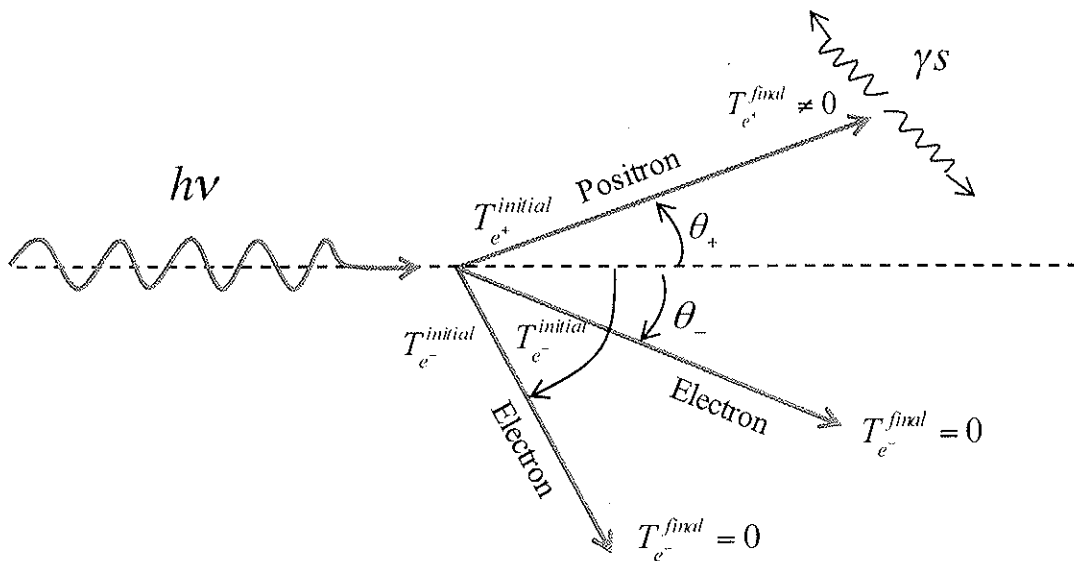
Figure 6.4. The geometry of triplet production with a positron annihilation in flight.

[†]Actually, the positron still gets a bit more energy because of the push from the positively charged nucleus that most available electrons are finding themselves near.

The Triplet Production Cross Section

The triplet production cross section is combined with the pair production cross section by using a factor C to relate the triplet cross section to the pair production cross section because of electron exchange effects:

$$_a K_{triplet} = \frac{_a K_{pair}}{Cz} = \sigma_0 \frac{z\bar{P}}{C}. \tag{6.18}$$

where $C = 1.6 \pm 0.2$ for $(5 \text{ MeV} < hv < 20 \text{ MeV})$, and $C = 1.1 \pm 0.1$ for $(20 \text{ MeV} < hv < 100 \text{ MeV})$.

C has a negligible dependence on z, but notice the additional factor of z for triplet production. There are z targets per atom for triplet production, but only one target per atom for pair production.

The combined triplet and pair cross section and mass attenuation coefficient are as follows:

$$_a K = {_a K_{pair}} + {_a K_{triplet}} = \sigma_0 z \bar{P}(z + 1/C), \tag{6.19}$$

$$\frac{K}{\rho} = \left(\frac{N_A}{A}\right) \sigma_0 z \bar{P}(z + 1/C), \tag{6.20}$$

$$\frac{K_{tr}}{\rho} = \frac{K}{\rho} \cdot \frac{T_{avail}}{hv} = \frac{K}{\rho}\left(\frac{hv - 2m_0 c^2}{hv}\right). \tag{6.21}$$

The fraction of photon energy transferred to charged particles is T_{avail}/hv. Therefore, the combined triplet and pair mass energy transfer coefficient is given by the following:

$$\frac{K_{tr}}{\rho} = \frac{K}{\rho} \cdot \frac{T_{avail}}{hv} = \frac{K}{\rho}\left(\frac{hv - 2m_0 c^2}{hv}\right). \tag{6.22}$$

Notice that the $2m_0 c^2$ is for both pair and triplet production. Triplet has an extra momentum issue, but still just creating two particles. This is shared between either two or three particles.

Note that right near the threshold, the amount of energy transferred is small, but this cross section approaches the attenuation cross section at large energies.

Positron Annihilation in Flight

When the positron meets an electron, two gamma photons are released in opposite directions in the center-of-mass (or "center-of-momentum") frame. Therefore, an isotropic angular distribution in this frame will happen. Both photons have the same polarization, either both are right hand circular (RHC) or both are left hand circular (LHC) (Figure 6.5).
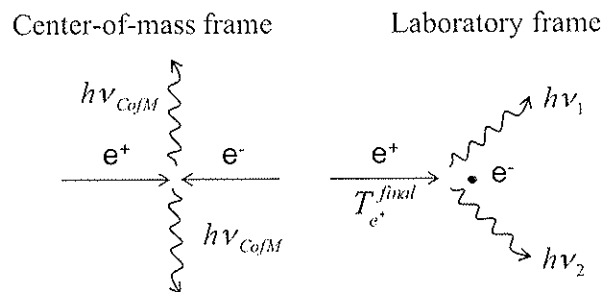
Figure 6.5. Two frames of reference for positron annihilation in flight.

$$h\nu_1 = 0.511\,\text{MeV}$$

$$T_{e^-}^{final} = 0 \quad \text{e}^{+/-}$$

$$h\nu_2 = 0.511\,\text{MeV}$$
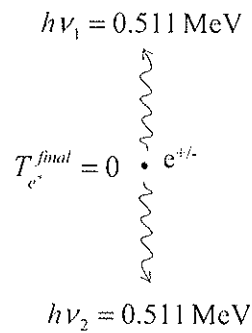
Figure 6.6. "Positronium."

The annihilation gammas in the lab frame will have a sum of energies as follows:

$$h\nu_1 + h\nu_2 = T_{e^-}^{final} + 2m_0c^2. \tag{6.23}$$

We will need to include the lost charged particle (positron) kinetic energy in the calculation of μ_{en} for this interaction. The mass annihilation coefficient was derived by Heitler as the following:

$$\frac{\sigma_{annihil}}{\rho} = \frac{N_A z}{A} \cdot \frac{\pi r_0^2}{(\gamma+1)}\left[\left(\frac{\gamma^2+4\gamma+1}{\gamma^2-1}\right)\ln\left(\gamma+\sqrt{\gamma^2-1}\right) - \frac{\gamma+3}{\sqrt{\gamma^2-1}}\right], \tag{6.24}$$

where:

$$\gamma = \frac{T_{e^-}^{final}}{m_0c^2} + 1 = \frac{1}{\sqrt{1-(v/c)^2}}. \tag{6.25}$$

Note that $\dfrac{\sigma_{annihil}}{\rho} \propto \dfrac{(z/A)}{T_{e^-}^{final}}$ for $T_{e^-}^{final} \gg m_0c^2$, so annihilation is much more likely at low energies.

"Positronium" (Figure 6.6) is the whimsical name given to the temporary positron-electron thing that exists for a short time when both have basically no kinetic energy—then they give off two identical, opposite gammas of 0.511 gammas in either frame.

References

Attix, F.H. *Introduction to Radiological Physics and Radiation Dosimetry.* Weinheim, Germany: WILEY-VCH Verlag GmbH & Co. KGaA, 2004.
Bethe, H. and W. Heitler. (1934). "On the Stopping of Fast Particles and on the Creation of Positive Electrons." *Proc. Roy. Soc. Lond.* A146:83–112.

7

Other Photon Interactions and Summary

Rayleigh (Coherent) Scattering

There are two kinds of *elastic* scattering for photons: Thomson scattering and Rayleigh scattering. While Thomson scattering is the scattering of photons by *free* electrons, in Rayleigh scattering, photons are scattered by whole atom. That is why it is called *coherent* scattering[†].

Rayleigh scattering occurs at low energies and can be 20% of the scattering for diagnostic energies. It's a significant issue for x-ray imaging. It is sometimes included with the Compton attenuation or scattering cross section. The scattering angle becomes more forwardly peaked as energy gets larger and z gets smaller.

We will not say much about Rayleigh scattering since it transfers absolutely zero energy. Therefore, energy transfer and absorption coefficients are both zero for Rayleigh scattering. For $2 < n < 2.5$, the attenuation cross section for Rayleigh scattering at x-ray energies is as follows:

$$_a\sigma_R \propto \frac{z^n}{(hv)^n}.$$

(7.1)

Photonuclear Interactions

Photonuclear interactions occur at high energies ($hv >> m_0c^2$). Typically a single nucleon is ejected, but multiple nucleons or alphas are also possible: (γ,n), (γ,p), (γ,α), $(\gamma,2n)$, $(\gamma,2p)$, (γ,np), etc. (Figure 7.1)
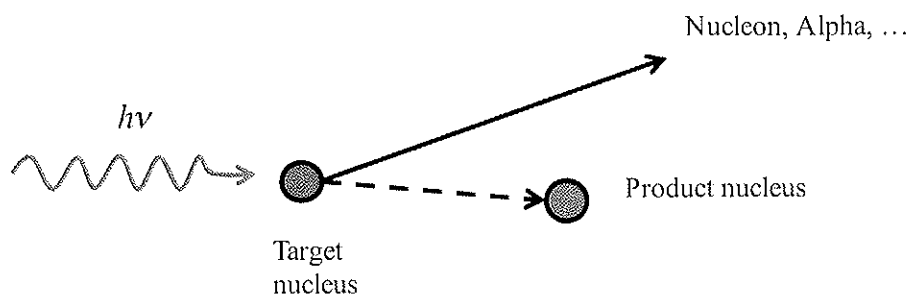

Figure 7.1. The geometry of photonuclear interactions.

[†] It is called "Bragg scattering" if it scatters off of a whole crystal plane.

The nucleus is usually left in an excited state and often de-excites with a γ-ray, etc. The threshold energy for the interaction—the smallest interaction threshold dominates—is the following:

$$(h\nu)_{min} = -BE\left(1 - \frac{BE}{2Mc^2}\right), \tag{7.2}$$

where BE is the energy of the binding of nucleon in the nucleus[†], and Mc^2 is the rest mass of the target nucleus. Energy balance for this interaction is given by the following:

$$BE = E^* + \sum Q. \tag{7.3}$$

Here, E^* is the excitation energy of the product nucleus and $\sum Q$ is the net energy derived from rest mass. $\sum Q$ is calculated as follows:

$$\sum Q = \Delta E_{target\ nucleus} - \left(\Delta E_{product\ nucleus} + \Delta E_{nucleon}\right). \tag{7.4}$$

The quantity $\sum Q$ is positive if mass is converted to energy, and it is negative if energy is converted to mass. Note that $\left|\sum Q\right| > E^*$ is required so that $BE < 0$.

The quantity ΔE is the "mass excess" of the indicated particle. The nuclear mass excess is the difference between the rest mass of a nucleus from 1/12th the mass of ^{12}C:

$$\Delta E = Mc^2 - \frac{A \cdot M_{^{12}_6C}}{12}c^2, \tag{7.5}$$

where A is the mass number (the sum of protons and neutrons) and, thus, an integer. Note that $\Delta E_{^{12}_6C} = 0$ for ^{12}C. For atomic mass numbers, refer to Anderson (1984), appendix 5, atomic mass tables.

Example Problem: In the following, assume that the product nucleus is not excited—that it goes directly to the ground state so that $E^*_{^{15}_8O} = 0$.

$$^{16}_8O \rightarrow\ ^{15}_8O + n \quad \Leftrightarrow \quad ^{16}_8O(\gamma,n)^{15}_8O.$$
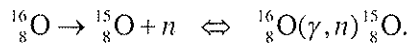
Using the atomic mass tables, find $\Delta E_{target\ nucleus}$, $\Delta E_{product\ nucleus}$, and $\Delta E_{nucleon}$.

Solution: We can get ΔEs for Equation (7.4) from tables as follows:

$\Delta E_{target\ nucleus} = \Delta E_{^{16}_8O} = -4736.6$ keV.

$\Delta E_{product\ nucleus} = \Delta E_{^{15}_8O} = 2859.9$ keV.

$\Delta E_{nucleon} = \Delta E_n = 8071.4$ keV.

Notice that sign is important. Therefore, the binding energy is calculated as follows:

$BE = (-4736.6\ keV) - [(2859.9\ keV) + (8071.4\ keV)] = -15.7$ MeV.

Since $-BE \ll 2(M_{^{16}_8O})$, the threshold for $^{16}_8O(\gamma,n)^{15}_8O$ is as follows:

$$(h\nu)_{min} = -BE\left(1 - \frac{BE}{2Mc^2}\right) \cong -BE = 15.7\ MeV.$$

[†] It is negative for bound state.

Any energy above the threshold is often given to just the kinetic energy of the nucleon released. The nucleon may not be a charged particle, and there may be other neutral particles, like gammas, because of the mass difference from the nucleus.

$$T_{nucleon} = h\nu - (h\nu)_{min}.$$

(7.6)

The reaction (γ,n) contributes only a negligible amount of energy to the recoil energy of the nucleus. However, (γ,p), for example, can contribute significant amounts of charged particle kinetic energy.

The reaction (γ,n) is a potential hazard for the use of high-energy linacs for radiotherapy, and extra neutron shielding is required. This would involve low-z materials, as we will see later.

Relative Importance of Each Interaction Type

Figure 7.2 is illustrated cross sections for each of the three main interaction types for x-rays or γ-rays. The main independent variables are incident photon energy and target atomic number.

In general, we can summarize volcano's plot as follows: the photoelectric effect dominates at low energy, the Compton effect dominates at intermediate energies, and pair production is dominant at high energies. Also note that the "volcano" gets wider for low-z materials. Figure 7.3 demonstrates mass attenuation coefficients for photons in air[‡].

Total Cross Sections (or Coefficients)

Altogether, the *total mass attenuation coefficient* is found as follows:

$$\frac{\mu}{\rho} = \frac{\tau}{\rho} + \frac{\sigma}{\rho} + \frac{\kappa}{\rho} \quad + \quad \frac{\sigma_R}{\rho} \quad + \quad \frac{\sigma_{(\gamma,n)}}{\rho} + \frac{\sigma_{(\gamma,p)}}{\rho} + \dots .$$

(7.7)
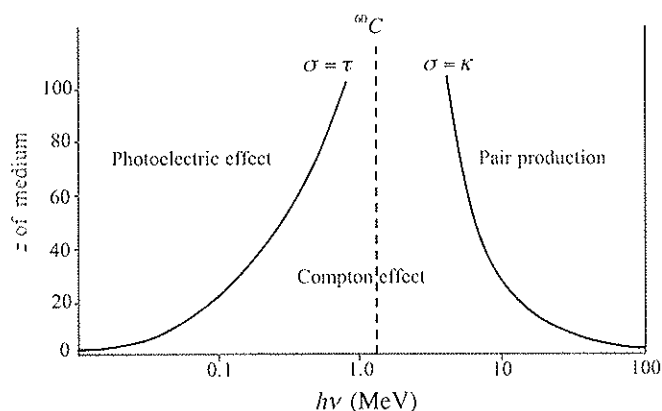
Figure 7.2. "Volcano plot" of cross sections for each of the three main interaction types for photons showing where they dominate. Note that ^{60}C is exactly at the middle of the plot.
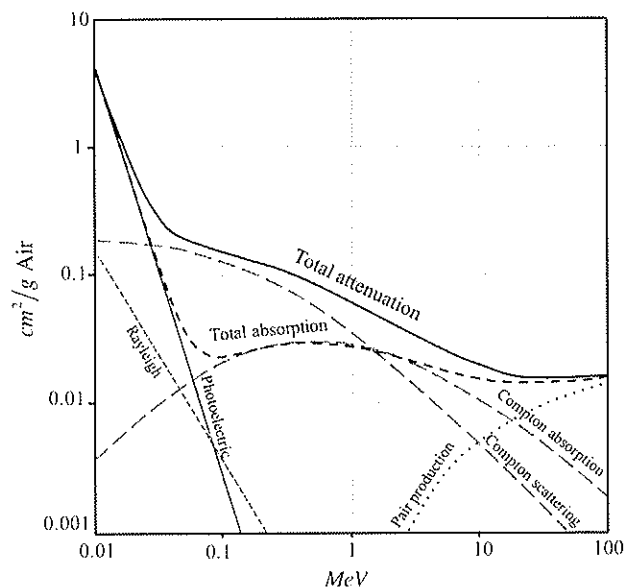
Figure 7.3. Attenuation in air showing its various components. Note the log-log scale. From Evans (1955) with permission.

[‡] For a series of mass attenuation and energy transfer coefficients plots for some common materials, see Evans (1955), pages 713–17.

The *mass energy transfer coefficient* is calculated by the following:

$$
\begin{aligned}
\frac{\mu_{tr}}{\rho} &= \frac{\tau_{tr}}{\rho} + \frac{\sigma_{tr}}{\rho} + \frac{\kappa_{tr}}{\rho} \quad + \quad \frac{\sigma_{(\gamma,p)}}{\rho} + \dots \\[2mm]
&= \frac{\tau}{\rho}\left(\frac{h\nu - P_K \cdot Y_K \cdot (h\bar{\nu})_K - (1 - P_K) \cdot P_L \cdot Y_L \cdot (h\bar{\nu})_L}{h\nu} \right) + \\[2mm]
&\quad \frac{\sigma}{\rho}\left(\frac{\bar{T}_c}{h\nu} \right) + \\[2mm]
&\quad \frac{\kappa}{\rho}\left(\frac{h\nu - 2m_0 c^2}{h\nu} \right) + \\[2mm]
&\quad \frac{\sigma_{(\gamma,p)}}{\rho}\left(\frac{\bar{T}_p}{h\nu} \right) + \text{other photonuclear terms possible} \dots .
\end{aligned}
\tag{7.8}
$$

And the *mass energy absorption coefficient* is found as follows:

$$
\frac{\mu_{en}}{\rho} = (1 - g)\frac{\mu_{tr}}{\rho}.
\tag{7.9}
$$

Cross Sections for Compounds and Mixtures

Bragg's rule states that atoms contribute independently to photon attenuation, and molecular or crystalline structures/states are not important[†]. For calculating mass attenuation coefficient and mass energy transfer coefficient, simply add each element or isotope together with respect to its mass fraction.

$$
\left(\frac{\mu}{\rho} \right)_{mix} = \left(\frac{\mu}{\rho} \right)_A f_A + \left(\frac{\mu}{\rho} \right)_B f_B + \left(\frac{\mu}{\rho} \right)_C f_C + \dots
\tag{7.10}
$$

$$
\left(\frac{\mu_{tr}}{\rho} \right)_{mix} = \left(\frac{\mu_{tr}}{\rho} \right)_A f_A + \left(\frac{\mu_{tr}}{\rho} \right)_B f_B + \left(\frac{\mu_{tr}}{\rho} \right)_C f_C + \dots .
\tag{7.11}
$$

where, f_A, f_B, and f_C are mass fractions for components A, B, and C, respectively. For mass energy absorption, however, it is a little different, with $g_{A\,or\,B\,or\,C,\,etc.}$ as the individual fractions for radiative losses.

$$
\left(\frac{\mu_{en}}{\rho} \right)_{mix} = \left(\frac{\mu_{tr}}{\rho} \right)_{mix} (1 - f_A g_A - f_B g_B - f_C g_C - \dots).
\tag{7.12}
$$

By defining $g_{mix} \equiv f_A g_A + f_B g_B + f_C g_C + \dots$, we can now write the mass energy absorption as follows:
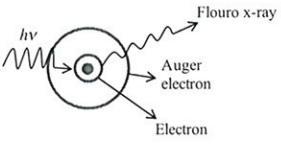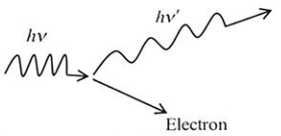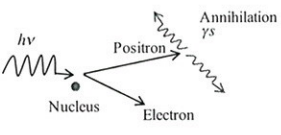
$$
\left(\frac{\mu_{en}}{\rho} \right)_{mix} = \left(\frac{\mu_{tr}}{\rho} \right)_{mix} (1 - g_{mix}).
\tag{7.13}
$$

Figures 7.4 and 7.5 below summarize all important interactions for dosimetry: the photoelectric effect, Compton effect, and pair and triplet production.

[†]The rule breaks down at very low energies (UV, for example).

References

Anderson, D.W. *Absorption of Ionizing Radiation*. Baltimore: University Park Press, 1984.

Attix, F.H. *Introduction to Radiological Physics and Radiation Dosimetry*. Weinheim, Germany: WILEY-VCH Verlag GmbH & Co. KGaA, 2004.

Evans, R.D. *The Atomic Nucleus*. Malabar, Florida: Krieger Publishing Co., 1955.

Process	Target	Secondary Particle	Diagram	Energy range it dominates (Water)	Energy range it dominates (Bone)
Photoelectric	Bound electron In atom	Electron (Fluorescent x-ray, Auger electron important here)		$h\nu < 30 keV$	$h\nu < 50 keV$
Compton	Electron	Electron Scattered photon, Fluoro, Auger energy is small		$30 keV < h\nu < 30 MeV$	$50 keV < h\nu < 25 MeV$
Pair Production	Nucleus	Electron Positron Annihilation		$h\nu > 30 MeV$	$h\nu > 25 MeV$

Process	Energy transferred to charges (sometimes Auger emitted, too)	Z dependency of attenuation coefficient	Energy dependency of attenuation coefficient
Photoelectric	$T_{e^-} = h\nu - E_b$ Any/all electron kinetic energy. Auger important.	$\dfrac{\tau}{\rho} \sim z^4 \;\; (h\nu < 100 keV)$	$\dfrac{\tau}{\rho} \sim (h\nu)^{-3}$ But max just over E_b
Compton	<u>Complex</u>: electron energy gets increasing fraction with increase and scattered photon angle increase.	$\dfrac{\sigma}{\rho} \sim z^0$	$\dfrac{\sigma}{\rho} \downarrow$ when $h\nu \uparrow$
Pair Production	$T_{e^-} + T_{e^+} = h\nu - 1.022\,MeV$	$\dfrac{\kappa}{\rho} \sim z^2$	$\dfrac{\kappa}{\rho} \uparrow$ when $h\nu \uparrow$ Threshold of $1.022\,MeV$

		General	Photoelectric	Compton	Pair Production+ Triplet Production
Terma		$T = \dfrac{\mu}{\rho}\Psi$ $= (_a\sigma N_A/A)\cdot\Psi$			
	Mass Attenuation Coefficient	$\dfrac{\mu}{\rho} = \dfrac{_a\sigma N_A}{A}$	$\dfrac{\tau}{\rho} = {_a\tau}\dfrac{N_A}{A}$	$\dfrac{\sigma}{\rho} = {_e\sigma}\dfrac{N_A Z}{A}$ $\dfrac{\sigma}{\rho} = \dfrac{\sigma_{tr}}{\rho} + \dfrac{\sigma_s}{\rho}$	$\dfrac{\kappa}{\rho} = \left(\dfrac{N_A}{A}\right)\sigma_0 z\bar{P}(z+1/C)$
Kerma		$K = \dfrac{\mu_{tr}}{\rho}\Psi$ $= (\bar{T}/h\nu)\cdot T$			
	Mass Energy Transfer	$\dfrac{\mu_{tr}}{\rho} = \dfrac{\bar{T}}{h\nu}\cdot\dfrac{\mu}{\rho}$ Or: $\dfrac{\mu_{tr}}{\mu} = \dfrac{\bar{T}}{h\nu}$ Where: $\bar{T} = (1/n)\sum_{i=1}^{n}(\varepsilon_{tr})_i$	Above K-edge: $\dfrac{\tau_{tr}}{\rho} =$ $\dfrac{\tau}{\rho}\left(\dfrac{h\nu - P_K\cdot Y_K\cdot(h\bar\nu)_K - (1-P_K)\cdot P_L\cdot Y_L\cdot(h\bar\nu)_L}{h\nu}\right)$ Below K-edge: $\dfrac{\tau_{tr}}{\rho} =$ $\dfrac{\tau}{\rho}\left(\dfrac{h\nu - P_L\cdot Y_L\cdot(h\bar\nu)_L}{h\nu}\right)$	$\dfrac{\sigma_{tr}}{\rho} = \dfrac{\bar{T}}{h\nu}\dfrac{\sigma}{\rho}$	$\dfrac{\kappa_{tr}}{\rho} = \dfrac{\kappa}{\rho}\left(\dfrac{h\nu - 2m_0c^2}{h\nu}\right)$ With condition that: $(h\nu)_{min} = 2m_0c^2\left(1+\dfrac{2m_0c^2}{2Mc^2}\right)$
Collision Kerma		$K_c = \dfrac{\mu_{en}}{\rho}\Psi$ $= (1-g)\cdot K$			
	Mass Energy Absorption	$\dfrac{\mu_{en}}{\rho} = (1-g)\dfrac{\mu_{tr}}{\rho}$ Where: $(1-g) = \dfrac{(1/n)\sum_{i=1}^{n}(\varepsilon_{tr}^{net})_i}{(1/n)\sum_{i=1}^{n}(\varepsilon_{tr})_i}$	$\dfrac{\tau_{en}}{\rho} \approx \dfrac{\tau_{tr}}{\rho}$	$\dfrac{\sigma_{en}}{\rho} = (1-g)\cdot\dfrac{\sigma_{tr}}{\rho}$	$\dfrac{\kappa_{en}}{\rho} = (1-g)\cdot\dfrac{\kappa_{tr}}{\rho}$
Dose		$D = \dfrac{\Delta\bar\varepsilon}{(\Delta m = \rho\Delta V)}$			

Figure 7.5. Summary of the dose-related quantities for the main photon interactions. Note that σ is not in the same units as $_a\sigma$ and $_e\sigma$.

8

Charged Particle Interactions with Matter

The photon interactions transfer energy to electrons, and it is these electrons that deliver dose as they slow down in matter. To understand the basic physics involved, we will start with an important derivation for heavy charged particles that will then be generalized to eventually work for electrons slowing down in condensed matter. It is in fact remarkable that this extension to electrons works as well as it does.

Interactions of Heavy Charged Particles

In Figure 8.1, let's consider a heavy charged particle with kinetic energy, T, and velocity, v, going very quickly by an atom with an impact parameter, b. Here we use simple description of the nucleus, which is the "liquid drop model." From this model, we get the nuclear radius is $R_{nuc} \approx 1.4 \times 10^{-13} A^{1/3} \text{cm}$ where A is the mass number[*]. The radius of the atom is about $a \approx 0.18\beta\lambda$ from Bohr's theory, where λ is the wavelength of the electron in an outer shell and $\beta = v/c$ is the particle speed compared to the speed of light. The radius of the atom is much larger than the nuclear radius. It is like a baseball (nucleus) in Camp Randall stadium (atom). Note that there is a velocity dependence to all of this, and this is just order of magnitude validity anyway.
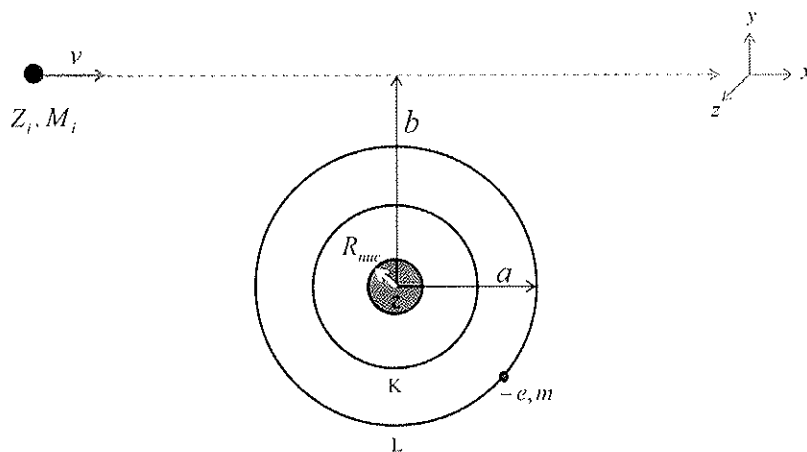

Figure 8.1. Geometry of a heavy charged particle interacting with a single atom. Note: this figure is not to scale.

---

[*]Mass number variable, A, here is the number of protons plus the number of neutrons, and it is an integer for just this discussion.

The "heavy and fast" particle at the base of the arrow in Figure 8.1 has a charge, Z_i, and a mass, M_i, and a significant energy, $\gamma M_i c^2$, such that $\gamma = 1 / \sqrt{1 - v^2 / c^2} \gg 1$. Notice that "fast" here means Born approximation[‡]. The atomic bound electron, on the other hand, has only a charge, $-e$, a mass, m, and bound energy such that kinetic energy, T, roughly equals its potential energy. In other words: $mv^2 / 2 \sim e^2 / a_0$ where $a_0 \approx \hbar^2 / me^2$, which gives $v^2 / c^2 \sim e^4 / \hbar^2 c^2 \sim (1 / 137)^2$, the fine structure constant, α squared. Therefore, the incident particle needs to have more kinetic energy than this ($T > mc^2 \alpha^2$). This implies that only about 53 keV is needed for the incident particle in this treatment. Other generalizations beyond these assumptions will also be possible[§].

In general we will be categorizing reactions according to impact parameter[§] b:

1. **Soft collisions ($b \gg a$)**: Continuous energy loss with many atoms at once—interactions with orbiting electrons. Soft collisions lead to excitations. Soft collisions are about half of what is happening.

2. **Hard collisions ($b \approx a$)**: Hard collisions are also near half of the interactions, but large events that can lead to the liberation of other charges with their own trajectories are more rare. We will need to carefully account for this. The liberated secondary charges are outer-shell-orbiting electrons. Hard collisions give ionizations with resulting excitations.

3. **Nuclear electric field interactions ($b \approx R_{nuc}$)**: This results in *elastic* collisions (mostly) and bremsstrahlung (only 2–3% for radiation therapy energies). Note that only light particles, like electrons, will show any significant bremsstrahlung.

4. **Nuclear interactions ($b < R_{nuc}$)**: Nuclear reactions will only occur here.

Stopping Power and Mass Stopping Power

One of the most important concepts in the physics of dosimetry is **stopping power**, $\dfrac{dT}{dx}$. Stopping power is defined as the rate of energy loss for distance traveled into the medium. The mass stopping power, $\dfrac{dT}{\rho dx}$, is then obtained by dividing stopping power by the density of the material. Mass stopping power is usually divided into two terms: one for (soft and hard) collisional energy losses and the other for radiative (bremsstrahlung) energy losses as follows:

$$\frac{dT}{\rho dx} = \left(\frac{dT}{\rho dx} \right)_c + \left(\frac{dT}{\rho dx} \right)_r . \tag{8.1}$$

The units of stopping power and mass stopping power are MeV/cm and MeV/(g/cm²), respectively.

Radiative stopping power is the production of bremsstrahlung. Heavy charged particles do not produce much bremsstrahlung: i.e., a proton is ~2000 times heavier than an electron and, therefore, 4×10^6 times less bremsstrahlung is produced. Thus, if M is much heavier than an electron, then we will assume radiative loss is negligible:

$$\left(\frac{dT}{\rho dx} \right)_r \sim \frac{1}{(Mc^2)^2} \approx 0. \tag{8.2}$$

However, for electrons and positrons, this radiative term will not be negligible. Later in this chapter, we will discuss the mass stopping power for electrons and positrons.

[‡] For more discussion about the Born approximation, visit Evans (1955), page 887.
[§] Note we are using slightly different notations: T and m and z versus Z.
[§] Note that this categorization is general and not just for heavy charged particles.

Collisional Mass Stopping Power for Heavy Charged Particles

Returning to Figure 8.1, consider the momentum impulse as we integrate in time the rate of momentum change (Gaussian units here):

$$\vec{F} = \frac{d\vec{P}}{dt} = -e\left(\vec{E} + \frac{1}{c}\vec{v} \times \vec{B} \right).$$

(8.3)

However, only the electric field part is important, since $v/c \sim \alpha$. For the geometry given above, and for a given b, the kicks in x and y are given by the following:

$$E_x = \frac{-Ze\gamma vt}{\left(b^2 + \gamma^2 v^2 t^2 \right)^{3/2}}.$$

(8.4)

$$E_y = \frac{-Ze\gamma b}{\left(b^2 + \gamma^2 v^2 t^2 \right)^{3/2}}.$$

(8.5)

One then integrates from $-$ infinity to $+$ infinity in time while noticing that the kick in E_x vanishes because it is an odd function. Therefore, only the y-kick comes into the momentum change:

$$\begin{aligned} \Delta P = \Delta P_y &= \int_{-\infty}^{\infty} dt \; eE_y(t) \\ &= 2\frac{Ze^2 b}{v} \int_0^{\infty} \frac{d(\gamma vt)}{\left(b^2 + (\gamma vt)^2 \right)^{3/2}} \\ &= \frac{2Ze^2}{bv}. \end{aligned}$$

(8.6)

This is like an impulse with $P_{y\_initial} = 0$. The energy lost is simply obtained then by $(\Delta P)^2 / 2m$ to arrive at the following very important result for the interaction with a single electron:

$$\Delta T(b) = \frac{(\Delta P)^2}{2m} = \frac{2Z^2 e^4}{mv^2}\left(\frac{1}{b^2} \right).$$

(8.7)

Notice that this energy loss is independent of the incident particle mass, M_i, even though a large mass is assumed, given that the incident particle does not change directions in this approximation. Also notice that the energy loss is proportional to $1/v^2$. This is a very important result that remains dominant as we proceed further. However, that was only for a given b, but in our problem, we have a whole range of b values. Therefore, we need to integrate over the full range of the impact parameter, b.

According to Figure 8.2, the number of electrons in the differential annulus of volume $(dx) \cdot (2\pi b db)$ is $[(2\pi b db) \cdot (dx)] \cdot \rho \cdot (N_A z/A)$. The differential energy loss experienced by the particle having an impulse with this annulus is then[†] the following:

$$dT = \left[(2\pi b db) \cdot (dx) \right] \cdot \rho \cdot \left(N_A z / A \right) \cdot \frac{2Z^2 e^4}{mv^2}\left(\frac{1}{b^2} \right).$$

(8.8)

[†]Note that the small Z is the material atomic number here, opposite from most books.
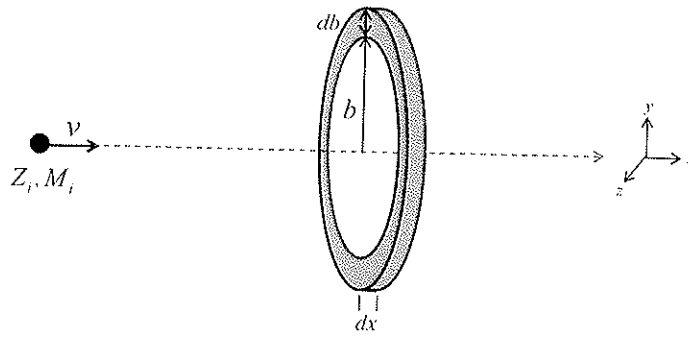
Figure 8.2. Geometry of a heavy charged particle interacting with a differential ring of atoms.

Rearranging and noting that we need to integrate over all possible b values:

$$\left(\frac{dT}{\rho dx}\right)_c = 4\pi \left(\frac{N_A z}{A}\right) \frac{Z^2 e^4}{mv^2} \int_{b=0}^{\infty} (db/b). \tag{8.9}$$

The critical issue is how to perform the integral. Since with integrating from zero to infinity, the stopping power would diverge. Instead of the full integral, we will then take the integral from a b_{min} to b_{max}, which results in the following:

$$\left(\frac{dT}{\rho dx}\right)_c = 4\pi \left(\frac{N_A z}{A}\right) \frac{Z^2 e^4}{mv^2} \ln \left(\frac{b_{max}}{b_{min}}\right). \tag{8.10}$$

According to the Equation (8.8), if b goes to zero, then dT will rise without any limit. However, there is a certain maximum for energy loss and that occurs with a head-on collision. So we need to choose a minimum for b which gives the maximum magnitude for energy loss.

After derivations of energy transfers with bound electron shell states in quantum mechanics, and some complicated Bessel function math[†], the stopping power is given by the following:

$$\left(\frac{dT}{dx}\right) = 4\pi \left(n\right) \frac{Z^2 z e^4}{mv^2} \left[\ln\left(B_c\right) - \beta^2/2\right], \tag{8.11}$$

where,

$$B_c \equiv \frac{b_{max}}{b_{min}} = (1.123) \frac{\gamma^2 mv^3}{Z_i e^2 \langle \omega \rangle}. \tag{8.12}$$

Here, $\langle \omega \rangle$ is the average motion frequency of electrons, and n is the number density of atoms[‡]. Note and remember from earlier chapters that $(\gamma - 1) = T/Mc^2$ and $\gamma = 1/\sqrt{1-\beta^2}$.

[†]For more discussion regarding this topic, see J.D. Jackson's *Classical Electrodynamics*, Chapter 13.
[‡]The factor 1.123 is from $1.123 = 2/\exp(0.577...)$, and $0.577...$ is Euler's constant.

Table 8.1: Maximum Energy Transferred for Various Situations*

Particle	Value of T'_{max}
For electrons	$T'_{max} = T/2$
For positrons	$T'_{max} = T$
For a heavy charged particle with mass M	$T'_{max} = T \left(\dfrac{1 + (2Mc^2/T)}{1 + (M+m)^2 c^2 / (2m/T)} \right)$
For a heavy charged particle with mass M, which $M \gg m$ and $T \ll Mc^2$	$T'_{max} \approx 2mc^2 \dfrac{\beta^2}{1 - \beta^2} \approx 2mv^2$

*Note that for positrons, the maximum energy transferred to an electron is twice what it is for electron to another electron. That is because the particles are different, and the secondary is not simply the one with the lower energy.

Let's separate the collisional mass stopping power into two terms: one for hard collisions and one for soft collisions. We will start out with an arbitrary energy cutoff, H, that will separate the two by an impact parameter or, equivalently in this case, an energy. If σ_s and σ_h are cross sections for soft and hard collisions, respectively:

$$\left(\frac{dT}{\rho dx} \right)_c = \left(\frac{dT_s}{\rho dx} \right)_c + \left(\frac{dT_h}{\rho dx} \right)_c = \left(\frac{N_A z}{A} \right) \left[\int_{T'_{min}}^{H} \frac{d\sigma_s}{dT'} T' dT' + \int_{H}^{T'_{max}} \frac{d\sigma_h}{dT'} T' dT' \right]. \tag{8.13}$$

The quantity T' here is the energy transferred by the fast charged particle to electrons. The quantity H here is somewhat arbitrary, but it should be about the value of the minimum energy at which the electron is ejected for hard collisions. Table 8.1 illustrates the values of T'_{max}.

Soft Collision Mass Stopping Power for Heavy Charged Particles

If the energy transferred, T', is less than the ionization potential, only excitations can occur. If it is larger, then ionizations can occur, but they will also have excitations as well, and the energy must be larger than H.

The quantity I is defined as the **mean excitation potential** of the absorbing medium; it includes both excitations and ionizations. See Attix (2004), Appendix B.1 and B.2. There is a lot of uncertainty to I, but at least it is in the logarithm, which reduces the sensitivity to that uncertainty. I is approximately proportional to z, the atomic number of the medium.

Derived using the Born approximation[†] ($\beta \gg zZ/137$)), then the soft collision mass stopping power is the following:

$$\left(\frac{dT_s}{\rho dx} \right)_c = 2\pi r_0^2 mc^2 \left(\frac{N_A z}{A} \right) \frac{Z^2}{\beta^2} \left[\ln \left(\frac{2mc^2 \beta^2}{I^2 (1 - \beta^2)} H \right) - \beta^2 \right]$$

$$= (0.1535) \left(\underbrace{\frac{z}{A}}_{material} \cdot \underbrace{\frac{Z^2}{\beta^2}}_{particle} \right) \left[\ln \left(\frac{2mc^2 \beta^2}{I^2 (1 - \beta^2)} H \right) - \beta^2 \right]. \tag{8.14}$$

[†] The particle's kinetic energy is much greater than an electron's potential (orbital) energy.

Here the quantity $2\pi r_0^2 mc^2 N_A = 0.1535$ (MeV/(g/cm^2)). For ease later, we can define the following:

$$k = (0.1535)\left(\frac{z}{A} \cdot \frac{Z^2}{\beta^2}\right). \tag{8.15}$$

The units of k are MeV/(g/cm^2). In fact, very important dependencies are in k. The $\frac{z}{A}$ term is a property of only the material, and $\frac{Z^2}{\beta^2}$ is a property of only the incident particle, and it is this part that produces the Bragg peak. The above applies to electrons, positrons, and heavy charged particles. Soft collisions are most, or at least half, of the collisions for radiation therapy energies.

Hard Collision Mass Stopping Power for Heavy Charged Particles

A hard collision is often further defined as when an electron is ejected with a considerable fraction of the maximum energy transferable, T_{max}. These recoil electrons are called "delta-rays" or "knock-on" electrons, and they can be seen in bubble chambers.

The **differential hard collision cross section per electron** for heavy charged particles is given by the following:

$$\frac{d\sigma_h}{dT'} = 2\pi r_0^2 mc^2 \frac{Z^2}{\beta^2}\left(\frac{1-\beta^2(T'/T'_{max})}{(T')^2}\right). \tag{8.16}$$

There is some dependence on particle spin for this differential hard collision cross section per electron. We will use the form for zero spin particles (like alpha, pion, …), but it will apply to spin ½ particles (like protons, electrons, muon, …) provided $T' \ll Mc^2$.

Then the **hard collision mass stopping power** for $H \ll T'_{max}$ is the following:

$$\begin{aligned}
\left(\frac{dT_h}{\rho dx}\right)_c &= \left(\frac{N_A z}{A}\right)\left[\int_H^{T'_{max}} \frac{d\sigma_h}{dT'} T' dT'\right] \\
&= k\left[\int_H^{T'_{max}} dT'/T' - (\beta^2/T'_{max})\int_H^{T'_{max}} dT'\right] \\
&= k\left[\ln(T'_{max}/H) - (\beta^2/T'_{max})(T'_{max} - H)\right] \\
&= k\left[\ln(T'_{max}/H) - \beta^2\right].
\end{aligned} \tag{8.17}$$

Now with combining Equations (8.13), (8.14), and (8.17), mass stopping power for heavy charged particles can be written as the following:

$$\left(\frac{dT}{\rho dx}\right)_c = \left(\frac{dT_s}{\rho dx}\right)_c + \left(\frac{dT_h}{\rho dx}\right)_c = k\left[\ln\left(\frac{2mc^2\beta^2}{I^2(1-\beta^2)}H\right) - \beta^2\right] + k\left[\ln(T'_{max}/H) - \beta^2\right]. \tag{8.18}$$

Table 8.2: Magnitudes for Parameters Related to High-energy Particle Speed Relative to the Speed of Light

β	T_p	β^2	$\ln(\beta^2/(1-\beta^2))$	$\ln(\beta^2/(1-\beta^2))-\beta^2$
0.80	626	0.64	0.57	−0.07
0.90	1214	0.810	1.45	1.17
0.95	2067	0.903	2.23	1.33
0.99	5713	0.980	3.89	2.91

With a bit of math, and recalling that for a heavy charged particle $T'_{max} \approx 2mc^2 \dfrac{\beta^2}{1-\beta^2} \approx 2mv^2$, the Equation (8.18) simplifies as follows:

$$\left(\frac{dT}{\rho dx}\right)_c = 2k\left[\ln\left(\frac{2mc^2\beta^2}{I(1-\beta^2)}\right)-\beta^2\right].$$
(8.19)

There is also a more handy form for mass collisional stopping power for spin ½ and $T' << Mc^2$ as follows:

$$\left(\frac{dT}{\rho dx}\right)_c = (0.3071)\underbrace{\left(\frac{z}{A}\right)}_{medium}\underbrace{\left(\frac{Z^2}{\beta^2}\right)}_{particle}\left[13.84+\ln\left(\frac{\beta^2}{1-\beta^2}\right)-\beta^2-\ln I\right].$$
(8.20)

Here, mean excitation potential, I, has units of eV. Note that the energy dependence in the brackets of Equation (8.20) is weak (see Table 8.2).

Shell Correction

The complex motion of the orbital electrons is accounted for with the shell correction. When the particle velocity is less than the orbital velocity of the electrons in that shell, then those electrons do not participate significantly in collisions with the particle.

The shell correction factor is written as C/z, and it (mostly) decreases the mass collisional stopping power by a small amount as follows:

$$\left(\frac{dT}{\rho dx}\right)_c = 2k\left[\ln\left(\frac{2mc^2\beta^2}{I(1-\beta^2)}\right)-\beta^2-C/z\right].$$
(8.21)

The shell correction is a function of the particle velocity and the atomic number of the medium. See Attix (2004), page 172, Figure 8.3 for the magnitude and proton kinetic energy dependence of the shell correction, as an example. Note that it is more important at lower energies.

Dependence of the Stopping Power on the Medium

The factor z/A has a value near 0.5 ±0.05 for most elements, dropping to lower values at higher z. Hydrogen-1 has the highest value of 1, which is why it is used to slow or shield fast charged particles. See appendix B.1 in Attix (2004), page 527, for z/A values.

The term $\ln I$ also makes high-z materials have lower stopping power. Also, the shell correction generally decreases the stopping power.
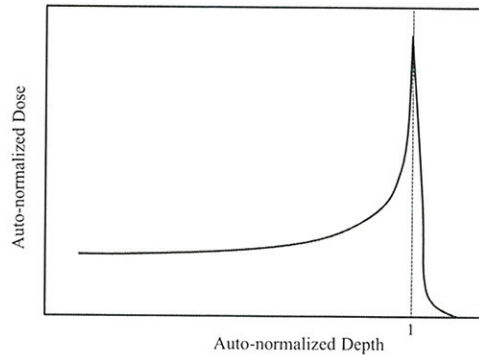
Figure 8.3. Dose depth curves for heavy ions along the centered axis of a broad beam. Note that the Bragg peak is due to the $1/\beta^2$ in k.

Mass Collisional Stopping Power Dependence on Particle Velocity

The term $1/\beta^2$ is dominant at low energies. It causes the mass collisional stopping power to sharply increase as the particle slows down. The result is the so-called "Bragg Peak" (see Figure 8.3).

When $\beta = v/c \approx 1$, the energy increases quickly as the speed creeps up against c. The linac accelerating microwave cavity uses this fact to keep the particle in phase with the phase velocity of the standing or traveling microwave. The cavity is loaded with periodic barriers to slow the phase velocity below c.

Also, when $\beta \approx 1$, the $1/\beta^2$ term has little influence, but the $\beta^2/(1-\beta^2)$ term increases. See Table 8.2.

The kinetic energy of a particle is directly proportional to its rest mass.

There is no mass dependence on the heavy charged particle stopping power. Therefore, any heavy particle with the same velocity and charge will have the same stopping power, *but the scatter and range straggling could be different.*

Mass Collisional Stopping Power Dependence on Particle Charge

At low energies (speeds $\beta < 0.1$), there is an effective charge, Z^*, to be used instead of the charge, Z, because of the attachment of the incident particle's electrons. Higher-energy particles are more likely to be fully ionized. See Anderson (1984), page 21, Figure 2.4.

The Z^2 factor means that particles with multiple charges have a much higher mass collisional stopping power than singly charged particles. For example, if $\beta_{\alpha^{2+}} = \beta_{p^+}$, then:

$$\left(\frac{dT}{\rho dx}\right)_c^{\alpha^{2+}} = 4 \cdot \left(\frac{dT}{\rho dx}\right)_c^{p^+}. \tag{8.22}$$

This fact can be used to obtain stopping powers for any heavy charged particle from a table of mass collisional stopping powers for protons. For this purpose, do the following steps:

1. Look up or calculate β for particle x with kinetic energy, T_x.
2. Look up or calculate the proton kinetic energy, T_p, for the same β.
3. Look up the mass stopping power for a proton with kinetic energy T_p.
4. Multiply the mass stopping power for a proton by $(Z_x^*/Z_p^*)^2$. Note that Z_p^* is unity, and Z_x^* is the effective charge on particle x at its speed.
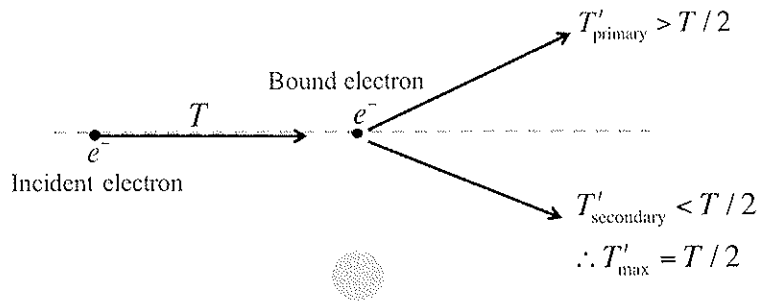
Figure 8.4. Kinetic energy after a hard collision by an electron. By convention, the primary charge has more energy than the secondary charge.

It should be emphasized that through the decades, the stopping power formula has been progressively refined. One of the most important refinements was to cure the high-speed (v approaching c) limit. As explained in Jackson (1999), page 636, the very fast particle causes so much ionization from relativistic effects that it self-shields its charge from the plasma effect of the ionizations it creates. The time scale associated with this shielding is manifest by the plasma frequency quantity that appears in this limit. Yet, the fundamental relations covering most of the important physics for most applications and for most particles are described by the simple derivation at the start of chapter, and this fact is remarkable in the history of modern physics.

Electron and Positron Interactions

In hard collisions by *electrons*, one cannot tell which was the primary or which was the secondary—by convention, the one with the highest energy (that is, the faster electron) is the "primary." Therefore, the maximum kinetic energy transferable is the amount that the lower-energy electron can have (Figure 8.4).

However, in the *positron* case, we *do* know which particle is which, and we cannot reassign the primary label, so the maximum kinetic energy transferred is $T'_{max} = T$ (look at Table 8.1). Therefore, the maximum kinetic energy transferred is $T/2$ for electrons, and it is T for positrons.

The differential cross section for the electron hard collisions—which describes the collision between two free electrons—was derived by Möller (1932) as follows:

$$\frac{d\sigma_h}{dT'} = 2\pi r_0^2 mc^2 \frac{1}{\beta^2 (T')^2} \left(\frac{T}{T-T'}\right)^2 \left\{1 - \left[3 - \left(\frac{T}{T-mc^2}\right)^2\right]\frac{T'}{T}\left(1-\frac{T'}{T}\right) + \left(\frac{T}{T-mc^2}\right)^2\left(\frac{T}{T-T'}\right)^2\right\}. \qquad (8.23)$$

Note that z dependence here is implicit in β^2 via mass stopping power. The differential cross section for positron-electron collisions is even more complex, and it was derived by Bhabha (1936).

Mass Collision Stopping Power for Electrons and Positrons

The mass collision stopping power for either electrons or positrons is given by the following:

$$\left(\frac{dT}{\rho dx}\right)_c = k\left\{\ln\left(\frac{\tau^2(\tau+2)}{2(I/mc^2)^2}\right) + F^{\pm}(\tau) - \delta - 2\frac{C}{z}\right\}. \tag{8.24}$$

where, with $\tau = \dfrac{T}{mc^2}$, the two quantities $F^-(\tau)$ and $F^+(\tau)$ are defined for electrons and positrons, respectively, as follows:

$$F^-(\tau) = 1 - \beta^2 + \frac{(\tau^2/8) - (2\tau+1)\ln 2}{(\tau+1)^2}. \tag{8.25}$$

$$F^+(\tau) = 2\ln 2 - \frac{\beta^2}{12}\left\{23 - \frac{14}{(\tau+2)} + \frac{10}{(\tau+2)^2} + \frac{4}{(\tau+2)^3}\right\}. \tag{8.26}$$

The term δ is a polarization or density effect correction that we will discuss in the next section. Recall that $k = (0.1535)\left(\dfrac{z}{A}\cdot\dfrac{Z^2}{\beta^2}\right)$ and its units are MeV/(g/cm²). The shell correction term, C/z, is the same for electrons and positrons as it is for protons, provided that β is the same. At low positron energy, the positron mass stopping power is slightly greater than that for electrons, and at higher energies, the opposite is true.

Polarization or Density Effect Correction

Atoms are much closer together in condensed matter (liquids and solids) than in gases, and this will be an important factor for the density effect. The electric field will be reduced by some self-shielding, and it happens for these light particles more easily because of their higher speed. Recall that the light particles are more relativistic for a given energy. The relativistic effect here comes from the field line contraction in the direction of the electric field momentum transfer. The relativistic field line contraction leads to an increased polarization of charges in the atoms. This effect reduces the mass collisional stopping power.

The density effect is roughly proportional to the following quantity (see Attix, Figure 8.4, page 173):

$$\chi = \log_{10}\left(\beta\sqrt{1-\beta^2}\right). \tag{8.27}$$

In the highly relativistic cases (Figure 8.5.b), the field lines get Lorentz-contracted (locally and temporarily stronger), and they strengthen the field, enhancing the polarization of the *nearby* medium by some ionizations (self-shielding the way a plasma does). Atoms away from the trajectory will see a smaller impulse from the passing charged particle. This effect happens significantly for electrons and positrons because they are faster and, therefore, more relativistic. In the slower cases (Figure 8.5.a), the atoms (electron shells) are more spherical relative to the passing charged particle.

The density effect is larger for low-z materials since they polarize more readily. To a very good approximation, $\delta \approx 0$ for gases. So water and air can be very different for this. Above 10 MeV, this factor becomes more significant (see Figure 8.5 in Attix, page 175). The density effect is important in ion chamber dosimetry where the cavity is a gas and the wall is a solid. The fast charged particles come from the wall, but we measure the ionization in the gas. This energy-dependent term can lead to a big difference between an ion chamber and a phantom dose in some cases. This effect can lead to a violation of Fano's theorem.
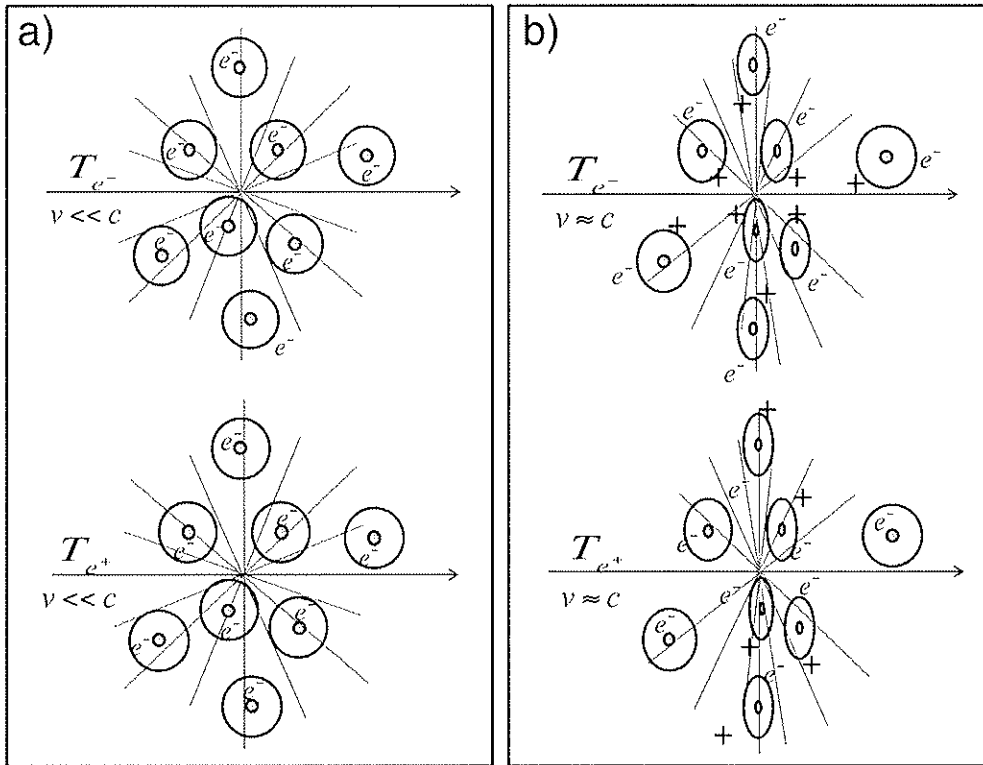
Figure 8.5. A non-relativistic particle (a) does not experience the Lorentz contraction that a relativistic particle does (b) which acts to enhance the polarization of the medium by contracting field lines near the fast particle.

Restricted Mass Stopping Power

Consider a thin foil. If we did not remove fast δ-rays from the collisional mass stopping power, then dose calculated from stopping power would be overestimated. That is because the thin foil would not have δ-rays equilibrium—there would be no δ-rays coming into the region, only leaving. These δ-rays deposit most of their energy near the end of their track, like all charged particles (see Figure 8.6).
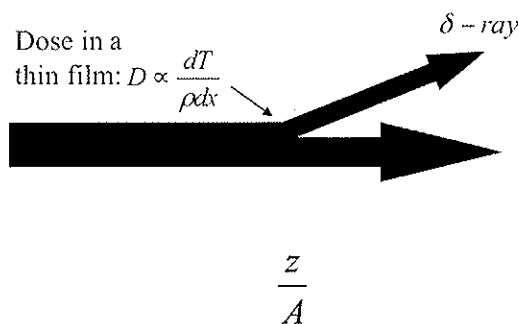
Figure 8.6. We need to use restricted stopping power with a proper value called Δ. The dose is overestimated with unrestricted stopping power. The foil is so thin that the stopping power is the same.

Energetic δ-rays or knock-on electrons leave the region (the particle track) with significant amounts of kinetic energy. However, the stopping power considers the primary particle loss to be deposited locally and continuously to the particle track. For this reason, sort of as we do with uncharged particles, the δ-rays should be treated as carriers of energy more than depositors of energy in this context. They should be treated separately or just removed from the stopping power of the main particle altogether.

Later in Spencer–Attix cavity theory discussions, we will remove these energetic δ-rays from the stopping power calculation if they are energetic enough to cross the cavity. The δ-rays that do not cross the cavity will be treated as though they are immediately local to the primary charge path, are not tracked, and will be absorbed into the continuous slowing down stopping power. The important concept here is that the primary charged particle should cross the cavity. In fact, it should cross all the way. If a secondary particle (δ-ray) goes all the way through the cavity, then it, too, should be treated as a primary charged particle[†].

The restricted mass stopping power, $\left(\dfrac{dT}{\rho\,dx}\right)_{\Delta}$, will include energy losses up to an energy transfer equal to Δ. Those δ-rays with $T > \Delta$ will be treated as if they were primary charged particles. δ-rays with energy $T < \Delta$ are treated as having no energy and, therefore, their energy is deposited locally with a continuous slowing down of the primary electron. See Figure 8.7.

The cutoff energy is somewhat arbitrary, but it is chosen to fit a region of interest, like the main track of energy deposition or a small cavity: these δ-rays with $T < \Delta$ stay in the region of interest and get included in a continuous slowing down stopping power.

We can see that this variation in energy—from a few to several discrete scattering events—leads to **range straggling**. Note on Figure 8.8 how there will be a variation in ranges.

Also notice that $\left(\dfrac{dT}{\rho\,dx}\right)_{\Delta} < \left(\dfrac{dT}{\rho\,dx}\right)_{c}$. If $\Delta \rightarrow T^{initial}_{e^-\,primary}$, then the restricted mass stopping power will equal the unrestricted mass (collisional) stopping power.

$$\lim_{\Delta \rightarrow T^{initial}_{e^-\,primary}} \left(\frac{dT}{\rho\,dx}\right)_{\Delta} = \left(\frac{dT}{\rho\,dx}\right)_{c}. \tag{8.28}$$

The restricted mass stopping power for heavy charged particles is driven by just replacing T'_{max} with Δ in the integration to arrive at the following:

$$\left(\frac{dT}{\rho\,dx}\right)_{\Delta} = k\left\{ \ln\left(\frac{2mc^2\beta^2\Delta}{I^2(1-\beta^2)}\right) - 2\beta^2 - 2\frac{C}{z}\right\}. \tag{8.29}$$

The restricted mass stopping power for electrons and positrons is given by the following:

$$\left(\frac{dT}{\rho\,dx}\right)_{\Delta} = k\left\{ \ln\left(\frac{\tau^2(\tau+2)}{2(I/mc^2)^2}\right) + G^{\pm}(\tau,\eta) - \delta - 2\frac{C}{z}\right\}. \tag{8.30}$$

[†] Note that here we use the term primary charged particle, but it is secondary to the primary photon beam.
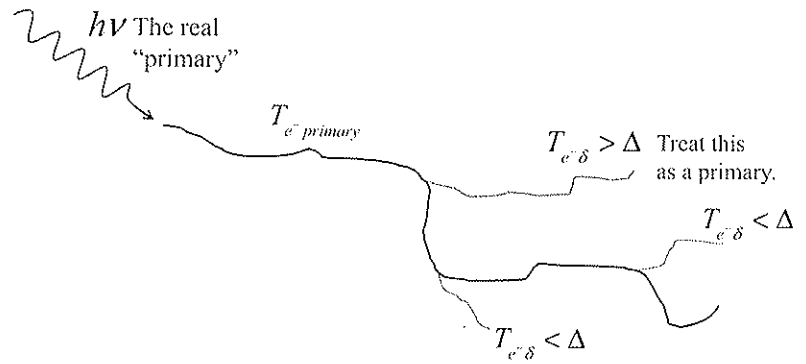
Figure. 8.7. The primary charged parti-
cle creates δ-rays, and some can be con-
sidered new primaries.
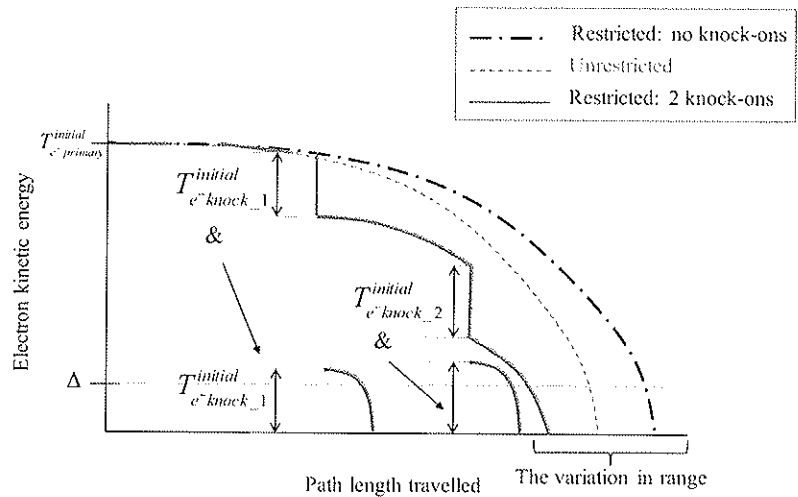
Figure 8.8. Two particular instances for
a restricted stopping power calculation,
such as one might do numerically: one
with two hard collisions big enough to
create δ-rays and one with no δ-rays.
They are compared to the unrestricted
case. Note the variation in range.

where, with $\tau \equiv T/mc^2$, $\eta \equiv \Delta/T$, and $k = (0.1535)\left(\dfrac{z}{A} \cdot \dfrac{Z^2}{\beta^2}\right)$, the two quantities $G^-(\tau,\eta)$ and $G^+(\tau,\eta)$ are defined for electrons and positrons respectively as follows:

$$G^-(\tau,\eta) = -1 - \beta^2 + \ln\left[4(1-\eta)\eta\right] + (1-\eta)^{-1} + (1-\beta^2)\left[\tau^2\eta^2/2 + (2\tau+1)\ln(1-\eta)\right], \tag{8.31}$$

$$G^+(\tau,\eta) = \ln 4\eta - \beta^2\left[1 + (2-\xi^2)\eta - (3+\xi^2)(\xi\tau/2)\eta^2 + (1+\xi\tau)(\xi^2\tau^2/3)\eta^3 - (\xi^3\tau^3/4)\eta^4\right]. \tag{8.32}$$

Here, $\xi \equiv (\tau+2)^{-1}$.

If $\Delta = T'_{max} = T/2$, then $\eta = 1/2$ and, therefore, $G^-(\tau,1/2) = F^-(\tau)$. And if $\Delta = T'_{max} = T$, then $\eta = 1$ and, therefore, $G^+(\tau,1) = F^+(\tau)$.

Note that *without scattering* and *without δ-rays,* etc. there is a theoretical Bragg peak for electron beams. However, in all real situations, scattering dominates electron beams impinging on matter in such a way that the peak is completely blurred beyond recognition.

Linear Energy Transfer and Unrestricted Linear Energy Transfer

The stopping power is the amount of energy lost from the particle's point of view. **Linear energy transfer (LET)**, however, is the restricted stopping power from the point of view of the medium. It does not include nuclear reactions either. The linear energy transfer symbol is L_Δ as follows:

$$L_\Delta = \left(\frac{dT}{dx}\right)_\Delta = \rho\left(\frac{dT}{\rho dx}\right)_\Delta.$$ (8.33)

Linear energy transfer often has the units of keV/μm. The **unrestricted linear energy transfer** is when $\Delta \to \infty$ (or T, even if T is very big). So the unrestricted linear energy transfer is written as follows:

$$S = L_\infty = \left(\frac{dT}{dx}\right)_c = \rho\left(\frac{dT}{\rho dx}\right)_c,$$ (8.34)

and has the units of keV/μm.

Mass Radiative Stopping Power

Bremsstrahlung (German for "braking radiation") is the production of x-rays due to an acceleration or de-acceleration of charged particles in a strong electric field. The differential cross section for bremsstrahlung production by a charged particle is given by the following:

$$\frac{d\sigma_{rad}}{d(hv)} = \frac{1}{137}\left(\frac{e^2}{mc^2}\right)^2 z^2 \left(\frac{T+mc^2}{T\cdot(hv)}\right)B.$$ (8.35)

Here, m is the mass of the fast charged particle[*] and z^2 is the material effective atomic number squared. The factor B is a dimensionless parameter that depends on the ratio of x-ray energy to charged particle kinetic energy, hv/T.

The z^2 dependence means that bremsstrahlung is much more likely to occur in high-z materials. X-ray anodes are often made with tantalum or tungsten partly for this reason. The more important reason is that x-ray anodes need a high melting temperature.

The $1/hv$ dependence means that low-energy x-rays are created more often. However, an energy of $hv \approx T$ is possible, but unlikely.

The mass radiative stopping power is given by the following:

$$\begin{aligned}
\left(\frac{dT}{\rho dx}\right) &= \frac{N_A}{A}\int_0^T \frac{d\sigma_{rad}}{d(hv)}(hv)d(hv) \\
&= \sigma_0 \frac{N_A}{A}z^2(T+mc^2)\int_0^1 Bd(hv/T) \\
&= \sigma_0 \frac{N_A}{A}z^2(T+mc^2)\,\bar{B}_r,
\end{aligned}$$ (8.36)

---

[*]Note that m can be for heavy particles, but the $1/m^2$ factor means, for us in medical applications, it is always electrons that we are concerned about for radiative losses.

where[*]:

$$\overline{B}_r = \int_0^1 B d(h\nu / T).$$ (8.37)

Note that $\sigma_0 = \dfrac{1}{137}\left(\dfrac{e^2}{mc^2}\right)^2 = \dfrac{r_0^2}{137}$.

For $T < mc^2$, $\overline{B}_r = 16/3$. If $mc^2 < T << 137\ mc^2 z^{-1/3}$, then there would be no screening and no z dependence and $\overline{B}_r = 4\ln\left(2\dfrac{(T + mc^2)}{mc^2} - \dfrac{1}{3}\right)$. There would be complete screening but no T dependence for $T >> 137\ mc^2 z^{-1/3}$ and $\overline{B}_r = 4\left(\ln(183 z^{-1/3}) - \dfrac{1}{18}\right)$.

Heitler's derivation of radiative stopping power is not particularly accurate by today's standards. The ICRU Report 37 is much more accurate. Tables 8.3, 8.4, and 8.5 compare Heitler's derivations and ICRU-37 with respect to the radiative stopping power for three elements: carbon, aluminum, and lead, respectively. Nevertheless, Heitler's work is illustrative and simple (elegant), and a huge accomplishment for its time.

At high energies $(T >> mc^2)$ and, therefore, complete screening, the mass radiative stopping power is given by the following:

$$\left(\frac{dT}{\rho dx}\right)_r = \sigma_0 \frac{N_A}{A} z^2 T\left[\ln(183 z^{-1/3}) - 1/18\right].$$ (8.38)

The comparison between mass collisional and radiative stopping powers for electrons in carbon, copper, and lead is plotted in Figure 8.6 of Attix (2004).

The dependencies on the medium and the particle kinetic energy are different for the two types of stopping powers at high energy. For $T >> mc^2$, the dependencies are as the following:

$$\left(\frac{dT}{\rho dx}\right)_c \propto \frac{N_A}{A} z,$$ (8.39)

$$\left(\frac{dT}{\rho dx}\right)_r \propto \frac{N_A}{A} z^2 T.$$ (8.40)

Table 8.3: Stopping Power for Carbon $(z = 6)$

T (MeV)	Heitler $(dT/\rho dx)_r$	ICRU-37 $(dT/\rho dx)_r$	% Difference
0.01	0.00291	0.00315	−7.6
0.1	0.00341	0.00341	−0.06
1.0	0.0109	0.0105	3.3
5.0	0.0705	0.0658	7.3
10.0	0.163	0.151	8.0
20.0	0.376	0.342	10.2
40.0	0.792	0.751	5.5

[*]See Evans (1955), page 603, Figure 1.1.

Table 8.4: Stopping Power for Aluminum (z = 13)

T (MeV)	Heitler $(dT/\rho dx)_r$	ICRU-37 $(dT/\rho dx)_r$	% Difference
0.01	0.00608	0.00656	−7.3
0.1	0.00713	0.00748	−4.6
1.0	0.0227	0.0212	7.3
5.0	0.147	0.126	16.7
10.0	0.341	0.286	19.4
40.0	1.56	1.38	13.4

Table 8.5: Stopping Power for Lead (z = 82)

T (MeV)	Heitler $(dT/\rho dx)_r$	ICRU-37 $(dT/\rho dx)_r$	% Difference
0.01	0.0315	0.0205	54.0
0.1	0.0369	0.0445	−17.1
1.0	0.118	0.129	−8.7
5.0	0.764	0.577	32.3
10.0	1.77	1.21	46.6
40.0	6.97	5.40	29.1

Therefore, with the input units for T, the ratio is given by the following for $T \gg mc^2$:

$$\left\{ \left(\frac{dT}{\rho dx} \right)_r \Big/ \left(\frac{dT}{\rho dx} \right)_c \right\} \approx \frac{zT(MeV)}{700}. \tag{8.41}$$

Radiation Length

The radiative stopping power energy dependence (T) can be separated out in this approximation by the following:

$$\frac{dT}{dx} = -\frac{\rho}{\chi_0} T. \tag{8.42}$$

The solution of this differential equation is as follows:

$$T = T_0 e^{-\rho x / \chi_0}. \tag{8.43}$$

Here T_0 is the initial kinetic energy at $x=0$. The quantity $\dfrac{1}{\chi_0}$ is called the **radiation length,** and it is defined through this procedure. It is the distance it takes very high-energy charged particles to reduce their kinetic energy

to $1/e$ of their original value by radiative interactions alone. The radiation length is a characteristic of the material and is given by the following:

$$\frac{1}{\chi_0} \equiv 4\sigma_0 \frac{N_A}{A} z^2 \left[\ln(183 z^{-1/3}) - \frac{1}{18} \right].$$

(8.44)

Note that z in Equation (8.44) is for material. The units of the radiation length are $\frac{cm^2}{g}$.

Radiation Yield

The **radiation yield**, $Y(T_0)$, is the average fraction of energy emitted by bremsstrahlung as the charged particle slows down from an energy T_0 to rest[*] (Figure 8.9). The radiation yield is given mathematically by the following:

$$Y(T_0) \equiv \frac{1}{T_0} \int_0^{T_0} \frac{(dT / \rho dx)_r}{(dT / \rho dx)} dT,$$

(8.45)

where,

$$(dT / \rho dx) = (dT / \rho dx)_c + (dT / \rho dx)_r.$$

(8.46)

The average amount of energy radiated is $T_0 Y(T_0)$. Thus, according to Figure 8.9, the average amount of radiated energy between two kinetic energies is the following:

$$\sum (h\nu)_{T_1 \to T_2} = T_1 Y(T_1) - T_2 Y(T_2).$$

(8.47)

If $Y(T_0)$ is averaged over all initial energies of electrons and positrons set in motion by photons, then the result is g, the average fraction of the initial kinetic energy lost due to radiative interactions (positron annihilation-in-flight is ignored at this moment, i.e., we do not count the annihilation photons as part of the bremsstrahlung). Therefore,

$$g = \frac{1}{\Phi} \int_0^{T_{max}} Y(T_0) \Phi'(T_0) dT_0.$$

(8.48)

where the quantity Φ is the initial fluence of electrons set in motion, which is given by the following:

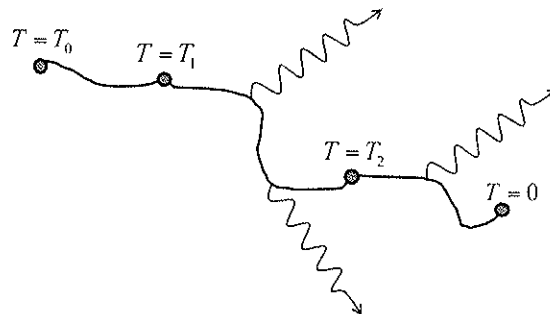$$\Phi \equiv \int_0^{T_{max}} \Phi'(T_0) dT_0.$$

(8.49)

Figure 8.9. Geometry of bremsstrahlung radiation in the particle's track.

[*]In ICRU-37, it is assumed that the charged particle doesn't create any secondaries as it slows down: continuous slowing down.

The quantity $\Phi'(T_0)$ is the initial energy spectrum of electrons set in motion by all photon interactions, and T_{max} is the maximum initial kinetic energy.

Elastic Scattering

When a charged particle interacts with a nucleus and there is no bremsstrahlung, the most likely thing to have happened is elastic scattering (Figure 8.10). Ernest Rutherford (1911) explored the elastic scattering cross section while he was studying the structure of the nucleus. Regarding Figure 8.10, Rutherford's (elastic) scattering cross section is given by the following:

$$\frac{d\sigma_{Ruth}}{d\Omega_\theta} = \frac{z^2}{4}\left(\frac{e^2}{Mc^2}\right)^2\left(\frac{(1-\beta^2)}{\beta^4}\right)\left(\frac{1}{\sin^4(\theta/2)}\right). \tag{8.50}$$

Note that the elastic cross section is proportional to $1/M^2$, so heavy charged particles scatter *much less* than electrons and positrons. The cross section is also proportional to $1/\beta^4$, therefore scattering is much more likely for low-energy (speed) particles and the $1-\beta^2$ factor further decreases the scattering probability as $\beta \to 1$.

According to Equation (8.50), an individual elastic scattering event is much more likely to happen for small angles since the Rutherford cross section is proportional to $1/\sin^4(\theta/2)$.

The Rutherford theory *really* only applies to *heavy* charged particles of zero spin, so its application to electrons is a stretch. This cross section also doesn't really apply to $\beta > 2z/137$ (Born approximation). Mott (1929, 1932) used both the relativistic Dirac theory of the electron and the Born approximation. McKinley and Feshbach (1948) found an acceptable analytical formulation of Mott's result for most situations. For electrons, their formulation is as follows:

$$\frac{d\sigma_{M-F}}{d\Omega_\theta} = \frac{d\sigma_{Ruth}}{d\Omega_\theta}\left[1 - \beta^2\sin^2(\theta/2) + \pi\beta(z/137)(1-\sin(\theta/2))\sin(\theta/2)\right]. \tag{8.51}$$

The McKinley–Feshbach result is valid for $\beta \approx 1$ if $(z/137) < 0.2$, so it is more appropriate for describing electron and positron scattering in low-atomic-number materials. We can see that for small scattering angles or low particle velocity, the McKinley–Feshbach equation reduces to the Rutherford equation.

Multiple Scattering

After a large number of small scattering events, the particle's direction can change significantly: this is called
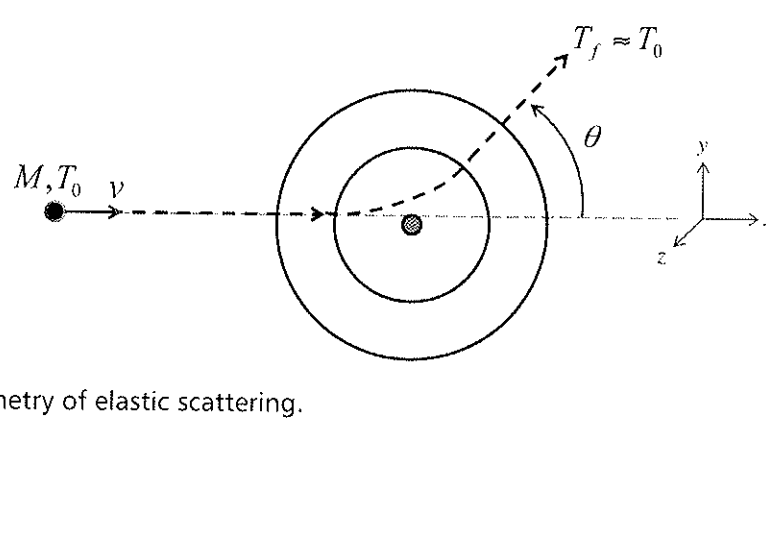

Figure 8.10. The geometry of elastic scattering.

to $1/e$ of their original value by radiative interactions alone. The radiation length is a characteristic of the material and is given by the following:

$$\frac{1}{\chi_0} \equiv 4\sigma_0 \frac{N_A}{A} z^2 \left[\ln(183 z^{-1/3}) - \frac{1}{18} \right].$$ (8.44)

Note that z in Equation (8.44) is for material. The units of the radiation length are $\frac{cm^2}{g}$.

Radiation Yield

The **radiation yield**, $Y(T_0)$, is the average fraction of energy emitted by bremsstrahlung as the charged particle slows down from an energy T_0 to rest[*] (Figure 8.9). The radiation yield is given mathematically by the following:

$$Y(T_0) \equiv \frac{1}{T_0} \int_0^{T_0} \frac{(dT/\rho dx)_r}{(dT/\rho dx)} dT,$$ (8.45)

where,

$$(dT/\rho dx) = (dT/\rho dx)_c + (dT/\rho dx)_r.$$ (8.46)

The average amount of energy radiated is $T_0 Y(T_0)$. Thus, according to Figure 8.9, the average amount of radiated energy between two kinetic energies is the following:

$$\sum (h\nu)_{T_1 \to T_2} = T_1 Y(T_1) - T_2 Y(T_2).$$ (8.47)

If $Y(T_0)$ is averaged over all initial energies of electrons and positrons set in motion by photons, then the result is g, the average fraction of the initial kinetic energy lost due to radiative interactions (positron annihilation-in-flight is ignored at this moment, i.e., we do not count the annihilation photons as part of the bremsstrahlung). Therefore,

$$g = \frac{1}{\Phi} \int_0^{T_{max}} Y(T_0) \Phi'(T_0) dT_0.$$ (8.48)

where the quantity Φ is the initial fluence of electrons set in motion, which is given by the following:

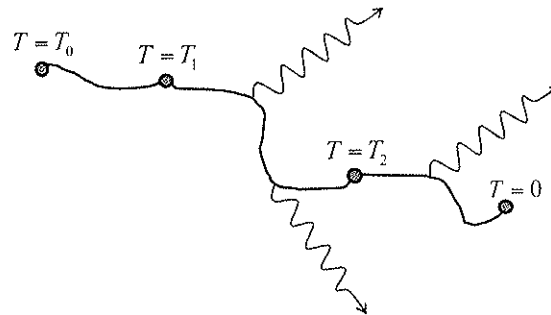$$\Phi \equiv \int^{T_{max}} \Phi'(T_0) dT_0.$$ (8.49)

Figure 8.9. Geometry of bremsstrahlung radiation in the particle's track.

[*]In ICRU-37, it is assumed that the charged particle doesn't create any secondaries as it slows down: continuous slowing down.

The quantity $\Phi'(T_0)$ is the initial energy spectrum of electrons set in motion by all photon interactions, and T_{max} is the maximum initial kinetic energy.

Elastic Scattering

When a charged particle interacts with a nucleus and there is no bremsstrahlung, the most likely thing to have happened is elastic scattering (Figure 8.10). Ernest Rutherford (1911) explored the elastic scattering cross section while he was studying the structure of the nucleus. Regarding Figure 8.10, Rutherford's (elastic) scattering cross section is given by the following:

$$\frac{d\sigma_{Ruth}}{d\Omega_\theta} = \frac{z^2}{4}\left(\frac{e^2}{Mc^2}\right)^2\left(\frac{(1-\beta^2)}{\beta^4}\right)\left(\frac{1}{\sin^4(\theta/2)}\right). \tag{8.50}$$

Note that the elastic cross section is proportional to $1/M^2$, so heavy charged particles scatter *much less* than electrons and positrons. The cross section is also proportional to $1/\beta^4$, therefore scattering is much more likely for low-energy (speed) particles and the $1-\beta^2$ factor further decreases the scattering probability as $\beta \to 1$.

According to Equation (8.50), an individual elastic scattering event is much more likely to happen for small angles since the Rutherford cross section is proportional to $1/\sin^4(\theta/2)$.

The Rutherford theory *really* only applies to *heavy* charged particles of zero spin, so its application to electrons is a stretch. This cross section also doesn't really apply to $\beta > 2z/137$ (Born approximation). Mott (1929,1932) used both the relativistic Dirac theory of the electron and the Born approximation. McKinley and Feshbach (1948) found an acceptable analytical formulation of Mott's result for most situations. For electrons, their formulation is as follows:

$$\frac{d\sigma_{M-F}}{d\Omega_\theta} = \frac{d\sigma_{Ruth}}{d\Omega_\theta}\left[1 - \beta^2\sin^2(\theta/2) + \pi\beta(z/137)(1-\sin(\theta/2))\sin(\theta/2)\right]. \tag{8.51}$$

The McKinley–Feshbach result is valid for $\beta \approx 1$ if $(z/137) < 0.2$, so it is more appropriate for describing electron and positron scattering in low-atomic-number materials. We can see that for small scattering angles or low particle velocity, the McKinley–Feshbach equation reduces to the Rutherford equation.

Multiple Scattering

After a large number of small scattering events, the particle's direction can change significantly: this is called
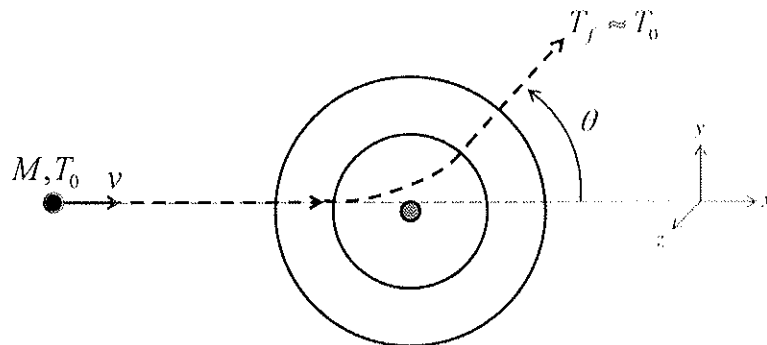

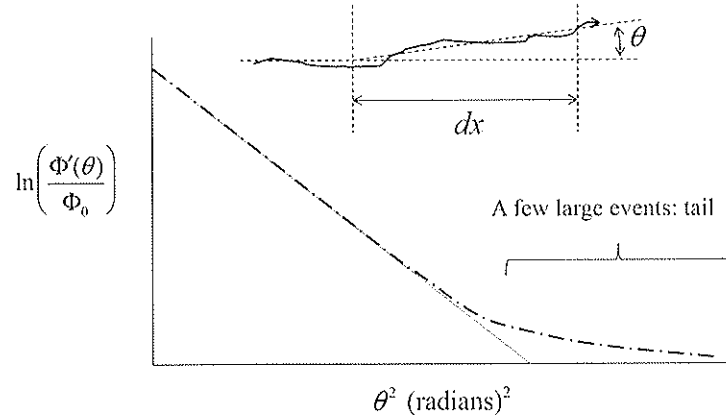**Figure 8.10.** The geometry of elastic scattering.

Figure 8.11. Gaussian multiple scattering showing an additional non-Gaussian component.

multiple scattering. The distribution of angle from the original electron direction after a beam of electrons have traveled a distance, dx, is illustrated in Figure 8.11.

In Figure 8.11, the quantity $\Phi'(\theta)/\Phi_0$ is the angular distribution of electrons having an angle θ normalized to the direction of the incident fluence Φ_0. The plot in Figure 8.11 suggests that the multiple small-angle scattering events are basically Gaussian, with a tail described by a deviation from a Gaussian. The equation for multiple Gaussian small-angle scattering is given by the following:

$$\frac{d\Phi}{d\theta} = \frac{\Phi_0}{\sqrt{2\pi\left\langle\theta^2\right\rangle}}\exp\left\{-\theta^2/2\left\langle\theta^2\right\rangle\right\},$$

(8.52)

where $\left\langle\theta^2\right\rangle$ is the mean square scattering angle and represents the variance (square of the standard deviation) in the angle of scattering.

Let's assume that a particle traverses a medium between x and $x+dx$ with a density ρ. The value of $\left\langle\theta^2\right\rangle$ at $x+dx$ is $\left\langle\theta^2\right\rangle+d\left\langle\theta^2\right\rangle$. Thus,

$$\frac{d\left\langle\theta^2\right\rangle}{\rho dx} = 2\pi\frac{N_A}{A}\int_{\theta_{min}}^{\theta_{max}}(\theta^2)\frac{d\sigma_{Ruth}}{d\Omega_\theta}\sin\theta d\theta.$$

(8.53)

The **maximum scattering angle** occurs when the particle comes very close to the nucleus. For this case, the finite size of the nucleus has to be accounted for. Also, there is a **minimum scattering angle** because of the electron screening of the nuclear charge. These limits are as follows:

$$\theta_{max} \cong 280A^{-1/3}\frac{\sqrt{1-\beta^2}}{\beta},$$

(8.54)

$$\theta_{min} \cong \frac{1}{137}z^{1/3}\frac{\sqrt{1-\beta^2}}{\beta}.$$

(8.55)

Now substituting Rutherford's scattering formula and using the *small-angle* approximation that $\theta \Rightarrow \theta$, **multiple angle scattering power** is given by the following:

$$\frac{d\langle\theta^2\rangle}{\rho dx} = 2\pi \frac{N_A}{A} \frac{z^2 r_0^2}{4} \frac{(1-\beta^2)}{\beta^4} \int_{\theta_{min}}^{\theta_{max}} (\theta^2) \frac{1}{(\theta/2)^4} \theta d\theta,$$

$$= 8\pi \frac{N_A}{A} z^2 r_0^2 \frac{(1-\beta^2)}{\beta^4} \ln\left(\frac{\theta_{max}}{\theta_{min}}\right), \qquad (8.56)$$

$$= 16\pi \frac{N_A}{A} z^2 r_0^2 \frac{(1-\beta^2)}{\beta^4} \ln\left(196(z/A)^{1/6} z^{-1/3}\right).$$

To a good approximation, Equation (8.56) can be expressed in terms of the radiation length, χ_0, as follows:

$$\frac{d\langle\theta^2\rangle}{\rho dx} \cong \frac{4\pi}{1/137} \frac{(1-\beta^2)}{\beta^4} \frac{1}{\chi_0}. \qquad (8.57)$$

The complete treatment of electron scattering should use Mott scattering and include the effects of a few large plural scatterings, as well as include the elastic and inelastic interaction with electrons and inelastic bremsstrahlung interactions. The complexity of electron scattering, with some non-Gaussian behavior as well, has so far only yielded to detailed analysis with Monte-Carlo computer simulation methods. One can also always create empirical tabulated data for standard field shapes and experimental setups, but then the tables are not easy to translate into non-standard situations.

Particle Range

The **range**, R, is the expectation value of the path length (not a straight line, in general) through a medium as a particle comes to rest. The range is a derived quantity, and there are various ways to describe it, as we will discuss.

If the energy loss were truly continuous, then all of the particles would have the same path length. That range approximation is called the **continuous slowing down approximation (CSDA)** and is given by the following:

$$R_{CSDA} \equiv \int_0^{T_0} \left(\frac{dT}{\rho dx}\right)^{-1} dT. \qquad (8.58)$$

The stopping power only defines the *average* energy loss per unit distance. There can be differences in the rate of energy losses due to stochastic variation. More importantly, there can be large discrete energy losses due to knock-on or γ-ray production and bremsstrahlung production. The distribution of relative energy losses in crossing a path ρdx would look like Figure 8.12.

$\Phi'(T'/T_0)$

$\left(\frac{dT}{\rho dx}\right)_c \frac{\rho dx}{T_0}$ with statistical variations

Long tail due to discrete interactions

Almost zero probability of losing none its energy

Finite probability of losing all its energy

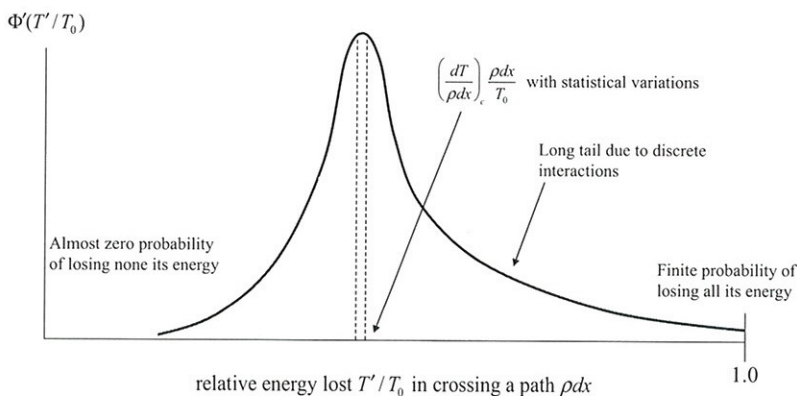relative energy lost T'/T_0 in crossing a path ρdx

1.0

Figure 8.12. The distribution of relative energy losses showing the most probable value and it's variation in crossing a path ρdx.
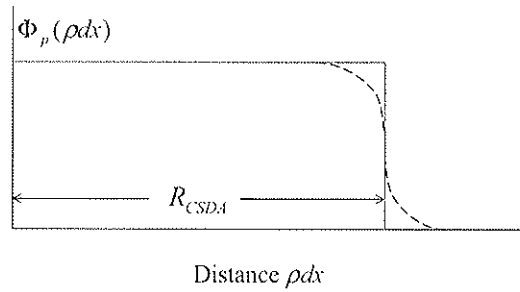
Figure 8.13. Heavy particle planar fluence over distance from a single beam from the left showing Gaussian range straggling.

The variation shown in Figure 8.12 is called **range** (or equivalently "**energy**") **straggling**: a particle may vary in range from another. When integrating along the path, considering net flow crossing the plane, one gets a more common picture (Figure 8.13). One can use the planar fluence $\Phi_p(\rho dx)$ to describe net flow in one direction: useful for some range calculations, but not useful for dosimetry, which does not care what the direction of travel is. Note that it will be very close to the fluence with small amounts of multiple scattering that can change net angle crossing a plane perpendicular to the original direction. See Kempe and Brahme (2010) for an analytical treatment of planar fluence versus ordinary fluence for Li ions, which have significant secondary fragment particles along their path. This is different from protons, which would look more like Figure 8.13.

Some heavy particles straggle significantly if not fully ionized: $(Z^*/Z)<1$. This leads to the range being slightly larger than the CSDA range for $Z>1$ particles.

Calculating the CSDA Range

Just as we could find the stopping power of any heavy particle knowing the proton stopping power, we can find the range of any heavy particle knowing the proton range. A table of proton ranges is given in Bichsel (1968).

All heavy particles (not electrons) with the same charge and speed have the approximately same stopping power. The kinetic energy of a particle is proportional to its rest mass: $T/Mc^2 = \gamma-1$. The stopping power of a multiply charged particle, m, has Z^{2m} times the stopping power of a singly charged heavy particle for the same β. Therefore, to calculate the CSDA range for any heavy ion, first look up the $(R_{CSDA})_{proton}$ for (a proton) of energy $T_p = (M_p/M)T$ where T and M are the energy and mass of a heavy charged particle, and M_p is the proton's mass. Then calculate the CSDA range by the following:

$$R_{CSDA}\left(\frac{Z^2}{M}\right) = (R_{CSDA})_p\left(\frac{(1)^2}{M_p}\right). \tag{8.59}$$

Projected Range

The **projected range**, $\langle t \rangle$, is the expectation value of the farthest depth (not a straight line in general, and may come back on itself) through a medium as a particle comes to rest. If N_0 is the incident number of particles, then the projected range is given by the following:

$$\langle t \rangle \equiv \frac{1}{N_0}\sum_1^{N_0} t_{farthest}. \tag{8.60}$$
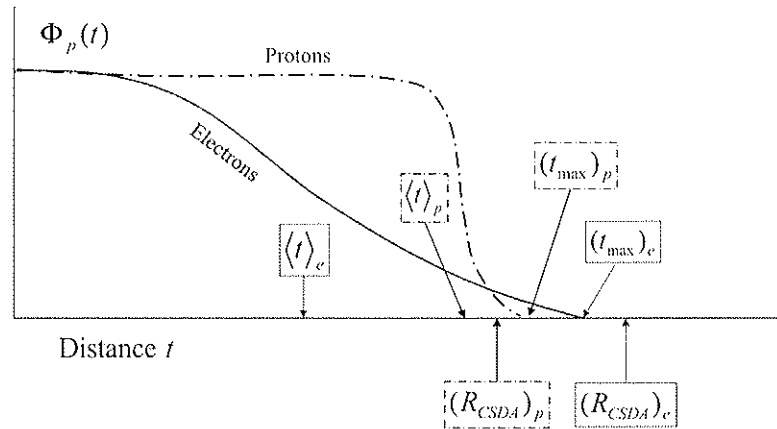
Figure 8.14. The projected ranges "$<t>$" are compared to the maximum ranges "(t_{max})" and the CSDA ranges "(R_{CSDA})" for heavy charged particles (such as protons) versus electrons. Note that the heavy scattering of electrons means that the *CSDA* range overestimates range for electrons—a useful way to make conservative approximations. For the heavy particles, all three values are close together: the heavier the particle, the more this is true.

For low-energy electrons, the projected range is less than R_{CSDA} because of scattering, so the CSDA range for electrons is a convenient overestimate. The amount of multiple scattering and energy straggling for protons and other heavy charged particles is small so that $\langle t \rangle_p \sim (R_{CSDA})_p$ (Figure 8.14). The amount of multiple scattering for electrons is high (recall that the scattering cross section is proportional to $1/M^2$). In fact, the amount of electron scattering is so high that it is unlikely that an electron could have penetrated without scattering. Therefore, $R_{CSDA} \geq t_{max}$ for electrons where t_{max} is the maximum penetration depth for electrons.

Practical Range

The **practical range** or **extrapolated range**, R_p, is used for electron beams and is defined at the intersection of the fall-off in the electron dose extrapolated to zero dose, and the asymptotic extrapolation of the bremsstrahlung tail as shown in Figure 8.15. From Attix (2004), we have the following:

$$R_p \approx 0.54 \frac{\text{g}}{\text{cm}^2 \times \text{MeV}} \cdot T_0 - 0.30 \frac{\text{g}}{\text{cm}^2}. \tag{8.61}$$

Figure 8.15. Illustration of the method to obtain the practical range: used for electron beams.

The mean kinetic energy as a function of thickness, t, is given by a couple of formulas as follows:

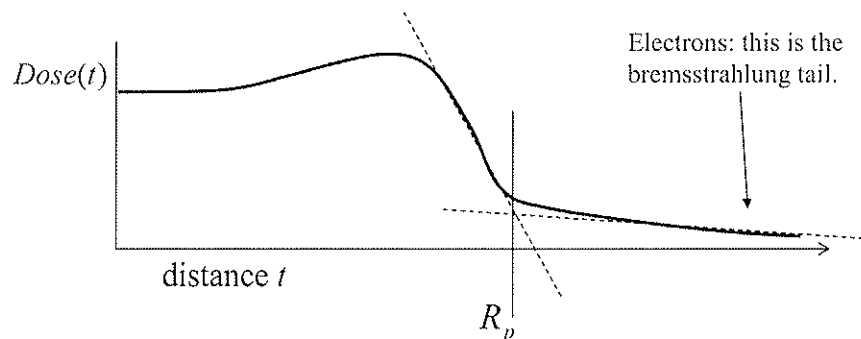$$\bar{T} = \frac{T_0}{(S_r)_0}\left\{\left[(S_r)_0 + (S_c)_0\right]e^{-(S_r)_0 t / T_0} - (S_c)_0\right\}.$$

(8.62)

where, $(S_r)_0 \equiv (dT_{(x=0)}/dx)_r$ and $(S_c)_0 \equiv (dT_{(x=0)}/dx)_c$ are the radiative and collisional stopping powers respectively, evaluated at the surface of the material, and T_0 is the initial electron energy. This gives a very handy equation as the following:

$$\bar{T} \approx T_0(1 - t/R_p).$$

(8.63)

The distribution of electrons in a medium is best modeled with Monte-Carlo methods: beyond the scope of this book.

References

Anderson, D.W. *Absorption of Ionizing Radiation*. Baltimore: University Park Press, 1984.

Attix, F.H. *Introduction to Radiological Physics and Radiation Dosimetry*. Weinheim, Germany: WILEY-VCH Verlag GmbH & Co. KGaA, 2004.

Bethe, H. and W. Heitler. (1934). "On the Stopping of Fast Particles and on the Creation of Positive Electrons." *Proc. Roy. Soc. Lond.* A146:83–112.

Bhabha, H.J. (1932). "The Scattering of Positrons by Electrons with Exchange on Dirac's Theory of the Positron." Proc. *Roy. Soc.* London, A 154:195.

Bichsel, H. "Charged-Particle Interactions." In *Radiation Dosimetry*, Vol 1. F.H. Attix, W.C. Roesch, and E. Tochilin, Eds. New York: Academic Press, 1968.

Bohr, N. (1913). "On the Theory of the Decrease of Velocity of Moving Electrified Particles on Passing Through Matter." *Phil. Mag. and J. of Sci.* 25:10–31.

Evans, R.D. *The Atomic Nucleus*. Malabar, Florida: Krieger Publishing Co., 1955.

Fermi, E. (1940). "The Ionization Loss of Energy in Gases and in Condensed Materials." *Phys. Rev.* 57:485.

Hall, E.J. *Radiobiology for the Radiologist*, 6th ed. Philadelphia: Lippincott Williams & Wilkins, 2006.

ICRU. *Radiation Dosimetry: Stopping Powers for Electrons and Positrons*. Report No. 37. Washington, D.C.: International Commission on Radiation Units and Measurements, 2007.

Jackson, J.D. *Classical Electrodynamics*, 3rd Ed. New York: Wiley, 1999.

Kempe, J. and A. Brahme. (2010). "Analytical Theory for the Fluence, Planar Fluence, Energy Fluence, Planar Energy Fluence, and Absorbed Dose of Primary Particles and Their Fragments in Broad Therapeutic Light Ion Beams. *Phys. Med.* 26:6–16.

McKinley, W.A. and H. Feshbach. (1948). "The Coulomb Scattering of Relativistic Electrons by Nuclei." *Phys. Rev.* 74:1759.

Möller, C. (1932). "Zur Theorie des Durchgangs schneller Elektronen durch Materie." *Ann. Phys.* 14:531.

Mott, N.F. (1932). "The Polarisation of Electrons by Double Scattering." *Proc. R. Soc. London A* 135:411–28.

Rutherford, E. (1911). "The Scattering of α and β Rays by Matter and the Structure of the Atom." *Philos. Mag.* 21:669–88.

Swann, W.F.G. (1938). "Theory of Energy Losses of High Energy Particles by L. W. Nordhein, Ph.D. Discussion." *J. Frank. Inst.* 226:598–600.

Weaver, B.A. and A.J. Westphal. (2002). "Energy loss of relativistic heavy ions in matter." *Nucl. Instrum. Methods. Phys. Res. B.* 187:285–301.

9

Radiation Equilibrium

Following a similar treatment in Attix (2004) assume a spatially infinite source of radiation. It can be both ionizing or nonionizing. A perfect example would be radioactivity in the ocean. As long as the dimensions of the space are much larger than the mean free path of the radiation, it will approach this ideal situation. The ideal situation we are describing has the following characteristics:

- homogeneous atomic composition,
- homogeneous density,
- homogeneous distributed source, and
- homogeneous electric and magnetic fields: zero is even better (what we will consider).

The most important assumption to remember for equilibrium is *for every interaction sequence, there is a spatially reciprocal sequence*[*].

Therefore, radiation equilibrium means that the number and energy (i.e., the energy spectrum) of particles going into a volume must be the same as leaving the volume dv with a mass dM. See Figure 9.1.

As a result, radiation equilibrium exists under the following conditions:

1. **Spectrum of photons entering = spectrum of photons leaving**

$$\Phi'(hv)\,|_{in} = \Phi'(hv)\,|_{out} \tag{9.1}$$

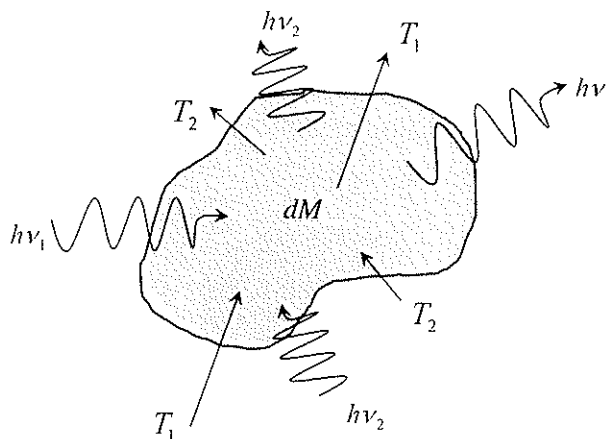$$\Psi'(hv)\,|_{in} = \Psi'(hv)\,|_{out} \tag{9.2}$$

Figure 9.1. A differential mass and volume experiencing radiation equilibrium.

*Some condition on the continuity and homogeneity of the radiation field is required.

2. Spectrum of charged particles entering = spectrum of charged particles leaving

$$\Phi'(T)\big|_{in} = \Phi'(T)\big|_{out},\tag{9.3}$$

$$\Psi'(T)\big|_{in} = \Psi'(T)\big|_{out}.\tag{9.4}$$

In a relaxation of the spectrum constraint, if the above is true, then we can say that the radiant energy "in" must be the same as the radiant energy "out" for all types of particles, charged and uncharged.

$$R_{in}\big|_u = R_{out}\big|_u,\tag{9.5}$$

$$R_{in}\big|_c = R_{out}\big|_c.\tag{9.6}$$

The *energy imparted* to a volume is given by the following:

$$\varepsilon = R_{in}\big|_u - R_{out}\big|_u + R_{in}\big|_c - R_{out}\big|_c + \sum Q\tag{9.7}$$

where $\sum Q$ is the sum of the rest mass energy converted to kinetic energy (excludes neutrinos). This is best way to express the energy imparted. It is positive if rest mass is lost. For radiation equilibrium, the energy imparted is given as follows:

$$\varepsilon = \sum Q.\tag{9.8}$$

The *absorbed dose* for radiation equilibrium in this ideal case is equal to the following:

$$D = \frac{d\varepsilon}{dM} = \frac{d\left(\sum Q\right)}{dM}.\tag{9.9}$$

The radiation equilibrium concept is especially important for nuclear medicine and health physics issues. For external beam radiotherapy, we will have to make conceptual adjustments: the spatial invariance cannot be strictly satisfied.

If all the secondary particles are in equilibrium (secondary electrons and photons), then the attenuation of the primary beam will equal the dose. The energy imparted is simply the energy removed from the primary beam. In most cases, the secondary photons will not be in equilibrium from a unidirectional beam. This will lead to the transient charged particle equilibrium concept, discussed in detail later. Therefore, the following upper limit on dose is an idealized situation (Figure 9.2). In general, terma sets an upper limit to dose as follows:

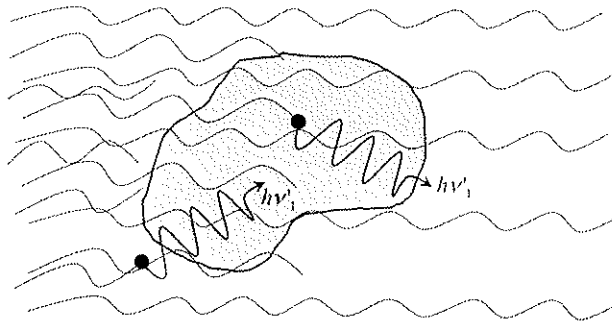$$D \Leftarrow TERMA = \Psi \frac{\mu}{\rho}.\tag{9.10}$$

Figure 9.2. A differential volume experiencing equilibrium of secondary photons which is, in general, not likely. In this case, the dose would be the terma.
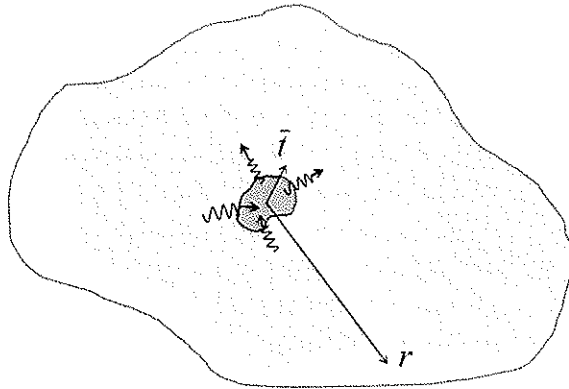
Figure 9.3. This inner medium is experiencing radiation equilibrium even though it is part of a larger but finite medium.
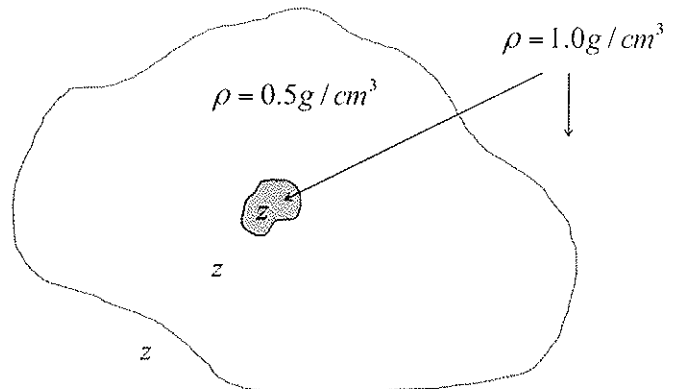

Figure 9.4. Fano's theorem would say that the mass attenuation coefficient and the mass stopping power would be uniform in this figure.

The concept of radiation equilibrium will still apply for media that don't fit the stringent conditions above. An infinite medium is not required as long as the mean free path of the uncharged particle is much less than a typical radius to the edge of the volume. That is, $\bar{l} \ll r$, where $\bar{l}$ is mean free path of the photons and r is the radius to the edge of the volume (Figure 9.3).

Note that we have left out the charged particles lately. In general, if $\bar{l} \ll r$, then $t_{max} \lll r$ where t_{max} is the maximum range of charged particles: usually $t_{max} \ll \bar{l}$ is a safe assumption in medical applications.

Fano's Theorem

Simply stated, Fano's Theorem is that a homogeneous density is not required for radiation equilibrium as long as the source strength, the attenuation of uncharged particles, and the stopping power are all proportional to density.

A rigorous treatment of this theorem has been formulated by Spencer (1975). Fano's theorem is normally roughly true. The stopping power and the attenuation coefficient are dominantly proportional to density: that's why we use *mass* attenuation and *mass* stopping powers. However, at therapy energies, say >1 MeV, the density effect will cause Fano's theorem violations.

The various materials that make up the region of interest must have the same or very similar atomic composition. This leads to the "*tissue equivalent*" concept one often hears: amounts to a z-effective requirement.

For radiation equilibrium to apply in the 0.5 g/cm³ region illustrated in Figure 9.4, the source density must be 1/2 of the rest of the media, and the atomic numbers must be equal in all the regions.

Charged Particle Equilibrium

For charged particle equilibrium, we need to address the situation of $\bar{l} \not< r$, and yet $t_{max} \ll r$. It is still based on $t_{max} \ll \bar{l}$. Therefore, we do not satisfy radiation equilibrium. However, let's observe that we *do* have an equilibrium for charged particles:

$$R_{in}\big|_u \neq R_{out}\big|_u,$$

(9.11)

$$R_{in}\big|_c = R_{out}\big|_c.$$

(9.12)

Therefore, the energy imparted is equal to the following:

$$\varepsilon = R_{in}\big|_u - R_{out}\big|_u + \sum Q.$$

(9.13)
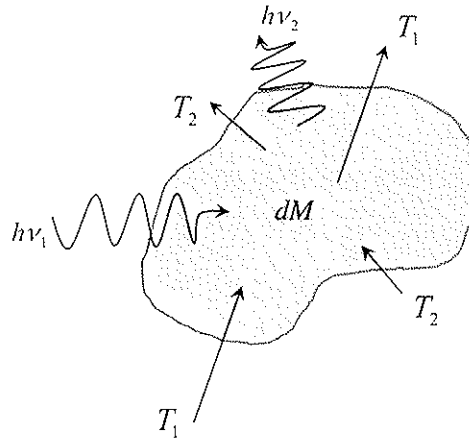
Figure 9.5. A differential mass and volume experiencing charged particle equilibrium.

If radiation equilibrium exists, then so does charged particle equilibrium, but the reverse is not true since $t_{max} \ll \bar{t}$. So, charged particle equilibrium can exist without radiation equilibrium (Figure 9.5), and it usually does.

If $\bar{t} \gg r$, then almost no uncharged particles will interact. Therefore, the absorbed dose in dV will only be due to radioactive decays that produce charged particles (β-decay and α-decay):

$$R_{out} \big|_u = R_{in} \big|_u + \left(\sum Q \right)_u . \tag{9.14}$$

By substituting Equation (9.14) into (9.13), the energy imparted will then be given by the following:

$$\varepsilon = \left(\sum Q \right)_c . \tag{9.15}$$

So then the dose would be the following:

$$D = \frac{d \left(\sum Q \right)_c}{dM} , \tag{9.16}$$

where, $\left(\sum Q \right)_u = \left(\sum Q \right) - \left(\sum Q \right)_c$, the rest energy given to uncharged particles (like photons or neutrons, but not neutrinos that have fantastically huge mean free paths).

The dose is difficult to calculate analytically in the following situations:

1. Charged particle equilibrium does not exist because source region is too small ($r \leq t_{max}$).
2. Charged particle equilibrium does exist, but a *significant amount of photons interact in the source volume*; however, the source volume is not large enough to establish radiation equilibrium ($t_{max} \ll r \leq \bar{t}$).
3. The source volume is large enough to establish radiation equilibrium, but the atomic composition is not homogeneous or the source strength is not proportional to density.

For these types of cases, Monte-Carlo calculations should be used. The reader is encouraged to see Attix (2004) for discussions about the inclusion of electric and magnetic fields for radiation and charged particle equilibrium.

Exposure

The old quantity of **exposure**, X, or long ago called *exposure dose*, has an equilibrium concept intrinsic to its formal definition, but it is often used informally.

Exposure, X, is defined via the ICRU (1980) definition as: "The quotient of the dQ by dm, where the value of dQ is the absolute value of the total charge of the ions of one sign produced in air when all of the electrons (negatrons and positrons) liberated by photons in air of mass dm are completely stopped in air." In this definition, note that the charges are *liberated*, not collected. They are liberated by *photons*, and only in *air*. Also note that the secondary electrons are starting and *completely stopping* in the air. The *completely stopped in air* implies CPE. Therefore, exposure is given by the following:

$$X = \psi \left(\frac{\mu_{en}}{\rho} \right)_{E,air} \left(\frac{1}{\overline{W}/e} \right)_{air} = \frac{(K_c)_{air}}{(\overline{W}/e)_{air}} = (K_c)_{air} / (33.97 J/C). \tag{9.17}$$

Under CPE conditions, the dose is proportional to exposure ($X \propto (K_c)_{air}$), and it was originally called "exposure dose."

The SI unit of exposure is C/kg for dry air. The historical unit is the roentgen (R), and it is defined as the exposure that produces one *esu* of charge of either sign in 1 cm^3 of dry air at 760 torr and 0 °C. ρ_{air} at these conditions is 0.001293 g/cm^3):

$$1R = \frac{1 \text{ esu}}{\text{cm}^3} \cdot \frac{1}{0.001293 \text{ g}/\text{cm}^3} \cdot \frac{1 \text{ C}}{2.998 \times 10^9 \text{esu}} \cdot \frac{10^3 \text{g}}{\text{kg}} = 2.58 \times 10^{-4} \text{C}/\text{kg}. \tag{9.18}$$

Attix (2004) calls the exposure the third most important quantity, and that is certainly true historically. He says one would "puzzle" over the definition to get the following interpretation: "The exposure X is the ionization equivalent of the collision kerma, K_c, in air for x-rays and γ-rays."[*]

However, kerma places no conditions that one is at equilibrium.

The phrase "completely stopped in air" is certainly implying some type of charged particle equilibrium. So, it is probably fine to rigorously use it for typical diagnostic energies, but it's a real conceptual stretch for its use in radiotherapy beams. Just be aware that many people use it like Attix does—as a stand-in for collision kerma.

If the *photon* beam is not monoenergetic, then do the following:

$$X = \int_{hv=0}^{hv_{max}} \psi'(hv) \cdot \left(\frac{\mu_{en}}{\rho} \right)_{air} \cdot \frac{1}{(\overline{W}/e)_{air}} d(hv), \tag{9.19}$$

where $\psi'(hv)$ is the energy spectrum of the energy fluence for photons, and μ_{en}/ρ depends on photon energy.

The exposure rate then is calculated by the following:

$$\dot{X} = \int_{hv=0}^{hv_{max}} \dot{\psi}'(hv) \cdot \left(\frac{\mu_{en}}{\rho} \right)_{air} \cdot \frac{1}{(\overline{W}/e)_{air}} d(hv). \tag{9.20}$$

The CPE condition is fulfilled for many diagnostic energy situations. For a therapy beam, though, it is generally not. However, people use exposure for all types of situations as a stand-in for collision kerma. Since air is reasonably close to tissue equivalence, it is also a stand-in for dose. However, at low energies, this equivalence is less valid, and yet, that is where the implied CPE condition is more likely to be satisfied. This quantity is, therefore, problematic if taken too literally.

---

[*]Find more of Attix's (2004) feelings about exposure on pages 32–34.

The only way to directly measure exposure according to the 1980 ICRU definition is with a free-air ionization chamber, a very specialized open-cavity well described in Attix (2004). In general, one can only do this practically up to photon energies of 300 keV.

For a typical therapy energy beam, the dimensions of the region-of-interest for CPE must be greater than the range of charged particles in that medium.

Transient Charged Particle Equilibrium

Up to now, we have anchored the discussion on uniformly distributed radioactivity. However, much of the time we are using external beams. To handle the nonuniformity of an external photon beam, another type of charged particle equilibrium is considered. With transient charged particle equilibrium, the secondary charges from the photon interactions have a relationship that is constant in space. That relationship is not an equality between dose and collision kerma; it is a proportionality between dose and collision kerma.

In Figure 9.6, the dose builds up to a maximum at d_{max}, and then reduces with depth. At depths $x > t_{max}$, the maximum range of the charged particles, the dose follows the collision kerma proportionally. This is **transient charged particle equilibrium**, TCPE, and it can be thought of as a spatial shift, $\bar{x}$, as the following:

$$D(x) = K_c(x - \bar{x}).$$ (9.21)

It can also be thought of as a constant buildup with a factor, β, as the following:

$$D(x) = K_c(x)\beta.$$ (9.22)

β is dimensionless and greater than or equal to 1.

The collision kerma is directly proportional to the fluence, which decreases exponentially due to attenuation as follows:

$$K_c(x) = K_c(x - \bar{x})e^{-\mu\bar{x}}.$$ (9.23)

This allows for us to relate the collision kerma ratio from Equation (9.23) to β as the following:

$$\beta = e^{\mu\bar{x}} \cong 1 + \mu\bar{x}.$$ (9.24)

Note that μ here is generally μ'. It depends on the geometry.
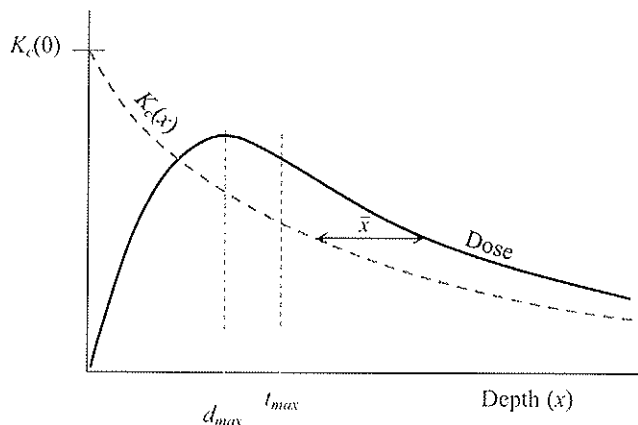
Figure 9.6. Transient charged particle equilibrium exists for x > t$_{max}$ where the ratio of Dose to collision kerma, K_c, does not change.

The issue for both TCPE and CPE is that the secondary photons (scattered, fluorescent, annihilation) will not contribute to the dose within a distance, $\bar{x}$. Therefore, CPE and TCPE are approximations that do not directly account for secondary, mostly scattered, photons.

Mackie et al. (1988) computed a table with $\bar{x}$ and β in 1993 with Monte-Carlo for monoenergetic photons (no scattered photons).

In summary, for the CPE for a photon beam, we have the following:

$$D \propto K_c, \tag{9.25}$$

$$D = \beta K_c, \tag{9.26}$$

$$D = (1 + \mu'\bar{x})K_c. \tag{9.27}$$

Note that this β is not the same as the Burlin cavity theory β.

References

Attix, F.H. *Introduction to Radiological Physics and Radiation Dosimetry.* Weinheim, Germany: WILEY-VCH Verlag GmbH & Co. KGaA, 2004.

Mackie, T.R., A.F. Bielajew, D.W.O. Rogers, and J.J. Battista. (1988). "Generation of photon energy deposition kernels using the EGS Monte Carlo code," *Phys. Med. Biol.* 33:1–20.

Spenser, L.V. (1975). "Some Comments on Fano's Theorem." *Radiat. Res.* 63:191–99.

10

Absorbed Dose in Media Containing Radioactive Materials

In this chapter, after briefly explaining radioactive decay, we will discuss five important radioactive decay processes and their dose rate calculations. Finally, we will generalize dose rate calculation for all five processes in one equation.

Radioactive Decay

For a large number N of identical radioactive atoms, the rate of disintegrations, $\dfrac{dN}{dt}$, is proportional to N at any time as follows:

$$\frac{dN}{dt} = -\lambda N, \qquad (10.1)$$

where the coefficient of proportionality, λ, is called **total radioactive decay constant** and has the units of s^{-1}. Note that the minus sign shows that as time increases, the number of radioactive atoms will decrease. The quantity of λN is called radiation **activity**, A, and is defined as the total number of atoms that disintegrate per unit time. The SI unit of radioactivity is the becquerel (Bq) and simply given by the following:

$$1 \text{ Bq} = 1 \text{ disintegration/s.} \qquad (10.2)$$

The total decay constant, λ, is related to the **half-life** of the radioactive nuclide $t_{1/2}$ (the time needed for half of the radioactive atoms to disintegrate) by the following:

$$\lambda = \frac{\ln 2}{t_{1/2}}. \qquad (10.3)$$

Alpha Decay

As a quick conceptual introduction, alpha decay occurs mainly in heavy nuclei with atomic numbers greater than 82. In this process, a heavy nucleus emits an alpha particle to reach a stable nuclear configuration. An "alpha" particle is a helium nucleus. Equation (10.4) illustrates an example of alpha decay:

$$^{222}_{88}\text{Ra} \rightarrow {}^{218}_{86}\text{Rn} + {}^{4}_{2}\text{He}. \qquad (10.4)$$

There is also energy released that goes into the products of the reaction. Until 1929, people thought each alpha-emitting species had only an alpha energy. The fine structure (alpha decay to several different excited
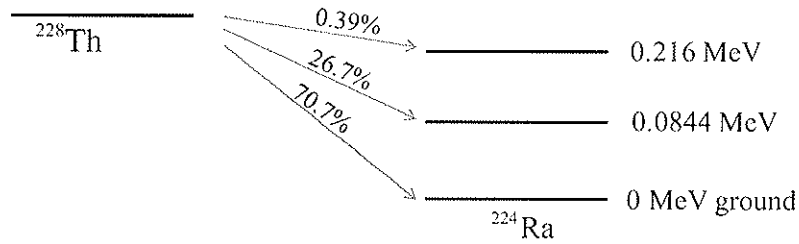
Figure 10.1. Example alpha decay showing higher probability of decay to ground state.
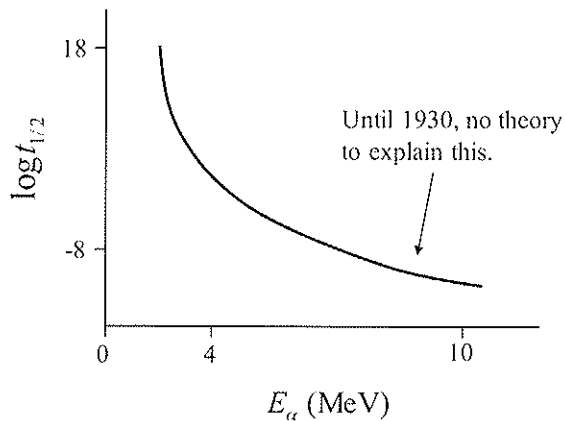

Figure 10.2. Characteristic relationship for alpha decay between half-life and alpha energy. Higher energy decays are more likely to occur, and large alpha energies have short half-lives.
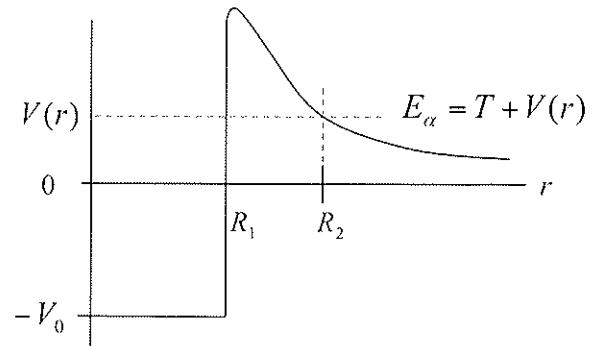
Figure 10.3. At large distances, when the nuclear electrostatic potential is very weak, the kinetic energy of the alpha particle is equal to its total energy. The nuclear force is very short range and plays no role beyond the nuclear radius.

states) was hard to observe at that time. There is a very strong dependence of decay probability on the decay energy for each resulting excited state. Decay to the ground state is much more likely.

Consider the example in Figure 10.1. The decay to the 0.216 MeV state happens only 0.39% of the time, and it's only 0.216 MeV less in energy. Therefore, it is very hard to observe. Figure 10.2 illustrates the relationship between the half-life and decay energy. This relationship derives directly from the physical nature of alpha decay.

The alpha particle (helium nucleus) is the first completed nuclear shell. It is very stable, but it is emitted out of a nucleus that is very unstable. It would be impossible from classical physics because it requires that the alpha particle "tunnel" through the potential barrier shown in Figure 10.3.

The mathematical description of alpha decay derives from a solution to the Schrödinger equation, and this was first explained by Gamow in 1928 (see Gamow, 1928). The solution provides for the probability of quantum tunneling through the potential barrier and is a function of the potential barrier height and width, as well as the total alpha energy. This probability then directly relates to the half-life[‡]. For example, one important fact is that angular momentum plays a very minor role in this case, but not for other decays, like beta and gamma. The total alpha energy and the recoil energy of the resulting (daughter) nucleus together share the total rest mass energy released in the reaction. For dosimetry, the energy of these particles and any gamma rays from an excited state are the main concern, so our focus will shift to energy balances now.

[‡]For more details and discussion of the nature of alpha decay, see Evans (1955).

Alpha Decay Specific to Dosimetry

In alpha decay, the *energy balance* is a main concern for us. Equation (10.5) shows an alpha decay process in general:

$$\,^A_Z X \rightarrow \,^{A-4}_{Z-2} Y + \,^4_2 He + \sum Q. \tag{10.5}$$

Alpha decay can result in an excited product (daughter) nucleus that then produces gamma decay (Figure 10.4).

The net rest mass energy released, $\sum Q$, is shared between the kinetic energy of the alpha, the recoil of the nucleus, and the subsequent gammas. Therefore, $\sum Q$ is calculated by the following from the mass excess tables[*]:

$$\sum Q = \Delta E_{parent} - (\Delta E_{daughter} + \Delta E_{\alpha}). \tag{10.6}$$

Note that the kinematics here are non-relativistic. The kinetic energy of the daughter product, T, is nowhere near the alpha rest mass:

$$T_{daughter} = \frac{\sum Q}{\dfrac{M_{daughter}c^2}{M_{\alpha}c^2}+1} = \frac{\sum Q}{\dfrac{A_{daughter}}{4}+1}. \tag{10.7}$$

Note that ΔE can be found in atomic mass excess tables. An example of an alpha decay energy calculation is the decay of radium to radon as the following:

$$\,^{226}_{88} Ra \rightarrow \,^{222}_{86} Rn + \,^4_2 He + 4.87 \text{ MeV}. \tag{10.8}$$

Radon is a major health physics concern. In addition, a gamma from this process is used for brachytherapy. Another example of the alpha decay process is the decay of radon to polonium. See Equation (10.9).

$$\,^{222}_{86} Rn \rightarrow \,^{218}_{84} Po + \,^4_2 He + 5.59 \text{ MeV}. \tag{10.9}$$

Here, only 5.49 MeV goes to the alpha particle. The quantity $\sum Q$ for the decay of $\,^{226}_{88} Ra$ is calculated as the following:

$$\sum Q = \Delta E_{Ra-226} - (\Delta E_{Rn-222} + \Delta E_{\alpha}) = 23623 \text{ keV} - (16329 + 2425) \text{ keV} = 4.87 \text{ MeV} \tag{10.10}$$
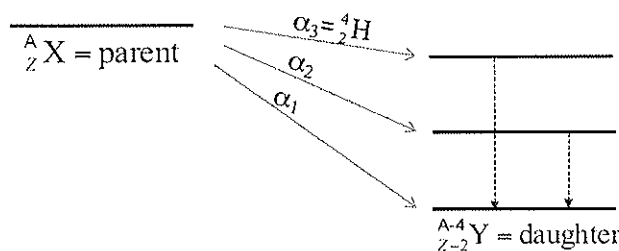
Figure 10.4. A general illustrative alpha decay showing possible excited states.

---

[*]Note that the mass excess is defined as the atomic mass differences relative to Carbon 12.
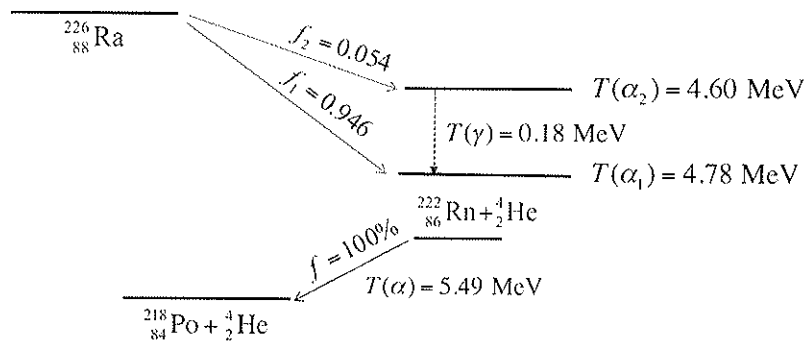
Figure 10.5. Example alpha decay scheme showing information important for dosimetry. Note the alpha energies are shown, not energy levels.

The kinetic energy of the radon is then equal to the following:

$$T_{(Rn-222)} = \frac{4.87 \text{ MeV}}{(222/4)+1} = 0.09 \text{ MeV}. \tag{10.11}$$

Therefore, energy available for the alpha and gammas is 4.87 MeV − 0.09 MeV = 4.78 MeV. For the decay of $^{222}_{86}\text{Rn}$, the quantity $\sum Q$ is calculated as follows:

$$\sum Q = \Delta E_{Rn-222} - (\Delta E_{Po-218} + \Delta E_\alpha) = 16{,}329 \text{ keV} - (8318 + 2425) \text{ keV} = 5.59 \text{ MeV}. \tag{10.12}$$

The kinetic energy of the polonium is then equal to the following:

$$T_{Po-218} = \frac{5.59 \text{ MeV}}{(218/4)+1} = 0.10 \text{ MeV}. \tag{10.13}$$

Energy available for the alpha in this process is then 5.59 MeV − 0.10 MeV = 5.49 MeV. The relative fraction of the decay that results in an alpha of kinetic energy T_α is f_i, which is called a "branching ratio." Figure 10.5 illustrates branching ratios for $^{226}_{88}\text{Ra}$ decay.

Dose Rate Calculations for Alpha Decay

For us, what we really need to care about the most is what to do with these energies in terms of equilibriums and dose *rates*. The dose rate is given by the following with mass, M, that receives the dose:

$$\dot{D}_\alpha = \frac{A}{M} \sum Q. \tag{10.14}$$

Therefore, in the case of *radiation equilibrium* (all photons interacting assumed) the dose rate is equal to the following:

$$\dot{D}_\alpha = \frac{A}{M} \sum Q = \frac{A}{M}\left(\left[\sum_{i=1}^{n} f_i\left(T_{\alpha_i} + h\nu_i\right) + T_{daughter}\right]\right). \tag{10.15}$$

However, in case of *charged particles equilibrium* (no photons interacting assumed) the dose rate is given by the following:

$$\dot{D}_\alpha = \frac{A}{M}\left(\sum Q\right)_c = \frac{A}{M}\left(\left[\sum_{i=1}^{n} f_i\left(T_{\alpha_i}\right) + T_{daughter}\right]\right). \tag{10.16}$$

Later, we will consider cases in between these limits. Before that point, we will explore these limits for each major decay.

Beta Decay

Beta decay is another radioactive process to reach a stable nuclear configuration. In this process, a proton is changed to a neutron or vice versa with emission 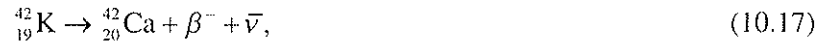of a beta particle. In changing a proton to neutron, the beta particle is an anti-electron, or positron, and is known as a beta plus, β^+. However, when a neutron is transformed to a proton, the beta particle is an electron, and is called a beta minus, β^-.

Beta minus decay tends to occur in nuclei with an excess of neutrons, and it is accompanied by a release of an anti-neutrino, $\bar{v}$, while beta plus decay tends to happen in nuclei with an excess of protons and is accompanied by a release of a neutrino, v. Equations (10.17) and (10.18) are examples of these two types of beta decay:

$$^{42}_{19}K \rightarrow {}^{42}_{20}Ca + \beta^- + \bar{v}, \tag{10.17}$$

$$^{23}_{12}Mg \rightarrow {}^{23}_{11}Na + \beta^+ + v. \tag{10.18}$$

Notice that in beta decay, the mass number stays the same. That is, the daughter product and the parent nuclei are the same isobar.

Beta Decay Specific to Dosimetry

As we mentioned before, for dosimetry, the energy balances of these radioactive processes are the main focus. Therefore, in general, we can write the β^- decay as follows:

$$^A_Z X + e^- \rightarrow {}^A_{Z+1}Y + \beta^- + \bar{v} + \sum Q. \tag{10.19}$$

The available energy is shared between the beta, the neutrino particles, and any gamma rays. The energy spectrum of each particle will be continuous, since it will vary randomly for each particular event. Some internal bremsstrahlung will also be possible.

The net rest mass energy released, $\sum Q$, for β^- decay is given by the following:

$$\sum Q = \Delta E_{parent} + 0.511\ MeV - (\Delta E_{daughter} + 0.511\ MeV),$$
$$= \Delta E_{parent} - \Delta E_{daughter}. \tag{10.20}$$

Also the β^+ decay is written as follows:

$$^A_Z X \rightarrow {}^A_{Z-1}Y + \beta^+ + v + e^- + \sum Q. \tag{10.21}$$

where, the quantity $\sum Q$ for that would be equal to the following:

$$\sum Q = \Delta E_{parent} - (\Delta E_{daughter} + 2 \times 0.511\ MeV),$$
$$= \Delta E_{parent} - \Delta E_{daughter} - 1.022\ MeV. \tag{10.22}$$

Note that the extra electrons are added to the balance. The atomic mass excess tables include electrons, so we need to carefully account for them. However, nuclear mass excess tables do not have this issue. The difference between atomic mass and nuclear mass is as follows:

$$m_{atomic}(_Z^A X_N)c^2 = m_{nuclear}(_Z^A X_N)c^2 + Z \cdot m_e c^2 - \sum_{i=1}^{Z} B_i. \tag{10.23}$$

The B terms are binding energies. Let's explore this electron balance issue more. Here is the mass-energy balance for β^- decay in more detail[†]:

$$Q_{\beta^-} = \left\{ \left[m(_Z^A X_N) - Z \cdot m_e \right] - \left[m(_{Z+1}^A Y_{N-1}) - (Z+1) \cdot m_e \right] - m_e \right\} c^2 + \underbrace{\left\{ \sum_{i=1}^{Z} B_i - \sum_{i=1}^{Z+1} B_i \right\}}_{small}. \tag{10.24}$$

Therefore, the quantity Q_{β^-} for β^- decay is given by the following:

$$Q_{\beta^-} \approx \left\{ m(_Z^A X_N) - m(_{Z+1}^A Y_{N-1}) \right\} c^2. \tag{10.25}$$

Here is an example of calculating Q_{β^-}. Consider the β^- decay of $_{83}^{210}\text{Bi}$ to $_{84}^{210}\text{Po}$ as the following:

$$_{83}^{210}\text{Bi} \rightarrow {}_{84}^{210}\text{Po} + \beta^- + \bar{\nu} + \sum Q. \tag{10.26}$$

The rest mass energy released for $_{83}^{210}\text{Bi}$ beta minus decay is given by the following:

$$
\begin{aligned}
Q_{\beta^-} &= \left[m(_{83}^{210}\text{Bi}) - m(_{84}^{210}\text{Po}) \right] c^2, \\
&= (209.984095 \text{ u} - 209.982848 \text{ u}) \cdot (931.502 \text{ MeV/u}), \\
&= 1.161 \text{ MeV}.
\end{aligned}
\tag{10.27}
$$

Note that here the mass difference is in the 6th significant digit, so it's much easier to use the mass *excess* tables that make the mass of each isotope relative to Carbon-12.

The mass-energy balance for β^+ decay in more detail is the following:

$$Q_{\beta^+} = \left\{ \left[m(_Z^A X_N) - Z \cdot m_e \right] - \left[m(_{Z-1}^A Y_{N+1}) - (Z-1) \cdot m_e \right] - m_e \right\} c^2 + \underbrace{\left\{ \sum_{i=1}^{Z} B_i - \sum_{i=1}^{Z-1} B_i \right\}}_{small}. \tag{10.28}$$

The quantity Q_{β^+} for β^- decay is then given by the following:

$$Q_{\beta^+} \approx \left\{ m(_Z^A X_N) - m(_{Z-1}^A Y_{N+1}) - 2m_e \right\} c^2. \tag{10.29}$$

Fermi Theory of Beta Decay

Just as we did with alpha decay, a little essential theory is important to know, especially for understanding decay charts. In alpha decay, we learned that the higher the alpha energy, the shorter the half-life. For beta decay, we will see that the momentum becomes important and that forbidden transitions are not strictly forbidden, just very unlikely.

[†]Here atomic/electron binding energy differences are neglected, since they are too small.

Following the treatment in Evens (1955) that reviews the original derivation by Fermi (1934), the rate of beta decay is proportional to the available phase space. Phase space has six dimensions—all three spatial and all three momentum values for each particle. If p is the momentum, the density of states is given by $\dfrac{dN}{dE} \sim \dfrac{4\pi}{h^3} p^2 dp$. It will be hard to explore the theory too deeply here, but to give a flavor of it, there is a concept of "comparative half-life" which is written by the following:

$$ ft_{1/2} = \frac{\text{constant}}{\left|M_{if}\right|^2}, \tag{10.30} $$

where, $\left|M_{if}\right|^2$ is a nuclear interaction term after atomic number and transition energy is removed. Given that w is the energy of the electron, the quantity f is given by the following:

$$ f = \int_0^w F(z, w')w'(w'-1)^{1/2}(w_0 - w')^2\, dw'. \tag{10.31} $$

The term $F(z,w)$ is a complicated term.

There are transition selection rules for angular momentum (I) and parity (π) for beta decay:

- Fermi rules (scalar): $\Delta I = 0$, $\Delta \pi = $ 'no'
- Gamow–Teller (vector): $\Delta I = 0, \pm 1$, $\Delta \pi = $ 'no'

The forbidden transitions do occur, but are very unlikely. These transitions are characterized by $\Delta I > 1$, $\Delta \pi = $ 'yes', $1 > 1$, and $\log f \cdot t$ will be large (about 9–15).

Here is an instructive example. An isotope important for dosimetry is $^{60}_{27}\text{Co}$ beta decay to $^{60}_{28}\text{Ni}$ (Figure 10.6).

The main beta energy is $(2.81 - 2.51)$ MeV $= 0.309$ MeV. The decay constants are related as follows:

$$ \lambda_i = f_i \lambda_{total} = f_i \cdot \ln 2 / t_{1/2}, \tag{10.32} $$

where, $\lambda_{total} = \lambda_1 + \lambda_2 + \lambda_3 + \lambda_4$. The transition to ground state, β_4, has not been observed. Log(ft) and ΔI are very high. Also note that $\log(ft) - \log(f) = 23 - 3 = 20$. Therefore, the half-life is very long. Table 10.1 gives a complete summary of the quantities in $^{60}_{27}\text{Co}$ beta decay.
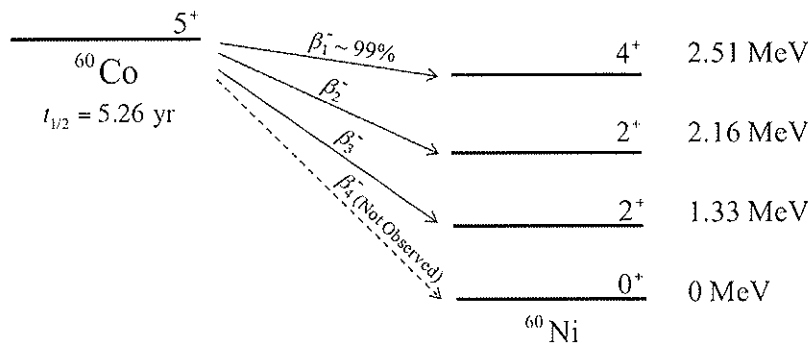

Figure 10.6. Decay scheme of Co-60 showing the unobserved decay to ground.

Table 10.1: Co-60 Decay Summary Showing the Parameters Related to the Decay to Ground State and Why the Allowed Transition is More Easily Observed

G-T rules	Log(ft)	Log(f)	$t_{1/2}$ (yr)	Branch	$f_{1/2}$	T_{max}	ΔI	$\Delta \pi$
$I = 1$ Allowed	7.6	−1.63	5.26	β_1	0.994	0.309	1	No
$I = 2$ Forbidden	12.7	0.63	4.05×10^4	β_2	1.3×10^{-4}	0.657	3	No
$I = 3$ Forbidden	13.1	2.0	4.38×10^3	β_3	0.12×10^{-2}	1.48	3	No
$I = 4$ Forbidden	>23	3.08	$\sim 10^{13}$	β_4	~ 0	2.82	5	No

Electron Capture (EC)

Electron capture is a closely related effect competing with β^+ decay. In this process, instead of emitting a positron, the nucleus may just capture an electron, and it is mostly (about 90%) from the K-shell. Of course, as with the photoelectric effect, there will also be fluorescent photons or Auger electrons emitted. In general, the electron capture equation is written as the following:

$$\prescript{A}{Z}{X} \rightarrow \prescript{A}{Z-1}{Y} + \nu + \sum Q. \tag{10.33}$$

Here,

$$\sum Q = \Delta E_{parent} - \Delta E_{daughter}. \tag{10.34}$$

Note that the additional electron need not be added. It is still there; it has just been eaten.

Even though electron capture competes with β^+ decay, a neutrino is still needed to conserve angular momentum. The subsequent gamma decays will be the same for electron capture as for β^+ decay, and the excited states are also the same. However, the quantity $\sum Q$ for electron capture is not the same as with β^+ decay. The rest mass energy released in the electron capture process is shared not just between the gammas and the neutrino, but also now between the fluorescent photons and Auger electrons. With electron capture, most of the energy is carried away with the neutrino, resulting in much less dose when compared to β^+ decay.

Dose Rate Calculations for Beta Decays and Electron Capture

Dose rate calculations for three radioactive processes—β^- decay, β^+ decay, and EC—are given by the following:

$$\dot{D} = \frac{A}{M} \sum Q' = \frac{A}{M} \left(\sum Q - E_\nu \right). \tag{10.35}$$

In Equation (10.35), $\sum Q$ is the rest mass energy released. $\sum Q'$ is the rest energy released, but not including the energy given to the neutrino or anti-neutrino. E_ν is the (anti)-neutrino energy.

Therefore, in the case of *radiation equilibrium* (all photons interacting assumed) the dose rates are equal to the following for each type of decay:

$$\dot{D}_{\beta^-} = \frac{A}{M}\left(\sum_{i=1}^{n} f_i\left(\overline{T}_i + h\nu_i\right)\right).$$ (10.36)

$$\dot{D}_{\beta^+} = \frac{A}{M}\left(\sum_{i=1}^{n} f_i\left(\overline{T}_i + h\nu_i\right) + 2mc^2\right).$$ (10.37)

$$\dot{D}_{EC} = \frac{A}{M}\left(\sum_{i=1}^{n} f_i\left(h\nu_i\right) + (E_B)_K\right).$$ (10.38)

where, $\overline{T}$ is the mean kinetic energy of the beta particle and $(E_B)_K$ is the K-shell binding energy available to fluorescent x-rays and auger electrons. Notice that $2mc^2$ in Equation (10.37) is for annihilation gammas.

In case of *charged particles equilibrium* (no photons interacting assumed) the dose rates are equal to the following for each type of decay:

$$\dot{D}_{\beta^-} = \frac{A}{M}\left(\sum_{i=1}^{n} f_i\left(\overline{T}_i\right)\right).$$ (10.39)

$$\dot{D}_{\beta^+} = \frac{A}{M}\left(\sum_{i=1}^{n} f_i\left(\overline{T}_i\right)\right).$$ (10.40)

$$\dot{D}_{EC} = \frac{A}{M}\left(\sum_{i=1}^{n} (T_{Auger})_i\right).$$ (10.41)

After nuclear reactions and alpha or beta decay, the daughter nucleus is often left in an excited state (which is indicated by an asterisk, i.e., $^A_Z X^*$). A nucleus in a long-lived or metastable excited state is called an *isomer*. A metastable state then de-excites by internal transition. This can be either *gamma decay* or *internal conversion*.

Gamma Decay

In this radioactive process, an excited nucleus reaches a stable nuclear configuration with the emission of a γ-ray. Gamma radiation is electromagnetic radiation emitted from a nucleus or from matter –antimatter annihilation, but it is nuclear decay that we consider here. Figure 10.7 illustrates a classic nuclear medicine example. In this process, the molybdenum nucleus decays to a technetium nucleus by emission of a β^- particle. The excited technetium nucleus, which is now an isomer[†], then emits a γ-ray to reach a lower energy state. Note that the isomer is denoted by an m next to the mass number of the technetium nucleus.

In nuclear medicine $^{99m}_{43}Tc$ is used for a various diagnostic purposes. The 140 keV gamma is ideal for a typically sized human in terms of contrast per dose.

$$^{99}_{42}Mo \xrightarrow[\beta^--decay]{\lambda=0.0104/hr} {}^{99m}_{43}Tc \xrightarrow[\gamma-decay, 140\ keV]{\lambda=0.115/hr} {}^{99}_{43}Tc$$
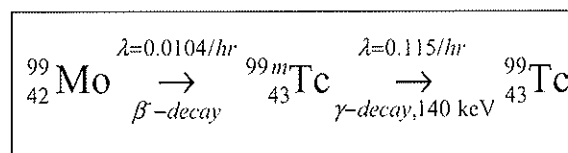
Figure 10.7. The Tc-99 process, the "workhorse of nuclear medicine."

[†]The isomeric or metastable state in this case happens about 86% of the time.

Internal Conversion

This is an alternative mechanism that competes with gamma decay. When the excitation energy of the nucleus is small, and the excited nucleus has a coherent coupling to an orbital electron (usually instead of emission of a γ-ray), the nucleus will pass the excitation energy to an atomic electron (mostly from K-shell) to eject from the atom. Note that the ejected electron in internal conversion is different from a β^- particle in energy. The energy of an electron ejected in the internal conversion process is always the same and is given by the following:

$$T_{IC} = h\nu - E_B. \tag{10.42}$$

The quantity E_B is the atomic shell binding energy, usually for the K-shell, and $h\nu$ is the energy of the competing gamma decay, the energy to be released, ΣQ. Just like electron capture, a vacancy in an electron shell induces fluorescence or Auger electrons.

Some Essential Gamma Decay Theory

Photons have spin of $1\hbar$. Therefore, they are bosons and follow Bose–Einstein statistics. The theory is complex. However, first recall that multi-pole fields arise from the spherical harmonics, (Y_{lm}), that describe the quantum states of the nucleus.

During the decay, angular momentum must be conserved in the vector sense:

$$\vec{I}_{parent} = \vec{I}_{daughter} + \vec{I}_{photon}. \tag{10.43}$$

The multi-pole order of radiation is set by the angular momentum of the photon, l. Since a photon is a boson, l has to be greater than zero. See Table 10.2.

There are also two rules related to angular momentum as follows:

$$\left| \vec{I}_{parent} - \vec{I}_{daughter} \right| \leq l \leq \left| \vec{I}_{parent} \right| + \left| \vec{I}_{daughter} \right|. \tag{10.44}$$

$$\Delta l \equiv \left| \vec{I}_{parent} - \vec{I}_{daughter} \right| > 0. \tag{10.45}$$

Parity of multi-pole radiation for electric multi-poles is given by $(-1)^l$ and for magnetic multi-poles is given by $(-1)^{l+1}$.

The rate of emission then is proportional to $S(l)\left(\dfrac{R_{nuc}}{\lambda_{h\nu}/2\pi} \right)^{2l}$, which is smaller than unity. The quantity $\lambda_{h\nu}$ is wavelength, R_{nuc} is the radius of the nucleus, and the quantity $S(l)$ is a statistical factor and a function of l as follows[†]:

$$S(l) = \frac{2(l+1)}{l[1 \cdot 3 \cdot 5 \cdot \ldots \cdot (2l+1)]^2} \cdot \left(\frac{3}{l+3}\right)^2. \tag{10.46}$$

Table 10.2: The 2^l-pole Designations (Note that there are no $l = 0$ multi-poles)

l		Designation
$l = 1$	$2^l = 2$	Dipole
$l = 2$	$2^l = 4$	Quadrupole
$l = 3$	$2^l = 8$	Octopole
l	2^l	2^l-pole

Table 10.3: Classification of Gamma Emissions

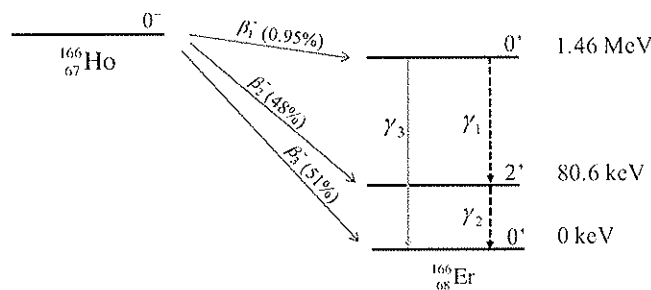| Classification	Symbol	l	$\Delta\pi$
Electric dipole	$E1$	1	"Yes"
Electric quadrupole	$E2$	2	"No"
Magnetic dipole	$M1$	1	"No"
Magnetic quadrupole	$M2$	2	"Yes"
Electric 2^l-pole	El	l	"No" for l-even; "Yes" for l-odd
Magnetic 2^l-pole	Ml	l	"Yes" for l-even; "No" for l-odd

Figure 10.8. Example decay scheme showing a third, but forbidden, gamma that violates selection rules.

Therefore, as l gets larger, the emission rate drops quickly, and large angular momentum transitions are very unlikely.

The multiple character of the emitted photons/radiation is based on angular momentum and parity, as Table 10.3 shows.

Figure 10.8 is an example of using angular momentum selection rules in decay of $^{166}_{67}\text{Ho}$ to $^{166}_{68}\text{Er}$. Note that γ_3 is forbidden, because a gamma must carry away at least the inherent spin of a photon, so a transition from a zero angular momentum state to another zero momentum state is not possible through a gamma decay. However, internal conversion would be possible for such a transition.

Absorbed Fraction (AF)

To properly discuss dose from gamma decay, first we need to define the concept of absorbed fraction. Recall that radiation equilibrium (RE) approximates the limit that "all gammas interact," and charged particle equilibrium (CPE) approximates the limit that "no gammas interact." Absorbed fraction handles much more common and realistic situations *in between* RE and CPE. Consider a small volume, dV, that has a uniform source which emits photons isotropically into a larger volume, V (see Figure 10.9):
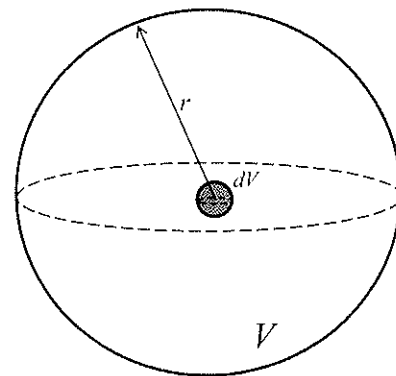

Figure 10.9. The geometry related to absorbed fraction and reciprocity discussions.

---

[1]See Evans (1995), page 214.

Absorbed fraction, $AF(r)$, is then defined as the relative amount of energy absorbed within a radius, r. Because of reciprocity[*], the expression also equals the right-hand side as follows:

$$AF(r) \equiv \frac{\text{Energy absorbed within } r}{\text{Radiant energy produced in } dV} = \frac{\text{Energy absorbed in } dV \text{ from activity at/within } r}{\text{Radiant energy produced in } V}. \quad (10.47)$$

If the source region is very large relative to the photon attenuation coefficient, then $AF \to 1$, that is, all gammas interacting in the source region. If the source region is very small relative to the photon attenuation coefficient, then $AF \to 0$, and that means no gammas interacting in the source region. The source region can be either dV or V in this discussion, as long as the detector region is as specified in Equation (10.47).

For a spherical source, if we know or can calculate the effective attenuation coefficient, $\mu'(r)$, the $AF(r)$ is as follows:

$$AF(r) = 1 - e^{-r \cdot \mu'(r)}. \quad (10.48)$$

In effect, Equation (10.48) is actually a type of definition for the effective attenuation coefficient. Accordingly, the effective attenuation coefficient can be given by the following:

$$\mu'(r) \Rightarrow \frac{1}{r} \ln\left(\frac{1}{1 - AF(r)}\right). \quad (10.49)$$

Figure 10.10 illustrates the absorbed fraction of photons in a volume. One side reads the source concentrated at the center with distributed detector, and the other side reads a distributed source and a concentrated central detector. Just turn this handy figure upside-down to see this reciprocity!

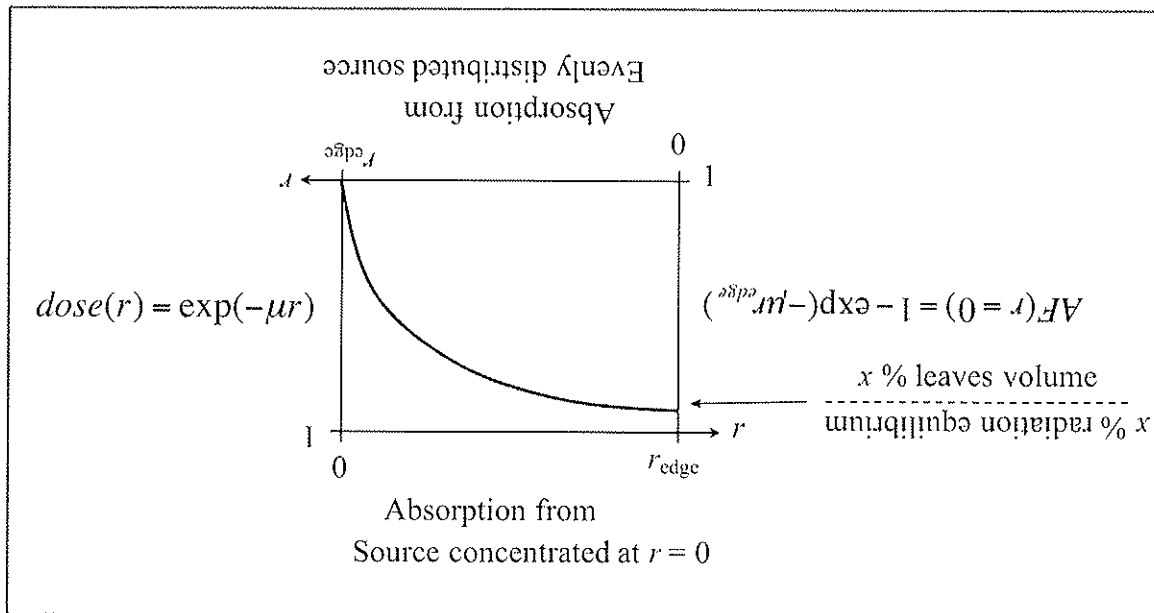

Figure 10.10. Memory aid for this particular reciprocity: flip upside-down for reciprocity. Note that the attenuation coefficients are really effective attenuation coefficients.

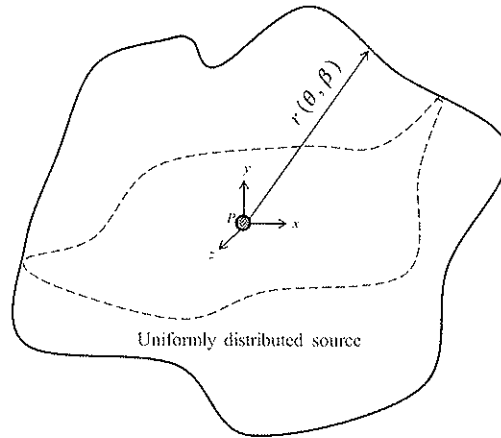[*] For reciprocity theorem see Attix (1986), page 55–59.

Figure 10.11. A generalization of the geometry of Figure 10.9.

We can generalize the above to cases where we do not have spherical symmetry (Figure 10.11); in these cases we will integrate over the source boundary (solid angles) to find the absorbed fraction at point P as follows:

$$AF = \frac{\int\limits_{\theta=0}^{\pi} \int\limits_{\beta=0}^{2\pi} \left(1 - e^{-[\mu'(r(\theta,\beta))\cdot r(\theta,\beta)]}\right) \sin(\theta) d\theta d\beta}{\int\limits_{\theta=0}^{\pi} \int\limits_{\beta=0}^{2\pi} \sin(\theta) d\theta d\beta},$$

$$= \frac{1}{4\pi} \int\limits_{\theta=0}^{\pi} \int\limits_{\beta=0}^{2\pi} \left(1 - e^{-[\mu'(r(\theta,\beta))\cdot r(\theta,\beta)]}\right) \sin(\theta) d\theta d\beta. \tag{10.50}$$

Then, we can define an average distance from the point P to the boundary as follows:

$$\bar{r} \equiv \frac{1}{4\pi} \int\limits_{\theta=0}^{\pi} \int\limits_{\beta=0}^{2\pi} r(\theta,\beta) \sin(\theta) d\theta d\beta. \tag{10.51}$$

and that will lead to a more compact approximate form for AF as follows, if one performs the usual approximation $\mu' \cong \mu_{en}$:

$$AF \approx 1 - e^{-\mu_{en} \cdot \bar{r}}. \tag{10.52}$$

Dose Rate Calculations for Gamma Decay and Internal Conversion

Now we consider gammas that partially interact, with the AF factor. Dose rate for non-RE photons, (in-between RE and CPE) is given by the following:

$$\dot{D} = \frac{A}{M} \sum_{i=1}^{n} AF_i \cdot f_i \cdot h\nu_i. \tag{10.53}$$

Of course, if no photons interact, then for the γ-decay, we have $\dot{D} = 0$.

For internal conversion, there is a dose from the IC electrons, and the f relates to the fraction not from fluorescence:

$$T_{IC} = h\nu - E_b \tag{10.54}$$

and the f becomes,

$$f_{IC} = h\nu - p_K Y_K h\overline{\nu}_K - p_L Y_L h\overline{\nu}_L. \tag{10.55}$$

The fraction of photons escaping the radioactive body is as follows:

$$p \approx 1 - AF = e^{-\mu_{en}\overline{r}}. \tag{10.56}$$

General Dose Rate Calculations

In general, the dose rate calculations for all these equations from each decay mode, all assembled as one, are given as follows:

$$\dot{D} = \frac{A}{M} \sum_{i=1}^{n} AF_i \cdot f_i \cdot E_i. \tag{10.57}$$

Here E_i is energy for each particular interaction as follows:

T_α	for α particle decay,
$T_{daughter}$	for recoil daughter in α decay,
$\overline{T}$	for β decay,
$2mc^2$	for annihilation photons in β^+ decay,
$h\nu$	for γ-rays, fluorescent photons, and internal bremsstrahlung photons (even though they are not discrete, they are often treated as such by binning the spectrum),
T_{Auger}	for Auger electrons, and
T_{IC}	for Internal Conversion electrons.

By defining the **equilibrium dose constant**, we can treat all these particles (charged and uncharged) the same way as follows:

$$\Delta_i = f_i E_i. \tag{10.58}$$

Equilibrium dose constant has the units of $\dfrac{\text{kg} \cdot \text{Gy}}{\text{Bq} \cdot \text{s}}$ or $\dfrac{\text{g} \cdot \text{rad}}{\text{mCi} \cdot \text{hr}}$, which are the units of energy.

Therefore, the general dose rate for radiation equilibrium (all gammas interacting) is given by the following:

$$\dot{D} = \frac{A}{M} \left(\sum_{i=1}^{n} \Delta_i \right). \tag{10.59}$$

The general dose rate for charged particles equilibrium (no gammas interacting) is then given by the following:

$$\dot{D} = \frac{A}{M}\left(\sum_{i=1}^{n} \Delta_i \right)_c .$$ (10.60)

Note that the subscript c in Equation (13.59) means that the sum is only over charged particles.

References

Attix, F.H. *Introduction to Radiological Physics and Radiation Dosimetry*. Weinheim, Germany: WILEY-VCH Verlag GmbH & Co. KGaA, 2004.
Evans, R.D. *The Atomic Nucleus*. Malabar, Florida: Krieger Publishing Co., 1955.
Fermi, E. (1934). "Versuch einer Theorie der beta-Strahlen. I." *Zeitschrift für Physik* 88:161.
Gamow, G. (1928). "Zur Quantentheorie des Atomkernes." *Zeitschrift für Physik* 51:204–22.

11

Dose from Directly Ionizing External Radiation Sources

In this chapter, we consider charged particle beams. An important consideration will be charged particle equilibrium (CPE) which requires that the energy deposition is spatially constant, but this condition will be hard to satisfy with an external source from one direction.

CPE can be defined for just the δ-ray component of the charged particle beam. Note that CPE for δ-rays doesn't exist near the surface or near the end of primary charged particle range. Also note that where CPE does exist, there is no need to consider the detailed dynamics of δ-rays. In other words, equilibrium means that for every δ-ray leaving a location, there is a similar one entering on average. Therefore, in terms of final dose, CPE implies less need for understanding the details of the δ-rays (Figure 11.1). This is an important concept.

Dose in Thin Films

I. Dose in Thin Films When δ-ray CPE Exists

Assume we have a *thin* foil. This assumption means we have constant (kinetic) energy, $T = T_0$, where T_0 is the initial energy onto the film in question. Also, this assumption implies a constant stopping power through the film for
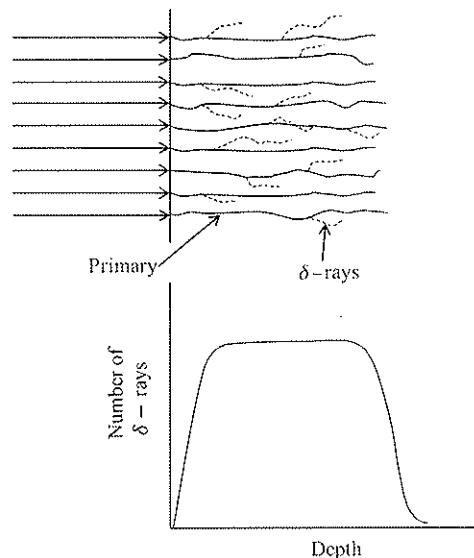

Figure 11.1. Illustration of the effects of δ-rays on dose.
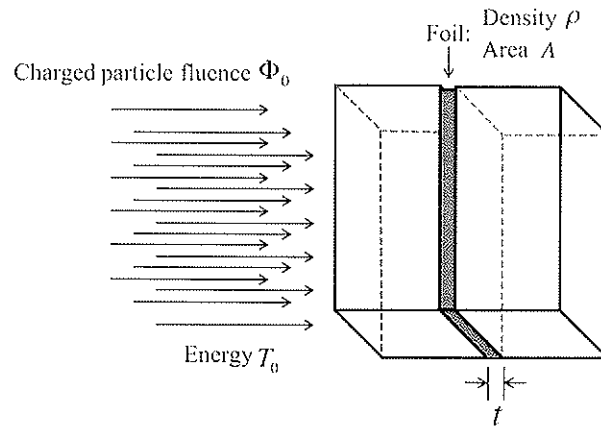
103

Figure 11.2. Illustration of a thin foil with buildup.

the primary particles. This happens when we sandwich the foil in between extra layers (*buildup layers*) that will establish the equilibrium. Figure 11.2 illustrates a picture of this thin foil in buildup.

We also assume that there is a very little scattering, that is $\langle \theta^2 \rangle \cong 0$. Under these assumptions, the energy deposited in the film is given by the following:

$$\varepsilon = \Phi_0 A \left(\frac{dT}{\rho dx} \right)_c \rho t. \tag{11.1}$$

Therefore, the dose for a particle beam is calculating as follows:

$$D = \frac{\varepsilon}{\rho t A} = \Phi_0 \left(\frac{dT}{\rho dx} \right)_c. \tag{11.2}$$

Notice that the dose is independent of the foil thickness and beam area if and only if there is negligible scatter and slowing down.

2. Dose in Thin Films When δ-ray CPE Does Not Exist

Without the extra layers to establish δ-ray charged particle equilibrium, δ-rays with energy larger than Δ can escape. Then, we would overestimate that actual dose if we did not take into account this energy escape. In other words, in terms of the CSDA range, we lose δ-ray CPE if $R_{CSDA}(\Delta) > t$. Therefore, the dose requires the restricted mass stopping power if δ-ray CPE doesn't exist, as in Equation (11.3):

$$D = \Phi_0 \left(\frac{dT}{\rho dx} \right)_{c,\Delta}. \tag{11.3}$$

Average Dose in Thick Foils

1. Average Dose in Very Thick Foils from Electrons

Electrons will scatter and will radiate very much more than protons, in general. If no electrons leave the foil, this case is actually fairly simple: just subtract off any radiated power from bremsstrahlung. So we now consider this

case, where the foil is much thicker than the maximum range of the electrons: $t \gg t_{max}$. If we ignore backscatter, then the amount of energy deposited in the layer is given by the following:

$$\varepsilon = \Phi_0 A T_0 \left[1 - Y(T_0) \right].$$

(11.4)

where, $Y(T_0)$ is the total radiation yield. As before, the dose is the following for very thick films:

$$D = \frac{\varepsilon}{\rho t A} = \frac{\Phi_0 T_0 \left[1 - Y(T_0) \right]}{\rho t}.$$

(11.5)

2. Average Dose in Thick Foils from Heavy Charged Particles

Heavy charged particles will have negligible scatter, but the stopping power and energy will change. Bremsstrahlung is negligible. Figure 11.3 is a picture of heavy charged particle radiation onto a thick foil, with a general incident angle.

The change in stopping power due to the change in energy across the foil will be handled by looking up the change in CSDA range. The **residual range** is what is left after the transit consumed some energy. With $l = \rho t / \cos \theta$, the residual range is given by the following:

$$R_{residual} = R_{CSDA}(T_0) - \frac{\rho t}{\cos \theta}.$$

(11.6)

We can also think of Equation (11.6) as follows:

$$(amount\ of\ range\ left) = (total\ potential\ range) - (amount\ of\ range\ used).$$

(11.7)

In this case, the energy deposited is equal to the following:

$$\varepsilon = \Phi_0 A \left(T_0 - T_f \right).$$

(11.8)

The dose is then the following for thick films (*not very thick*) for heavy charges at a general angle of incidence:

$$D = \frac{\varepsilon}{A \rho t / \cos \theta} = \frac{\Phi_0 \left(T_0 - T_f \right) \cos \theta}{\rho t}.$$
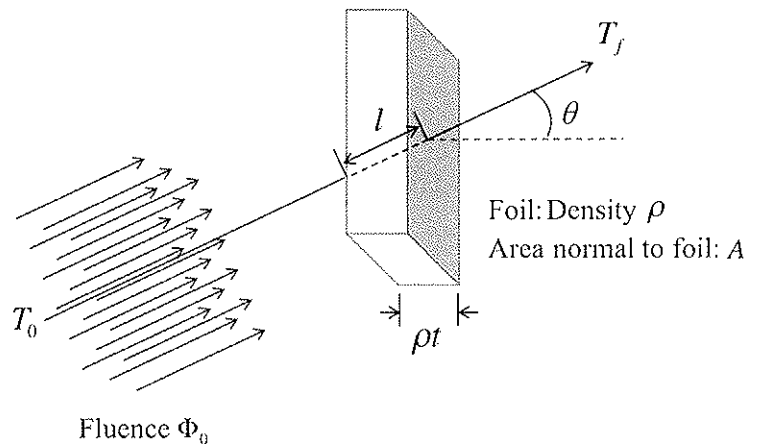
(11.9)

Figure 11.3. Heavy charged particles impinge upon a thick foil with at an angle.

3. Average Dose in Thick Foils from Electrons

This is the most difficult situation. Here we consider some complications: electrons do scatter considerably, and electrons produce bremsstrahlung. Most importantly, scattering will expand the path length up to 10%. If the layer were very thick, then it would not matter much, since all of their energy gets deposited. In this case, bremsstrahlung photons leave with a certain amount of energy that we will need to find. In order to do that, we will need to estimate the corrected path length. Figure 8.11 in Attix (2004) is a difficult figure that is required for this case. The procedure is as follows.

The path length *without* scattering is $l = \rho t / \cos\theta$. The *corrected path length*, l', which is illustrated in Figure 11.4, is the following:

$$l' = l \cdot \left[1 + (\%increase / 100) \right]. \tag{11.10}$$

Find the "% increase" from Figure 8.11 of Attix (2004) by first getting the following ratio:

$$\xi = \frac{l}{\chi_0}. \tag{11.11}$$

The quantity χ_0 is the radiation length, and a table of χ_0 can be found in Attix (2004) on page 190. Figure 8.11 in Attix is like a very long figure that is folded onto itself with arrows showing where to read the abscissa value for a given beam energy curve.

After that complicated step, the corrected path length, l', is used to determine the residual range as follows:

$$R_{residual} = R_{CSDA}(T_0) - l'. \tag{11.12}$$

The energy deposited is given by the following equation:

$$\varepsilon = \Phi_0 A \left\{ T_0 \left[1 - Y(T_0) \right] - T_f \left[1 - Y(T_f) \right] \right\}. \tag{11.13}$$
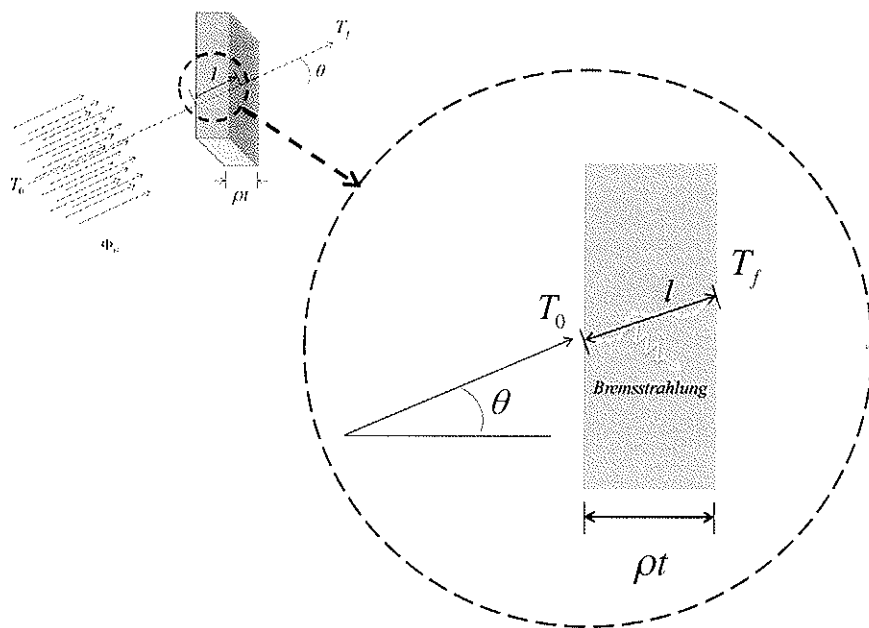

Figure 11.4. Two complications with electron beams: scatter increases the path length (white dashed line) and bremsstrahlung.

The quantity T_f is the final energy, which corresponds to $R_{residual}$. The range tables can be used in either direction. The dose is then the following for electrons in thick foils:

$$D = \frac{\varepsilon}{A\rho t / \cos\theta} = \frac{\Phi_0\left\{T_0\left[1-Y(T_0)\right]-T_f\left[1-Y(T_f)\right]\right\}\cos\theta}{\rho t}. \tag{11.14}$$

Dose When the Electron Energy Spectrum is Known

An electron spectrum can be measured with a magnetic spectrometer, expressed with analytical transport theory, or calculated with Monte-Carlo.

The following can work with δ-ray equilibrium for both directly or indirectly ionizing primary radiation:

$$D = \int_0^{T_{max}} \Phi'(T)\left(\frac{dT}{\rho dx}\right)_c dT, \tag{11.15}$$

where $\Phi'(T)$ is the charged particle energy spectrum.

A Monte-Carlo simulation is useful for exploring various components of the spectrum. For example, notice in Figure 11.5 that the Bragg peak for electrons is visible only when scattering is unrealistically turned off. Also notice that when the delta-rays are not changing over space between about 0.1 to 0.5 in normalized depth, then the dose is not sensitive to their explicit inclusion. Therefore, one really only needs to know the spectrum when it is changing: a key concept in charged particle equilibrium.
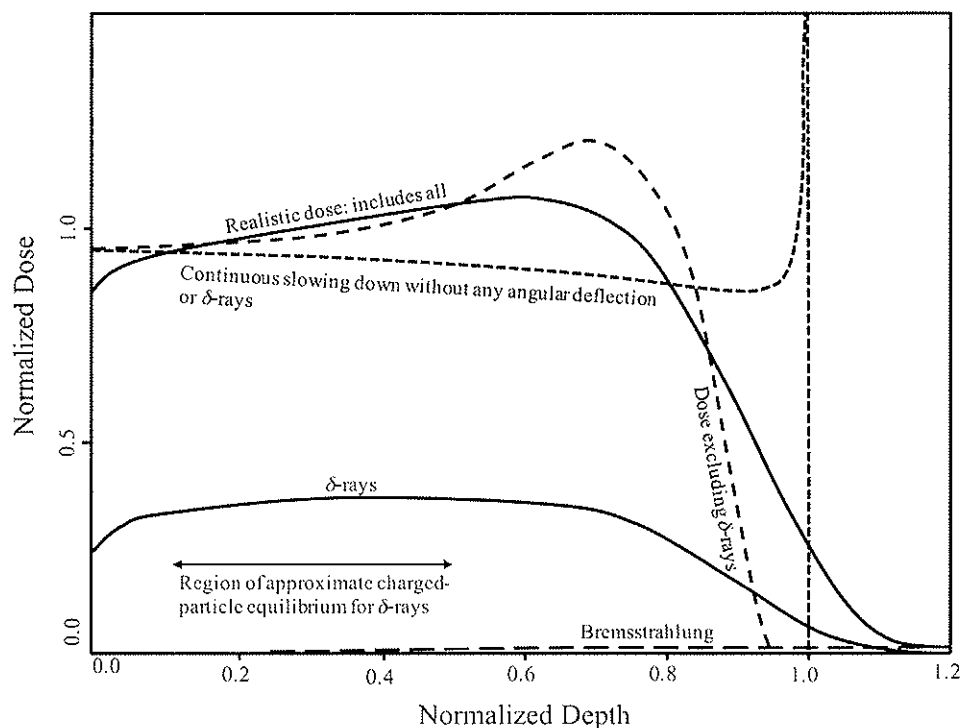
Figure 11.5. Energetic electrons impinge on condensed matter from the left side of the figure in a Monte-Carlo calculation. Note that in the region between normalized depth of 0.1 to 0.5 (the white region), the delta-ray spectrum is not changing and, therefore, the δ-rays are in equilibrium and are not explicitly needed to be separated out for a correct dose calculations. In regions very shallow and near the end of range, this delta-ray equilibrium is lost. Reprinted from Jenkins et al. (1988) with permission.

Table 11.1: Summary Table of Each Case Discussed in This Chapter.

DOSE	Without δ-CPE	With δ-CPE
Very thin	$\Phi_0 \left(\dfrac{dT}{\rho dx} \right)_{c,\Delta}$	$\Phi_0 \left(\dfrac{dT}{\rho dx} \right)_{c}$
Spectrum known	$\displaystyle\int_{\Delta}^{T_{max}} \Phi'_{\delta\,included}(T) \left(\dfrac{dT}{\rho dx} \right)_{c,\Delta} dT$	$\displaystyle\int_{\Delta}^{T_{max}} \Phi'(T) \left(\dfrac{dT}{\rho dx} \right)_{c} dT$

DOSE	Heavy Charge	Electron
Very thick	$\dfrac{\Phi_0 T_0}{\rho t}$	$\dfrac{\Phi_0 T_0 \left(1 - Y(T_0)\right)}{\rho t}$
Thick	$\dfrac{\Phi_0 (T_0 - T_f)\cos\theta}{\rho t}$	$\dfrac{\Phi_0 \left[\left(T_0(1 - Y(T_0)) - T_f \left(1 - Y(T_f)\right)\right)\right]\cos\theta}{\rho t}$
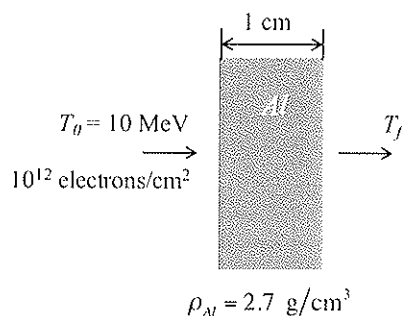
Figure 11.6. Figure for the example problem below.

Example Problem: Calculate the dose for the thin aluminum foil in Figure 11.6.

Solution: The path length is $l = (1 \text{ cm})(2.7 \text{ g/cm}^3) = 2.7 \text{ g/cm}^2$. The corrected path length is found from

$(\chi_0 = 24.46 \text{ g/cm}^2)$ as $\xi = \dfrac{2.7 \text{ g} / \text{cm}^2}{24.46 \text{ g} / \text{cm}^2} = 0.11$.

The graph gives $l' = l + 0.06\, l = 2.86 \text{ g/cm}^2$. The CSDA range for 10 MeV electrons from Appendix E of Attix (2004) is 5.86 g/cm². Therefore,

$R_{residual} = R_{CSDA} - l' = 5.86 \text{ g/cm}^2 - 2.86 \text{ g/cm}^2 = 3.0 \text{ g/cm}^2$.

Back to appendix E of Attix (2004) and using the interpolation technique, 3.0 g/cm² corresponds to an energy of $T_f = 4.84$ MeV as follows:

$\dfrac{(4.84) - 4.50}{3.00 - 2.79} = \dfrac{5.00 - 4.50}{3.092 - 2.79}$.

Again back to appendix E of Attix (2004), "radiation yield," the amount of energy *not* lost to bremsstrahlung is calculated as the following:

$$\frac{\varepsilon}{\Phi_0 A} = (10 \text{ MeV})(1 - 0.0745) - (4.84 \text{ MeV})(1 - 0.0357) = 4.59 \text{ MeV}$$

Therefore, the dose would be equal to the following:

$$D = \frac{\varepsilon}{A\rho t}(\cos\theta = 1) = \frac{(10^{12} \text{cm}^{-2})(4.59 \text{ MeV})\cos(0)}{(2.7 \text{ g/cm}^3)(1 \text{ cm})} = 1.70 \times 10^{12} \text{ MeV/g},$$

$$= (1.70 \times 10^{12} \text{ MeV/g}) \cdot (1.602 \cdot 10^{-10} \text{ Gy/(MeV/g)}) = 272 \text{ Gy}.$$

References

Attix, F.H. *Introduction to Radiological Physics and Radiation Dosimetry.* Weinheim, Germany: WILEY-VCH Verlag GmbH & Co. KGaA, 2004.

Jenkins, T.M, W.R. Nelson, and A. Rindi, Eds. *Monte Carlo Transport of Electrons and Photons.* New York: Plenum Press, 1988.

12

Dosimetry Introduction

Dosimetry is the determination of radiation dose or a related radiological quantity that results from the interaction of ionizing radiation with matter. A dosimeter is a device that provides a reading, R, that is a function of the dose absorbed in its sensitive volume. The dose in the dosimeter is related to the dose deposited in the surrounding medium. By analogy, the thermometer measures only the temperature of the thermometer itself—with an assumption that it is in thermal equilibrium with its surroundings so that we can infer the temperature of the surroundings. A truly absolute dosimeter is an ideal dosimeter that does not require calibration to some known radiation field.

Characteristics of Dosimeters

A colorimeter measures the temperature rise from *both* ionization and excitation. If there are no other reactions and in isolation, the relation between the temperature rise and the amount of energy deposited is the heat capacity, h. Recall from Chapter 1 how small the temperature rise would be for even a lethal beam. The calorimeter has the least amount of *theoretical* complications, except that they are hard to build and use.

Other dosimeters will generally have a more complicated relationship to the energy deposited: ion chambers for example, will measure ionization; they are very sensitive to the gas mass, which is complicated by uncertainties in volume and density and to some extent humidity and purity as well. The conversion coefficient in this case is $\bar{W}/e$, the average energy associated with forming an ion pair. Ferrous sulfate dosimetry solutions ("Fricke" solutions) measure the amount of chemical product produced. The conversion coefficient in this case is G, the chemical yield.

1. Precision or/vs. Accuracy

Precision is how close one expects to get, with confidence, to the expectation value. This aspect relates more to *quality*. However, **accuracy** (Figure 12.1) is how close the expectation value one obtains on average actually is to
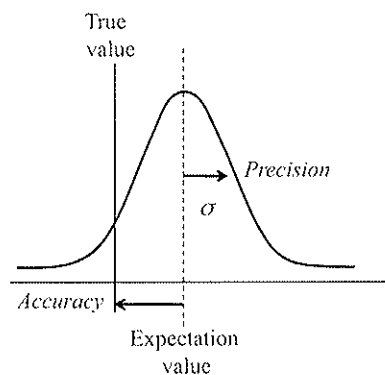

Figure 12.1. Simplistic conceptual illustration of the distinction between precision and accuracy.

the true value. This aspect relates more to *calibration*. The calibration of a dosimeter that provides accuracy is specific to a particular situation (like a particular beam's energy spectrum). The dosimeter itself, and how one uses it, is more of a determinant of its precision.

2. Dose Sensitivity

Few dosimeters are sensitive to both very low doses and very high doses of radiation. The *dynamic range* is this range of proper use, and it's limited in various ways for various dosimeters.

The lower limit of sensitivity is limited usually by stochastic variability. There may be statistical fluctuations in the particles received. That level may be similar to spurious readings that occur at zero dose, i.e., system noise. The zero dose readings need to be subtracted off the readings—for example, shielding cosmic ray background or cooling to reduce dark current in a photomultiplier.

There is an upper limit of sensitivity, as well, for most systems. If the dose rate is too high, a scintillation detector or a pulsed detector will have a finite dead time for which it needs to recover from the previous event. The sensitivity is diminished when the average time between pulses or events is less than the dead time of the detector. Recombination in ion chambers will reduce sensitivity if the density of the ions in the gas is too high— the ions recombine during the transit to the electrodes. Scintillation detectors can saturate.

Thermoluminescent detectors (TLDs) have a complicated response to high dose. The radiation damage can create more traps for a while until the damage is so large that the crystal's structure has been modified too much.

3. Stability

Ideally, the detector should always respond the same way to the same quality and quantity of radiation. Also, the detector should be stable *after* the radiation. Dosimeters that store dose until read-out—like TLDs, films, and chemical dosimeters—should not lose or alter the stored dose information between the irradiation time and the read-out time. For example, TLDs have low-energy traps that should not be read out if they can release fluorescent photons at room temperature. Another example is the light sensitivity for radiographic films.

4. Energy Dependence

Ideal responses could be responses *proportional* to energy (i.e., pulse size proportional to the deposited energy for determining dose) or responses *independent* of energy (i.e., a Geiger counter or other pulse-counting system that just counts up the number of events for determining radioactivity). In either case, we would want the ratio of the reading, R, to the radiological quantity of interest, J, to be independent of energy. So, for $E_1 \neq E_2$, we would like to have the following:

$$\left(\frac{R}{J}\right)_{E_1} = \left(\frac{R}{J}\right)_{E_2}, \tag{12.1}$$

where, R is charge collected and J is dose. However, few detectors meet this criterion to a good enough approximation. Therefore, energy dependence remains an important factor to include in the calibration. This means that some account should be taken of the energy spectrum differences between calibration and other beams. Attix (2004) discusses ways to modify the energy dependence in clever ways.

5. Angular Dependence

Ideal responses are isotropic. That seems to imply a spherical shape for all detectors, but that is not practical, and the small differences in this dependence can be corrected for, usually. However, one should be careful to have this characterized.
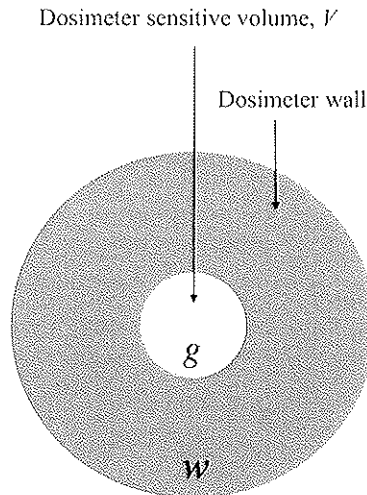
Dosimeter sensitive volume, V

Dosimeter wall

g

w

Figure 12.2. Idealized ion chamber geometry.

Ion Chamber Dosimetry

The ideal ion chamber is a prototypical dosimeter for ionizing radiation. It will measure ionization. Recall that ionization is not the only result of transferred energy. Consider a small cavity with volume, V, filled with a gas, labeled g. The cavity is embedded in a surrounding medium (dosimeter wall), labeled w. The filling medium, g, is sensitive to radiation, and it will be affected by the radiation's effect on the w medium (Figure 12.2).

The dosimeter wall can serve many functions other than simply a boundary. For a relatively energetic photon beam, such as those used for radiation therapy, all or most of the charged particles that are set in motion come from this wall. Sometimes the wall is made thick enough to shield the sensitive volume, V, from charged particles set in motion from *outside* this wall. The wall can act then as a radiation filter.

Now consider the small cavity of the ion chamber filled with air and the wall of the cavity being equivalent to some medium, like tissue or air ($z_{eff} \sim 7.5$ for a range of energies). An electric field is produced in the cavity volume to collect charges that are produced by the radiation. The electric field requires that a central electrode be inserted to form a potential relative to the wall. Another way is to have the wall be made of separate pieces in order to form the potential difference.

Fast electrons can enter the cavity, deposit their energy, and, therefore, ionize some molecules. The ionization products are usually a positive heavy ion and a negative electron attached to a neutral molecule. These charges then travel to the electrodes and create a small current. If the gas molecules cannot become negatively charged, the gas is called nonelectronegative. Methane is such a gas. If the ions encounter each other on their way to the electrodes, they can recombine. If the electric field is strong enough, then recombination is minimized to the point where the collection current does not change—the chamber is then said to be "saturated."

Energy corresponding to the ionization, charge pairs produced, Q, of gas, g, is equal to the following:

$$\varepsilon = Q \left(\frac{\bar{W}}{e} \right)_g . \tag{12.2}$$

The quantity $\bar{W} / e$ is always written this way and represents a single quantity: the average energy expended to produce an ion pair for the gas in a stated condition. For example, it is 33.9 eV/ion pair for dry air. Note that this is not the ionization potential. See Attix (2004) pages 339–41 for more details. This quantity includes energy that produces excitations as well as ionizations.

The dose to the chamber gas is then given by the following:

$$D = \frac{\varepsilon}{M} = \frac{Q}{M}\left(\frac{\bar{W}}{e}\right)_g. \tag{12.3}$$

See Attix (2004) Table 12.1 for $\bar{W}/e$ values for various gases. Major sources of error can involve the conditions for which $\bar{W}/e$ holds and uncertainties in the mass of the chamber gas in the sensitive volume, M. Even though ionization is only part of the energy, if its fraction of the total deposited energy is constant over energy, then the dosimetry will still be accurate.

Cavity Theory

1. Bragg–Gray Cavity Theory

Suppose that a monoenergetic beam of charged particles is passing through a medium labeled w that has a very small medium labeled g sandwiched in between, as shown in Figure 12.3.

We assume that we have δ-ray equilibrium, and we also assume that the fluence, Φ, and its spectrum are not perturbed (i.e., *scattering is not changing*). Then we can have the following for the doses to w and g:

$$D_w = \Phi\left(\frac{dT}{\rho dx}\right)_{c,w}, \tag{12.4}$$

$$D_g = \Phi\left(\frac{dT}{\rho dx}\right)_{c,g}. \tag{12.5}$$

Canceling the fluence, the ratio $\dfrac{D_w}{D_g}$ is calculated as the following, assuming monoenergetic particles:

$$\frac{D_w}{D_g} = \frac{\left(dT/\rho dx\right)_{c,w}}{\left(dT/\rho dx\right)_{c,g}}. \tag{12.6}$$

There are two Bragg–Gray conditions: the first Bragg–Gray condition is that we assume the g medium does not perturb the energy spectrum, $\Phi'(T)$, of the fluence of charged particles. The second Bragg–Gray condition is
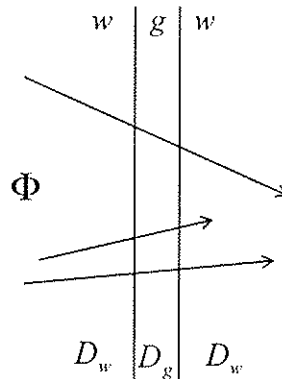

Figure 12.3. Idealized Bragg–Gray cavity.

that we also assume the particles are all crossing the g medium, not starting in or stopping in g. This amounts to a condition that the cavity size is small compared to the charged particle range. It is generally a good assumption for energies >100 keV. The range of charged particles in a gas is ~1000 longer than in a solid because of density.

With $\Phi'(T)$ as the fluence spectrum of charged particles, the dose is equal to the following:

$$D_g = \int_0^{T_{max}} \Phi'(T) \left(\frac{dT}{\rho dx} \right)_{c,g} dT. \tag{12.7}$$

Let's define the average mass collisional stopping power for a polyenergetic beam such that the dose is as follows:

$$D_g = \overline{S}_g \Phi. \tag{12.8}$$

The quantity $\overline{S}_g$ is a fluence-weighted average mass collisional stopping power[†]. We also have the same for the w medium as follows:

$$\overline{S}_w \equiv \frac{1}{\Phi} \int_0^{T_{max}} \Phi'(T) \left(\frac{dT}{\rho dx} \right)_{c,w} dT. \tag{12.9}$$

Now the Bragg–Gray relation is given by the following:

$$\frac{D_w}{D_g} = \frac{\overline{S}_w}{\overline{S}_g} \equiv \overline{S}_g^w = \frac{\int_0^{T_{max}} \Phi'(T) \left(\frac{dT}{\rho dx} \right)_{c,w} dT}{\int_0^{T_{max}} \Phi'(T) \left(\frac{dT}{\rho dx} \right)_{c,g} dT}. \tag{12.10}$$

Usually, g is a gas, and we know from before that $D_g = \frac{Q}{M} \left(\frac{\overline{W}}{e} \right)_g$. The quantity Q here is the charges produced (not necessarily collected), and M is the mass of the gas.

Therefore, the Bragg–Gray cavity theorem is stated as follows:

> *"The ratio of the doses is the ratio of the average mass collisional*
> *stopping powers if the charged particle fluence is unperturbed."*

Using the above equations, we now form the dose in the wall in these terms as follows:

$$D_w = \frac{Q}{M} \left(\frac{\overline{W}}{e} \right)_g \overline{S}_g^w. \tag{12.11}$$

This explains why we have a cavity in the first place; the above is a handy relation to get the dose in the w medium by measuring the ionization in the cavity.

2. Spencer–Attix Cavity Theory

Attix noticed that there were problems with Bragg–Gray cavity theory when he performed ionization measurements on chambers with small air cavities that have high-z (high atomic number) walls. The deviation of measurements from Bragg–Gray was most severe when the thickness of the cavity was small[‡]. Attix had the brilliant

---

[†]Fluence-weighted average mass collisional stopping power sometimes is written as $_m \overline{S}_g$.
[‡]See Attix (2004), page 242.

suggestion to Spencer that the "*local*" energy deposition should not include the generation of knock-on electrons (or δ-rays). Therefore, Spencer performed a re-derivation of Bragg–Gray. There was still CPE everywhere in the wall, from where the electrons are emitted. Again, no electrons generated in g, and bremsstrahlung photons are not produced. In order to do this, the knock-on electrons must not be considered part of the stopping power. Note that the issue is what happens to the spectrum. That is where the knock-on electrons, the δ-rays, are placed in the equation. First let us consider what to expect from the equilibrium spectrum. The word equilibrium in this sense refers to the shape of the distribution.

Consider a simple case: N_w electrons of energy T_0 produced per unit mass of medium w. The dose in w wherever CPE exists is given by the following:

$$D_w = (K_c)_w = N_w T_0. \tag{12.12}$$

However, what really is the meaning of N_w? Consider an analogy to radioactive decay and recall the dose rate, $\dot{D} = \dfrac{A}{M}\left(\sum_{i=1}^{n} \Delta_i\right)$, i.e., Equation (10.59). So, for monoenergetic particles from radioactive decay, D_w is given by the following:

$$D_w = \frac{1}{M}\left(\int A\,dt\right)T_0. \tag{12.13}$$

Therefore, according to Equations (12.12) and (12.13), the quantity N_w is equal to the following:

$$N_w = \frac{1}{M}\left(\int A\,dt\right). \tag{12.14}$$

In the case of CPE for an external photon beam, we have the following equality:

$$D_w = \left(\frac{\mu_{en}}{\rho}\right)\Psi_w = \left(\frac{\mu}{\rho}\frac{T_0}{h\nu}(1-g)\right)\Psi_w \cong \left(\frac{\mu}{\rho}\frac{T_0}{h\nu}\right)\Psi_w, \tag{12.15}$$

or equivalently,

$$D_w = \left((TERMA)_w\frac{T_0}{h\nu}\right). \tag{12.16}$$

Therefore, our meaning for N_w could then be simply the following:

$$N_w = (TERMA)_w / (h\nu). \tag{12.17}$$

Recall the dose expression for a spectrum of energies as follows:

$$D_w = \int_0^{T_0} \Phi'(T)\left(\frac{dT}{\rho\,dx}\right)_w dT. \tag{12.18}$$

Now consider an *equilibrium* spectrum of electrons (equilibrium in the sense of energy bins and, therefore, the shape of the spectrum), $\Phi_{equil}{}'(T) \equiv \Phi_T^e$. Thus, we can have the following:

$$D_w = N_w T_0 = \int_0^{T_0} \Phi_T^e \left(\frac{dT}{\rho dx} \right)_w dT, \tag{12.19}$$

$$\Delta D = N_w T_0 = \Phi_T^e \left(\frac{dT}{\rho dx} \right)_w \Delta T, \tag{12.20}$$

$$\Delta D / \Delta T = \Phi_T^e \left(\frac{dT}{\rho dx} \right)_w . \tag{12.21}$$

According to Equation (12.12), the *"energy bin equilibrium"* solution to the above is as the following:

$$\Phi_T^e = \frac{N_w}{\left(dT / \rho dx \right)_w}. \tag{12.22}$$

Therefore, we can see that $\left(d\Phi^e(T) / dT \right) \propto \left(dT / \rho dx \right)_w^{-1}$. It says that the equilibrium spectrum is proportional to the inverse of the mass collisional stopping power: "If passing rapidly from energy bin to energy bin, and no charges lost, then there are few charges in that bin" (Figure 12.4). Note the linear scale.

Holding to the Bragg–Gray condition that the same fluence and flux density traverses the cavity, we have the following expression for D_g:

$$D_g = \int_0^{T_0} \Phi_T^e \left(dT / \rho dx \right)_g dT = N_w \int_0^{T_0} \frac{\left(dT / \rho dx \right)_g}{\left(dT / \rho dx \right)_w} dT. \tag{12.23}$$

Figure 12.4. Electrons generated at T_0 slow down with a conservation of particles but travel through the bins faster as they lose energy faster at lower energies.

According to the Bragg–Gray relation, i.e., Equation (12.10), the ratio $\dfrac{D_g}{D_w}$ is given by the following:

$$\frac{D_g}{D_w} = \bar{S}_w^g = \frac{\displaystyle\int_0^{T_0} \Phi'(T)\left(dT/\rho\,dx\right)_g dT}{\displaystyle\int_0^{T_0} \Phi'(T)\left(dT/\rho\,dx\right)_w dT}. \tag{12.24}$$

Now substitute for the energy bin equilibrium:

$$\frac{D_g}{D_w} = \frac{\displaystyle\int_0^{T_0} \Phi_T^c \left(dT/\rho\,dx\right)_g dT}{\displaystyle\int_0^{T_0} \Phi_T^c \left(dT/\rho\,dx\right)_w dT} = \frac{N_w \displaystyle\int_0^{T_0} \frac{\left(dT/\rho\,dx\right)_g}{\left(dT/\rho\,dx\right)_w} dT}{N_w T_0} = \frac{1}{T_0}\int_0^{T_0} \frac{\left(dT/\rho\,dx\right)_g}{\left(dT/\rho\,dx\right)_w} dT. \tag{12.25}$$

This is just a special case of Bragg–Gray—no dependence on the spectrum with an energy bin equilibrium spectrum. For an equilibrium spectrum of electrons, the Bragg–Gray equation is merely the averaging of the stopping power ratio over the energy range from 0 to T_0.

Spencer–Attix cavity theory starts from assuming an equilibrium spectrum and Bragg–Gray cavity theory, but explicitly includes knock-on electrons into the equilibrium spectrum. The effect of this inclusion is to enhance the lower-energy part of the electron spectrum relative to the higher-energy parts (Figure 12.5).

The equilibrium spectrum for Spencer–Attix is the following:

$$(\Phi_T^c)_{S-A} = R(T_0, T)(\Phi_T^c)_{B-G}, \tag{12.26}$$

where the factor $R(T_0, T)$ is a multiplicative correction to the primary equilibrium spectrum, $(\Phi_T^c)_{B-G}$, and was obtained from the Möller cross section for knock-on electron production. We can also calculate the spectrum with Monte-Carlo methods.

Therefore, for Spencer–Attix, we will use the following:

$$\frac{D_g}{D_w} = \frac{\displaystyle\int_\Delta^{T_0} \frac{R(T_0, T)}{\left(dT/\rho\,dx\right)_w} L_g(T, \Delta)dT}{\displaystyle\int_\Delta^{T_0} \frac{R(T_0, T)}{\left(dT/\rho\,dx\right)_w} L_w(T, \Delta)dT} = \frac{\bar{L}_g}{\bar{L}_w} = \bar{L}_w^g. \tag{12.27}$$
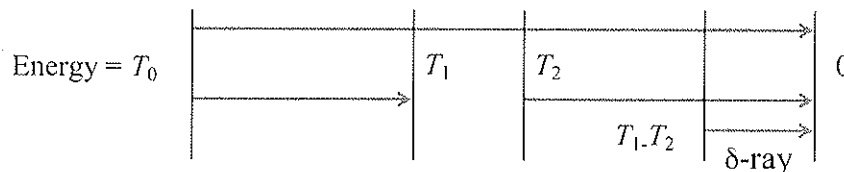

Figure 12.5. Illustration of how δ-rays shift the charged particle energy spectrum to lower energies.

Figure 12.6. The δ-rays that are generated within each medium are indicated with light small tracks. The heavy black tracks inside g are equivalent in range to the light small tracks in w. Spencer–Attix theory adds these heavy black lines to the primary fluence. After that, CPE is again assumed everywhere for the remaining δ-rays. (Not to scale.)
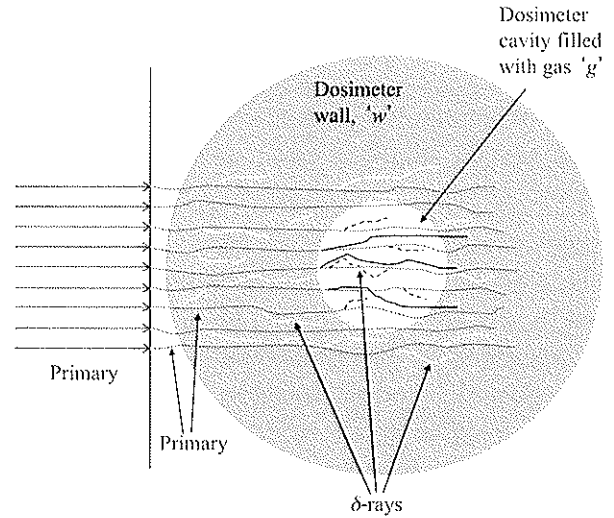
The restricted mass collisional stopping power values are the following:

$$L_g(T,\Delta) = \left(dT / \rho\,dx\right)_{g,\Delta}, \tag{12.28}$$

$$L_w(T,\Delta) = \left(dT / \rho\,dx\right)_{w,\Delta}. \tag{12.29}$$

In order to understand this better, let's consider disequilibrium of the hard δ-rays between the wall and the gas. In Figure 12.6, δ-rays are in CPE everywhere. Thus, Brag–Gray cavity theory applies. The δ-rays just within the gas must have very low energy.

If we call the original electrons the "primary" and the knock-on or δ-rays the "secondary," a spectrum would look like Figure 12.7.

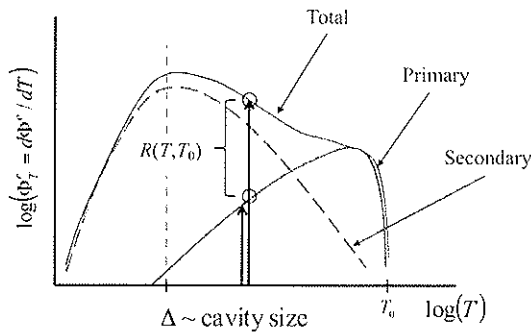The spectrum experienced by the gas is similar to Figure 12.8.

Figure 12.7. Secondaries (δ-rays) shown in the charged particle spectrum and characterized by the R factor shown.
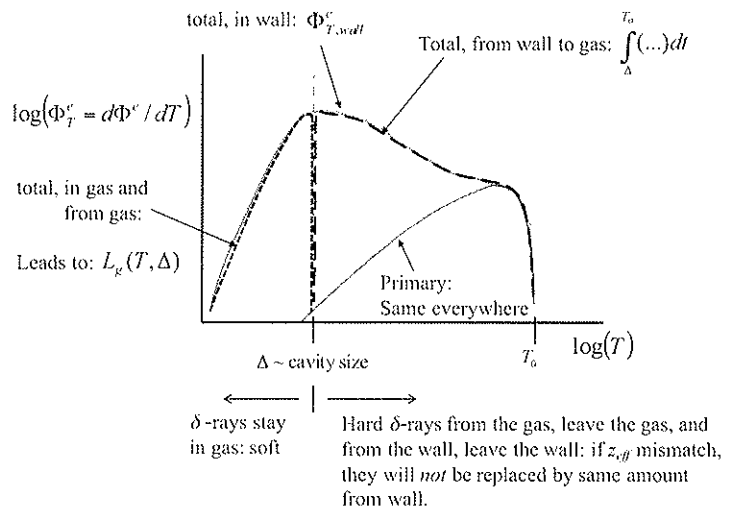

Figure 12.8. Perspective of the gas in the small cavity with z_{eff} match. Spencer–Attix theory divides the secondaries into two populations as shown in the figure at Δ.

Consider the equation for the dose to the gas with Spencer–Attix theory as follows:

$$D_{gas} = \int_{\Delta}^{T_0} \frac{R(T_0,T)}{(dT/\rho dx)_w} L_g(T,\Delta)dT. \qquad (12.30)$$

In Equation (12.30) above, the restricted stopping power of the medium g, $L_g(T,\Delta)$, excludes hard δ-rays that leave the medium g: they would have kinetic energies $T > \Delta$. We only want to keep δ-rays that locally deposit within g and so are truly part of the continuous slowing down in the stopping power. Spencer–Attix theory divides the δ-rays into these two distinct groups: those that stay local and are part of the stopping (restricted) power, and those that become part of the total fluence spectrum: $T > \Delta$. To that end, in Equation (12.30), the primary fluence is now enhanced by the R factor. Note that the limits of the integral start at the energy Δ. To do otherwise would be to effectively count the soft δ-rays twice. As the energy of the δ-rays increases, their ability to cross the cavity increases, and so the cutoff energy increases with chamber size. In the limit of a large cavity, no δ-rays make it out of the gas, and then $\Delta \to T_0$. In this limit, Spencer–Attix theory approaches Bragg–Gray theory. The R factor will approach unity, and the integral will reduce to the evaluation at T_0. Therefore, in the large cavity limit, Equation (12.30) reduces to the following:

$$\lim_{\Delta \to T_0} \{D_{gas}\}_{S-A} = \lim_{\Delta \to T_0} \int_{\Delta}^{T_0} \frac{R(T_0,T)}{(dT/\rho dx)_w} L_g(T,\Delta)dT \Rightarrow (N_w T_0) \cdot \bar{S}_w^g = (D_{gas})_{B-G}. \qquad (12.31)$$

This limit is very interesting. If there is an atomic number mismatch between the mediums g, the gas say, and w, the wall, then there will be a mismatch in the δ-rays that get generated. If the cavity is large enough, then this mismatch will represent a small part of the charged particle fluence spectrum (see Figure 12.9). In this case, Bragg–Gray theory will work well even if there is a mismatch of materials, and that is very robust.

In the limit of very small cavity, $\Delta \to 0$ and the secondary electrons take up much of the spectrum, shown in Figure 12.10. This is also for the case of mismatched secondaries between the wall and the gas from these materials having different effective atomic numbers. Now, there is a need for Spencer–Attix theory. Using Bragg–Gray theory would lead to incorrect answers, because δ-ray equilibrium would not be achieved between the gas and the wall.
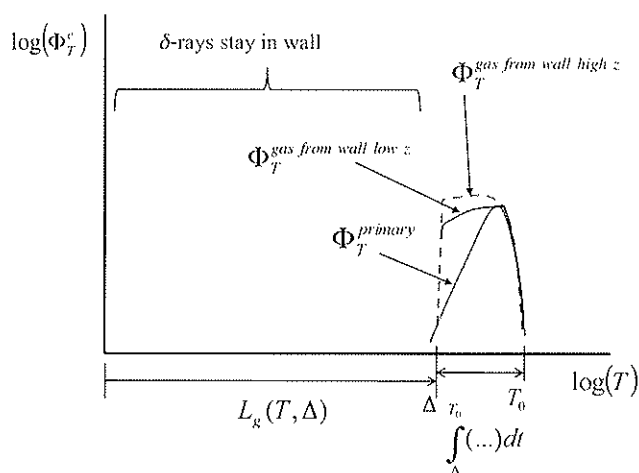

Figure 12.9. Perspective of the gas, large cavity limit. Note that the effects of a z mismatch are minimized because the primaries play a large role.
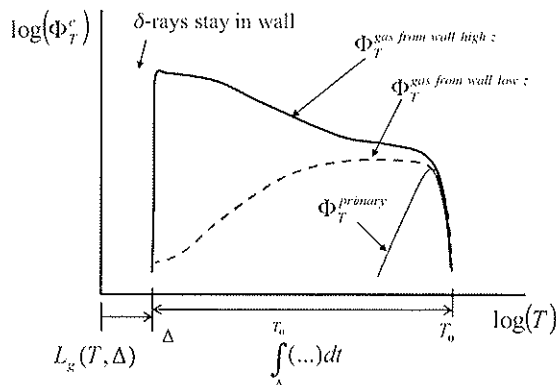
Figure 12.10. Perspective of the gas: very small cavity limit. Note that the effects of a z mismatch are significant in this case because the secondaries play such a large role.

The situation of a small cavity and very different z_{eff} between the gas and the wall provides the maximum deviation from Bragg–Gray. One can see this difference in data shown in Attix (2004) in his Figure 10.3 and in his Table 10.2. It is ironic, at first thought, that small cavities are more likely to deviate from Bragg–Gray. There are also other factors in real ion chambers that can affect equilibrium, such as lateral disequilibrium around the electrode guard rings, etc. In fact, lateral disequilibrium contaminates the data shown in Figure 10.3 in Attix (2004), and he admits this in the text on the facing page. The modern dosimetry protocols use Spencer–Attix theory, as we will see in later chapters.

More on Stopping Power Averaging

We can vary the initial starting energy. Recall that for Compton, the maximum starting electron energy is $T_{max} = \dfrac{hv \cdot 2\alpha_0}{1 + 2\alpha_0}$, where, $\alpha_0 = \dfrac{hv}{mc^2}$. This allows for some additional averaging over the initial energy of the "primary" electrons released from photons undergoing Compton interactions from a monoenergetic photon beam. Note that T_{max} is a function of photon energy as follows:

$$\overline{\overline{S}}_w(T_{max}(hv)) = \frac{\displaystyle\int_0^{T_{max}} N'(T_0)\overline{S}_w(T_0)dT_0}{\displaystyle\int_0^{T_{max}} N'(T_0)dT_0}. \tag{12.32}$$

With a distribution of photon energies, use the photon fluence spectrum as follows:

$$\overline{\overline{\overline{S}}}_w(hv_{max}) = \frac{\displaystyle\int_0^{hv_{max}} \Phi'[T_{max}(hv)]\overline{\overline{S}}_w[T_{max}(hv)]d(hv)}{\displaystyle\int_0^{hv_{max}} \Phi'(hv)d(hv)}, \tag{12.33}$$

In summary of averages: $\overline{S}$ represents an average over secondary e^-s up to a launching energy, $\overline{\overline{S}}$ represents an average over spectrum of launching (maximum) energies, $\overline{\overline{\overline{S}}}$ represents an average over photon energies, and finally, $\dfrac{\overline{\overline{\mu}}}{\rho}$ represents an average over photon energies.

There are some useful rules of thumb for photon beams. First, calculate the mean energy of the photon beam, $\overline{hv}$. For diagnostic energies, this is 40% to 50% of the maximum. For example, for 60 kVp, use 25–30 kV (kVp = peak kilovoltage of a bremsstrahlung spectrum, MV and kV are used for photon beam characterizations, the energy from this accelerating voltage). For therapy type, megavoltage beams, use 1/3 of the maximum, the accelerating MV voltage.

For Compton, one electron is set in motion, and the mean kinetic energy it will have is obtained from the following:

$$\overline{T}_0 = \frac{_c\sigma_{tr}}{_c\sigma}\overline{hv}. \tag{12.34}$$

Note that energies around 1 MeV are dominated by Compton. In general, one often uses the following:

$$\overline{T}_0 = \frac{\mu_{tr}}{\mu}\overline{hv}. \tag{12.35}$$

From this point, there are two ways to go for calculating the mass collisional stopping power ratios from this average initial electron energy:

1. Attix suggests to just use $\overline{T}_0 / 2$ and look it up. This assumes that the average particle energy, $\overline{T}$, is 1/2 the average initial particle energy. This works OK for ratios of stopping powers. Note that these ratios are robust to $\overline{T}$ estimates.

2. A better way is from Johns and Cunningham (1983), which is accurate to about 1/2%. Calculate it from Equation (12.36) by looking up these components in Appendix E of Attix (2004).

$$\overline{S} = \frac{\overline{T}_0 \left[1 - Y(\overline{T}_0) \right]}{R_{CSDA}(\overline{T}_0)}. \tag{12.36}$$

3. Other Cavity Theories for Photon Beams

For low energies, even Bragg–Gray will break down. There are two other theories that will handle some situations that deviate from the "only crossers" assumption for the cavity: "very large cavity theory" and "Burlin cavity theory."

Very Large Cavity Theory: Assuming CPE exists in the cavity and most of the charges there are from the cavity, the dose D_g is given by the following:

$$D_g \overset{CPE}{=} (K_c)_g = \Psi_g \left(\frac{\overline{\mu}_{en}}{\rho} \right)_g. \tag{12.37}$$

If the cavity were replaced by the wall material, and if there was CPE in the wall, the dose is then given by the following:

$$D_w \overset{CPE}{=} (K_c)_w = \Psi_w \left(\frac{\overline{\mu}_{en}}{\rho} \right)_w. \tag{12.38}$$

If the energy fluence of photons is unperturbed by the cavity (i.e., no attenuation or scattering difference, $\Psi_w \cong \Psi_g$), then for very large cavities we have the following:

$$\frac{D_g}{D_w} = \left(\frac{\overline{\mu}_{en}}{\rho} \right)_w^g. \tag{12.39}$$

Note that this is a mass energy absorption ratio, and contrast this with Bragg–Gray, which had a stopping power ratio.

Burlin Cavity Theory: Burlin cavity theory is an attempt to bridge a gap between the very small cavity (Bragg–Gray or Spencer–Attix) and the very large cavity case. This attempt is the simplest possible way, but Monte-Carlo simulation is the only good way to handle this situation.

Consider four types of particles:

1. *Crossers*: electrons cross the cavity. This is the ideal for small cavities, and Bragg–Gray assumes all primary charges are these and no δ-rays. Spencer–Attix assumes high-energy δ-rays are all crossers.

2. *Insiders*: electrons start and stop completely within the cavity. This is the ideal for very large cavity theory.

3. *Stoppers*: generated outside cavity, but stop within.

4. *Starters*: generated inside cavity, but stop outside it.

In Burlin theory, the *last two* are assumed to "cancel each other." Burlin theory can be considered to be a linear superposition of Bragg–Gray and very large theories as follows:

$$\frac{D_g}{D_w} = d\left(\frac{D_g}{D_w}\right)_{B-G} + (1-d)\left(\frac{D_g}{D_w}\right)_{\text{very large}} = d\cdot\left(\bar{S}_w^g\right) + (1-d)\cdot\left(\frac{\bar{\mu}_{en}}{\rho}\right)_w^g. \tag{12.40}$$

The quantity d is the fraction of electrons generated in the wall, and $1-d$ is the fraction that are not. For small cavities $d = 1$, and for very large cavities $d = 0$.

A very big assumption now is that the charged particles' fluence *decays* in distance exponentially (but we know this is not true). For a convex cavity, the mean cord length is given by the following:

$$L = \frac{4V}{A}, \tag{12.41}$$

where, A is the surface area and V is the volume. Then, we can write d an average of $e^{-\beta L}$ as the following:

$$d = \frac{\int_0^L \Phi'_e e^{-\beta l}\, dl}{\int_0^L \Phi'_e\, dl}. \tag{12.42}$$

If we assume that the equilibrium spectrum is unaltered, then d is simply equal to the following:

$$d = \frac{1 - e^{-\beta L}}{\beta L}. \tag{12.43}$$

Burlin uses the following equation to define β for electron beams:

$$0.01 = e^{-\beta t_{max}}, \tag{12.44}$$

where t_{max} is the maximum depth of electron penetration and has been arbitrarily assigned a value where the fluence is attenuated to 1% of its original value. Janssens (1974) found that a value of 4% is better. Note that Equation (10.47) from Attix (2004) has this form—watch units of β. Attix (2004) may not be consistent between cm^{-1} and g/cm^2. Beta is not sensitive to the exact value of z_{eff}. The rules of thumb for photon beams that we defined earlier this chapter are not useful for getting beta. Get z_{eff} and go to Table 8.5 of Attix (2004) for t_{max}/R_{CSDA}.

Burlin theory can be useful for intermediate cavity sizes and for liquid- or solid-filled cavities. The theory is empirically based, so if used in a new situation, be very careful. Burlin theory also works best when $S \sim \frac{\mu_{en}}{\rho}$.

Table 12.1: Summary of All Cavity Theories

	Bragg–Gray	Spencer–Attix	Very Large	Burlin
Assumptions	• electron fluence not perturbed • all electrons from walls, and considered to be primaries • CPE throughout wall • not sensitive to electron spectrum	• primary electron fluence not perturbed • CPE throughout wall • sensitive to delta ray spectrum that is not in equilibrium: $T_\delta < \Delta$ not in spectrum $T_\delta > \Delta$ act like primary	• all electrons come from the cavity • photon energy fluence is not perturbed	• electron fluence, photon energy fluence not perturbed
Indications	• for small cavities • wall and cavity with similar z or not very small	• for small cavities susceptible to δ-ray disequilibrium effects: dissimilar z	• for cavity size much larger than electron range in cavity • for photon beams	• for intermediate cavity sizes • for photon beams
Equations	$\dfrac{D_g}{D_w} = \bar{S}_w^g,$ with: $\bar{S}_w^g = $ $\dfrac{\int_0^{T_0} \Phi'(T)(dT/\rho dx)_g\, dT}{\int_0^{T_0} \Phi'(T)(dT/\rho dx)_w\, dT}.$	$\dfrac{D_g}{D_w} = \bar{L}_w^g,$ with: $\bar{L}_w^g = $ $\dfrac{\int_\Delta^{T_0} \dfrac{R(T_0,T)}{(dT/\rho dx)_g} L_g(T,\Delta)\, dT}{\int_\Delta^{T_0} \dfrac{R(T_0,T)}{(dT/\rho dx)_w} L_w(T,\Delta)\, dT}.$	$\dfrac{D_g}{D_w} = \left(\dfrac{\bar{\mu}_{en}}{\rho}\right)_w^g,$ with: $\left(\dfrac{\bar{\mu}_{en}}{\rho}\right)_w^g = \dfrac{(\bar{\mu}_{en}/\rho)_g}{(\bar{\mu}_{en}/\rho)_w}.$	$\dfrac{D_g}{D_w} = d \cdot \left(\bar{S}_w^g\right) + (1-d) \cdot \left(\dfrac{\bar{\mu}_{en}}{\rho}\right)_w^g,$ with: $d = \dfrac{1 - e^{-\beta L}}{\beta L},$ such that: $0.01 = e^{-\beta L}.$

Cavity Theory Examples and Discussion

Example Problem 1: Suppose we have a small cavity surrounded by a wall and placed in a water phantom. Suppose that the wall has almost the same atomic number as water. What is the dose ratio between the cavity air and the water medium from a monoenergetic electron beam of 10 MeV? (Ignore electron scattering.)

Solution: Bragg–Gray works well with electron beams. Also, we ignore electron scattering. Therefore, assume the spectrum is the same across boundaries. The dose ratio is then calculated as follows:

$$\frac{D_g}{D_w} = \frac{D_{air}}{D_{H_2O}} = \frac{\int_0^{T_{max}} \Phi'(T)(dT/\rho dx)_{c,air}\, dT}{\int_0^{T_{max}} \Phi'(T)(dT/\rho dx)_{c,H_2O}\, dT} = \frac{(dT/\rho dx)_{c,air}}{(dT/\rho dx)_{c,H_2O}}\Bigg|_{10\,MeV} \cdot \frac{\int_0^{T_{max}} \Phi'(T)\, dT}{\int_0^{T_{max}} \Phi'(T)\, dT}$$

$$= \frac{(dT/\rho dx)_{c,air}}{(dT/\rho dx)_{c,H_2O}}\Bigg|_{10\,MeV} = \frac{1.979\ \text{MeVcm}^2/\text{g}}{1.968\ \text{MeVcm}^2/\text{g}} = 1.006.$$

Example Problem 2: Suppose we have a $\beta-$ source with an average energy of 100 keV in CPE in bone. Assume that there is an equilibrium spectrum of charged particles present in the bone and in a small air cavity in the bone. What is the dose ratio between the cavity air and the bone?

Solution: The dose ratio is calculated as follows:

$$\frac{D_g}{D_w} = \frac{D_{air}}{D_{bone}} = \frac{1}{T_0} \int_0^{T_0} \frac{(dT/\rho dx)_{c,air}}{(dT/\rho dx)_{c,bone}} dT,$$

where from Attix, Appendix E, for energies near 100 keV, $\dfrac{(dT/\rho dx)_{c,air}}{(dT/\rho dx)_{c,bone}} \cong 0.99$. If this ratio was constant, the approximate answer would be the following:

$$\frac{D_{air}}{D_{bone}} = 0.99 \frac{1}{T_0} \int_0^{T_0} dT = 0.99.$$

Example Problem 3: Suppose we have a 10 cm radius cavity of a polystyrene-based scintillation dosimeter embedded in water. What is the ratio of dose between the dosimeter and the water for a 1.25 MeV photon beam? (Ignore attenuation.)

Solution: For a 1.25 MeV photon, the maximum kinetic energy of an electron set in motion is 1.03 MeV. For this energy, the range, R_{CSDA}, is about 0.5 cm $\ll$ 10 cm. See Attix (2004) page 580. So most of the electrons are going to be set in motion within the polystyrene—it's a very large cavity.

$$\frac{D_{polyst}}{D_{water}} = \frac{1}{(\bar{\mu}_{en}/\rho)_{polyst}^{water}} = \frac{1}{1.036} = 0.965.$$

Example Problem 4: Suppose the cavity in example 3 above is replaced by air. What is the ratio of the dose in the air to the water medium dose for the 1.25 MeV photon beam?

Solution: This time, the range is on the same order as the cavity size, so we must use Burlin cavity theory. For the small cavity part, since air and water have similar atomic numbers, Bragg–Gray will be fine.

$$\frac{D_{air}}{D_{water}} = d\left(\frac{D_{air}}{D_{water}}\right)_{small\ cavity} + (1-d)\left(\frac{\bar{\mu}_{en}}{\rho}\right)_{water}^{air}$$

$$= d\left(\bar{S}_{water}^{air}\right) + (1-d)\left(\frac{\bar{\mu}_{en}}{\rho}\right)_{water}^{air},$$

where $\beta = \ln(1/0.01)/t_{max}$ and $t_{max} = 0.5$ g/cm^2, so $\beta = 9.2$ cm^2/g. Assume the cavity is spherical, the mean cord length is $L = 4(4/3)\pi R^3/4\pi R^2 = 4R/3 = 13.3$ cm. Therefore, d is as follows ($\rho_{air} = 1.29 \times 10^{-3}$ g/cm^3):

$$d = \frac{1 - \exp\{(9.2\ cm^2/g)(1.29 \times 10^{-3}\ g/cm^3)(13.3\ cm)\}}{(9.2\ cm^2/g)(1.29 \times 10^{-3}\ g/cm^3)(13.3\ cm)} = 0.93$$

With $\bar{S}_{water}^{air} = 0.885$ and $(\mu_{en}/\rho)_{water}^{air} = 0.900$, the dose ratio would be as follows:

$$\frac{D_{air}}{D_{water}} = (0.93)(0.885) + (1 - 0.93)(0.900) = 0.886.$$

Since d is 0.93, one should ask if Burlin was worth the effort. If all we needed was a rough number, Bragg–Gray would have been fine.
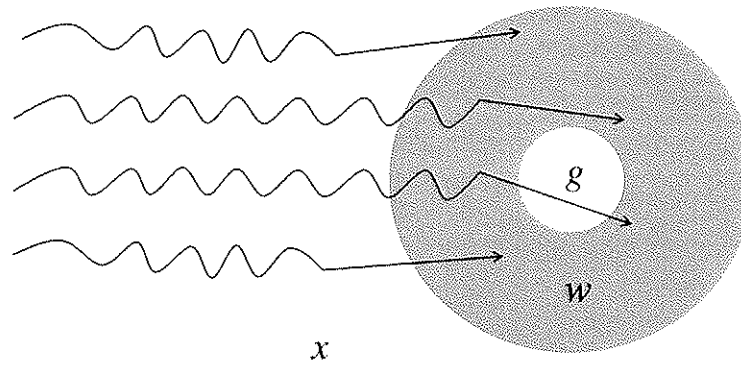
Figure 12.11. Illustration of a cavity embedded in a medium, x.

Dosimetry Fundamentals

Ideal Bragg–Gray Ion Chamber: Figure 12.11 illustrates a dosimeter with a cavity, g, and a wall, w, embedded in a medium labeled x.

Consider the following assumptions: the wall is thick enough to establish CPE, and none of the electrons in g come from x. The cavity g is very small so that none of the electrons are set in motion from there. The fluence entering the cavity is unperturbed. The energy fluence of photons in the medium, x, is not perturbed by the dosimeter. The dose to the medium is then calculated by the following:

$$D_x = D_w \frac{(\bar{\mu}_{en}/\rho)_x}{(\bar{\mu}_{en}/\rho)_w}. \tag{12.45}$$

We can use Bragg–Gray cavity theory to write Equation (12.45) as follows:

$$D_x = D_g \left(\frac{D_w}{D_g} \right)_{cavityTheory} \cdot \frac{(\bar{\mu}_{en}/\rho)_x}{(\bar{\mu}_{en}/\rho)_w} = D_g \bar{S}_g^w \cdot (\bar{\mu}_{en}/\rho)_w^x. \tag{12.46}$$

If the cavity is a gas, and $D_g = (Q/M)(\bar{W}/e)_g$, we can further write the following:

$$D_x = \frac{Q}{M} \left(\frac{\bar{W}}{e} \right)_g \cdot \bar{S}_g^w \cdot (\bar{\mu}_{en}/\rho)_w^x. \tag{12.47}$$

Advantages of Media Matching

If the wall and the cavity material are the same in atomic number, and if Fano's theorem applies[†], then $D_w \approx D_g$. In Burlin cavity theory, this would amount to $\bar{S}_g^w = (\bar{\mu}_{en}/\rho)_w^g = 1$:

$$\frac{D_g}{D_w} = d\left(\bar{S}_w^g\right) + (1-d)\left(\frac{\bar{\mu}_{en}}{\rho}\right)_w^g \Rightarrow 1. \tag{12.48}$$

For an ion chamber cavity, the quantity D_x is then:

$$D_x = \frac{Q}{M}\left(\frac{\bar{W}}{e}\right)_g \cdot 1 \cdot (\bar{\mu}_{en}/\rho)_w^x. \tag{12.49}$$

If the surrounding medium, the phantom that the chamber is embedded within, is also closely matched to the wall, then the Burlin theory example is the following:

$$\frac{D_g}{D_x} = \frac{D_g}{D_w} \cdot \frac{D_w}{D_x} = \left\{ d\left(\bar{S}_w^g\right) + (1-d)\left(\frac{\bar{\mu}_{en}}{\rho}\right)_w^g \right\} \cdot \left(\frac{\bar{\mu}_{en}}{\rho}\right)_x^w = d'\left(\bar{S}_x^g\right) + (1-d')\left(\frac{\bar{\mu}_{en}}{\rho}\right)_x^g. \tag{12.50}$$

In Equation (12.50), $d' = d \cdot \left(\bar{S}_w^x\right) \cdot \left(\frac{\bar{\mu}_{en}}{\rho}\right)_x^w = d$ and matched media $\left(\bar{S}_w^x\right) = \left(\frac{\bar{\mu}_{en}}{\rho}\right)_x^w = 1$. In effect, the medium has become the new wall when the wall and the medium are well matched. In reality, it's hard to match all three.

Consider the two situations of the energy fluence in Figure 12.12, one with and the other without the dosimeter in the medium, x, with broad beams.
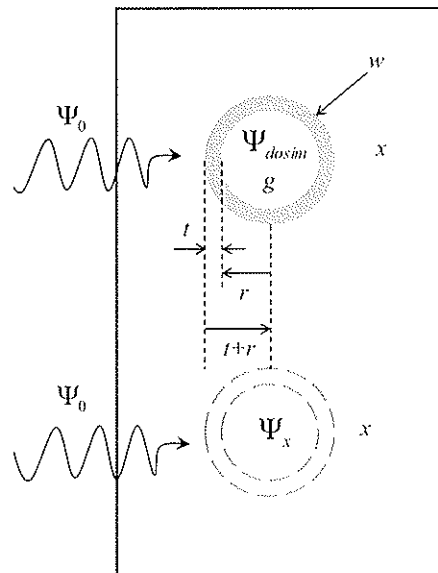

Figure 12.12. A goal of calibration is to correct for the perturbation caused by the dosimeter itself.

[†]Recall high energies and therefore high density effects can lead to violations of Fano's theorem.

The energy fluence for the cases with dosimeter, Ψ_{dosim}, and without dosimeter, Ψ_x, will be as follows:

$$\Psi_{dosim} = \Psi_0 e^{-\left\{(\mu_{en}/\rho)_w \rho_w t + (\mu_{en}/\rho)_g \rho_g r\right\}}.$$ (12.51)

$$\Psi_x = \Psi_0 e^{-\left\{(\mu_{en}/\rho)_x \rho_x t + (\mu_{en}/\rho)_x \rho_x r\right\}}.$$ (12.52)

The correction factor is then the ratio in the limit of a small[*] dosimeter:

$$(\Psi_x / \Psi_{dosim}) = 1 - \left[(\mu_{en}/\rho)_w \rho_w - (\mu_{en}/\rho)_x \rho_x\right]t - \left[(\mu_{en}/\rho)_g \rho_g - (\mu_{en}/\rho)_x \rho_x\right]r.$$ (12.53)

Figure 12.13 illustrates a diagram for choosing cavity theories.

References

Attix, F.H. *Introduction to Radiological Physics and Radiation Dosimetry*. Weinheim, Germany: WILEY-VCH Verlag GmbH & Co. KGaA, 2004.
ICRU. *Radiation Quantities and Units*. Report 33. Bethesda, MD: International Commission on Radiation Units and Measurements, 1991.
Janssens, A., G. Eggermont, R. Jacobs, and G. Thielens. (1974). "Spectrum perturbation and energy deposition models for stopping-power ratio calculations in general cavity theory." *Phys. Med. Biol.* 19;619.
Johns, H.E. and J.R. Cunningham. *The Physics of Radiology*, 4th Ed. Springfield, IL: Thomas, 1983.
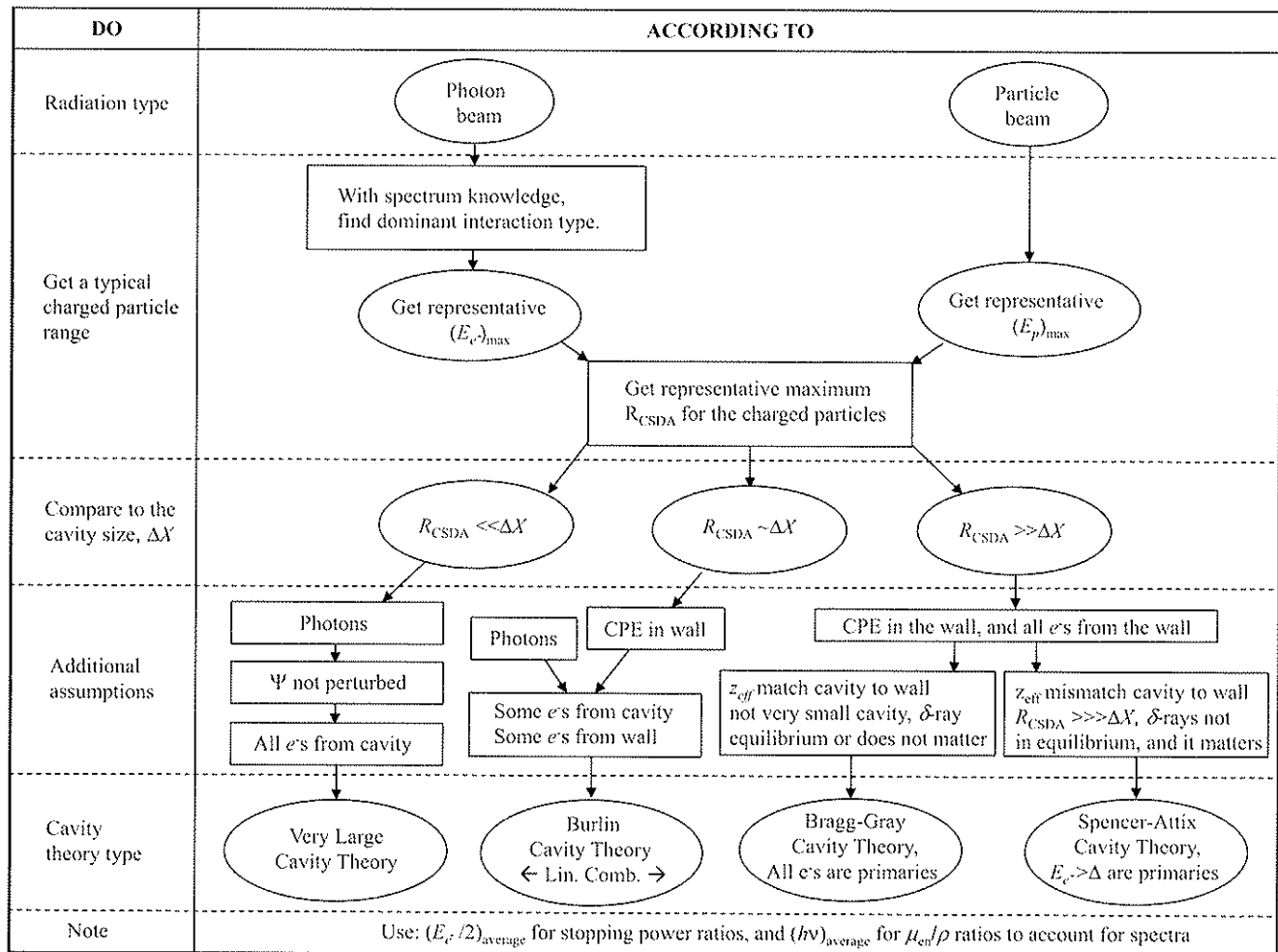

Figure 12.13. A diagram to aid in choosing the correct cavity theory.

---

[*] In Taylor series expansion keep linear terms.

13

Cavity Ionization Chambers, Circuits, and Corrections

Ion chambers (or equivalently, ionization chambers) are radiation dosimeters which, in general, vary a great deal in both volume and current. The volume is filled with a gas that typically gets ionized by energetic charged particles. The electrons often attach to a neutral molecule, and these negative ions, in addition to the positive ions, move to their respective electrodes and are collected by a circuit that includes an electrometer. Volumes vary from ~0.005 cc to ~800 cc. Currents vary from ~1 pA to ~1 μA. Note that these currents are very small. The total charge collected is likewise very small.

Ion chambers operate in the saturation region shown in Figure 13.1. The energy deposited in the sensitive volume that produces ionization is more directly connected to dose in this saturation region. However, since there is no multiplication of charge in this region, one needs a large enough fluence to operate an ion chamber. Hospital linear accelerators typically satisfy this requirement. The ion chamber is, therefore, the dosimeter of choice for the most careful calibrations that need to be done. We will focus on ion chambers for the remainder of this book.

Thimble-type Chambers

Thimble-type chamber is a fundamental tool for medical dosimetry physics and the main type used in the calibration protocols. It is a cylindrical or spherical cavity in which an electric field is applied between a conducting wall and a collector electrode along the center of the cavity (Figure 13.2).
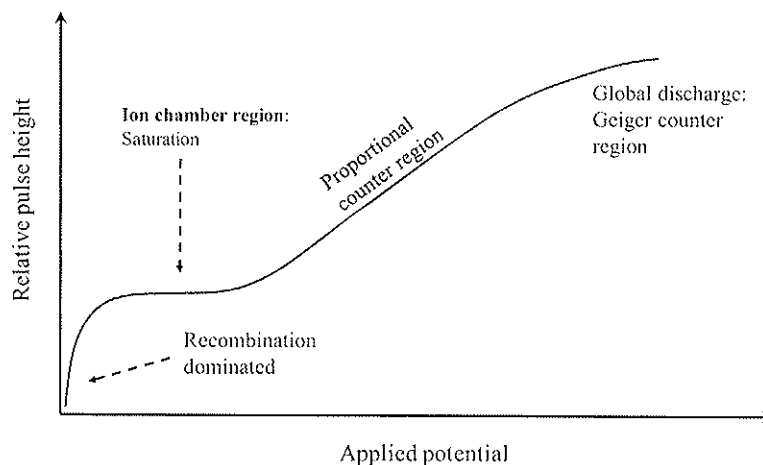

Figure 13.1. Ion chambers operate in a saturation region where ideally all the charges are collected, and without multiplication, such as in the proportional counter region.
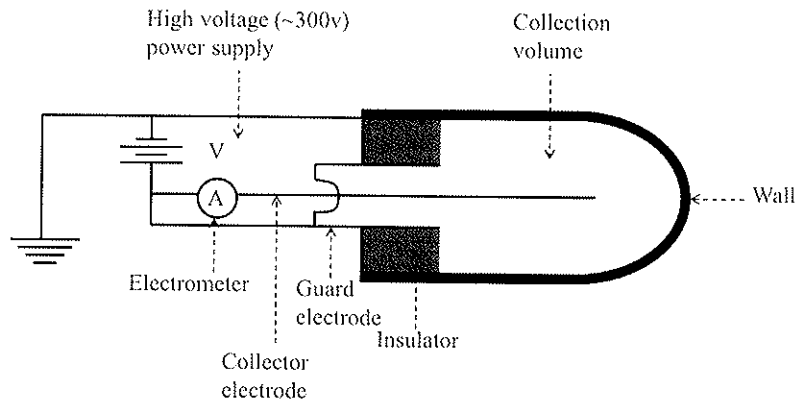
Figure 13.2. A thimble-type ion chamber shown in the context of a simplified circuit for collecting the ions.

The chamber wall, and also any other material surrounding it (phantom), is usually the main source of charged particles. The wall is often made from C-552 or graphite. It is often (but not always) made thick enough to establish CPE or TCPE that is fully characteristic of the photon interactions taking place in the wall material or thin enough to not perturb the fluence of charged particles, if charged particles are the primary radiation.

The current collected is very small. The voltage on the inner electrodes is high, and it usually uses a triaxial cable to include a guard. The guard electrode grounds the current that leaks between the wall and collector electrodes. The leaks mainly occur along the surface of the insulator separating the electrodes, but the cable joining the ion chamber to the electrometer can leak as well—especially if the triaxial cable is kinked and bent a lot, which always seems to happen in a busy hospital. The guard defines the collection volume of the ion chamber. The collection volume is impossible to manufacture to the precision needed in hospital applications, so each ion chamber and its electrometer must be calibrated in a known field regularly to make sure the ion chamber response remains a known quantity with the needed precision and accuracy.

Condenser-type Chambers

A condenser chamber is not connected to an electrometer during irradiation. Instead, a high voltage is placed between two electrodes (Figure 13.3). The condenser chamber can be thought of as an ion chamber in parallel with a capacitor (Figure 13.4), where the combined capacitance of the chamber and the capacitor is $C = C_{cap} + C_{chamb}$. The initial charging voltage is P_1. After irradiation, one gets the remaining voltage, P_2. The charge collected from the chamber, ΔQ, is given by the following:

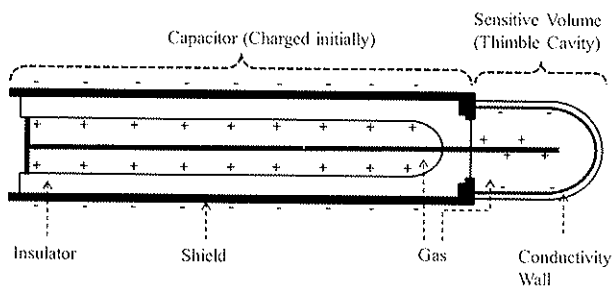$$\Delta Q = Q_1 - Q_2 = C(P_1 - P_2). \tag{13.1}$$

Figure 13.3. Condenser-type ion chamber. Radiation gradually discharges the capacitor.
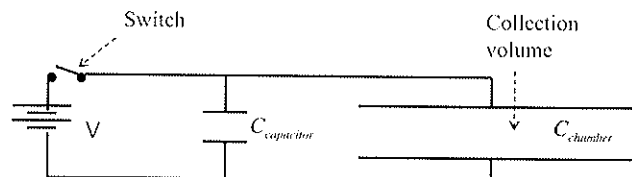

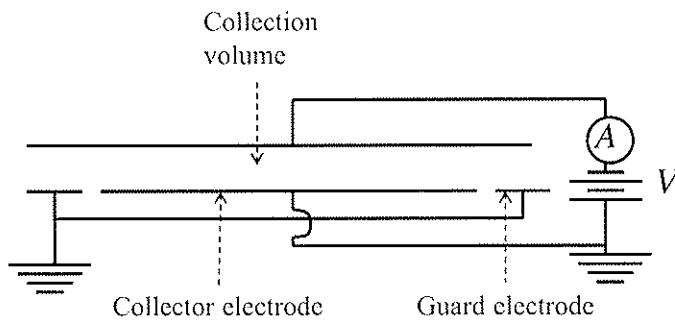**Figure 13.4.** Condenser-type ion chamber circuit.

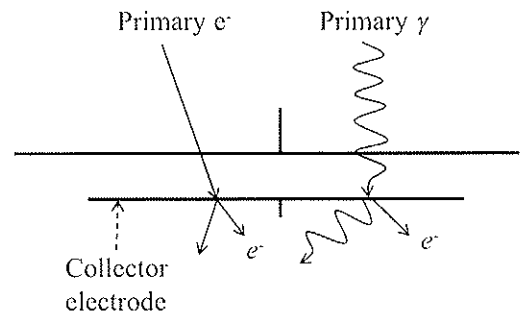**Figure 13.5.** Parallel plate ion chamber circuit.

Figure 13.6. False currents or charges can occur from radiation interacting with the collecting electrodes.

Since the voltage across the chamber decreases during the irradiation, there must eventually be recombination of some ions before they can reach the electrodes. This means that some ions produced will not be collected—a correction for this is discussed later. The recombination depends on voltage, so other ion chambers make efforts to keep the voltage constant.

Parallel Plate Chambers

In parallel plate chambers (Figure 13.5), the voltage across the plates is kept constant. One or both of the plates is thin enough, and conducting, to allow minimal attenuation or scattering of incident electrons or low-energy photons. The plate separation can be very small, and it can also be variable (an extrapolation chamber). In this way, one can get close to a surface dose, and if it is an extrapolation chamber, then the surface dose is inferred from the extrapolation of a series of measurements.

If the collector electrode is too thick, then extra electrons can be knocked out by photons, primary charged particles, or δ-rays, all of which will lead to an increase in positive charge. If charged positive originally, then it will appear as though fewer ions were created. If originally charged negative, then it will appear as though more ions are created in the cavity (see Figure 13.6.).

This "polarity" effect can be corrected for by taking measurements with both polarities and averaging the results. All chambers should have triaxial cables to guard against current leakage so leakage is not accidentally included in the measurement.

Charge and Current Measurements

The amount of charge of one sign is found, in general, by the following for an air-filled cavity:

$$D_{air} = \frac{Q}{M}\left(\frac{\overline{W}}{e}\right)_{air}.$$

(13.2)

The charge collected and current measured are very small. For example, if the dose to air in the cavity is 1 Gy and the volume of that air at 22 °C and 1 atm is the pressure of gas in a volume of 1 cc, then the charge collected is given by the following:

$$Q = \frac{D_{air}M}{(\bar{W}/e)_{air}} = \frac{D_{air}\rho_{air}V}{(\bar{W}/e)_{air}},$$

$$= \frac{(1 \text{ J/kg})(1.29 \times 10^{-3} \text{ g/cc})(1 \text{ cc})(10^{-3} \text{ kg/g})}{(33.97 \text{ J/C})} = 3.80 \times 10^{-8} \text{ C}.$$

(13.3)

The calculated charge is small. In radiotherapy, a dose like this can take only about 30 s of continuous beam-on time, so the current would be the following:

$$i = \frac{\Delta Q}{\Delta t} = \frac{3.80 \times 10^{-8} \text{ C}}{30 \text{ s}} = 1.27 \text{ nA}.$$

(13.4)

A typical ammeter cannot measure this small a current, and this is also the reason why you should treat your triax cable with care. A typical digital multimeter can sense ~2 mA. A high-end one can sense ~20 μA with 10^7 Ω input impedance. An electrometer is, therefore, used with ion chambers. An electrometer is a very high-impendence voltmeter that can be used to measure current or voltage on a calibrated capacitor on which this collected charge is accumulated. An electrometer typically has 10^{14} Ω input impedance and can cost between $2,000 to $10,000 dollars.

Charge Measurement Specifics

Modern electrometers use operational-amplifiers (op-amps) to amplify the voltage. Following Attix (2004), a simple configuration for an electrometer would be like in Figure 13.7, where G is the gain of the op-amp, and C_i is the ion chamber's and its cable's intrinsic capacitance. A charge, Q, flows from the ion chamber and responds to a potential, P_i.

The total potential across the capacitor, C, is $P_0 - (-P_i)$, and it holds a charge, $C(P_0 + P_i)$. This capacitor is in parallel with the inherent capacitance, C_i (the chamber and the cable). Therefore, the ion chamber charge is as follows:

$$Q = C\left(P_0 + P_i\right) + C_iP_i = CP_0 + \left(C + C_i\right)P_i = C(GP_i) + CP_i + C_iP_i.$$
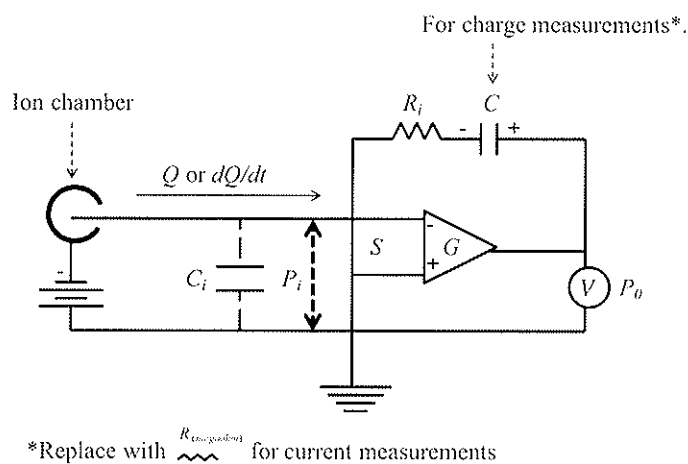
(13.5)

Figure 13.7. This simple op-amp circuit for an ion chamber is so simplistic the guard circuit is not even shown.

We can assume a large gain approximation, $CG \gg C_i$ and $G + 1 \approx G$. Therefore,

$$Q = CGP_i = CP_0. \tag{13.6}$$

Smaller capacitors, C, allow for smaller charges to be measured: the output voltage, P_0, is inversely proportional to C, that is, $P_0 \cong \dfrac{Q}{C}$.

Current Measurement Specifics

If one replaces the capacitor, C, in Figure 13.7 with a very large megaohm resistor, R, the current, I, that passes through both R and the inherent, R_i, is as follows by using $P_0 = GP_i$:

$$i(R + R_i) = P_0 + P_i = (G + 1)P_i. \tag{13.7}$$

With two assumptions, small inherent resistance, $R \gg R_i$, and large gain approximations, $G + 1 \approx G$, the current would be as follows:

$$i \cong \frac{GP_i}{R} = \frac{P_0}{R}. \tag{13.8}$$

Therefore, large resistors, R, allow for smaller currents to be measured.

Figure 13.8 illustrates a typical triax mode circuit, while Figure 13.9 shows a coax mode circuit with an external high voltage supply[*]. Note that the resistor for feedback to the inverting input makes the op-amp circuit look like a high-pass filter. Op-amps act to force the inverting input (−) to have equal voltage to the non-inverting input (+).

Density and Humidity Corrections to an Ideal Ion Chamber

An ion chamber (and its electrometer) gets calibrated at a National Institute of Standards and Technology (NIST) calibration lab at 22 °C and 760 torr[‡]. Therefore, $T_{cal} = (273 + 22)$ K = 295 K and $P_{cal} = 760$ torr.
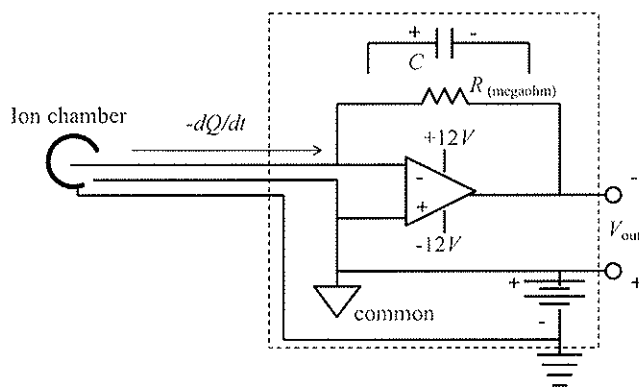

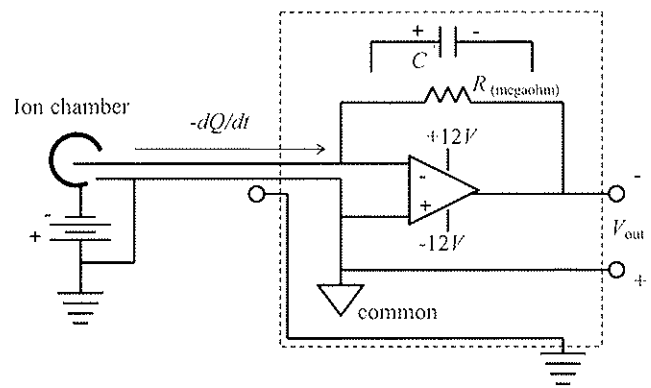**Figure 13.8.** Triax mode circuit.

Figure 13.9. Coax mode circuit (external HV supply).

---

[*]The circuits shown in Figures 13.8 and 13.9 are realistic circuits.
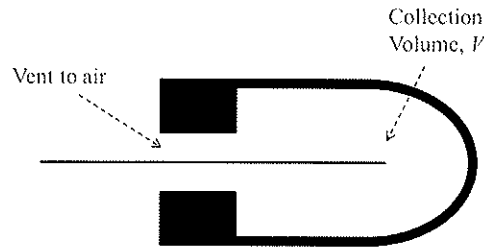[‡]1 torr = 1 mm Hg = 1/760 atm = 0.1333 kPa.

Figure 13.10. Geometry of an idealized ion chamber.

Consider an idealized ion chamber that vents to air in the atmosphere that is dry for the moment (Figure 13.10).

Using ideal gas law[*], we can relate the present gas density to that which occurred at calibration by the following equation:

$$\frac{\rho}{\rho_{cal}} = \frac{n}{n_{cal}} = \frac{T_{cal}}{T} \cdot \frac{P}{P_{cal}} = \frac{295K}{273K + T(^{\circ}C)} \cdot \frac{p \text{ (torr)}}{760 \text{ torr}}. \tag{13.9}$$

The density of dry air at 0 °C and 760 torr is $\rho = 0.0012929$ g/cc.

Now this time let's consider the ion chamber venting to air, which is humid. Humid air is less dense. The water vapor contains a lot of hydrogen. The density of humid air is calculated by the following:

$$\frac{\rho_h}{\rho_{cal}} = \frac{295K}{273K + T(^{\circ}C)} \cdot \frac{p(\text{torr}) - 0.3783 p_w}{760 \text{ torr}}. \tag{13.10}$$

where, ρ_h is the density of humid air and p_w is the partial pressure of water (torr) in the air. The partial pressure of water, p_w, is calculated as follows:

$$p_w = \left[19.827 \text{ torr} + 1.21\left(T(^{\circ}C) - 22\,^{\circ}C\right)\frac{\text{torr}}{^{\circ}C} \right]\frac{\text{RH}_{\%}}{100}. \tag{13.11}$$

In the above, $\text{RH}_{\%}$ is the relative humidity of the air.

The other humidity effect is that $(\overline{W}/e)_h$ for humid air is less than $(\overline{W}/e)_d$ for dry air (= 33.97 J/C); it is easier to ionize the hydrogen in water than the oxygen and nitrogen in the air. Recall that we find the dose, D, as $D = \frac{Q}{M}\left(\frac{\overline{W}}{e}\right)$. This allows us to express the ratio of charge produced in humid air, Q_h, to that in dry air, Q_d, as follows:

$$\frac{Q_h}{Q_d} = \frac{\left(D_h M_h / (\overline{W}/e)_h\right)}{\left(D_d M_d / (\overline{W}/e)_d\right)}. \tag{13.12}$$

Assuming Bragg–Gray theory applies ($D \propto \Phi(dT/\rho dx)$) and we also know $M = \rho V$, therefore,

$$\frac{Q_h}{Q_d} = \frac{\left(\Phi(dT/\rho dx)_h \rho_h V / (\overline{W}/e)_h\right)}{\left(\Phi(dT/\rho dx)_d \rho_d V / (\overline{W}/e)_d\right)}. \tag{13.13}$$

[†]$PV = nRT$, where, P, V, and T are pressure, volume, and temperature of the gas, respectively. The quantity n is number of moles of the gas, and R is the gas constant.

Note that the z/A dependence in the stopping power is quite different when something has a lot of H in it. The quantity z/A for hydrogen-1 is 1.0. The density of humid air is lower (as we all know from the weather). Therefore, we can write and summarize the effects of humidity as follows:

$$\frac{Q_h}{Q_d} = \overbrace{\frac{(\bar{W}/e)_h}{(\bar{W}/e)_d}}^{<1 \text{ less energy to ionize water}} \cdot \underbrace{\frac{(dT/\rho dx)_h}{(dT/\rho dx)_d}}_{>1 \text{ hydrogen has a high } z/A} \cdot \overbrace{\frac{\rho_h}{\rho_d}}^{<1 \text{ H}_2\text{O is lighter than O}_2 \text{ and N}_2} \cdot \tag{13.14}$$

Ion Chamber Saturation and Recombination

The dose in the ion chamber gas is proportional to the charge of one sign produced, Q. Both signs exist and travel in opposite directions, past each other, on their way to different electrodes. They can combine and neutralize each other. Recombination reduces with increasing potential between electrodes. Recombination also generally increases with density. When the recombination does not change upon further increases in electrode potential, the ion chamber is said to be saturated. When the electrode potential is increased further, then the migrating charges can cause subsequent ionizations (avalanches), and this process is used in proportional counters and in Geiger–Müller counters[†].

There is a recombination dependence on initial ion concentration. High-LET (linear energy transfer) particles, like alphas, produce so many ions that recombination will be larger than for low-LET particles, like electrons. Our focus is on volumetric or general recombination—initially uniformly distributed ion concentrations in the cavity.

Here we define the **charge collection efficiency**, f. It is defined as the ratio of the charge collected, Q', to the charge produced, Q.

The drift velocity of the ions across the chamber (mobility) is proportional to the electric field strength, E, as follows (units are volts/m):

$$v_1 = k_1 E, \tag{13.15}$$

$$v_2 = k_2 E. \tag{13.16}$$

Here k_1 and k_2 are the mobilities of the positive and negative ions, respectively, and their units are m^2/(volts · s). Note that "mobility" is a terminal velocity and not an acceleration, because it assumes a constant drag—continuous bumping of each other as the ions try to accelerate toward the electrodes. With an electronegative gas, an electron attaches to a gas molecule, and this makes the positive and negative ion mobilities about equal. With nonelectronegative gases—like N_2, CO_2, H_2, methane, and the noble gases—the electron does not attach, so the very light electrons have a much higher mobility, or about 10^3 cm^2/(volts · s).

[†] For proportional counters and Geiger–Müller counters, see Attix (2004), Chapter 15.
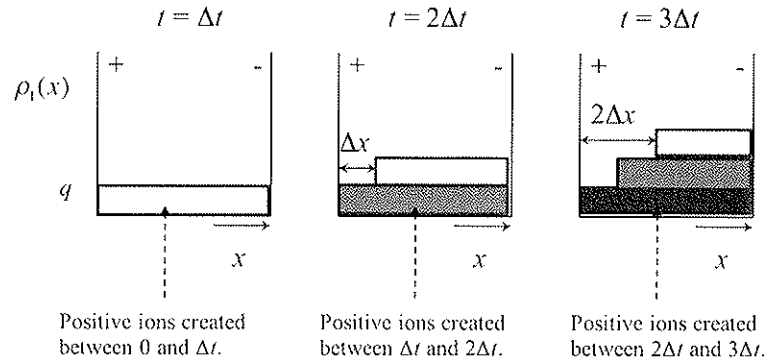
Figure 13.11. Simplified diagram of the creation and migration of charges in an ion chamber to show how the profile forms.

Consider the following situation: a parallel plate chamber with an electronegative gas in a continuous radiation field. Just after the irradiation starts, the positive ion charge density, $\rho_1(x)$, (units are C/m³), looks like Figure 13.11. The ions move the distance Δx ($= v_1 \Delta t = k_1 E \Delta t$) between frame 1 and 2 in time Δt. The ionization density rate is q (units are esu/m³s), and the time it takes a positive ion to cross the cavity from its creation at the opposite electrode is τ_1:

$$\tau_1 = d / v_1 = \frac{d}{k_1 E}.$$ (13.17)

There is an analogous relation for the negative ions, τ_2. At times greater than τ_1 and τ_2, the steady state charge density is achieved. The charge density of positive ions just next to the negative electrode is as follows:

$$\rho_1(x = d) = q \Delta t \frac{\tau_1}{\Delta t} = q \tau_1 = \frac{qd}{k_1 E},$$ (13.18)

and,
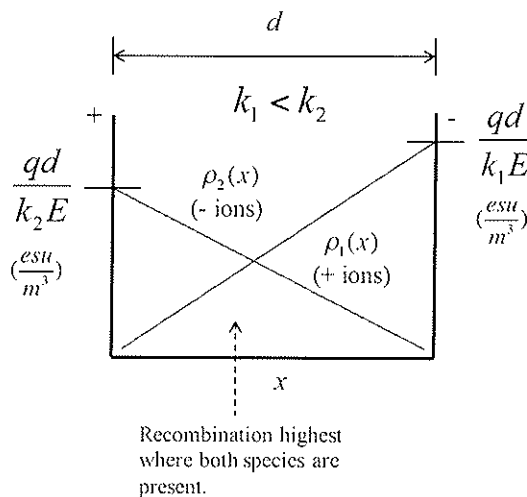
$$q = \frac{\rho}{t}.$$ (13.19)

Figure 13.12. Simplified charge profiles in an ion chamber assuming no recombination.

Likewise for the negative ions. If the mobility is different, then the steady state charge density will be different as well. In general, one might get a **steady state charge distribution** like in Figure 13.12. Note that the highest recombination would be in the middle. Also, the level depends on the mobility.

The above was derived *without* recombination, but it's a fine approximation if recombination is small. As mentioned, the recombination rate per volume, $r(x)$, with units of C/m^3s, is proportional to the charge densities of both species as follows:

$$r(x) = \frac{\alpha}{e} \rho_1(x)\rho_2(x),$$ (13.20)

where α is a the recombination constant with units m^3/s. The total (integrated) recombination rate, R, is as follows:

$$R = \frac{\alpha}{e} \int_0^d \rho_1(x)\rho_2(x)dx.$$ (13.21)

Inserting what we already have, the total (integrated) recombination rate would be as follows:

$$R = \frac{\alpha}{e} \int_0^d \left\{ \left(\frac{qd}{k_1 E}\right)\left(\frac{x}{d}\right) \cdot \left(\frac{qd}{k_2 E}\right)\left(1 - \frac{x}{d}\right) \right\} dx = \frac{\alpha q^2}{e k_1 k_2 E^2} \int_0^d \left\{ (x)\cdot(d-x) \right\} dx = \frac{\alpha q^2 d^3}{6 e k_1 k_2 E^2}.$$ (13.22)

Now we can use these equations for the collection efficiency, f. Note that the charge produced per unit area and per unit time is qd. Therefore,

$$f = 1 - \frac{R}{qd} = 1 - \frac{\alpha q d^2}{6 e k_1 k_2 E^2}.$$ (13.23)

For a parallel plate geometry, the electric field, E, is related to the potential, P, by $E = P/d$. Therefore, the collection efficiency is as follows:

$$f = 1 - \frac{1}{6}\xi^2.$$ (13.24)

We define ξ as follows:

$$\xi \equiv \frac{d^2\sqrt{q}}{P} \sqrt{\frac{\alpha}{e k_1 k_2}} = m \frac{d^2\sqrt{q}}{P},$$ (13.25)

where, $m = 36.7$ volts·$s^{1/2}$ cm$^{-1/2}$ esu$^{-1/2}$ for air at (one type of) STP (= 0 °C, 760 torr).

We actually overestimated the recombination, since we should have considered recombination when giving the charge densities. It can be fixed by integrating with the charge densities at the electrodes as $\frac{fqd}{k_1 E}$ and $\frac{fqd}{k_2 E}$. We would then get $(R/qd) = (f^2\xi^2/6)$ and $f = 1 - \frac{1}{6}f^2\xi^2 = \frac{Q'}{Q}$. However, this now underestimates the recombination because we have not considered the more complex shape of the charge densities—space charge alteration of the electric field (solid lines in Figure 13.13).
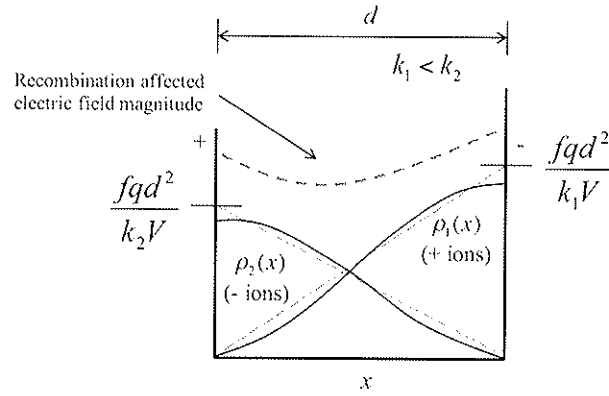
Figure 13.13. More realistic charge profiles in an ion chamber.

According to Mie's theory, $\dfrac{R}{qd} = \dfrac{1}{6} f \xi^2$ and $f = 1 - \dfrac{1}{6} f \xi^2$ (not quadratic this time), and this gives the following:

$$f = \frac{1}{1 + (\xi^2 / 6)}. \tag{13.26}$$

In summary then,

$$f = 1 - \frac{1}{6} f^{\overbrace{\{0,1,2\}}} \xi^2, \tag{13.27}$$

where an exponent of 0 is for an E constant and no recombination, an exponent of 1 is for E adjusted with recombination, and, finally, an exponent of 2 is for E constant with recombination[†].

Let's find the charge produced as follows (if f is not too far from 1):

$$\frac{1}{f} = \frac{Q}{Q'} \approx 1 + \frac{1}{6} \xi^2 = 1 + \frac{1}{6} \frac{m^2 d^4 q}{P^2}. \tag{13.28}$$

If the irradiation time, t, is much longer than τ:

$$Q = qVt \rightarrow \frac{Q}{Q'} = 1 + \frac{cQ}{P^2}. \tag{13.29}$$

Here, $c \equiv \dfrac{m^2 d^4}{6Vt}$, and dividing by Q gives the following linear equation:

$$\frac{1}{Q'} = \frac{1}{Q} + \frac{c}{P^2}. \tag{13.30}$$

[†]For another approach to this subject, see Johns and Cunningham (1983), Chapter 9.
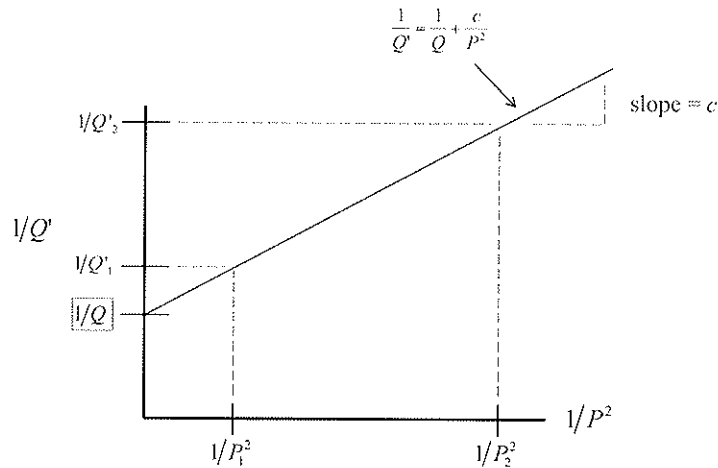
Figure 13.14. Jaffé plot for recombination.

Let's use this to produce the so-called Jaffé plot (Figure 13.14). See Attix (2004), page 335.

We can use this, extrapolating from two measurements, to get Q, the charge produced. This is also called the *"saturation charge."* If the radiation is pulsed, then this steady state will likely not be reached: a typical linac has 1 μs pulses that are 1 ms apart. Recombination requires significant overlapping charge densities. It is worth exploring confounding issues more closely. In both TG-21 (IV.c and Figure 4) and TG-51 (Equations 11 and 12), there is a "two-voltage" technique to correct for recombination that relies on the above figure being linear. For typical chambers, errors of <0.5% occur because of that assumption.

For typical ion chambers, there are other factors—such as prompt ("initial") recombination and ionic diffusion—that can also lead to charge reduction. The ion chamber plateau region of the response to applied potential is also not truly flat because of some charge multiplication.

In smaller chambers, like the A1SL, these effects can be more pronounced, since the region near walls, which has more varying electric fields, is a larger portion of the total volume. Therefore, deviations from linearity, or a pure ion chamber-type response, can be more pronounced in small chambers or micro-chambers.

In Zankowski and Podgorsak (1998), the following form is used to include these corrections:

$$\frac{1}{Q'} = \left(\frac{1}{Q} + \underbrace{\frac{\alpha}{P}}_{\substack{\text{initial} \\ \text{recombination,} \\ \text{ionic} \\ \text{diffusion}}} + \overbrace{\frac{\beta}{P^2}}^{\substack{\text{general} \\ \text{recombination}}} \right) \underbrace{\exp\{-\gamma P\}}_{\substack{\text{charge} \\ \text{multiplication}}}. \tag{13.31}$$

References

Attix, F.H. *Introduction to Radiological Physics and Radiation Dosimetry*. Weinheim, Germany: WILEY-VCH Verlag GmbH & Co. KGaA, 2004.

Johns, H.E. and J.R. Cunningham. *The Physics of Radiology*, 4th Ed. Springfield, IL: Thomas, 1983.

Zankowski, C. and E.B. Podgorsak. (1998). *Med. Phys.* 25:908–15.

14

Calibration of Ion Chambers and Photon Beams

The TG-21 protocol (AAPM 1983) is "a protocol for the determination of absorbed dose from high-energy photon and electron beam" and the result of a task group from the American Association of Physicists in Medicine (AAPM). In this chapter, first we explore this older and outdated protocol, and then discuss the newer clinical protocol, Task Group 51 (AAPM 1999) in a comparative way, showing how quantities in one are related to those in the other. The reasons for explaining TG-21 are both that, unfortunately, it may still be used somewhere, and more importantly, the cavity theory physics is more transparent. By learning TG-21 first, it will be easy to understand TG-51 later. The analogy is that it is easy to learn to drive with an automatic transmission after one learns to drive with a manual transmission first. TG-21 is analogous to the manual transmission car.

Note that what is left out of this discussion is the excess scatter correction for phantoms other than water, like acrylic. The reason is that this discussion of an old protocol is connected to the more modern protocol via dose to water at the end. The focus on an old protocol is for educational purposes of understanding theory, and not to be complete in how to use the outdated protocol. It also makes sense to neglect discussions of even older protocols that use concepts like C_λ, since they are *very* outdated now.

The basic issue is that each clinical linac beam is different in "quality." In other words, each beam will have some uniqueness to its energy spectrum. One "dials in" a "monitor unit." The monitor unit, MU, is calibrated to give 1 cGy at reference conditions. It would be obviously deceptive to have "cGy" on the linac dial, since it would give the false impression that it was always calibrated and always with a setup of reference conditions.

Inherent to this "reference condition" is an ion chamber. That ion chamber and its electrometer need to be calibrated. The only way to do this—considering that each linac has a unique energy spectrum and that each chamber has a unique charge collection volume at a microscopic level—is to send the chamber and electrometer to a place with a Co-60 source that is itself well calibrated. In the United States, the various Accredited Dosimetry Calibration Laboratories (ADCL) do this very task. They work in concert with the National Institute of Standards and Technology (NIST) to maintain the source: Co-60 always has the same beam quality. It only gets less radioactive as time progresses.

These calibration laboratories can provide the "exposure" from the Co-60 source in a volume of air. They can characterize your ion chamber's response to their source. They provide that "response" to you in the form of a factor called N_x, and you then use all the physics we have just learned, wrapped in factors that we will now learn about, to be able to determine what the dose in the reference condition is for your linac. Then you will be able to adjust the linac, if needed, to provide for 1 MU = 1 cGy at the reference conditions, and the patients will get their planned dose to well within 1% from physics considerations alone (neglecting all biology). A 1% uncertainty is possible with TG-51, but not really with TG-21.

Note that TG-21 has its own notations that might be different from notations that have been used in this book until now. In this chapter, notations are as what they are in TG-21.
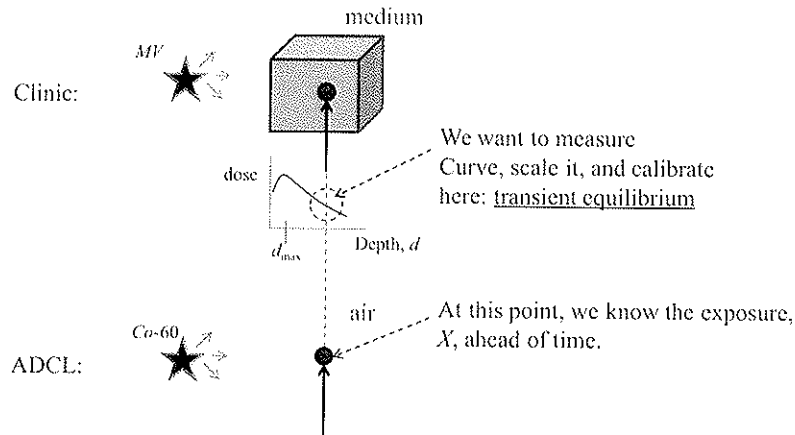
Figure 14.1. The TG-21 protocol converts a chamber response from the ADCL to the clinic situation.

Understanding TG-21 at the NIST Calibration Lab (ADCL)

At the NIST lab (or ADCL), they put the chamber and electrometer in their Co-60 beam and get the relation between the exposure and the dose to the chamber gas (Figure 14.1). The NIST lab knows the exposure, X. A clinician's chamber is placed where they know the exposure, X, and an electrometer reading, M, is obtained (units of charge, C). That reading is corrected to 22 °C and 1 atm. The value of N_X is obtained as follows (Equation 2 of TG-21):

$$N_X = \frac{X}{M}.$$

(14.1)

How does the NIST lab get X? They know and calculated X from a variety of measurements. See Equation 1 in TG-21 and the preceding text:

$$X = k^{-1} J_{gas} \left(\frac{\bar{L}}{\rho}\right)^{wall}_{gas} \left\{\frac{\bar{\mu}_{en}}{\rho}\right\}^{air}_{wall} \beta^{-1}_{wall} \left(\prod_i K_i\right).$$

(14.2)

In Equation (14.2), $k = 2.58 \times 10^{-4}$ C/kg/R. The next quantity, J_{gas}, is defined as the *charge per unit mass of the cavity gas*[†].

We assume a Spencer–Attix cavity theory for the chamber, $\left(\dfrac{\bar{L}}{\rho}\right)^{wall}_{gas}$. Also we assume the photon energy fluence through the room air is unperturbed by the chamber wall, $\left\{\dfrac{\bar{\mu}_{en}}{\rho}\right\}^{air}_{wall}$, at zero thickness. The quantity β_{wall} is the ratio of dose to collision kerma in the chamber wall, and it is equal to 1.005 (i.e., the ADCL must use a carbon wall to get "X"). The "K" factors represent water vapor content of the room air, ionization recombination losses, scatter from the stem of chamber, correction to zero wall thickness, and some other factors as follows:

$$\prod_i K_i \cong \frac{1}{A_{ion} A_{wall}},$$

(14.3)

[†] In the chamber is a "gas." It is almost always air, but in the protocol they write "gas" for the air *inside* the chamber. The word "*air*" will refer to the air in the ADCL room.

where, A_{ion} accounts for ion recombination losses for the Co-60 beam. It is Q'/Q in our previous notation, the ratio of charge collected to charge produced in the cavity gas, the charge collection efficiency, f, and A_{wall} accounts for the wall thickness effects different from zero on the collision kerma.

We will use A_{ion} and N_X to calculate N_{gas}, which is a property of the chamber and buildup cap, but not the phantom, in the clinic.

The following equation relates the dose in chamber gas to dose in the wall:

$$D_{gas} = \left(\frac{D_{gas}}{D_{wall}} \right) [D_{wall}]. \tag{14.4}$$

Wall dose in TCPE is a buildup (β_{wall}) from its collision kerma (graphite walls with Co-60). (See the text near Equation 1 in TG-21.) Therefore, Equation (14.4) can be turned into the following:

$$D_{gas} = \left(\frac{D_{gas}}{D_{wall}} \right) [\beta_{wall} (K_c)_{wall}]. \tag{14.5}$$

Note that wall includes a cap ($\alpha = 1$), i.e., the same z_{eff} for now. Also, β_{wall} is actually a correction for charged particle fluence changes. The buildup is needed to relate collision kerma to dose (see Figure 14.2).

Equation (14.5) relates to kerma in the room air (at the ADCL) as follows:

$$D_{gas} = \left(\frac{D_{gas}}{D_{wall}} \right) \left[\beta_{wall} \left\{ \frac{(K_c)_{wall}}{(K_c)_{air}} \right\} (K_c)_{air} \right]. \tag{14.6}$$
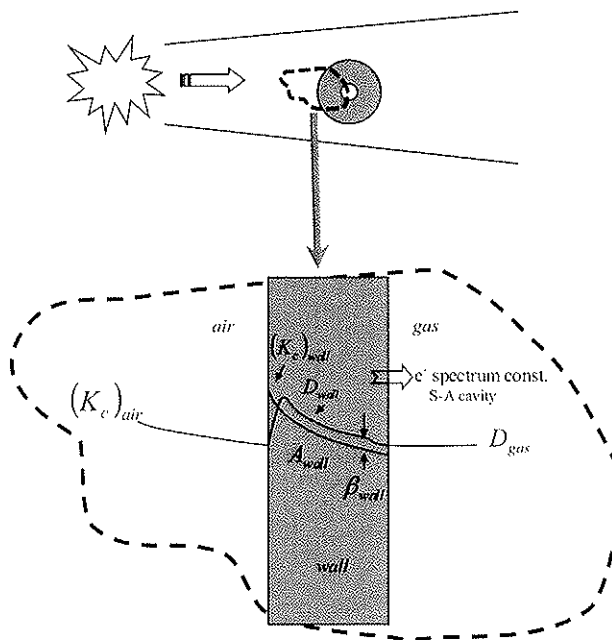

Figure 14.2. The factors A_{wall} and β_{wall} account for fluence perturbations and buildup in the wall. In effect, factors like these make up for the assumptions needed to apply cavity theory.
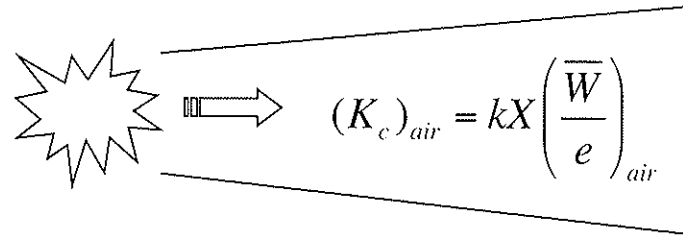
Figure 14.3. The ADCL knows X in the room, and so also $(K_c)_{air}$ is known.

In order to relate the room air kerma to the ADCL room air, $(K_c)_{air}$ is replaced by $kX\left(\dfrac{\bar{W}}{e}\right)_{air}$ as follows (see Figure 14.3):

$$D_{gas} = \left(\frac{D_{gas}}{D_{wall}}\right)\left[\beta_{wall}\left\{\frac{(K_c)_{wall}}{(K_c)_{air}}\right\}kX\left(\frac{\bar{W}}{e}\right)_{air}\right]. \tag{14.7}$$

Note that $\left(\dfrac{\bar{W}}{e}\right)_{air}$ is *not* a function of beam energy. Now assume that photon energy spectrum is unperturbed until corrected for attenuation in the wall[*] (A_{wall}):

$$D_{gas} = \left(\frac{D_{gas}}{D_{wall}}\right)\left[A_{wall}\beta_{wall}\left\{\frac{\bar{\mu}_{en}}{\rho}\right\}_{air}^{wall}kX\left(\frac{\bar{W}}{e}\right)_{air}\right]. \tag{14.8}$$

Applying Spencer–Attix cavity theory results in the following[*]:

$$D_{gas} = \left(\frac{\bar{L}}{\rho}\right)_{wall}^{gas}\left[A_{wall}\beta_{wall}\left\{\frac{\bar{\mu}_{en}}{\rho}\right\}_{air}^{wall}kX\left(\frac{\bar{W}}{e}\right)_{air}\right]. \tag{14.9}$$

With Equation (14.1), we can relate exposure, X, to the charge collected, M, as follows:

$$D_{gas} = \left(\frac{\bar{L}}{\rho}\right)_{wall}^{gas}\left[A_{wall}\beta_{wall}\left\{\frac{\mu_{en}}{\rho}\right\}_{air}^{wall}MkN_X\left(\frac{\bar{W}}{e}\right)_{air}\right]. \tag{14.10}$$

We rearrange to get the following equation in which recombination has not yet been accounted for:

$$D_{gas} = M\left[A_{wall}\beta_{wall}\left(\frac{\bar{L}}{\rho}\right)_{wall}^{gas}\left\{\frac{\mu_{en}}{\rho}\right\}_{air}^{wall}N_X k\left(\frac{\bar{W}}{e}\right)_{air}\right]. \tag{14.11}$$

[†]Note the photon fluence correction: $A_{wall} = e^{-\mu'\ell} \cong 1 - (\mu'/\rho)\rho\ell$. Also note that the photon fluence correction is decoupled from the charged particle fluence correction: β_{wall} for Co-60 beam at ADCL.

[‡]Bragg–Gray would have been fine, with errors of only a few tenths of a percent if the wall is almost water equivalent. The $\Delta = 10$ keV and the R_{CSDA} in air is 0.25 cm. Table 13.2 Attix (2004) shows the error if one were to use Bragg–Gray.

We know that the dose to the chamber gas is found by the following (Equation 3 of TG-21):

$$D_{gas} = J_{gas}\left(\frac{\bar{W}}{e}\right)_{gas}.$$ (14.12)

The energy deposited for an ion pair for room air (not dry air) in our energy range is provided to be 33.7 J/C. The J_{gas} is assumed to be corrected for recombination here, so if not, write as follows:

$$D_{gas} = (J_{gas}A_{ion})\left(\frac{\bar{W}}{e}\right)_{gas}.$$ (14.13)

Equation 4 of TG-21 is:

$$D_{gas} = N_{gas}\left(M / A_{ion}\right).$$ (14.14)

Recognize now N_{gas} by comparing Equation (14.14) to Equation (14.11) as follows:

$$N_{gas} \equiv A_{wall}\beta_{wall}\left(\frac{\bar{L}}{\rho}\right)_{wall}^{gas}\left\{\frac{\mu_{en}}{\rho}\right\}_{air}^{wall} A_{ion}N_{x}k\left(\frac{\bar{W}}{e}\right)_{air}.$$ (14.15)

With some rearrangements we get to Equation 5 of TG-21:

$$N_{gas} = N_{x}\frac{A_{wall}\beta_{wall}A_{ion}k\left(\frac{\bar{W}}{e}\right)_{air}}{\left(\frac{\bar{L}}{\rho}\right)_{gas}^{wall}\left\{\frac{\bar{\mu}_{en}}{\rho}\right\}_{wall}^{air}}.$$ (14.16)

An advantage of N_{gas} is that it is a property only of the chamber. Note that all of these correction factors are for Co-60 beam quality—this is essentially a correction that takes this beam quality out so that another beam quality can be used for this chamber. However, this is an intermediate stage that cannot be directly measured; one must apply N_{gas} to measure it. So N_{gas} is somewhat abstract.

Now, if we get N_{x} from the NIST lab, we can use this to calculate N_{gas} such that N_{gas} has the meaning: $D_{gas} = M \cdot N_{gas}$. Here we assume "$M$" is corrected for recombination. Be careful to note that TG-21 gets confusing where A_{ion} gets included or not. Also, M here must be corrected for temperature and pressure.

The NIST lab gives us N_{x} and A_{ion}. Next at the clinic, we need to calculate N_{gas} ourselves. Then, we will have our own correction factors: *P-factors for the clinic versus A-factors for the NIST lab.*

Understanding TG-21 at the Clinic

In the clinic, we will have a medium (a phantom). At the ADSL, it had one too, even if it is just a buildup cap. The beam energy is also different, and it is pulsed in the clinic. TG-21 says all we need is TCPE in the phantom (medium), and suggests the depths shown in Table 14.1. As a rough rule of thumb, consider: $d_{max}(cm) \sim E(MV) / 4$. For TCPE, the depth needs to exceed d_{max}.

Table 14.1: Suggested Depths for TCPE from TG-21

Beam Nominal Energy (MV)	Depth (cm)
Co-60–15	5
16–25	7
26–50	10

The dose to the medium is built up the same way as before, Equation (14.4):

$$D_{med} = \left(\frac{D_{med}}{D_{gas}} \right) D_{gas}.$$ (14.17)

Then the dose to the cavity gas is given by the following:

$$D_{gas} = (M \cdot P_{ion}) N_{gas}.$$ (14.18)

Pay attention that $(M \cdot P_{ion})$ is charges liberated and M is charges collected. Expect very small or very large chambers to have complicated recombination dynamics. Note, we also needed to use a different factor for the ion recombination losses: P_{ion}, but strangely enough, it is the inverse (Q/Q') of A_{ion}. Most common ion chambers have $P_{ion} = 1/A_{ion}$. The older approach to recombination is as follows:

$$P_s = a_0 + a_1 \left(\frac{R_1}{R_2} \right) + a_2 \left(\frac{R_1}{R_2} \right)^2,$$ (14.19)

where, R_1 is read at −300 v, and R_2 is read at −100 v, for example.

More general than just TG-21, charges collected, M, must be corrected for temperature, pressure, and some other things at this stage. Later, other factors are explicitly corrected for outside of "M." For now, we correct M as follows:

$$M = M_{raw} \cdot P_{t,p} \cdot P_h \cdot P_{pol},$$ (14.20)

where, M_{raw} is the uncorrected ion chamber reading. The part $P_{t,p}$ is temperature and pressure correction that, as you would expect, is given by the following:

$$P_{t,p} = \frac{273.15 \,\text{K} + T(^{\circ}\text{C})}{295.15 \,\text{K}} \cdot \frac{760 \,\text{torr}}{p \,(\text{torr})}.$$ (14.21)

The humidity correction, P_h, for a wide range of average humidity, is just unity.

The polarity correction, P_{pol}, is more explicit in TG-51, but here one should do the following, calculated with the raw reading (M^+ or M^-) at a "+" or "−" polarity, respectively:

$$P_{pol} = \frac{(M^+ - M^-)}{[2(M^+ \,or\, M^-)]}.$$ (14.22)

Polarization effects are caused by two currents:

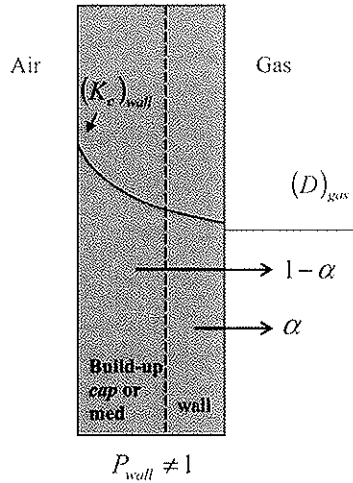1. *Compton current*: electrons liberated from other stuff like electrodes and guard.

Figure 14.4. The quantities P_{wall} and A_{wall} both account for electron contributions that differ between the wall and the medium. For A_{wall}, the medium is air.

2. *Extracameral current*: cable irradiation or charges collected outside of gas sensitive volume.

Define α as the fraction of ionizations in the cavity gas by electrons from the wall, proper (see Figure 14.4). Therefore, $1-\alpha$ is that fraction from the medium or the phantom instead. Now, use these fractions to get N_{gas} as follows (Equation 6 in TG-21):

$$N_{gas} = N_X \frac{A_{wall}\beta_{wall}A_{ion}k\left(\frac{\overline{W}}{e}\right)_{air}}{\alpha\left(\frac{\overline{L}}{\rho}\right)_{gas}^{wall}\left\{\frac{\overline{\mu}_{en}}{\rho}\right\}_{wall}^{air} + (1-\alpha)\left(\frac{\overline{L}}{\rho}\right)_{gas}^{med}\left\{\frac{\overline{\mu}_{en}}{\rho}\right\}_{med}^{air}}. \tag{14.23}$$

All of the quantities in Equation (14.23) are for Co-60. Find α in Figure 1 of TG-21 for Co-60[†].

Going back to Equation (14.17), let's assume Spencer–Attix also applies here. So $\left(\frac{\overline{L}}{\rho}\right)_{gas}^{med}$ can be substituted

for $\left(\frac{D_{med}}{D_{gas}}\right)$, provided we use factors described next, because we skipped the wall in this ratio. If the wall is very different from the phantom, it can be accounted for with P_{wall}. The replacement correction factor, P_{repl}, allows us to use Spencer–Attix by correcting for the photon fluence perturbations caused by the whole chamber's displacement of the medium. It does not include electron fluence corrections if the chamber is placed at TCPE[‡] ($d > d_{max}$).

What if the medium and the wall material both provide electrons to the cavity gas? Then the wall correction factor, P_{wall}, accounts for the medium being different from the wall. If different materials and both provide charges to the gas in the cavity, then $P_{wall} \neq 1$, otherwise it is unity.

At the ADSL, attenuation in the wall is given by the following:

$$A_{wall} = \frac{\psi_{wall}}{\psi_{air}}, \tag{14.24}$$

[†]Figure 7 of TG-21 is for another quality.
[‡]See Figure 5 in TG-21.

where, air is the "medium." Therefore, $A_{wall} = \dfrac{\psi_{wall}}{\psi_{med}}$.

At the clinic,

$$\frac{D_{med}}{D_{gas}} = \frac{D_{med}}{D_{wall}} \cdot \frac{D_{wall}}{D_{gas}} = P_{repl}(P_{wall})\left(\frac{\bar{L}}{\rho}\right)_{gas}^{med}. \tag{14.25}$$

The part $\dfrac{D_{med}}{D_{wall}}$ is covered by P_{repl}. With the same material of wall and medium, then $P_{wall} = 1$ by definition (and for electron beams). Otherwise we use the following:

$$P_{wall} = \frac{\alpha \left(\dfrac{\bar{L}}{\rho}\right)_{gas}^{wall} \left\{\dfrac{\bar{\mu}_{en}}{\rho}\right\}_{wall}^{med} + (1-\alpha)\left(\dfrac{\bar{L}}{\rho}\right)_{gas}^{med}}{\left(\dfrac{\bar{L}}{\rho}\right)_{gas}^{med}}. \tag{14.26}$$

Therefore, from Figure 7 in TG-21, for beam quality Q, the dose to medium is given by the following, which is Equation 9 of TG-21 if $P_{wall} = 1$:

$$D_{med} = M \cdot N_{gas}\left(P_{ion} \cdot P_{wall} \cdot P_{repl}\left(\frac{\bar{L}}{\rho}\right)_{gas}^{med}\right). \tag{14.27}$$

Here is how these complimentary terms are handled in the protocol. At the ADCL, the calibration is "in-air," and all the factors at ADCL are for Co-60: i.e., use Figure 1 in TG-21 for α. Therefore,

$$\left(\frac{\bar{L}}{\rho}\right)_{gas}^{wall}\left\{\frac{\bar{\mu}_{en}}{\rho}\right\}_{wall}^{air} \Rightarrow \alpha\left(\frac{\bar{L}}{\rho}\right)_{gas}^{wall}\left\{\frac{\bar{\mu}_{en}}{\rho}\right\}_{wall}^{air} + (1-\alpha)\left(\frac{\bar{L}}{\rho}\right)_{gas}^{cap}\left\{\frac{\bar{\mu}_{en}}{\rho}\right\}_{cap}^{air}. \tag{14.28}$$

At the clinic with, in general, $P_{wall} \neq 1$, and the calibrations happen "in-phantom" (relate to Equation 10 in TG-21), use Figure 7 in TG-21 for α:

$$\left(\frac{\bar{L}}{\rho}\right)_{gas}^{med} P_{wall} \Rightarrow \alpha\left(\frac{\bar{L}}{\rho}\right)_{gas}^{wall}\left\{\frac{\bar{\mu}_{en}}{\rho}\right\}_{wall}^{med} + (1-\alpha)\left(\frac{\bar{L}}{\rho}\right)_{gas}^{med}\underbrace{\left\{\frac{\bar{\mu}_{en}}{\rho}\right\}_{med}^{med}}_{=1!}. \tag{14.29}$$

The α factor in Equation (14.28) is different from that in Equation (14.29) since they are for different beam qualities. However, they represent the same correction fundamentally. Note that A_{wall} is unaffected by α, and A_{wall} corrects only for photons. Also note that "gas" and "air" must be distinguished to derive all this; the worksheet at the end of TG-21 does not distinguish.

Now noting that with $D_{gas} = M \cdot N_{gas}$, Equation 9 in TG-21 becomes: ($\alpha = 1$)

$$D_{med} = \left(P_{ion}P_{wall}P_{repl}\left(\frac{\bar{L}}{\rho}\right)_{gas}^{med}\right)_Q D_{gas}. \tag{14.30}$$

Substitute now with Equation 14.16 to *finally* get: ($\alpha = 1$)

$$D_{med} = M\left(P_{ion}P_{wall}P_{repl}\left(\frac{\bar{L}}{\rho}\right)^{med}_{gas} \right)_Q \left[A_{wall}\beta_{wall}\left(\frac{\bar{L}}{\rho}\right)^{gas}_{wall} \left\{\frac{\bar{\mu}_{en}}{\rho}\right\}^{wall}_{air} A_{ion}N_X k\left(\frac{\bar{W}}{e}\right)_{air} \right]_{Co-60}. \tag{14.31}$$

Rearrange to see more clearly: ($\alpha = 1$)

$$D_{med} = (MP_{ion}A_{ion})\cdot(P_{wall}P_{repl}A_{wall}\beta_{wall})\cdot\left[N_X k\left(\frac{\bar{W}}{e}\right)_{air}\right]\cdot\left[\left\{\frac{\bar{\mu}_{en}}{\rho}\right\}^{wall}_{\substack{air\\Co-60}}\left(\frac{\bar{L}}{\rho}\right)^{gas}_{\substack{wall\\Co-60}}\left(\frac{\bar{L}}{\rho}\right)^{med}_{\substack{gas\\Q}}\right]. \tag{14.32}$$

The right-hand-side of Equation (14.32) has four components. Now we discuss each part's corrections. The first part, $MP_{ion}A_{ion}$, is recombination. Chamber/electrometer reading M, corrected for recombination difference between continuous Co-60 (A_{ion}) and the pulsed linac (P_{ion}). The second part, $P_{wall}P_{repl}A_{wall}\beta_{wall}$, is fluence. For ADCL, Co-60, β_{wall} corrects for Φ (charges), and ψ (photons) are corrected for by A_{wall}. Then, for the clinic linac, both are corrected for by the product: $P_{wall}P_{repl}$. The higher-energy linac has a coupled correction! Again, $P_{wall}= 1$ if $\alpha = 1$. The third component, $\left[N_X k\left(\frac{\bar{W}}{e}\right)_{air}\right]$, is energy corresponding to a charge pair in the ADCL, so that we can use N_X. And finally, the last part, $\left[\left\{\frac{\bar{\mu}_{en}}{\rho}\right\}^{wall}_{\substack{air\\Co-60}}\left(\frac{\bar{L}}{\rho}\right)^{gas}_{\substack{wall\\Co-60}}\left(\frac{\bar{L}}{\rho}\right)^{med}_{\substack{gas\\Q}}\right]$, accounts for attenuation and stopping power corrections.

At the clinic for photon beams, substitute the N_{gas} definition in Equation (14.30) to get Equation 9 of TG-21:

$$D_{med} = M\left(P_{ion}P_{wall}P_{repl}\left(\frac{\bar{L}}{\rho}\right)^{med}_{gas} \right)\left[N_{gas} \right]. \tag{14.33}$$

The part $P_{ion}P_{wall}P_{repl}\left(\frac{\bar{L}}{\rho}\right)^{med}_{gas}$ in the above is all for clinic-specific beam Q and the phantom corrected into it. The next part, N_{gas}, is a property of a chamber with Co-60 dependencies corrected out.

Calibration of Electron Beams

Our discussion of electron beams will be brief. Consider that we have N_{gas}, and let us suppose that we have a thin wall or one that matches the phantom (medium or cap) material. The dose in the phantom from an electron beam with mean energy, $\bar{T}$, crossing the cavity is the following:

$$(D_{med})_{\bar{T}} = M_E\left(P_{ion}P_{fl}\left(\frac{\bar{L}}{\rho}\right)^{med}_{gas} \right)_{\bar{T}}\left[N_{gas} \right]. \tag{14.34}$$

Table 14.2: Average Point of Electron Entry into Cavity

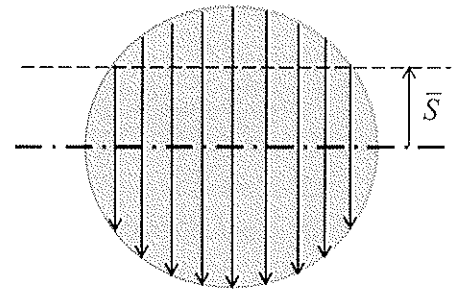| Cavity Type	Dimension	$\overline{S}$
Parallel	d = thickness	$d/2$
Cylindrical	r = radius	$0.85\ r$
Spherical	r = radius	$0.75\ r$

Figure 14.5. Depth of the effective center of the ion chamber.

The quantity $\left(D_{med}\right)_{\overline{T}}$ is the dose at the average point at which electrons enter the cavity, which is displaced a distance, $\overline{S}$, *upstream* of the geometric center of the cavity (see Table 14.2 and Figure 14.5).

The quantity M_E is the pressure- and temperature-corrected electrometer reading in the electron beam, and P_{fl} is the electron fluence correction. Only very small cavities will not perturb an electron beam. This perturbation is mainly due to a spatial variation of scatter. Thin parallel plate chambers have $P_{fl} \approx 1$, and extrapolation chambers can extrapolate to $P_{fl} = 1$. See Attix (2004) Table 13.9 for P_{fl} for cylindrical chambers. It is less than unity, and gets smaller for lower electron energies in cylindrical chambers.

Figure 14.6 shows the effects of differently shaped cavities on the electron scattering—the effects can be complex.

The part $\left[\left(\dfrac{L}{\rho}\right)_{gas}^{med}\right]_{\overline{T}}$ is the ratio of restricted stopping powers evaluated at the average energy $\overline{T}$. Table 13.11 of Attix (2004) has the ratio of restricted stopping powers for water, polystyrene, and Lucite. Notice that it increases with decreasing energy for water or plastic phantoms. The TG-21 protocol recommends $\Delta = 10$ keV. Recall that the average electron energy decreases linearly with depth. R_p is the practical range, d is the depth beneath the surface, and T_0 is the energy of the beam at the surface[†]:

$$\overline{T} \cong T_0(1 - d / R_p).$$
(14.35)

Electron beam coming from above.

Homogeneous phantom

Phantom with cavity:
Wide: less scattering
and decreased dose in
the cavity.

Phantom with cavity:
Long: more in-scattering
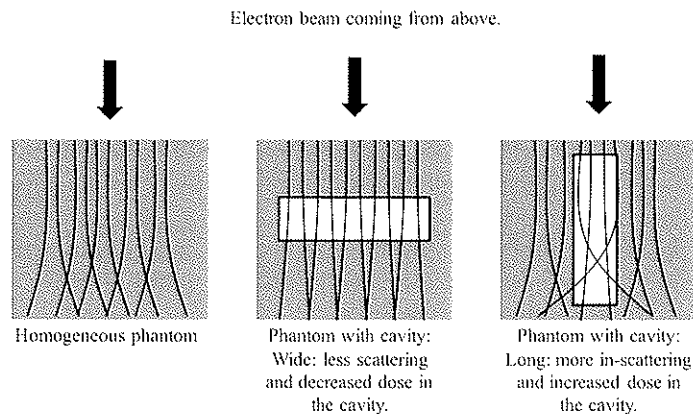and increased dose in
the cavity.

Figure 14.6. The effect of a cavity on electron beam scattering in matter.

[†]Attix (2004) uses the CSDA range, but TG-21 uses the practical range.

Updated Calibration Protocol for Medical Photon Beams (TG-51)

This improved protocol replaces the AAPM TG-21 protocol, and it can be applied to both photon and electron beams, but we will only focus on photon beams here.

One must use water phantoms for this protocol, and it is not based on exposure or even air kerma. This move simplifies the calculations. It also uses a better set of restricted mass stopping powers for the Monte-Carlo calculations of some parameters. Note that tap water is fine to use.

The dose to water, D_w^Q, for a beam "quality" ("quality" refers to beam type and energy spectrum), Q, in a reference condition is given by the following:

$$D_w^Q = M N_{D,w}^Q, \tag{14.36}$$

where M is the ion chamber reading (absolute charge value) and $N_{D,w}^Q$ is the absorbed dose to water calibration factor for an ion chamber located in the reference condition in a beam of quality Q. The key $N_{D,w}^Q$ quantity is determined from the calibration factor obtained in a calibration laboratory using a Co-60 beam again. It is found from the following:

$$N_{D,w}^Q = k_Q N_{D,w}^{^{60}Co}. \tag{14.37}$$

Here, k_Q converts the absorbed dose to water calibration factor for a Co-60 beam into the calibration factor for an arbitrary beam of quality Q, photon or electron. A lot of the physics discussed previously is now wrapped into this one factor: k_Q.

The reading, M, now must be fully converted from the raw reading, M_{raw}. Now, more factors than just the temperature and pressure corrections end up in this correction step as follows:

$$M = M_{raw} \cdot P_{ion} P_{TP} P_{elec} P_{pol}. \tag{14.38}$$

We must consider for these factors. P_{TP} corrects for temperature and pressure as before, and now is stated as follows:

$$P_{TP} = \frac{273.2 + T(^\circ C)}{295.2} \cdot \frac{101.33 \text{ kPa}}{P \text{ (kPa)}}. \tag{14.39}$$

The term P_{elec} corrects for the electrometer being calibrated at a separate time or procedure, and P_{pol} corrects for polarization effects. One takes a reading at each polarity, "+" and "−." Then, these readings respectively, M_{raw}^+ and M_{raw}^-, are used in the equation below. Important: retain the signs of these readings. The reading M_{raw}^- is the one used in the reference condition dosimetry, and it should be the same as used in the Co-60 calibration as well, either + or −:

$$P_{pol} = \left| \frac{M_{raw}^+ - M_{raw}^-}{2M_{raw}} \right|. \tag{14.40}$$

The next term is P_{ion}, which corrects for ion recombination. Recall the linearity discussion. An ion chamber should be used in the saturation region: voltage should be large enough to prevent recombination, but small enough so that electrons do not further ionize on their way to the central electrode. Note that small chambers will have trouble finding this regime. Recombination is more likely for high LET, high dose rate, higher temperatures, less voltage, and more space between electrodes. The procedure for calculating this is very elegant here. For the continuous beam, Co-60, P_{ion} is given by the following:

$$P_{ion} = \frac{1 - (V_H / V_L)^2}{(M_{raw}^H / M_{raw}^L) - (V_H / V_L)^2}. \tag{14.41}$$

For a pulsed beam (linac), it is like the following (note the exponent changes):

$$P_{ion} = \frac{1-(V_H/V_L)}{(M_{raw}^H / M_{raw}^L)-(V_H/V_L)}.$$

(14.42)

Here, V_H and V_L are the high and low voltage settings (by at least a factor of two), and M_{raw}^H and M_{raw}^L are the corresponding readings, respectively. Note that the two-voltage technique ignores initial recombination, ionic diffusion, and any charge multiplication. Therefore, it is an incomplete account of recombination.

Now, the improved ICRU-37 restricted collisional mass stopping power tables are used in Monte-Carlo calculations for k_Q. One must have an ion chamber that is listed or shown in Table 1 and the graph of Table 4 in TG-51 or provided in an update. The beam quality is specified by the percent depth dose found at 10 cm depth: $\%dd(10)_x$.

For beams with a nominal energy greater than or equal to 10 MV, TG-51 recommends that one use a 1 mm thick lead foil about 50 cm from the source to *standardize* (not eliminate) the electron contamination. There is a legitimate debate on this issue—it may add a complication that introduces errors for no good reason. The IAEA protocol does not recommend this foil. The $\%dd(10)_x$ is the result of first doing $\%dd(10)_{Pb}$ or just $\%dd(10)$ if no lead is used. One goes into the tables with $\%dd(10)_x$. Figure 1 in Rogers (1999) article shows the error one gets from the lead foil correction not being used. It is suggested by some that one need only use the lead if the $\%dd(10)_{Pb}$ is bigger than 75.

Tailor et al. (2002) produced a table showing only a 0.2% error if lead foil is not used. Page 1855 of TG-51 claims 2% error in $\%dd(10)_x$, therefore, only a 0.4% dose error in extreme cases.

One must also shift the chamber *reading* upstream for the effective point of measurement—it is an implicit correction for the chamber's inherent charged particle fluence perturbation. For photon beams, we shift the reading upstream by $0.6 \cdot r_{cav}$ (see Figure 14.7), where r_{cav} is the radius of the ion chamber cavity.

Since this protocol does not use an ionization ratio for beam quality, it is important to perform this shift. A ratio like TPR would be more robust to this issue. Therefore, TG-51 instructs us to perform this *shift of the curve*. Note that TG-51 defines the shifted curve as the depth-ionization curve.

Note that the caption in Figure 1 of TG-51 explains that for photons, the shifted curve is the depth-ionization curve, and that it is the same as the depth-dose curve. For electrons near d_{ref}, that is not true, and a second shift at one point is needed.
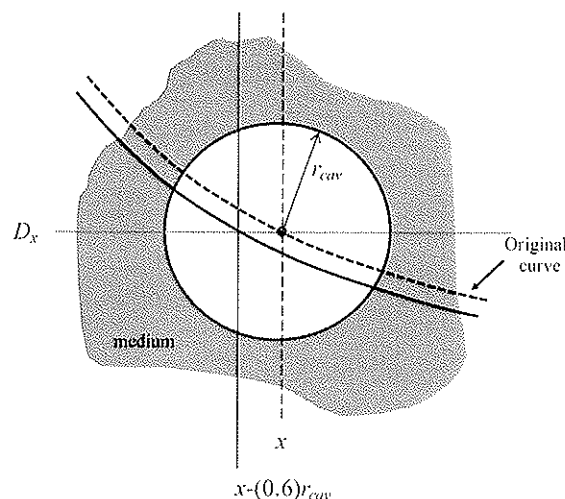

Figure 14.7. $x - (0.6)r_{cav}$ shifts the curve (reading) to the place where the same reading would occur if the chamber were not there.

In TG-21 terms, k_Q is written as the following:

$$k_Q = \frac{\left\{ (\bar{L}/\rho)_{air}^{water} P_{wall} P_{fl} P_{gr} P_{cel} \right\}_Q}{\left\{ (\bar{L}/\rho)_{air}^{water} P_{wall} P_{fl} P_{gr} P_{cel} \right\}_{{}^{60}Co}} = \frac{N_{D,w}^{Q}}{N_{D,w}^{{}^{60}Co}}.$$ (14.43)

A new factor is considered here, P_{cel}. It is the correction to account for the central electrode. Also, another new factor is here, P_{gr}, which is the correction to account for the effective center of the ion chamber. Note that $P_{fl} P_{gr} = P_{repl}$.

If we were to discuss electrons, we would have $N_{D,w}^{Q_{ecal}}$ instead of $N_{D,w}^{Q}$. Also there would be a more complicated gradient correction, $P_{gr}^{Q_{ecal}}$, and k'_{ecal} with $k'_{R_{50}}$. However, the spirit is the same.

A good way to compare TG-21 and TG-51 may be to access the discussion in TG-21 that describes the absorbed dose to water as a calibration basis, instead of exposure—the predecessor of TG-51 (see Equation 8 in TG-21):

$$N_{gas} = N_D \frac{A_{ion} A_{repl}}{\left(\frac{\bar{L}}{\rho} \right)_{gas}^{wall} \left\{ \frac{\bar{\mu}_{en}}{\rho} \right\}_{wall}^{water}},$$ (14.44)

where N_D is given by the following:

$$N_D \equiv \frac{D_{water}}{M}.$$ (14.45)

Compare this to Equation (14.16) (Equation 5 in TG-21)[*] and, therefore, the following equivalence must be true:

$$N_X \frac{A_{wall} \beta_{wall} k \left(\frac{\bar{W}}{e} \right)_{air}}{\left\{ \frac{\bar{\mu}_{en}}{\rho} \right\}_{wall}^{air}} \Leftrightarrow N_D \frac{A_{repl}}{\left\{ \frac{\bar{\mu}_{en}}{\rho} \right\}_{wall}^{water}}.$$ (14.46)

So N_X would be written as follows:

$$N_X = N_D \left(\frac{A_{repl}}{A_{wall} \beta_{wall}} \right) \left\{ \frac{\bar{\mu}_{en}}{\rho} \right\}_{water}^{air} \left[k \left(\frac{\bar{W}}{e} \right)_{air} \right]^{-1}.$$ (14.47)

Substitute this into D_{med} with $\alpha = 1$, replacing medium with water, cancel terms, and consider a beam quality, Q, the dose to water can be written as follows for each protocol:

TG-21: $$D_{water}^{Q} = M N_D \left(P_{ion}^{Q} A_{ion} \right) \left(P_{repl}^{Q} A_{repl} \right) \left(\frac{\bar{L}}{\rho} \right)_{wall\,Co-60}^{water\,Q} \left\{ \frac{\bar{\mu}_{en}}{\rho} \right\}_{water\,Co-60}^{wall\,Co-60} \left(\frac{\bar{L}}{\rho} \right)_{wall\,Q}^{water\,Co-60},$$ (14.48)

TG-51: $$D_{water}^{Q} = M k_Q N_{D,w}^{Co-60} = M N_{D,w}^{Q}.$$ (14.49)

We now define our own variables to better compare A factors versus P factors as follows:

$$P_{ion}^{Co-60} \equiv A_{ion}^{-1},$$ (14.50)

$$P_{repl}^{Co-60} \equiv A_{repl}^{-1}.$$ (14.51)

---

[*] It is easier to derive when "air" is distinguished from "gas."

Recall $k_Q \equiv \dfrac{N_{D,w}^{Q}}{N_{D,w}^{Co-60}}$ from Equation (14.37), and we would have the following:

$$k_Q = \frac{D_{water}^{Q}}{D_{water}^{Co-60}}. \tag{14.52}$$

Using the above, to convert between TG-21 and TG-51:

$$k_Q = \left(P_{ion}P_{repl}\right)_{Co-60}^{Q}\left[\frac{\left(\dfrac{\overline{L}}{\rho}\right)_{gas}^{water}}{}\right]_{Co-60}^{Q}, \tag{14.53}$$

$$N_{D,w}^{Co-60} = N_D\left[\left(\frac{\overline{L}}{\rho}\right)_{wall}^{water}\left\{\frac{\overline{\mu}_{en}}{\rho}\right\}_{water}^{wall}\right]_{Co-60}. \tag{14.54}$$

where, N_D is given by the following:

$$N_D = N_X k\left(\overline{W}/e\right)_{air}\left(\frac{A_{wall}\beta_{wall}}{A_{repl}}\right)\left\{\frac{\overline{\mu}_{en}}{\rho}\right\}_{air}^{water}. \tag{14.55}$$

A key point is that TG-51 has no in-between step like N_{gas}. Tailor and Hansen (2002) provide a numerical comparison between TG-21 and TG-51.

A Few Key Concepts for TG-51 Calibration

In TG-51 for electron beams, a big change is that we now have a specific reference position, d_{ref}. See Figure 2 in TG-51 and just below to the end of the section and Equations 16 and 17. Note that d_{ref} is on a gradient. The text says to shift the measured curve to get the depth-ionization curve and get I_{50}. One then shifts again, but only one point, to get R_{50} via Equations 16 and 17, and then we calculate d_{ref}.

Remember, we want to get the effective position for the chamber reading, given its current position. That will mean we need to not only correct for the effective center relative to where the electrons are launched, as with photon beams. But there is a second shift, and it is a conceptually very important CPE concept.

The second shift accounts for disequilibrium gradient effects, because we are not in transient charged particle equilibrium at d_{ref}. A single shift does not work for all depths, as it did for photons.

Now see Figure 1 of TG-51, and read the caption carefully as one also reads the text following Figure 2. The solid lines are the depth ionization curves, after a first shift from the raw data for both photons and electrons:

   i. For photons, the depth-ionization is the same as the depth-dose because of transient charged particle equilibrium, TCPE past d_{max} is rigorous for all energies.

   ii. For electrons, the depth-ionization is *different* from the depth-dose, and this difference is almost maximum right where the d_{ref} is located.

   iii. For lower-energy electron beams, $d_{max} \sim d_{ref}$, but for higher-energy electron beams, the situation gets more complicated. The caption says the whole depth-dose curve is not needed for this protocol, but a second shift is needed (so the last sentence of that caption could have been more clear).

For electron beams, follow the instructions in the text below to get R_{50}, and then one can get d_{ref}. Note that gradient corrections are already in the depth-ionization curve. For parallel-plate chambers, the chamber averaging implicitly averages to the correct effective measurement position. In a sense, then, this shift is really a shift to account for a finite lateral ion chamber dimension, like cylindrical chambers.

Table 14.3: Some Key Differences between Two Common Calibration Protocols: TG-51 Replaces TG-21

TG-21	TG-51
Air kerma-based (or really exposure-based)	Water dose based
Beam quality = TPR^{20}_{10} (ionization ratio)	Beam quality = $\%dd(10)_x$
Water or solid water type phantoms can be used	ONLY water can be used
No inclusion of the central electrode	Central electrode included
Intermediate factors: various P variables and N_{gas} cannot be directly measured	One can directly measure the intermediate factors like k_Q
Complicated—more errors possible	Simpler—more robust for a busy clinic
Uses ICRU 35 stopping powers (1% off) (Worse at lower e-beam energies)	Uses better ICRU 37 tables
Overall precision 3–4%, but errors mostly can cancel by luck. (TG-40 requires 2%, so potentially an issue)	Overall precision <1%

Now, we have curve II in TG-51, Figure 1, the depth-ionization curve, but for high-energy electron beams measured with an ion chamber, this is not the depth-dose curve. See Figure 1 of Hug et al. (1997), which is much more clear than the short dashes and solid lines in TG-51's Figure 1b. The second shift is then the conversion between I_{50} and R_{50}. It depends on energy, and it is handled empirically. See Equations 16 and 17 in TG-51. Two other ways to calibrate are mentioned: use a solid state detector or correct the whole curve with knowledge of the spectrum. These are all clues to the origin behind this second shift.

The real answer is found in Figure 11.5, which is also a high-energy electron beam[†]. Recall in Spencer–Attix theory, we worried about some of the delta-rays being like primary particles depending on the size of the ion chamber. In a solid state detector, this would not be an issue because the radiological distance is so different (see Rikner (1985)). In an ion chamber, the stopping powers need to have Spencer–Attix corrections, but in this case, the corrections will vary with depth, and this is handled by adding a second shift. Therefore, I_{50} and R_{50} will not be the same because of the distances the charged particles move. Because of delta-ray disequilibrium that changes with depth, electrons need a further correction.

Note that there is now an Addendum to TG-51 where the k_Q values have been refined, as well as good uncertainty analysis being added. See Figure 2 in Appendix B of McEwen (2014).

Also, TG-51 is further corrected for electrons by more accurate shifts to get R_{50}. See Table III of Muir (2014). In this table, note that the numbers in the last column are all very different from 0.5.

Table 14.3 summarizes key differences between the two protocols: TG-21 and TG-51.

References

AAPM. (1983). Radiotherapy Task Group 21. "A protocol for the determination of absorbed dose from high-energy photon and electron beams." *Med. Phys.* 10:741–71.

Almond, P.R., P.J. Biggs, B.M. Coursey, W.F. Hanson, M.S. Huq, R. Nath, and D.W.O. Rogers. (1999). Radiotherapy Task Group 51. "AAPM's TG-51 protocol for clinical reference dosimetry of high-energy photon and electron beams." *Med. Phys.* 26:1847–70.

Attix, F.H. *Introduction to Radiological Physics and Radiation Dosimetry.* Weinheim, Germany: WILEY-VCH Verlag GmbH & Co. KGaA, 2004.

Ding, G.X., D.W. Rogers, and T.R. Mackie. (1995). "Calculation of stopping-power ratios using realistic clinical electron beams." *Med. Phys.* 22:489–501.

Huq, M.S., N. Yue, and N. Suntharalingam. (1997). "Experimental determination of fluence correction factors at depths beyond dmax for a Farmer type cylindrical ionization chamber in clinical electron beams." *Med. Phys.* 24:1609–13.

[†]Notice below where the delta-rays (knock-ons) lose CPE: it would be right where d_{ref} is located.

Jenkins, T.M., W.R. Nelson, and A. Rindi. *Monte Carlo Transport of Electrons and Photons*. Proceedings of the international school of radiation damage and protection (8th, 1987, Erice, Italy). New York: Plenum Press, 1988.

McEwen, M., L. DeWerd, G. Ibbott, D. Followill, D.W. Rogers, S. Seltzer, and J. Seuntjens. (2014). *Med. Phys.* 41:041501.

Muir, B.R. and D.W. Rogers. (2014). "Monte Carlo calculations of electron beam quality conversion factors for several ion chamber types." *Med. Phys.* 41:111701.

Rikner, G. (1985). "Characteristics of a P-Si Detector in High Energy Electron Fields." *Acta Radiol. Oncol.* 24:71–4.

Rogers, D.W. (1999). "Correcting for electron contamination at dose maximum in photon beams." *Med. Phys.* 26:533–7.

Tailor R.C. and W.F. Hanson. (2002). "Calculated absorbed-dose ratios, TG51/TG21, for most widely used cylindrical and parallel-plate ion chambers over a range of photon and electron energies." *Med. Phys.* 29:1464–72.

Looking for a book that will deepen your knowledge about the particle interaction physics hidden inside radiation dosimetry protocols like TG-51 or its predecessor, TG-21? Unlike a cumbersome textbook with more overhead than insight, this nimble text distills actual lectures from a leading medical physics graduate program. In fact, the University of Wisconsin course this book is based on was previously taught by Frank Herbert Attix and Thomas Rockwell Mackie, legends whose insights are still found in these pages, refined and added to by the authors. After reading and studying this book, you will feel that even routine clinical tasks will remind you of the deep historical physics breakthroughs of generations of physicists who got us where we are today.

mpp